Unveiling the Mechanisms that Contribute to the Vascular Smooth Muscle Cell Response to Matrix Rigidity

---

Reesha Solanki

100113109

A thesis submitted for the degree of Doctor of Philosophy (Ph.D.)

University of East Anglia School of Pharmacy

September 2024

1.1 Abstract

Vascular smooth muscle cells (VSMCs) are the predominant cell type that make up the tunica media in the arterial wall. They exist in a quiescent, contractile state and regulate vascular tone and compliance. In ageing and disease, the extracellular matrix (ECM) stiffens, and vascular compliance is reduced. VSMCs are mechanosensitive and can respond to the stiffened ECM by dedifferentiating to a proliferative phenotype and becoming hypertrophic. The exact mechanism driving this change remains elusive, therefore, our work focuses on the VSMC response to rigid ECM.

We seed human aortic-VSMCs onto polyacrylamide hydrogels (PAHs) of two tensile strengths biomimicking a physiological (12 kPa) and pathological (72 kPa) aorta. In this thesis we have identified multiple VSMC volume regulators. Additionally, we have been able to identify that VSMCs seeded on rigid (72 kPa) PAHs stimulated with angiotensin II or growth media are hypertrophic in nature but also experience increased DNA damage.

We find that HDAC3 inhibition plays a beneficial role in restoring healthy morphology on a rigid matrix, whilst HDAC6 inhibition caused a hypertrophic response in those seeded on a pliable (12 kPa) PAHs as well as greater DNA damage accumulation. We find that microtubule stability does not drive this mechanism as we first hypothesised.

We highlight a novel piezo1/PKC/aquaporin-1 mediated pathway driving VSMC hypertrophy. We find that the pharmacological targeting of this pathway (even in the longer term) inhibits the increased VSMC volume response to ECM rigidity. We utilised the allosteric activator of piezo1, Yoda1, as well as siRNA-mediated knockdown and the inhibition of PKC and aquaporin-1 to determine this result. We also confirm that PKC regulates aquaporin-1 localisation in VSMCs, which was not fully elucidated until now. Our findings provide novel therapeutic targets for stiffness-induced VSMC hypertrophy and dysregulation.

1.2 The work in this thesis has contributed to several recently published papers:

Johnson RT*, Solanki R*, Wostear F*, Ahmed S, Taylor JCK, Rees J, et al. **Piezo1- mediated regulation of smooth muscle cell volume in response to enhanced extracellular matrix rigidity**. British Journal of Pharmacology 2023

Johnson R*, Wostear F*, Solanki R*, Steward O, Morris C, Bidula S, et al. **A microtubule stability switch alters isolated vascular smooth muscle calcium**. Paper published in Journal of Cell Science 2024.

*Joint first author

1.3 Contents

1.4 List of figures

1.5 Acknowledgements

I am deeply grateful to all those who have supported me throughout my PhD journey. First and foremost, I would like to extend my heartfelt thanks to my supervisor, Dr. Derek Warren. Your unwavering support, insightful guidance, and friendship have been invaluable to me. I could not imagine completing this chapter of my life in any other lab than yours. Your belief in me and encouragement have made this challenging journey not only possible but profoundly rewarding. Only a great leader can make a lab feel like family and for that I am so grateful. I would also like to thank the rest of my supervisory team especially Dr Julie Sanderson and Dr Stefan Bidula.

To my colleagues, Rob and Finn, you have been more than just peers. It would have been hard to get through these four years without you. Knowing that you were in lab made even the hardest days easier. Rob, I cannot thank you enough for your help, reassurance and caring messages of support whenever things were not working, or I was feeling down. I also am so grateful that you allowed me to bother you at any time with my silly questions even after you left for Denmark! I wouldn't have made it to this point without you. Finn, I could not have thought of anyone better to join our team three years ago. You have become an incredible friend and now can never imagine life without your humour, even if it is at my expense! Your ever-willingness to help has made this whole process a lot easier. It is hard to believe we got anything done with all the ruckus we caused.

I'd like to thank my parents, who have been my twin pillars without whom I could not stand. I am proud to be your daughter and would not have made it this far without your unwavering support and guidance. Anneka, you have been the greatest source of motivation and someone who knew I could get through the toughest times before even I could myself. I cherish the countless ways you support me everyday and the special bond we share. I'd also like to thank Alex Jones for providing a safe haven through the PhD storms, your hard work and motivation is inspirational and I would be happy to achieve half of what you have.

I cannot forget you Alex Merchan, I would never have thought at the beginning of my PhD that this path would also lead me to you. Thank you for looking after me and Lyra everyday, the late night pickups from the lab and constant words of encouragement. You have believed in me more than I could imagine anyone could and I am incredibly fortunate to have you by my side.

Finally, I must acknowledge my beloved cats Lyra, Chico and Johnny, whose companionship has provided much-needed comfort and joy throughout this process. Their presence has been a soothing and reassuring constant amid the whirlwind of research.

Thank you all for your incredible support and for being an integral part of this achievement.

1.6 Abbreviations

2D- Two-dimensional

3D- Three dimensional

53BP1- p53-binding protein 1

α-SMA – Alpha-Smooth Muscle Actin

AFM- Atomic force microscopy

AngII- Angiotensin II

APES - (3-Aminopropyl)triethoxysilane

APS - Ammonium persulfate

BSA - Bovine Serum Albumin

CVD – Cardiovascular disease

DAG – Diacylglycerol

DAPI - Diamidino-2-Pheylindoledihydrochloride

DDR - DNA damage response

DMSO - Dimethyl sulfoxide

DMEM – Dulbecco's Modified Eagle Medium

DNA – Deoxyribonucleic Acid

ECM – Extracellular matrix

FA – Focal Adhesion

F-actin – Filamentous Actin

FBS- Fetal bovine serum

HRP - Horseradish peroxidase

IF – Immunofluorescence

kPa – Kilopascals (for stiffness measurement)

MAP - Microtubule associated protein

MAPK – Mitogen-Activated Protein Kinase

MMP – Matrix Metalloproteinase

MLC - Myosin light chain

MLCK - Myosin light chain kinase

MLCP - Myosin light chain phosphatase

NO - Nitric oxide

NT- Non-targeting

PAH- polyacrylamide hydrogel

PBS - Phosphate Buffered Saline

PFA - Paraformaldehyde

PIP2 - Phosphatidylinositol 4,5-bisphosphate

PKC – Protein kinase C

PLC - Phospholipase C

pMLC - Phosphorylated myosin light chain

RhoA – Ras Homolog Family Member A ROCK - Rho-associated protein kinase

ROI - Region of interest

RPM- Revolutions per minute

RT – Room temperature

SAC - Stretch-activated ion channel

SDS - Sodium Dodecyl Sulfate

SDS-PAGE – Sodium Dodecyl Sulfate-Polyacrylamide Gel Electrophoresis

siRNA – Small Interfering RNA

SM-myosin II - Smooth muscle myosin II

SR - Sarcoplasmic reticulum

TEMED - Tetramethylethylenediamine

TFM – Traction force microscopy

TRP - Transient receptor potential

TRPV - Transient receptor potential-vanilloid

UV – Ultraviolet (used in crosslinking)

VSMC – Vascular smooth muscle cell

VGCC - Voltage-gated calcium channel

WB- Western blot

Chapter 1: Introduction

Cardiovascular disease (CVD) is one of the leading causes of death with coronary heart disease being the most common cause of premature deaths in western countries. In the UK its totals 25% of all deaths (1,2). It was calculated in 2019 that England spent £9 billion on CVD related healthcare (3). CVD is an umbrella term that encapsulates multiple diseases such as atherosclerosis, hypertension, coronary heart disease and stroke (4). Although diabetes, smoking and cholesterol levels are prominent risk factors of CVD, ageing has proven to be the most significant (5).

Ageing impacts the structure and functionality of blood vessels mirroring the changes observed in hypertension(5,6). Vascular compliance is the ability of the vessel to expand and contract in response to fluctuations in hydrostatic pressure generated by the cardiac cycle. Vascular remodelling is associated with structural changes in the extracellular matrix (ECM). Specifically, increased collagen deposition along with greater elastin degradation results in increased stiffness and reduced vessel compliance. This reduced vessel compliance means blood vessels are exposed to far greater levels of shear stress and is the key aetiology of several vascular diseases such as hypertension and aortic aneurysm (7).

1.1 The aorta

1.1.1 Aortic structure

The aorta provides oxygen rich blood to the body. The aorta is the largest vessel in the human body and is composed of three major layers. These layers - in order of innermost to outermost - are named tunica intima, tunica media and tunica adventitia (8,9) as can be seen in **Figure 1.1**. The tunica intima is composed of a single layer of endothelial cells. This layer of cells has a role to separate the blood from vessel tissue as well as producing signalling molecules to aid in the regulation of vascular tone. Endothelial cells also play a role in haemostasis, coagulation and inflammation (10).

The tunica media is the thickest layer and is predominantly made up of vascular smooth muscle cells (VSMCs). It also contains ECM with a higher elastin to collagen ratio. Most mechanical properties of the aorta are due to the tunica media where stiffness is determined by the contraction of VSMC and the molecular composition of the ECM. The VSMC secrete most extracellular matrix proteins found in the vessel. The outermost layer is the tunica adventitia. It is composed primarily of stiffer ECM components such as collagen and provides essential support to prohibit overexpansion of the vessel (9,11).

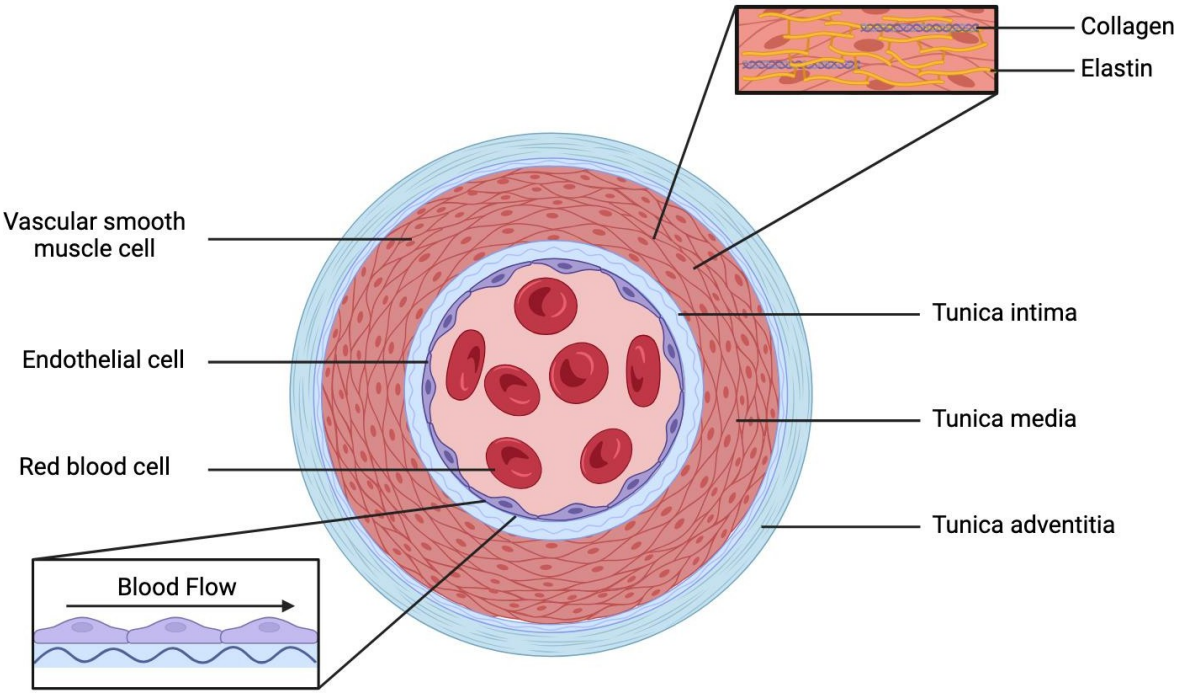

Figure 1.1 *A schematic diagram of the aorta representing the three layers (innermost to outermost): tunica intima, tunica media and tunica adventitia.*

1.1.2 Aortic Compliance and ageing

Aortic compliance is the ability of the aorta to change shape in response to changes in blood pressure. The balance between collagen and elastin defines aortic compliance and modulates mechanical pressures from increased blood pressure in the vessel (8). Collagen provides the tensile strength counteracting the pressure placed on the vessel, whereas elastin imparts its elastic ability to allow flexibility in the vessel to undergo vasoconstriction and vasodilation (12,13). The aorta acts as an elastic reservoir behind the heart, known as the elastic buffering chamber. This mechanism labelled as the Windkessel effect, aids in converting the pulsatile nature of blood flow from the heart into a more continuous smooth flow within the arterial system. This elastic property of the aorta allows for a reduction in cardiac workload by storing energy during systole and releasing it during diastole. The Windkessel effect can be disrupted when there is a loss of elasticity affecting arterial stiffness(14).

Ageing creates a negative feedback loop in aortic compliance whereby an increase in nonelastic proteins such as fibronectin and collagen are compounded by increased degradation of elastin (15,16). The turnover rate of elastin fibres is considerably lower than that of collagen thus creating an imbalance exposing the artery to mechanical damage overtime(8,17). Maintaining aortic compliance as we age is of utmost importance to avoid the pathogenesis of CVD. The effect of vessel compliance on blood pressure can be seen in **Figure 1.2**. Decreased aortic compliance is now considered a major risk factor in the development of CVD (18,19). The tunica media plays a vital physiological role in blood vessels as they bear 60% of the load under circumferential tension and is, therefore essential to vascular compliance. The adventitia bears the remaining 40% (8). VSMCs respond to varied blood pressure by contracting and relaxing the blood vessel. VSMCs use actomyosin attached to the extracellular matrix to generate contraction within the cell. In healthy tissue, these actomyosin forces contract the cell in response to mechanical signals to maintain vessel tone. In ageing and disease, VSMCs respond to increased matrix stiffness by generating increased actomyosin forces. This results in even greater vessel stiffness and increased pathogenesis. The specific mechanisms driving this VSMC contribution are yet to be elucidated.

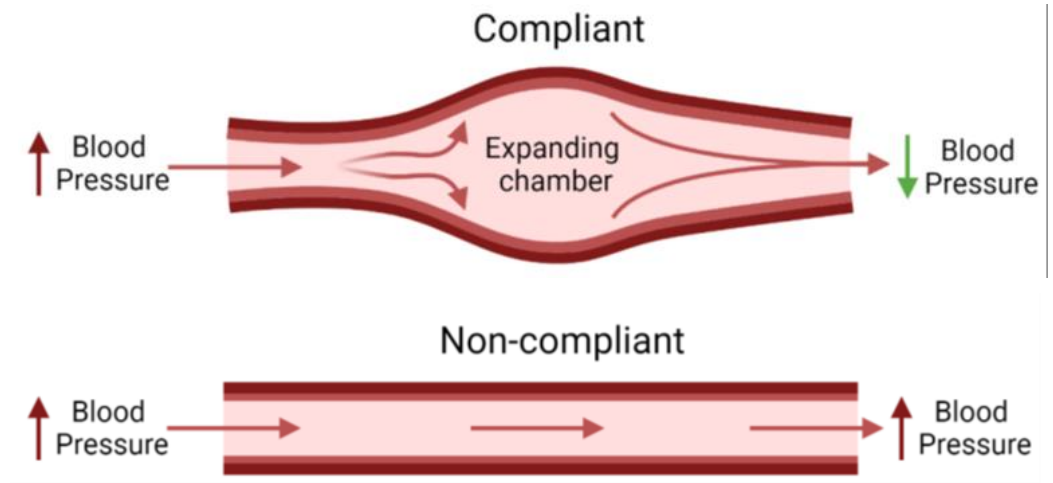

Figure 1.2 *A diagram to show a compliant vs non-compliant artery with its resultant effect on blood pressure.*

1.2 VSMC Contraction

In healthy aorta, VSMCs are found to be in the quiescent phenotype. This means they are highly contractile. This contraction is primarily regulated via the activity of calcium ions (Ca^{2+}) and their downstream signalling pathways. The release of Ca^{2+} stimulates the production of actomyosin force generation. In the first instance, Ca^{2+} ions enter from the extracellular environment through selective voltage gated or non-selective cation channels located on the plasma membrane (20). There are five voltage gated calcium channels, L, P, N, R and T found in varying locations within the human body. The L-type calcium channel is the predominant route of calcium entry in VSMCs (21).

The calcium dependent pathway starts with the binding of a ligand to a G-protein coupled receptor that is coupled to a Gq heterotrimeric G-protein. The α-subunit of Gq binds to and induces phospholipase C (PLC) activity. PLC converts phosphatidylinositol-4,5-bisphosphate (PIP_2) into secondary messengers inositol- 1,4,5-triphosphate (IP_3) and diacylglycerol (DAG). IP_3 binds to IP_3 receptors in the sarcoplasmic reticulum triggering the release of Ca^{2+} ions. Cytosolic calcium ions bind calmodulin, a regulator of myosin light chain kinase (MLCK). MLCK phosphorylates the light chain of myosin at the Serine 19 or Threonine 18 residues. MLCK is an essential kinase in VSMC as it is the only kinase able to phosphorylate myosin light chain, as observed in MLCK knockout mice. Activation of MLCK therefore stimulates cross-bridge cycling as the myosin filament pulls on the actin filament anchored to the membrane. This initiates contraction of the VSMC (22). Deletion of MLCK impairs contractile force proving its essential role in contraction (22,23).

In addition to the calcium-dependent pathway, the contraction of VSMCs can be stimulated/maintained via the RhoA pathway (24). This is also known as the calcium-independent pathway as it regulates the phosphorylation of myosin light chain. The activation of GPCRs catalyse the exchange of GTP for GDP in RhoA. RhoA is a small G-protein along with its associated kinase Rho kinase (ROCK) alters myosin light chain calcium sensitivity. GTP bound RhoA activates ROCK which in turn inhibits MLC phosphatase (MLCP), via phosphorylation (25). Customarily, the removal of phosphate allows for smooth muscle cell relaxation, thus inhibition of MLCP maintains

VSMC contraction. The RhoA/ROCK pathway is regularly found in tonic smooth muscle, where prolonged contraction of the cell occurs as opposed to phasic, contracting in bursts via the calcium influx (26–28). This pathway has been represented by **Figure 1.3** which shows the RhoA-ROCK pathway and the calcium-dependent pathway that regulated the contractile mechanism for VSMC contraction.

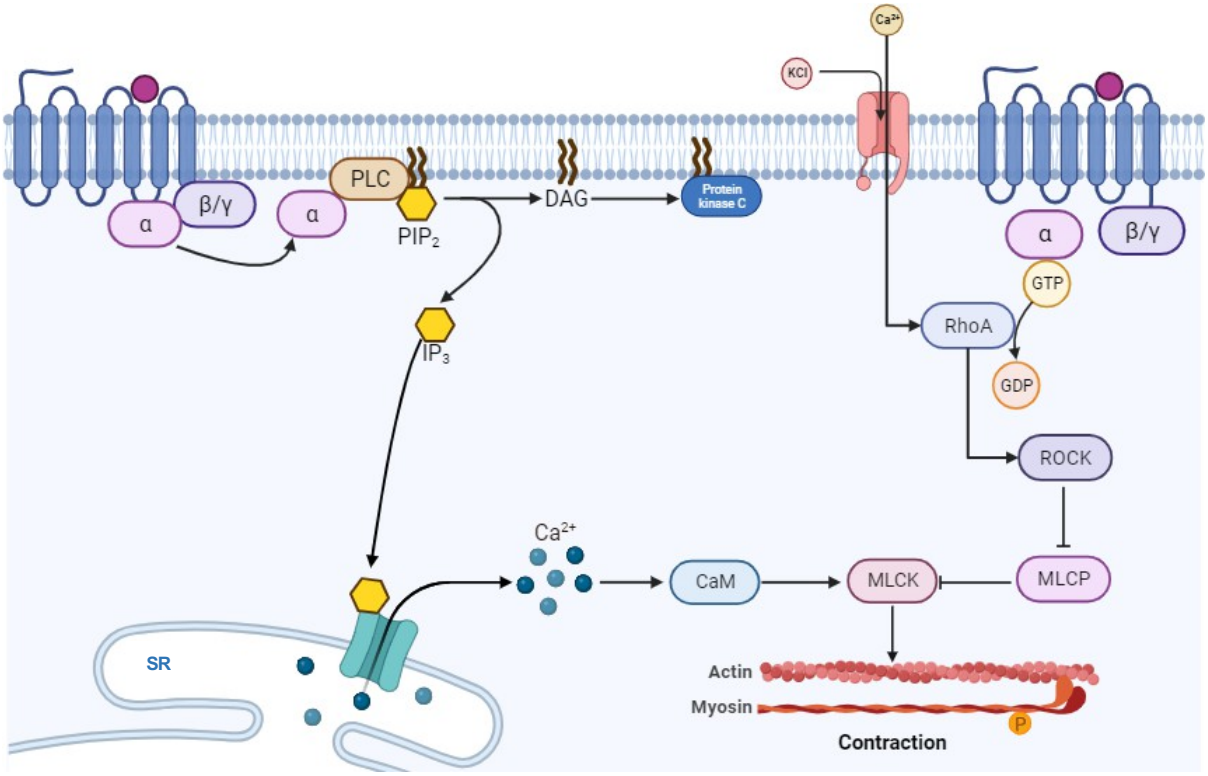

Figure 1.3 *This figure shows the contractile mechanisms for VSMC contraction, depicting the RhoA-ROCK pathway and calcium-dependent pathway and their interconnection which regulates VSMC contraction.*

1.3 Vascular Smooth Muscle Cell Phenotype

VSMCs have the unique ability to retain plasticity once matured. In healthy vessels, VSMCs are found in the quiescent phenotype which is also known as the contractile phenotype. Typical contractile proteins found in this state are smooth muscle α-actin, smooth muscle myosin heavy chain (SM-MHC), desmin and smoothelin. SM-MHC is a VSMC specific marker. These marker proteins are essential in VSMC contraction and for providing structure to the contractile components of the cell. It is the α-actin and myosin that construct the actomyosin unit which enables vasoconstriction.

In response to vascular injury or changes in cell-matrix interactions, VSMCs de- differentiate into a synthetic phenotype. This phenotype is associated with the downregulation of contractile filaments alongside the increase in ability to proliferate and migrate as well as ECM remodelling (11,29). This proliferation contributes to an increase in VSMC population. The decrease in contractile proteins means that VSMCs cannot contract as effectively as the quiescent type (30). The simultaneous increase in matrix metalloproteinases (MMPs) causing VSMCs to migrate within the vessel wall and can lead to intimal thickening and atherosclerotic plaques (30–32). It has been observed that SM-MHC and smoothelin are absent in studies of arterial injury with myofibroblast cells, which correlates to studies showing both proteins being downregulated in the synthetic phenotype (33). The synthetic phenotype contributes to the pathophysiology of multiple cardiovascular diseases such as hypertension, inflammation, and atherosclerosis (34–36).

Enhanced synthetic activity also leads to the increase in ECM production. This means the increase in both collagen and elastin secretion. This secretion is essential in tissue repair, however, in excess amounts can lead to certain CVDs such as atherosclerosis
(30). The extracellular matrix can affect VSMC phenotype and vice versa specifically through integrin mediated cell-matrix interactions. In addition to collagen and elastin, proteoglycans are another vital component in the ECM. For example, heparin has been associated with the maintenance of the contractile phenotype and the reduction of VSMC proliferation. Fibronectin, a glycoprotein in the ECM stimulates the synthetic phenotype, and is known to be upregulated in stiffer matrix environments (33,37,38).

An increase in some ECM proteins has been observed in atherosclerotic injury across many studies (32,39).

The phenotypic switch from quiescent to synthetic is also seen in an aged vessel as damage overtime creates a dysfunction in VSMC homeostasis (30). The cell shape associated with quiescent and synthetic phenotype can be seen in **Figure 1.4**. In ageing and hypertensive mice models, there was a decrease in contractile proteins whilst concomitantly detecting an increase in synthetic phenotype markers (40). Senescent cells upregulate the synthesis of MMPs and pro-inflammatory markers which can exacerbate inflammation and remodeling whilst also promoting the synthetic phenotype. The increase in MMPs aide the breakdown of the ECM allowing VSMCs to migrate through the vessel walls (30). Together these synthetic proteins lead to atherosclerosis which can further promote senescent cells also causing an increase in VMSC stiffness, all looping into a negative cycle (41).

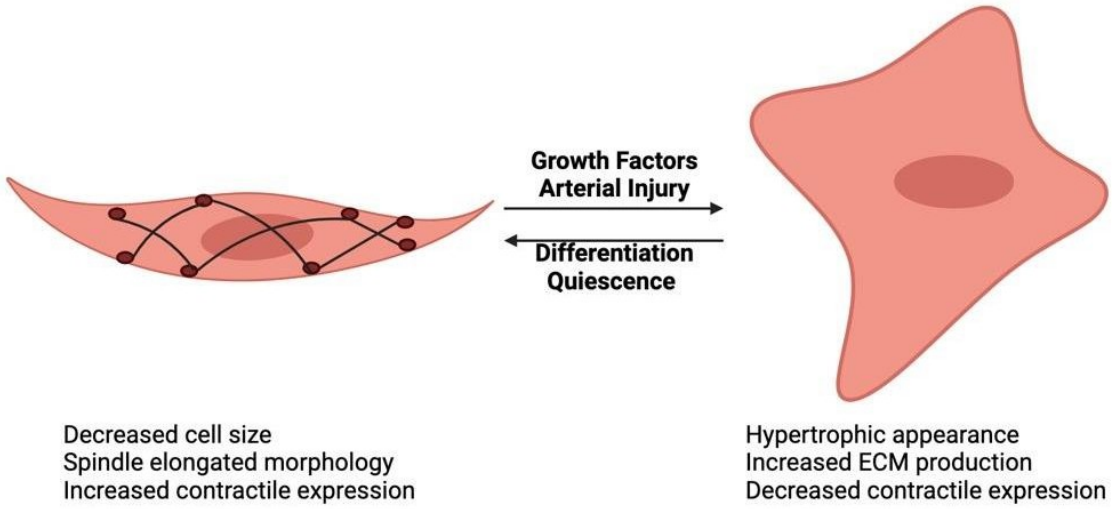

Figure 1.4 *A figure to represent the vascular smooth muscle cell phenotypes, quiescent cell on left and proliferative cell on right.*

Shear stress is the biomechanical force produced by blood flow that is imposed on the tunica intima, the level of force is known to impact phenotype modulation. Higher shear stress, as sensed by endothelial cells has been associated with the synthetic phenotype and an increase in proliferation (42). Through BrdU labelling it was confirmed that VSMCs exposed to a higher shear stress had elevated levels of proliferation (43). Overtime it is known that the endothelial layer becomes thicker as a response to higher blood pressure (42). Contractile protein markers of VSMCs, mentioned earlier, are also increased as the cell attempts to maintain contractile

capability. It has also been observed that upon detection of wall stress, collagen synthesis is upregulated further stiffening the environment (44,45). These maladaptive processes, regulated through cell-matrix interactions, lead to de-differentiation into the synthetic phenotype.

1.4 The role of actin in VSMC mechanotransduction

Actin makes up 20% of the total protein content of VSMCs. Research from *Qui et al* shows that VSMCs of older monkeys have a higher elastic modulus compared to young monkeys. A greater elastic modulus suggests aging creates a stiffer environment; this decrease in elasticity was related to an increase in actin filaments. This study proved that actin filaments played a key role in VSMC stiffness. Supporting this data when *Qui et al* further reported that when VSMCs are treated with Cytochalasin D (an actin depolymerising agent) a reduction in the elastic modulus is seen in both old and young monkeys. Two variations of actin exist in VSMCs, a globular monomeric form, called G-actin, as well as a linear polymer form called F- actin. It is the ratio between these two actin forms that affect elasticity and stress- relaxation patterns within the cell(46). Actin filaments in VSMCs attach to the ECM via integrins, it is through this adhesion that the structure of the ECM regulates the contractile functions of VSMCs. Integrins are composed of alpha and beta subunits. They are essential for cell adhesion, migration, proliferation, survival and differentiation.

Alongside integrins, actin requires scaffold proteins aiding in signalling, stabilisation and motility. Focal adhesions are essential in creating a link between the ECM and actin cytoskeleton. A representative figure can be seen in **Figure 1.5** which highlights the cell-matrix interaction via integrins. This connection allows for the transduction of mechanical signals into biochemical signals to adapt cell behaviour (28). These scaffolding molecules are, α-actin, vinculin, paxillin and talin. Activation signals such as collagen binding promote Talin to attach to the β subunit of the integrin. This attachment leads to the conformational changes to both integrin subunits to facilitate the binding of focal adhesions in the extracellular environment. Talin and α-actin bind directly to the integrin, it is understood that talin promotes the binding of the additional scaffold proteins. An example of this is vinculin which crosslinks the actin cytoskeleton and talin (46). This strengthens the focal adhesion. This mechanism is also known as “Inside-out” signalling (47). The α5β1 integrin; binds to fibronectin another extracellular matrix protein (48). In some age-related cardiovascular diseases, the expression of α5β1 integrin increases alongside a greater elastic modulus, which in turn increases fibronectin binding. It is unknown whether this response further accelerates VSMC stiffness. The ECM-integrin and α-actin interaction impact bio-mechanical responses in the cell, and the dysfunction of these can create maladaptation in vascular tone (49,50).

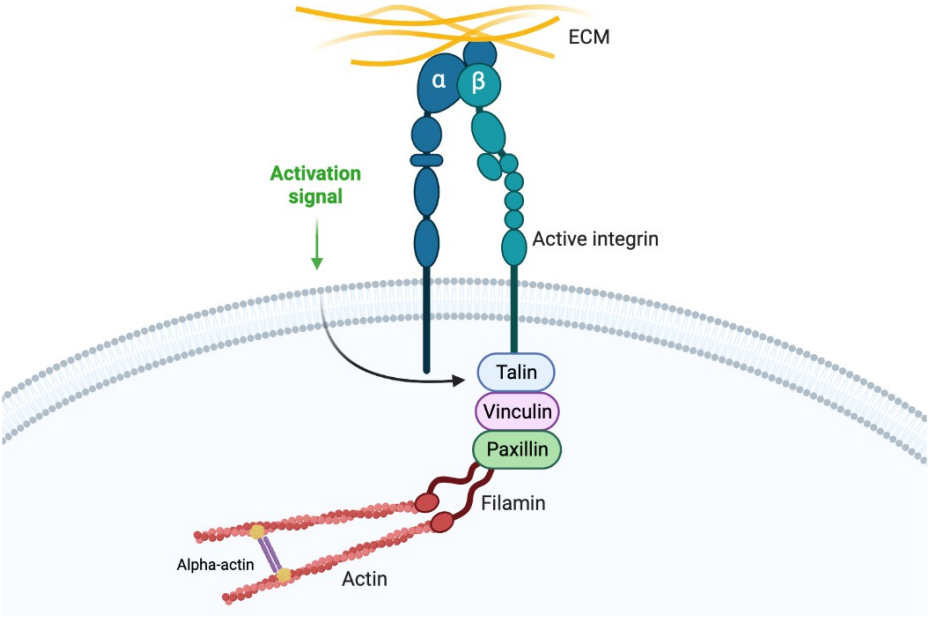

Figure 1.5 *A representation of cell-matrix interaction via integrin focal adhesion. Active integrins connect actin cytoskeleton to the extracellular matrix allowing for the transduction of mechanical signals into the cell.*

1.5 Microtubules

Vascular smooth muscle cells are mechanosensitive. They respond via changes in shape and structure to biological stimuli surrounding them (51). The ability for VSMCs to respond to mechanical stimuli is essential for maintaining vascular tone ensuring a constant force across the blood vessel wall. Integrin proteins bind across the cell membrane, linking ECM with the intracellular actin filaments. They are essential in transducing stimuli from outside the cell to the actin filaments and regulate a range of processes including cell contractility, gene transcription and proliferation. Microtubules and intermediate filaments are other components of the cytoskeleton that are essential in transducing stimuli from the outside to the inside of the cell.

Microtubules play a role in mechanotransduction and execute a multitude of cellular activities such as regulating cell shape, cell contractility and transport. The microtubule structure is made up of thirteen protofilaments consisting of a-tubulin and b-tubulin heterodimers. As microtubules are found ubiquitously in the cell, the abnormal function of microtubules consequently leads to a diverse number of diseases including cancer and has been implicated in CVD. Microtubules help maintain cell contractility through regulation of actin and myosin organisation. Microtubules are known to sense stress, as they respond with cellular shape changes by growing in the direction of stress. This theory can be applied to VSMCs, with key cell area changes occurring possibly due to microtubule reorganization (52).

Microtubules exist in the state of polymerisation and depolymerisation, this is known as dynamic instability. This process allows the microtubules to rapidly assemble and disassemble when required in response to external stimuli. The process of polymerisation involves two steps called nucleation and elongation where heterodimers of α- and β-tubulin form protofilaments that bind together to form the hollow microtubule. β- tubulin binds to GTP which induces polymerisation at the positive end. Depolymerisation leads to the disassembly via the removal of tubulin. The depolymerisation of MTs leads to cytoskeletal reorganization and altered cell stiffness. Depolymerised microtubules are believed to enhance force generation and whilst impeding vasodilation. It is thought that stable microtubules provide a resistance to the intracellular tension generated by actomyosin forces as they are suggested to be compression bearing. This can be seen in **Figure 1.6**. The resistance to compression affects cell morphology

and stability (51,53). This resistance in force is described in the tensegrity model and suggests that microtubules have a protective effect in the cell when stable. In other studies, porcine coronary VSMCs have shown to have increased intracellular calcium levels when treated with a microtubule depolymerising agent. This suggests that microtubules dynamics can influence calcium induced signalling (51).

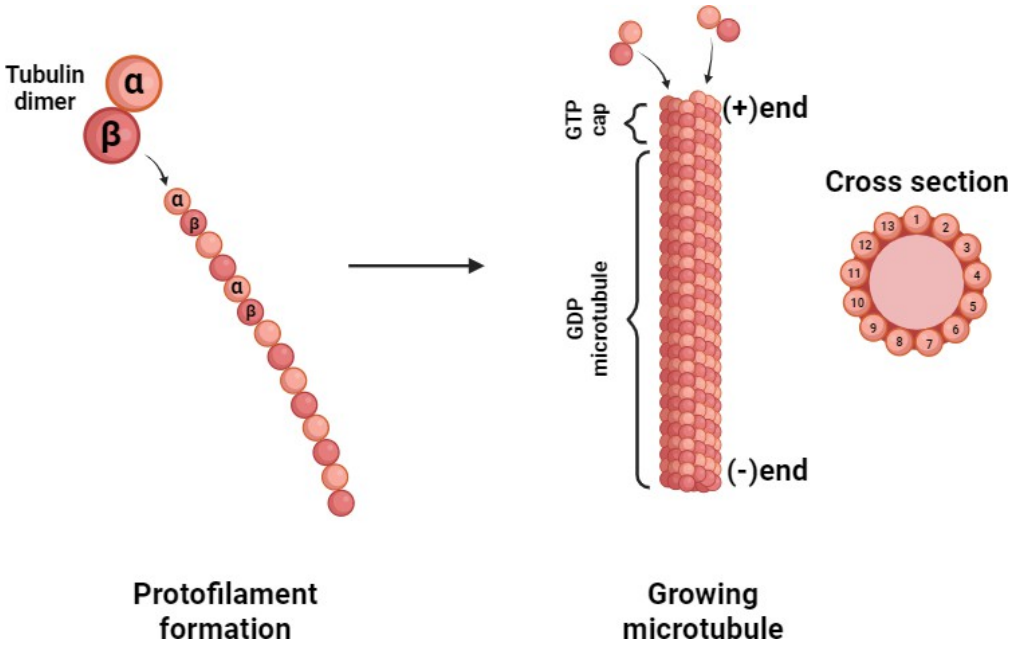

Figure 1.6 *A diagram to show microtubule formation and structure with cross section to represent 13 profilaments binding to make a hollow microtubule.*

Microtubule dynamics can be regulated via accessory proteins that can bind to microtubule preventing or promoting depolymerisation (54). The three most researched microtubule associated proteins (MAPs) are MAP2, MAP4 and TAU. These proteins enhance stabilisation and therefore microtubule polymerisation. Protein binding is regulated by kinases that phosphorylate the MAP family which can detach the MAP and destabilise the microtubule. Examples of these kinases would be microtubule affinity regulating kinase (MARK), protein kinase C (PKC) and cell division cycle protein 2 (CDK1). The increase of MAP4 proteins have been marker of oesophageal squamous cell carcinoma. Evidence also indicates that MAP4 is the predominant form of MAP expressed in the heart, suggesting it plays a significant role in CVDs. Studies have suggested that the phosphorylation of MAP4 mediated by the p38/MAPK pathway promotes cellular proliferation and migration in hypoxic endothelial cells. It also induced microtubule disassembly and cardiomyocyte apoptosis prior to cardiac remodelling in mice. MAP4 is also upregulated in hypertrophic cardiomyocytes (55). MARK4 has shown to promote atherosclerosis, with its knockdown being associated with lower cholesterol and fat

mass levels (56,57). Furthermore, TAU provides stabilisation as it transforms tubulin into microtubules. In Alzheimer's disease, TAU becomes hyperphosphorylated, reducing its ability to bind to microtubules, encouraging destabilisation. In addition to this, the hyperphosphorylated TAU begins to form aggregates creating dense structures called neurofibrillary tangles (58,59). "Tauopathies", which are the disorders characterised by the abnormal TAU aggregation may not only be confined to neurodegenerative disease of the brain. It was recently observed that an increase of hyperphosphorylated TAU was detected in heart failure (60).

Due to the importance of microtubules in VSMC structure and function, it is plausible that TAU levels are upregulated in other CVDs such as atherosclerosis or hypertension. In general, MAPs seem to play a significant role in multiple diseases and have become emerging targets in certain CVDs. Their roles in VSMC function are yet to be fully understood.

Microtubules can also be stabilised via tubulin acetylation. This in turn leads to polymerisation of G-actin leading to actin filament formation. It is postulated that acetylation increases the flexibility of the microtubules. This flexibility is thought to increase their resistance to mechanical stresses (61). Tubulin acetylation occurs through post translational modifications (PTM) of the microtubule via acetylases. Research indicates that microtubule acetylation is correlated with increased stiffness and microtubule density in cardiomyocytes (57).

The use of certain drugs to inhibit microtubule acetylation are now of increased interest such as histone deacetylase 6 (HDAC6) which can bind to free tubulin (57). There is probability that the hyperacetylation of microtubules could impact VSMC stiffness or the VSMC response to ECM rigidity.

1.6 Histone deacetylases

DNA is packaged around proteins called histones. This mixture of protein and DNA make up chromatin which is essential for structure in a chromosome. There are several ways in which histone modifications can regulate gene repression or expression. Examples of post translational modifications are histone acetylases/deacetylases that modify the lysine residue in the NH2 terminal tails of a histone(62). For example, histone deacetylases (HDACs) are enzymes which remove acetyl groups from histone tails. HDAC inhibitors can inhibit the deacetylation of the histone. This process can lead to the hyperacetylation of histones resulting in epigenetic modification (63). The addition of acetyl groups lead to a more open chromatin structure as the histone tails lose their affinity to DNA. Another example is histone (de)methylation, the reaction of adding or removing a methyl group on a histone lysine residue (63)

There are 4 classes of HDAC. These are classes I (HDACs 1, 2, 3 and 8), II (HDACs 4, 5, 6, 7, 9 and 10) and IV (HDAC 11). Class III (SIRT1,2,3,4,5,6 and 7) are sirtuins which are nicotinamide adenine dinucleotide (NAD+) dependent as opposed to zinc dependent enzymes. HDAC11 is the only class IV HDAC, and it is present in smooth muscle, however, is known to be a weak deacetylator. HDAC11 is over 10,000 times more efficient in its defatty-acylase activity than its deacetylase activity. HDACs have been shown to be key regulators of various cell functions. These functions include cell cycle, motility, cell differentiation, proliferation and immunity (63,64) **Figure 1.7** represents the roles that have been identified for HDACs in cancer biology.

Histone deacetylase 6 (HDAC6), a member of the class IIb histone deacetylases and is a microtubule associated deacetylase primarily located in the cytoplasm (64). HDAC6 is key to maintaining homeostasis and removes the acetyl group from b9 lysine residues located on α-tubulin. HDAC6 is involved in multiple cellular processes such as cell motility, signalling and vehicle transport. It has been shown that excessive or insufficient acetylation of α-tubulin can alter microtubule stability and organisation, leading to CVD (65,66). HDAC6 has been posited as a potential therapeutic target in cancer and heart disease. Acetylation of tubulin results in stabilised microtubules. Therefore, the destabilisation of microtubules through deacetylation can be prevented inhibiting the activity of HDAC6, thus preventing the removal of the acetyl

group. Class IIa HDAC-inhibitors have been seen to be beneficial in reducing pressure induced cardiac hypertrophy (67,68). In one study using a mouse model of hypertension induced by a high-fat diet, it was observed that valproic acid exhibited a preventative effect on the progression of hypertension. Valproic acid caused the downregulation of angiotensin II and its receptor by inhibiting HDAC1 (69). Symptoms seen in CVD such as inflammation of the vessel wall and cell proliferation were also reduced upon treatment. Histone acetylation is proving to have a significant role in some epigenetic modifications that are linked to ageing (63,70).

Studies have shown that HDAC3 is essential in DNA replication and repair. Additionally, it plays a vital role in maintaining chromatin structure and genome stability (71–73). It has been observed that the lack of HDAC3 in endothelial cells results in cell death and the development of atherosclerosis through the activation of an inflammatory response (73,74). Alongside this, it was observed that in HDAC3 deficient macrophages they upregulated the Nrf2-dependent antioxidant genes possibly to combat the oxidative stress (75).

Another potential therapeutic target is HDAC8 which has also been affiliated with α- tubulin aiding in cell migration like its HDAC6 counterpart. In addition to this it has also been seen to promote tumour growth and cell proliferation and inhibiting apoptosis. HDAC8 also is involved in the immune response like HDAC3 (76) HDAC8 has been notified to have a pathological role in cardiovascular disease (77,78).

SIRT 1, a class III HDAC is known to delay cell senescence and is recognised as a longevity gene (79). SIRT1 exerts cardiovascular protective effects and may protect against VSMC hypertrophy. This has been confirmed in mouse models that overexpress SIRT1. In angiotensin receptor AT-1 knockout mice, it was found that reactive oxygen species (ROS) were lower than control and had a prolonged lifespan
(80). SIRT1 may be able to regulate fat and cholesterol synthesis which may have beneficial effects in combating atherosclerosis (80).

Histone deacetylases have already shown great potential in cancer treatment due to their antineoplastic effects. An increased level of HDAC activity was observed in various tumors further highlighting the benefit of HDAC inhibitors as strategies to treat disease (81). There are currently four possible inhibitors in clinical trials to date, Vorinostat, Romidepsin, Palobinostat

and Belinostat (82).

Aortic constricted mouse models have shown the potential of HDAC inhibitors as treatments for heart disease. In this study, mice with pressure overload-induced hypertrophy were treated with a pan-HDAC inhibitor showed a reduction in hypertrophic response and the progression of heart failure (83,84).

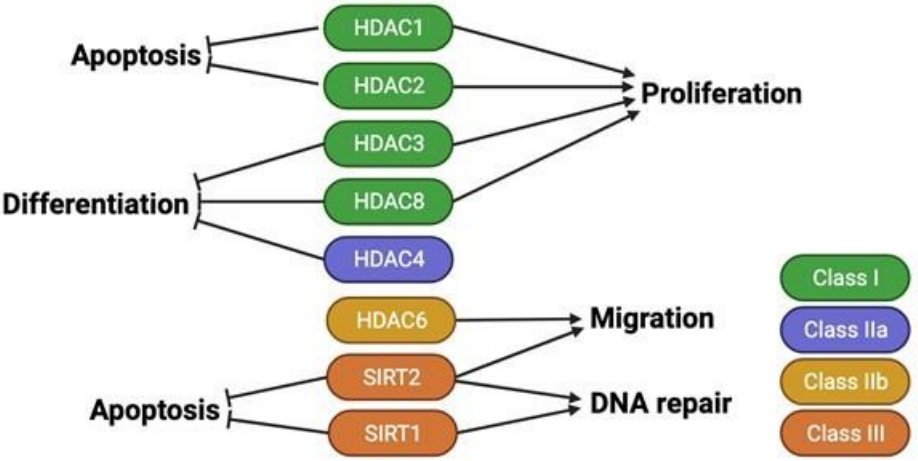

Figure 1.7 *HDAC roles in cancer biology. Class I HDACs promote cell proliferation and initial apoptosis and cell differentiation. Class IIa HDACs inhibit differentiation. Class IIb HDACs promote cell migration. Class III HDACs (sirtuins) promote migration, DNA repair and inhibit apoptosis. Arrows signify inhibition. Adapted from (132).*

1.7 Other epigenetic modifications and Vascular Smooth Muscle Cells

Post translational modifications are also essential epigenetic mechanisms in regulation of cytoskeletal function. These modifications also impact the nucleus and thus the regulation of gene expression. Increased PTM via methylation or acetylation has been implicated in atherosclerosis, where a reduction in tri-methylation of H3K27 in the tunica media correlates with a progression of the disease (85,86).

The reduction of histone methylation has also been implicated in maintaining the proinflammatory phenotype of vascular smooth muscle cells(87). Histone deacetylase 3 has been known to influence VSMC phenotype switching via reduction in F-actin, promoting a synthetic phenotype (35,87,88). Chromatin can exist in an 'open' or 'closed' state when packaged around histones. When in the 'open' state the chromatin is defined as active. This is represented in **Figure 1.8** below. This is because transcription factors can bind to and promote transcription of DNA in the 'open' region. Histone post translational modifications have been shown to play a role in chromatin structure. Histone acetylation is more commonly seen in an 'open' chromatin unit whereas increased methylation is seen in 'closed' chromatin, (89). Our current understanding of how epigenetic mechanisms regulate gene expression in VSMCs is limited. Further research is required to fully elucidate the role these processes pay in VSMCs and CVDs.

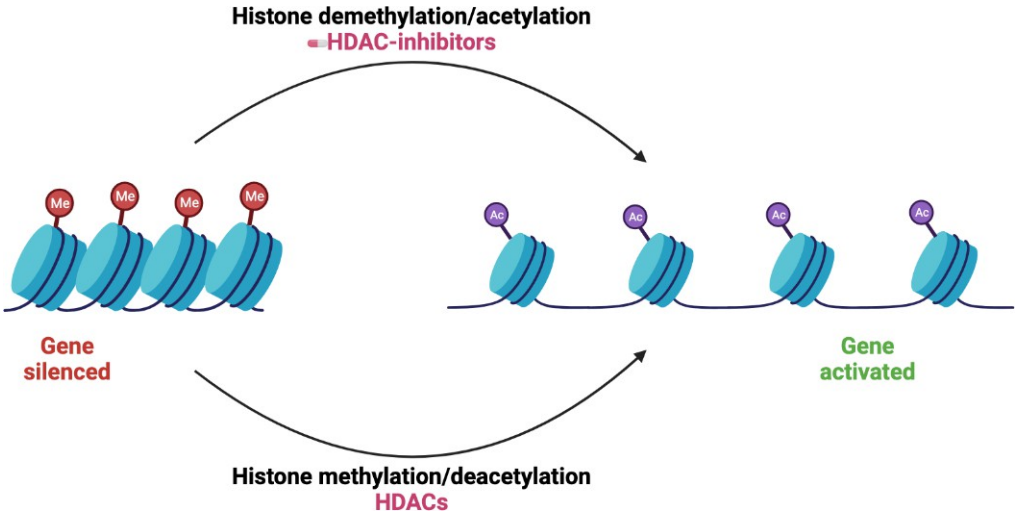

Figure 1.8 *A figure to represent the effect of post-translational modifications from histone demethylation/acetylation and methylation/deacetylation of the histones and how this affects gene activation/silencing. HDAC inhibitors promote the acetylation of the histone, activating the gene. HDACs deacetylate the histone causing gene silencing.*

1.8 VSMC senescence and the DNA damage response

Cell function is progressively lost during ageing as the accumulation of cell senescence markers increases. This leads to a host of age-related disease including cardiovascular disease. The senescence of VSMCs has a great impact on the mechanistic role of the vasculature. Senescent cells can no longer undergo mitotic division and are known to experience phenotypic switching. The increase in cell senescent markers such as γH2AX, which indicates the presence of DNA damage as well as p53 and p16 create a negative cycle of arrested growth and senescence.

Mechanisms of VSMC senescence include telomere shortening, oxidative stress and DNA damage. Oxidative stress is due to the increase in reactive oxygen species (ROS) in the vessel walls in atherosclerosis. ROS alters protein confirmations, protein-protein and protein-DNA interactions resulting in knockdown effects and stimulating the DNA damage response pathway. Other effects of ROS include the peroxidation of lipids creating DNA adducts further contributing to DNA damage. Histone methylation and acetylation has also been implicated in the production of ROS. This epigenetic transformation is impacted by age. In an aged mouse model it has been shown that H3-Ac, H3K9-Ac and H3K4-tri-Me regulate the expression of $p66^{shc}$, $p66^{shc}$ promotes ROS production, resulting in VSMC senescence(90).

VSMC senescence is affected by the RAAS signalling pathway. RAAS is activated by angiotensin II binding to AT1 and AT2 receptors. AT1 and AT2 are G-protein coupled receptors. Angiotensin II binds to AT1 triggering vasoconstriction, pro-inflammation and hypertrophy. Angiotensin II has shown to induce oxidative stress and promotes the proliferative phenotype in VSMCs via the release of growth factors. The adverse modulation of the extracellular matrix is also influenced by angiotensin II and has been shown to prompt various vascular diseases especially atherosclerosis (91).

The DNA damage response pathway is additionally stimulated by telomere shortening which intensifies with age. This occurs through the gradual loss of the telomere cap and leaves the ends of chromosomes exposed. This exposed end triggers the DNA damage response (DDR) inducing replicative senescence. This beneficial in tumour

suppression but comes at the cost of inhibits DNA repair. Studies have shown an increase in DNA damage in aged arterial vessels compared to young healthy ones. As arteries age, they tend to become stiffer, mirroring findings in cancer research that have demonstrated DNA damage accumulation in response to ECM alterations (92).

1.9 Vascular smooth muscle cell hypertrophy and matrix stiffness

VSMCs play a role in the remodelling processes of the vessel wall. This remodelling can be driven by changes in phenotype with the up or downregulation of contractile/proliferative markers. VSMCs respond to external stimuli such as injury, shear stress from blood flow provoking a maladaptive stiffening response (93). Previous work in the Warren Lab has found that when stimulated with a contractile agonist such as Angiotensin II, VSMCs cultured on a rigid surface have a greater cell spread than those on a pliable surface. This suggests that there may be a hypertrophic response to rigid ECM (94). The remodelling of the extracellular matrix via collagen-I deposition and elastin degradation creates a stiffer environment. Vessel non-compliance has been liked to VSMC hypertrophy in aged and hypertensive populations (95).

Studies conducted on glass or plastic cannot accurately measure VSMC behaviour as these substrates are roughly a thousand times stiffer than that of a healthy or even diseased aorta (8,94,96). This is because VSMCs are mechanosensitive and are therefore highly sensitive to the stiffness of their underlying substrate. The stiffness of a substrate can be measured with Young's modulus (96). Vascular smooth muscle cells are mechanosensitive and play an important part in maintaining vascular tone. For example, as extracellular matrix rigidity increases, VSMCs increase actomyosin force generation which, in turn, increases VSMC stiffness. VSMC stiffness has been linked to hypertrophy which is defined as the increase in cell mass without an increase in cell number (97). VSMC hypertrophy in turn leads to an increase in vessel wall thickness as well as rigidity (98).

The underlying mechanisms for VSMC hypertrophy and stiffness has not been well explored. Our efforts are now targeted towards the VSMC response to ECM stiffening to develop strategies to target CVD in ageing.

1.10 Stretch activated channels

Mechanosensitive channels also known as stretch activated ion channels (SACs) allow vascular smooth muscle cells to respond to the mechanical perturbations incurred on vessel walls such as shear stress. Stretch induces a contractile response via an inward current of non-selective cations. The sudden influx of cations causes plasma membrane depolarisation which triggers the opening of cell surface calcium channels allowing for influx of Ca^{2+}, eventually allowing the release of calcium from intracellular stores and inducing vasoconstriction (99).

Additionally, Ca^{2+} influx into SACs activates other Ca^{2+} dependent pathways such as protein kinase C (PKC). PKC is ubiquitous in VSMCs and is known to be a regulator of VSMC contraction. Another way it is known to be activated is angiotensin II, a contractile agonist. Angiotensin II activates phospholipase C producing diacyl glycerol (DAG), this in turn stimulates PKC. In a cyclic manner PKC stimulates more Ca^{2+} entry via non-selective calcium channels. Studies have shown an increase in PKC-α levels in vascular smooth muscle cells with increased actin levels (100). This suggests that shear stress induces the contractile phenotype. Furthermore, the activation of PKC has been seen to increase the sensitivity of Ca2+ within the cell. Calcium levels in VSMC are tightly regulated due to the necessity of myogenic tone to ensure the appropriate fast response to intraluminal pressure (101).

Piezo1 is an example of a stretch activated channel (SAC) that responds to the elevation of blood flow and pressure. Piezo-1 is a non-selective cation channel that allows the inward current of cations when membrane stretch is detected. The activation of Piezo1 leads to a rise in cytosolic Ca2+ levels, promoting the activity of transglutaminase II (TGII), an enzyme crucial for cytoskeleton and extracellular matrix (ECM) remodeling. Upon membrane tension, Piezo1 adopts a flattened configuration attempting to accommodate the extra blood flow, this can be seen in **Figure 1.9** (102). The specific changes in structure of Piezo-1 when activated remain unknown, as well as how it detects changes to stretch in the membrane (103). Piezo-1 is known to be upregulated in atherosclerosis, hypertension and abdominal aortic

aneurysm-mediated VSMC dysfunction (102).

Yoda1 is a Piezo1 agonist that can increase the sensitivity of Piezo1 so that it can activate without the need of an external mechanical force (104). On the other hand, GSMTx4 is known as a gating modifier that blocks some SACs such as Piezo1. It is a toxin that is extracted from the venom of Grammostola spatulate (Chilean Rose Tarantula). It relaxes cell membrane tension close to the channel resulting in their inhibition (102). For this reason, the use of a SAC blocker like GSMTx4, could be a therapeutic agent in reducing VSMC hypertrophy.

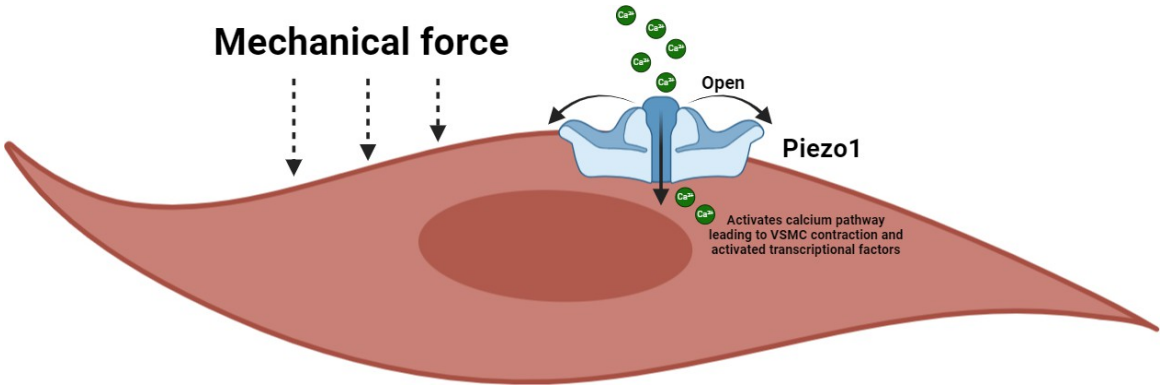

Figure 1.9 *Piezo1 adopts the flattened, open configuration when mechanical force is detected This leads to the influx of calcium ions which can promote VSMC contraction and activation of transcriptional factors.*

1.11 Aquaporin-1 mediated water influx into VSMC

Aquaporin-1 is expressed in vascular smooth muscle cells (105). The arterial wall is described as poro-elastic as it possesses both porous and elastic characteristics. This ability allows for stretch when subjugated to external forces such changes in blood pressure (106). When pressure increases the vessel wall can expand and the opposite when pressure decreases, however, the wall can still allow for the exchange of fluids or nutrients from the blood to surrounding tissue. Aquaporins enhance this ability through the transfer of water into the cell. This may have a significant impact on cell contraction due to the increase in cell volume creating tension and an increase in cell stiffness. The impact of VSMC stiffness may impact contractility leading to disease. Therefore, aquaporin-1 may play a fundamental role in VSMC function in disease. It has been observed that disrupting Aquaporin-1 can decelerate the movement of water in human vascular endothelial cells and has led to a reduction in the thickness of the left ventricular wall

in mice (107–109). Stiffened atherosclerotic arteries exhibit an increased expression of Aquaporin-1 and has shown to contribute to further stiffening (110).

The expression Aquaporin-1 has been associated with hypertension and atherosclerosis, with significantly elevated expression observed in hypertensive rats compared to their normotensive counterparts (111). Some studies have shown that aquaporin-1 is ubiquitous in healthy endothelial cells however when knocked out can lead to Angiotensin II driven atherosclerosis (112,113).

1.12 Current in vitro limitations

VSMCs switch to a synthetic phenotype when passaged in vitro, which is associated with the diseased state (114). Typically, cells are seeded onto glass and plastic with a tensile strength of 10,000 kPa, which is around a thousand times stiffer than a healthy artery. This high elastic modulus may induce VSMCs into the synthetic phenotype. Healthy arterial stiffness is in range of 10 - 20 kPa whereas that of a diseased artery is 60 - 200 kPa (115). This is represented in **Figure 1.10**.

It has been shown that matrices above 135 kPa affect the VSMC force generation. Polyacrylamide hydrogels (PAHs) aid the investigation of matrix rigidity on VSMC response as they allow the biomimicking of healthy and diseased aortae. Studies using PAHs have shown that matrix rigidity is a key regulator of VSMC morphology. VSMCs seeded onto a stiffer matrix presented a greater cell area and volume when treated to contractile agonist, Angiotensin II (94). This finding supports work showing that VSMC sourced from older monkeys have a greater cell volume compared to VSMC from younger monkeys (49). This phenomenon may be caused by the increase in adhesion sites observed when cells are surrounded by a stiffer substrate, causing cells to spread out with larger adhesions (116).

To understand the role the ECM plays on VSMC biomechanics, importance must be given to how cells are grown in vitro. Experimental systems such as 2D or 3D PAHs allow for tailored stiffness gradients and are necessary to understand VSMC mechanics related to ECM composition in ageing and disease (117). In certain environments, phenotype can also be controlled via seeding with growth (proliferative) or basal (quiescent) media. It is clear that

matrix stiffness has an important role in the pathology of cardiovascular disease, however its effect on VSMC biology remains elusive. As VSMCs are the predominant cell in the aorta, it is important to understand the morphological changes that occur in response to increased matrix (5,8). Microtubules provide a novel pathway to explore in understanding VSMC contraction, however the mechanism is still not understood and requires additional work. Furthermore, adaptations at the epigenetic level via post-translational modifications have been linked to vascular diseases, with the unravelling of these mechanisms fundamental to providing potential novel therapeutic avenues.

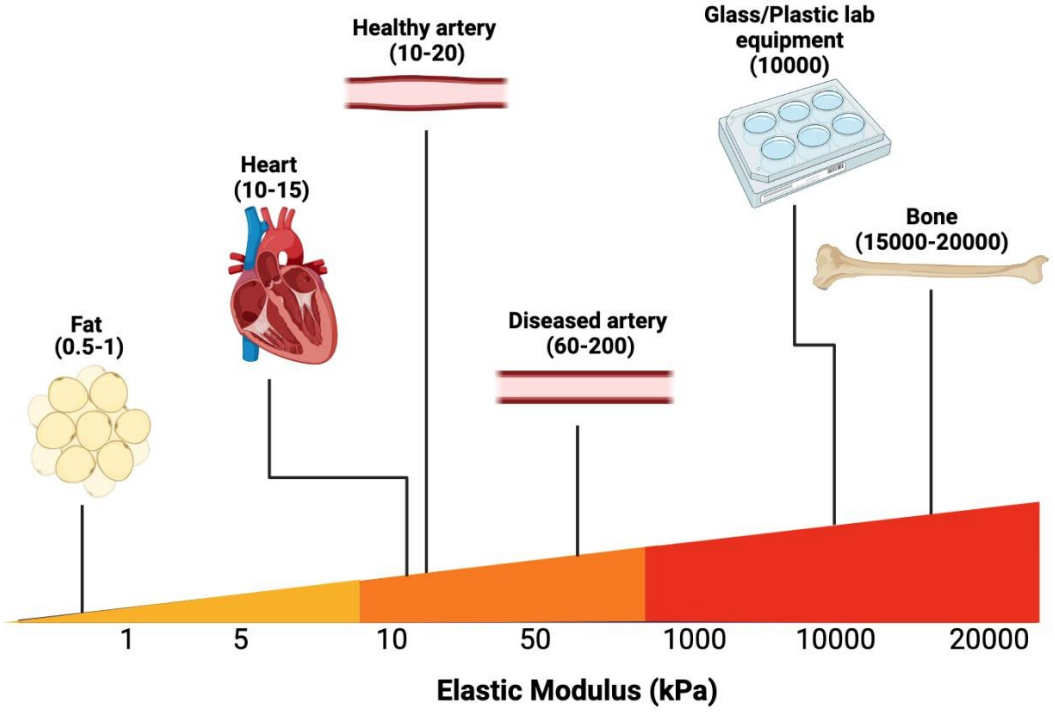

Figure 1.10 *The varying elastic modulus of human tissue in comparison to glass and plastic lab equipment used to seed cells. (Adaptation from Handorf et al, 2015).*

1.13 Hypothesis and project aims

The decrease in vascular compliance is the key aetiology of many cardiovascular diseases. Ageing contributes to extracellular matrix stiffening further reducing compliance, with VSMCs being a major regulator of compliance. Increased vascular stiffening promotes VSMCs to generate enhanced contractile forces which contribute to VSMC stiffening causing further stiffening of the vessel. Previous studies on VSMC function have been conducted on plastic or glass that do not accurately represent the properties of the aortic wall. Our use of polyacrylamide hydrogels (PAHs) allows us to biomimic healthy and diseased vessels. Previous work has shown that cells seeded on 12kPa PAHs treated with a contractile agonist (angiotensin II) were smaller than those on a stiffer 72kPa PAH. Specific mechanisms driving this VSMC response to matrix rigidity remain elusive.

We propose that HDACs are regulating the cellular mechanisms that are contributing to this hypertrophic like effect of VSMCs on stiffer matrices. We hypothesise that altered VSMC mechanotransduction in response to matrix stiffness is regulated by:

- Tubulin acetylation
- HDACs are regulators of VSMC volume regulation.

  We also hypothesise other pharmacological pathways contribute to VSMC volume regulation such as:

- Stretch activated channel: Piezo1 and subsequent Ca^{2+} influx
- Activation of PKC and aquaporin-1.

  The specific objectives within this project were:

1. To understand the role of various HDACs on VSMC and nuclear area.

2. To investigate and validate the pharmacological benefits, if any, of HDAC inhibitors on VSMC dysfunction and volume response caused by matrix stiffening.

3. To identify regulatory pathways of VSMC volume regulation to matrix rigidity by investigating Piezo1 and subsequent downstream regulators of cell volume aquaporin-1 and protein kinase C (PKC).

4. To evaluate pharmacological interventions of the Piezo1/PKC/Aquaporin-1 pathway and whether this can be used to block enhanced VSMC volume on rigid matrices without impairing VSMC contractility on pliable matrices.

Chapter 2: Material and Methods

2.1 Antibodies

Antibody	Product code/Cat. No.	Host	Company	Application	Dilution
53BP1	4937S	Rabbit	Cell signalling Technology	IF	1:100 3% BSA in PBS
Acetyl α-Tubulin	5335s	Rabbit	Cell Signalling Technology	WB	1:500 5% BSA in TBST
Alexa Fluor 488 anti-mouse	A32723	Goat	Invitrogen	ICC/IF	1:400 3% BSA in PBS
Alexa Fluor 488 anti-goat	A32814	Donkey	Invitrogen	ICC/IF	1:400 3% BSA in PBS
Alexa Fluor 568 anti-rabbit	A143157	Goat	Invitrogen	ICC/IF	1:400 3% BSA in PBS
Anti-aquaporin1		Rabbit	Merck	ICC/IF	1:400 3% BSA in PBS
Anti-Histone H3 (acetyl k9)	ab4441	Rabbit	Abcam	WB/IF	1:1000 5% BSA in TBST
Anti- Histone H3 (acetyl k9)	ab10812	Rabbit	Abcam	WB/IF	1:1000 3%BSA in PBS
Anti- Histone H3 (tri methyl K9)	ab8898	Rabbit	Abcam	WB/IF	1:1000 WB- 5% BSA in TBST IF- 3% BSA in PBS
Anti- Lamin A/C	SAB4200236	Mouse	Sigma	ICC/IF	1:100 3% BSA in PBS
Anti- Piezo1	NBP1-78537	Rabbit	Novus	WB	1: 500 5% BSA

					in TBST
GAPDH	2118s	Rabbit	Cell Signalling Technologies	WB	1:6000 5% BSA in TBST
Mouse Horseradish peroxidase linked whole Ab	NA931	Sheep	Amersham	WB	1:4000 In 5% Milk in TBST
p- Histone H2A.X	5438S	Rabbit	Cell signalling Technology	IF	1:100 in 3% BSA in PBS
Rabbit IgG Horseradish peroxidase linked whole Ab	NA934V	Donkey	Amersham	WB	1:4000 In 5% Milk in TBST
Rhodamine Phalloidin	R415		Invitrogen	ICC/IF	1:400 3% BSA in PBS
α- Tubulin	3873s	Mouse	Cell Signalling Technology	WB	1:500 5% BSA in TBST/Milk

2.2 Lab consumables

Lab consumable	Product number	Source
(3-Aminopropyl)triethoxysilane (APES)	A3678	Sigma
13mm Coverglass	631-0149	VWR
30mm Coverglass	631-0174	VWR
6 well plates	130184	Thermo Scientific
24 well plates	1450-603	Perkin-elmer
Acrylamide 30%	A3574	Sigma
Acrylamide 40%	A7802	Sigma
AllStars Negative Control siRNA	1027280	Qiagen
Bis-acrylamide 2%w/v	BP1404250	Fisher Scientific
Bovine Serum Albumin (BSA)	A2153	Sigma
Collagen-1	A1048301	Gibco
Dimethyl sulfoxide (DMSO)	D8418	Sigma
Earle's Balanced Salt Solution	E6267	Sigma
Filter paper	88600	Thermoscientific
GeneSolution siRNA HDAC6	1027416	Qiagen
Glutaraldehyde solution	G6257	Sigma
HiPerFect Transfection Reagent	301704	Qiagen
Immuno-Blot PVDF 0.2 µm, 26 cm x 3.3 m	1620177	BIO-RAD
Methanol	M/4000/17	Fisher Scientific
Nonidet P-40 (NP40) 10% w/v aqueous solution	85124	Thermo Scientific
Parafilm	P7793	Sigma
Paraformaldehyde (PFA)	P6148	Sigma

Phosphate Buffered Saline (PBS)	D8537	Sigma
Smooth muscle cell basal media	132-500	Sigma
Smooth muscle cell growth media	311-500	Sigma
Smooth muscle cell growth supplement	311-GS	Sigma
Sulfo-SANPAH	Ab145610	Abcam
Tetramethylethylenediamine (TEMED)	17917	Thermo Scientific
Thermo Scientific Biolite Cell Culture Treated Flasks T25	11884235	Fisher Scientific
Thermo Scientific Biolite Cell Culture Treated Flasks T75	11884235	Fisher Scientific
Triton x-100	X100	Sigma
Tru-page transfer buffer 20X	PCG3011	Sigma
Trypsin-EDTA solution	T3924	Sigma
Vectashield mounting media	H-1400	Vector
Vectashield mounting media with DAPI	H-1500	Vector

2.3 Compounds

Compounds	**Product name**	**Source**	**Vehicle**	**Concentration range**	**Working concentration**
Angiotensin II	Sigma A9525	Sigma	dH_2O	0.01 100 µM	10 µM
AK-7 (SIRT2i)	Sigma 566331	Sigma	DMSO	0.01 - 100 µM	-
BRD9757 (HDAC6i)	Tocris 6040	Tocris	dH2O	0.001 - 1000 nM	-

EX-527 (SIRT1i)	Sigma E7034	Sigma	DMSO	0.001 - 100 nM	-
Go6983 (PKCi)	2285	Tocris	DMSO	0.01 - 100 nM	100 nM
GSMTx-4	Ab141871	Abcam	dH_2O	0.5 - 5000 nM	500 nM
MS275 (HDAC1i)	Tocris 6208	Tocris	DMSO	0.01 -1000 nM	-
PCI34051 (HDAC8i)	Tocris 4643	Tocris	DMSO	0.01 - 10 µM	-
RGFP- 966 (HDAC3i)	Tocris 6278	Tocris	DMSO	0.01 100 µM	10 µM
Santacruzamate A (HDAC2i)	Tocris 7191	Tocris	DMSO	0.001 - 100 nm	-
TC AQP1 1 (AQP1i)	Tocris 5412	Tocris	DMSO	0.01 100 nM	100 nM
Tubastatin (HDAC6i)	Sigma 382187	Sigma		0.01 - 100 µM	1 µM
Yoda1	5568	Tocris	DMSO	-	1 µM

2.4 Cell culture

Human aortic smooth muscle cells (Sigma 354-05A) were used in this study. These cells came from a pooled sample of three patients between 25-60 years old, with no underlying health conditions. Cells were grown in a T75 flask (Thermo Scientific 130190) at 37°C with 5% CO_2 in smooth muscle cell growth medium (Sigma 311-500) with smooth muscle cell growth supplement (Merck 311-GS). Cells were passaged upon reaching 70-80% confluency. Spent growth medium was aspirated and cells were washed with 10 mL Earle's Balanced Salts (EBS) solution (Sigma E6267). EBS was aspirated and cells were detached with 12.5% Trypsin-EDTA solution (Sigma T3924) for 3-5 minutes at 37°C. A further 10.5 mL of fresh growth media enhanced with supplement were added. Cells were seeded into two T75 flasks at a 1:2 split. Both flasks were brought up to a total volume of 12 mL each with additional growth media containing supplement.

2.5 Polyacrylamide hydrogel fabrication

Approximately 200 µL of (3-Aminopropyl)triethoxysilane (Sigma A3648) was added to a sheet of Parafilm, ensuring the saturation of one side of a 30 mm coverslip (VWR 631-0174). Coverslips were incubated at room temperature (RT) for 2 minutes before being transferred into 6-well plates (Thermo Fisher 130184/Starlab CC7682-7506) with saturated side facing up. Coverslips were washed with ddH_2O three times before being immersed in 2 mL of 1:50 glutaraldehyde in ddH_2O for 40 minutes. Glutaraldehyde solution (Sigma G6257) was removed from all wells and coverslips were washed a further three times with ddH_2O. Coverslips were then removed from the 6-well plates and placed activated side up to dry, preferably overnight, however, a minimum of 30 minutes.

2.6 Preparing the polyacrylamide hydrogel

PAHs used in this study were of stiffness 12 kPa and 72 kPa. Solution was prepared to allow for 50 µL per coverslip. A ratio of 1:100 dilution 10% APS (Sigma A3678) and 1:1000 TEMED (Thermo scientific #17919) was added to the appropriate strengths of polyacrylamide solution.

Ensuring the solution was thoroughly amalgamated, 50 µL was added per glass slide (Fisherbrand 1237-3118). Dried, activated coverslips were added face down onto a drop of the solution and allowed to adhere for 3-8 minutes. Coverslips were carefully peeled off the glass slide, resulting in a fully adhered hydrogel layer onto its activated side. Hydrogel coverslips were washed three times to ensure excess solution was removed, remaining in third wash to remain hydrated. Prepared hydrogel coverslips were kept at 4°C for a maximum two weeks.

2.7 Cell seeding

Hydrogel coverslips were crosslinked with 1:3000 sulfo-SANPAH with ddH2O at 2 mL per well. The 6-well plate was placed in a Benchtop UV Transilluminator for 5 minutes and then a further 30 minutes with the lid off. Lids were replaced onto the plate and

transferred to an aseptic tissue culture hood. Sulfo-SANPAH solution (Abcam ab145610) was removed from the PAHs and washed with phosphate buffered saline (PBS) (OXOID BR00149). PBS was replaced with a 1:30 dilution of Collagen type 1 (Thermo Fisher A1048301) in PBS at a total of 2 mL per well. This was incubated at RT for 10 minutes. Wells were once again washed with PBS. Cells were seeded with a 1:2 split for Western blot, 1:4 for immunofluorescence assays, with the flask intended for seeding brought up to 24 mL with growth or basal media allowing for a total of 12 wells to be seeded. Cells were incubated for a minimum 24 hours at 37°C, 5% CO_2.

2.8 Western Blot

Cells were seeded as mentioned in *section 2.7* with growth media. Cells were left for a period of 2 days. If basal medium was necessary, this was changed after the first day.

2.9 Generating protein lysates

To produce protein lysates, media was removed from wells and washed with PBS. Cells were lysed with 50 µL of 4X Lamelli's buffer for 5 minutes. As cells cannot be scraped off PAHs as in a standard Western blot protocol, 6-well plates were stood on an angle after the 5-minute incubation to allow protein sample to pool, increasing sample volume. Protein lysates were stored at -20°C.

2.10 Performing the western blot

Protein lysates were heated at 94°C for 5 minutes followed by centrifugation. Lysate samples (20µL) were separated with SDS-Page on a 4-20% Polyacrylamide gel (Merck PCG2004-10EA). The separated proteins were transferred onto polyvinylidene difluoride (PVDF) membrane (BioRad 1620177). Membranes were blocked with 5% non-fat milk powder (Melford M17200-500) in TBST (Sigma T9039-10PAK) for 1 hour. Membranes were subsequently incubated with primary antibodies at 4°C overnight. Antibody dilutions can be found in the table above. Membranes were washed with TBST and incubated with the appropriate secondary antibodies horseradish peroxidase-conjugated diluted 1:4000 in 5% milk-TBST at RT for 2 hours. Membranes

were vigorously washed with TBST for a period of 30 minutes and treated with a 1:1 Amersham ECL Prime Western Blotting Detection Reagent. Chemiluminescent membranes were imaged with BioRad ChemiDoc XRS+ imaging system.

Western blots were analysed via densitometry using ImageJ. GAPDH was used as loading control, with all detected bands normalized to the control.

2.11 Growth vs Basal medium assay

Lysates were produced from cells seeded on 12 or 72 kPa PAHs, all cells were seeded with growth medium for 24h with a 1:2 split. Following 24h, cells to be treated with basal media (Sigma 310-500) had media replaced and incubated for a further 24h at 37°C. Lysates were produced with western blot protocol in section. Western blots were probed for primary antibodies, Anti histone H3 acetyl k9, Anti histone H3 tri-methyl K9, Ac-α tubulin, α-tubulin and GAPDH.

2.12 HDAC6-Inhibitor dose contractile assay

A serial dilution for Tubastatin doses 100µM, 10µM, 1 µM, $1x10^{-1}$µM, $1x10^{-2}$, $1x10^{-3}$ µM, $1x10^{-4}$ µM and $1x10^{-5}$µM were prepared. Cells were seeded straight onto the 6- well plates with growth media for the first 24h with a 1:2 split. Following this, media was replaced with basal media (Merck 310-500) for another 24h. Appropriate doses of Tubastatin were added to each well for 1h at 37°C. This was followed by the western blot protocol. All HDAC6-Inhibitor treated lysates were treated with primary antibodies, Ac-α tubulin, α-tubulin and GAPDH.

2.13 Membrane stripping

To probe for a different protein, membranes were stripped by applying a mild stripping buffer for 5 -10 mins for a total of two times. Buffer comprised of the following: 15 g glycine, 1 g SDS, 10 mL Tween 20, prepared in dH_2O (brought to 1 L), pH 2.2. Buffer is 0.2M. Membranes underwent a 2 x 10 mins PBS wash followed by a 2 x 10 mins TBST wash. Membranes were then ready for blocking in 5% milk in TBST for 1 hour.

2.14 Growth vs Basal medium assay

Cells were split in a 1:4 ratio as stated in the section 3.5. Cells were either split with basal or growth media and left to adhere for 24hrs. After 24hrs cells were fixed and stained for imaging.

2.15 siRNA Knockdown

2.15.1 *HDAC6*

SiRNA transfection on VSMC was performed with HiPerFect (Qiagen) as per manufacturer's instructions. The HDAC6 siRNA was used at 20 µM, thus 50 µL of basal was media was added. 2 µL of oligonucleotide was combined and vortexed with an additional 430 µL of basal media, then 28 µL of HiPerfect was added. The solution was left to incubate for 10 minutes before being resuspended. This oligonucleotide solution was added dropwise to the cells growing in a T25 flask with 4 mL of growth media. Cells were treated within flask at least 24 hours prior to cell seeding onto PAHs. Once cells were settled onto PAHs, the growth media was replaced with basal media to induce quiescence for approximately 18 hours. On day 3, VSMCs were stimulated with contractile agonist, Angiotensin II (10 µM) for 30 minutes. VSMCs were fixed and prepared for immunocytochemical analysis.

siRNA #5	CACCGTCAACGTGGCATGGAA
siRNA #10	CCGGAGGGTCCTTATCGTAGA

2.15.2 *Piezo1*

SiRNA transfection on VSMC was performed with HiPerFect (Qiagen) as per manufacturer's instructions. The above method remains the same for Piezo1 siRNA.

siRNA #5	CCGCGTCTTCCTTAGCCATTA
siRNA#7	CGGCCGCCTCGTGGTCTACAA

2.16 Immunocytochemistry

2.16.1 *VSMC Area and Volume*

In preparation for confocal imaging, media was aspirated from treated cells and washed with PBS. PBS was removed from wells and replaced with 4% PFA for 10 minutes at RT for fixing. Wells were subsequently washed with PBS. Following the fixing protocol, wells were incubated overnight with primary antibody solution anti-lamin A/C (Sigma) 1:400 in 3% BSA in PBS at 4°C in a humidity chamber protected from light. After 24 hours cells were incubated with secondary antibody solution, Alexa Fluor® 488 1:400 and rhodamine phalloidin 1:400 in 3% BSA in PBS for 2 hours at RT in a humidity chamber, ensuring protection from light. Antibody solution is washed from Polyacrylamide hydrogels (PAHs) 3x with PBS, store in PBS for imaging at 4°C. Prior to imaging, PAH coverslips were mounted onto a clean glass slide with 30 µL with hard set mounting media no DAPI (Vectashield H1-400 ZG1201).

For the localisation assay the primary antibody was anti- aquaporin-1 antibody. Secondary staining was performed with alexa-fluor 568 (red). Mounted with hard set mounting media DAPI vectashield media (Vectashield H-1500).

2.16.2 *VSMC DNA Damage*

VSMCs were fixed and washed as aforementioned. VSMC nuclei were incubated overnight with primary antibody solution γH2AX (Cell signalling Technology 5438S) or 53BP1 (Cell signalling Technology 4937S) as appropriate diluted as 1:100 in 3% BSA in PBS at 4°C in a humidity chamber protected from light. After 24 hours cells were incubated with secondary antibody solution, Alexa Fluor® 568 1:400. The following process was the same as mentioned above. PAH coverslips were mounted with Vectashield Antifade mounting medium with DAPI (Vectashield H-1200-10) for imaging.

2.16.3 *Cold-stable microtubule stability assay*

After treatment, cells were placed on ice for 15 minutes then washed once with PBS and twice with PEM buffer (80 µM PIPES pH 6.8, 1 mM EGTA, 1 mM MgCl2, 0.5% Triton X-100 and 25% (w/v) glycerol) for a duration of 3 minutes.2.08mM? Cells were then fixed for 20 minutes with ice-cold MeOH and prepared for staining as detailed above using anti a-tubulin as primary and Alexa Fluor 528 as the secondary antibody. Cell nuclei were identified using DAPI. Images were captured at 40x magnification using an Axioplan Epifluorescent microscope.

2.17 Microscopy and Image Analysis

All slides for volume data were viewed with Zeiss LSM510-META or Zeiss LSM980- Airyscan confocal with a x20 objective.
Additionally, x10 objective was used for cell and nuclear volume data whereas x40 was used for microtubule analysis.

It was aimed that a total of 5 images were taken of each slide, one per quadrant and one in middle of sample slide with 3 cells per image.

2.17.1 Image analysis

Method for Zeiss LSM510-META images: Cells were analysed for area with programme ImageJ. To set the scale, select “analyse” then “distance in pixel” to 1 with a “known distance” of 0.323, this allowed for 3.096 pixels/µm, the appropriate scale for a x20 objective with eyepiece lense of x10.

Method for Zeiss LSM908-Airyscan images: Cells were analysed for area with programme ImageJ. Scale was not set as the confocal automatically assigns this.

2.17.2 *Measuring Total Cell area*

The images were split by colour channel to process cell actin area and nuclei area separately. As images were taken with a “Z Stack”, images were stacked for max intensity to ensure full image visibility. Consequently, the “freehand tool” was used to accurately draw around the cell membrane. To store the measurement, select “analyse” then “measure”.

2.17.3 *Measuring Nuclear Area*

The green channel represented the nuclei in staining. The image was separated, and Z-stacked. The image was processed into an 8-bit file, inverted and threshold was set to ensure a solid contrast outline of nuclei. The same process was used to draw around the nuclei as the total cell area.

2.17.4 *Measuring Total Cell Volume*

Cell volume was measured with Volocity 3D image analysis. From "measurements" select "restore protocol", select "Sultan ROI" a to allow volume measurement of total cell volume. Cells were carefully drawn around with the "freehand ROI tool".

This protocol was adapted when the University of East Anglia ended Volocity 3D licensing.

2.17.5 *Updated Volume Analysis Protocol*

Cell area and volume was measured using FIJI, open-source software. Channels were separated with the split channel function. The F-actin (phalloidin stain) image was thresholded on the brightest slice using the Otsu method, this removes gaps. The cell edge was carefully drawn around using the region of interest (ROI) function. Cell area was measured on the image channel for the nuclei and recorded by selecting the ROI on the image. If measuring nuclei an ROI was drawn around the nucleus on the alexa- fluor 488 (green) nuclei channel. In the set measurements menu, 'area' and 'limited to threshold' options were selected before the total volume of thresholded objects was calculated by running the ImageJ macro code (freely available from Visikol at https://visikol.com/blog/2018/11/29/blog-post-loading-and-measurement-of-volumes- in-3d-confocal-image-stacks-with-imagej/).

2.17.6 *Measuring Nuclear Volume*

Cell volume was initially measured with Volocity 3D image analysis. From "measurements", "restore protocol" was selected, then "Sultan volume" to allow volume measurement of nuclei volume. All nuclei should be selected automatically with this protocol.

This protocol was updated due to the expiration of Volocity 3D licensing. Volume was measured in FIJI (FIJI is just ImageJ), see above for updated volume analysis protocol.

2.17.7 *Measuring DNA Damage γH2AX Foci*

The images were split by colour channel to process immunofluorescent identified foci and nuclei area separately. Foci image was turned into an 8-bit file and inverted. This foci image was then thresholded using the 72 kPa Angiotensin II only image as a baseline for DNA damage as this was how gain was determined during imaging. The DAPI stained nuclei image was overlayed allowing us to use the ROI tool to mark the outline of the nuclei. This was then processed using the "analyse particles" function.

2.17.8 *Measuring DNA Damage 53BP1+ Cells*

The initial protocol involved a similar method to thresholding the foci identified image to gH2AX, however, this method introduced bias when counting 53BP1+ cells. Other problems with this method of analysis were noisy background in images prevented actual foci from being displayed, as well as false positives when little to no 53BP1 stain due to the increase in noise when thresholding.

The updated protocol utilises the "renyientropy" function which is a method of autothresholding to allow for only the brightest of foci to be displayed. This removed any leniency with foci counting when DNA damage was to be expected.

2.17.9 *Measuring Cold-stable Microtubules*

The image was split by colour channels, the image with stained microtubules was turned into an 8-bit image, inverted and thresholded until microtubules (MTs) are easily identifiable. The DAPI stained nuclei image is overlayed onto this image to ensure only those with a present nucleus are counted. MTs are counted manually with each crossover counted as another MT.

2.18 Data Analysis

Statistical analysis was conducted in GraphPad Prism 9.5. Results are presented as a combination of all data points or a mean ± SEM, these can be represented by small dots and are specified in figure legends. The number of repeated independent experiments and cells analysed are also listed within the figure legend. The Shapiro- Wilk normality test was used on data sets with all displaying a normal distribution. To compare concentration responses at either 12 kPa or 72 kPa stiffness, an unpaired student's t-test was performed. Concentration-response curves are presented as mean ± SEM plotted on a logarithmic scale. Log (agonist) vs response curves were generated using non-linear regression. To determine statistical significance between more than two groups, one-way ANOVA was performed followed by Tukey's multiple comparison test. Statistical significance is represented by: *=P<0.05, **=P<0.01,

***=P<0.001 and ****=P<0.0001. No statistical significance is represented by "ns". Post-hoc tests were run only if F achieved $P \leq 0.05$ and there was no significant variance inhomogeneity.

Chapter 3: Deciphering the role of histone deacetylases in smooth muscle cell response to matrix rigidity

3.1 Introduction

Vascular stiffness is a major risk factor in the development of cardiovascular disease. Stiffness can be impacted by VSMC morphology and maladaptive changes to the ECM around it. *Sehgel et al.* found that the aortic stiffness of rodent models exhibiting hypertension was increased 4-fold compared to control mice (49). However, the mechanism of this is not fully understood. This stiffening was attributed to ECM remodeling and demonstrates the feedback between pathophysiology and vessel composition.

Differentiated VSMCs retain their phenotypic plasticity and possess the ability to de-differentiate into a highly proliferative and migratory 'synthetic' phenotype in disease (30,118,119) This phenotype has also been associated with that of old age and the downregulation of contractile proteins (119,120). This results in ECM remodeling and reduce vascular compliance (121). Moreover, ECM changes can introduce a shift in VSMC phenotype, resulting in a negative feedback loop of increased vascular stiffness (122,123). We therefore wanted to model physiological and pathological stiffnesses in our VSMC assays.

Previous work by *Warren* Lab has investigated VSMC morphology and structure in response to matrix stiffness. To achieve this the Warren Lab established a method of using polyacrylamide hydrogels (PAHs) that can bio-mimic the tensile strength of healthy and diseased vessels (94). The physiological stiffness of blood vessels is approximately 10-20 kPa therefore we fabricate a 12 kPa hydrogel. Additionally, we mimic the pathological/aged stiffness (60 - 200 kPa) of the vessel wall using a 72 kPa hydrogel.

Previous work using this assay has shown cells seeded on 12 kPa PAHs treated with the contractile agonist angiotensin II (angII) were smaller than those seeded on 72 kPa PAHs. It was found that VSMCs seeded on a pliable PAH functioned as normal with the ability to contract when stimulated by angiotensin II. VSMCs seeded on 72 kPa PAHs lost their contractile function resulting in VSMC swelling. This suggests that contractile stimulation of VSMCs on rigid environments promotes cytoplasmic and

nuclear spreading compared to those seeded on 12 kPa PAH. The exact mechanism of action for this VSMC response to matrix rigidity remains elusive. However, it is known that the increase in matrix rigidity caused the remodelling of the actin cytoskeleton and the promotion of stress fibre formation which led to an increase in VSMC stiffness (124,125). It has also been observed that VSMCs enhance actomyosin forces when subjected to a rigid matrix leading to increased compression and a decrease in arterial compliance (126). Previous work from the Warren lab have shown that microtubules are essential in being load bearing components that can resist deformational stress from increased actomyosin activity (127). This deformational stress can promote the opening of stretch activated channels leading to VSMC dysfunction (128). This relationship between microtubules and actomyosin is known as the tensegrity model. Due to their dynamic instability the acetylation and deacetylation of microtubules is known to alter MT stability. It is proposed that K40 acetylation promotes the stabilisation of MTs. This refers to the acetylation of the lysine 40 on the a-tubulin subunit. This post-translational modification is thought to make the MT more resistant to mechanical stress and thereby depolymerisation. Little is known of the implications of K40 acetylation in VSMCs, however, previous studies have shown that the increase of MT stability decreases VSMC actomyosin activity and vice versa (128–131)

We utilized our PAHs to screen various pharmacological compounds in VSMCs to generate a matrix-dependent response. This allowed us to dissect VSMC signalling pathways in both health and disease. HDACs are known to be regulators of various cellular processes. For example, proliferation, differentiation, cell cycle and motility. Certain HDACs, such as HDAC6, are microtubule specific, and HDAC6 inhibition leads to the acetylation of microtubules. We were especially interested in understanding the effect of MT acetylation on VSMC matrix rigidity response. Some studies have suggested that targeted inhibition of HDACs may be beneficial in the treatment of some cardiovascular diseases. As detailed in the introduction four HDAC inhibitors have entered clinical trials as anti-cancer drugs. Specifically, these are Vorinostat, Romidepsin, Panobinostat and Belinostat. These HDAC inhibitors are being used as novel treatments for hematological cancers (132). However, the effect of these novel compounds has not been fully elucidated in cardiovascular disease and some may have a contradictory impact on disease.

3.2 Hypothesis

We hypothesise that HDAC inhibitors will influence the VSMC response to matrix stiffness. This concentration response assay will reveal more information on both healthy and diseased VSMC morphology. My assumption is that HDAC inhibitors will have varying responses at different concentrations on VSMCs seeded on both 12 kPa and 72 kPa PAH. These results will allow us to determine if targeted inhibition of specific HDACs have, if any, therapeutic effect on VSMCs. I will be able to determine the therapeutic dose as well as compare if any HDAC inhibitors have a greater beneficial effect. Equally, I will be able to rule out HDAC inhibitors that also impact healthy VSMCs (those cultured on 12 kPa PAH).

3.3 Aims

This chapter aims to investigate the role of HDACs in VSMC dysfunction.

1. To examine the effect of HDAC inhibition on VSMCs seeded on both pliable and rigid matrices. Studying the following inhibitors for: HDAC 1/2/3/6 and 8. This will be conducted via a concentration response assay to determine cell and nuclear area.

2. To examine the effects of the sirtuin family on VSMCs seeded on both pliable and rigid matrices. Studying the following inhibitors for: SIRT1 and 2. This will be conducted via a concentration response assay to determine cell and nuclear area.

3.4 Results

3.4.1 HDAC1 inhibitor (MS275) concentration response assay

HDAC1 has been shown to influence cell proliferation, migration, apoptosis, differentiation and inflammatory effects (133,134). Further study was necessary to determine its role in VSMC stiffness.

Representative images were obtained with confocal microscopy of VSMCs seeded on 12k Pa PAH treated with a serial dilution of a class I HDAC1 specific inhibitor (MS275). The concentration range was initially between 0.01 - 1000 nM, cells were also stimulated with angII (10 μM). This concentration range was dropped to 100nM as we could see a significant difference at lower concentrations.

We set out to investigate the role of HDAC inhibitors on VSMC matrix stiffness response. We began by examining the impact of increasing concentrations of MS275, a class I HDAC inhibitor on the morphology of angiotensin II stimulated VSMCs on pliable PAHs. Analysis revealed that revealed that MS275 had no effect on VSMC area on pliable PAHs **Figure 3.1(A-C)**.

Next, we examined the impact of MS275 on the morphology of angiotensin II stimulated VSMCs seeded onto rigid PAHs. Analysis revealed the MS275 treatment evoked concentration dependent reduction in VSMC area **Figure3.2(A-C)**. Non-linear regression analysis revealed the IC50 to be 10^{-9} M **Figure3.2(B-C)**.

We saw no changes in nuclear area in VSMCs on either 12 or 72kPa PAHs when treated with HDAC1 inhibitor MS275, this can be seen in **(Appendix-Figure A2.1)**.

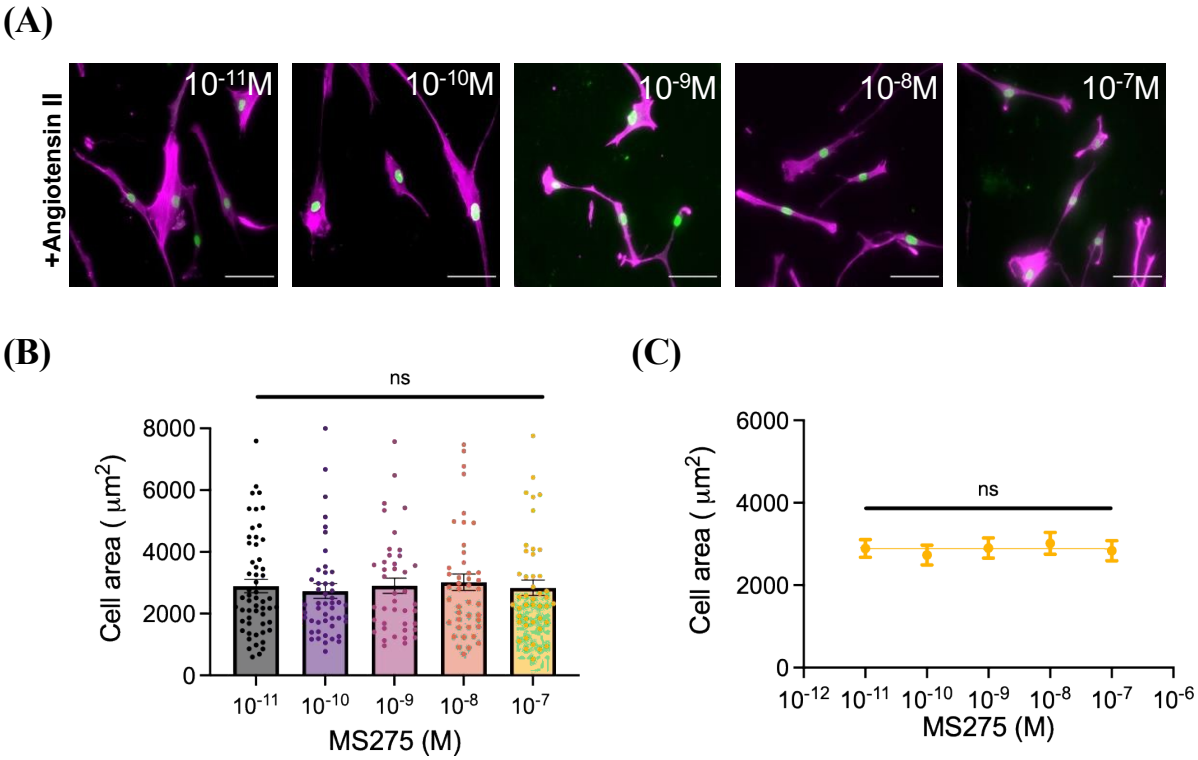

Figure 3.1 HDAC1 inhibitor (MS275) concentration response assay 12 kPa (A) *Representative immunofluorescence images showing isolated VSMC cultured on 12 kPa PAHs actin cytoskeleton stained using rhodamine phalloidin (magenta) and corresponding nuclei stained with lamin A/C (green) when treated with MS275 of increasing concentration for 1 hour. Scale bar represents 100µm. VSMCs were treated with increasing concentrations of MS275 (0.01nM-1000nM) for 1 hour.* ***(B)*** *Graph shows individual cell values (coloured dots) as well as the mean of 3 independent experiments with approximately ≥40 cells analysed. No significance was determined using one-way ANOVA followed by Tukey's multiple comparison test.* ***(C)*** *Corresponding line graph representing mean of 3 independent experiments with ≥40 cells. Statistical significance was determined with a one-way ANOVA (non-significant; p =>0.05).*

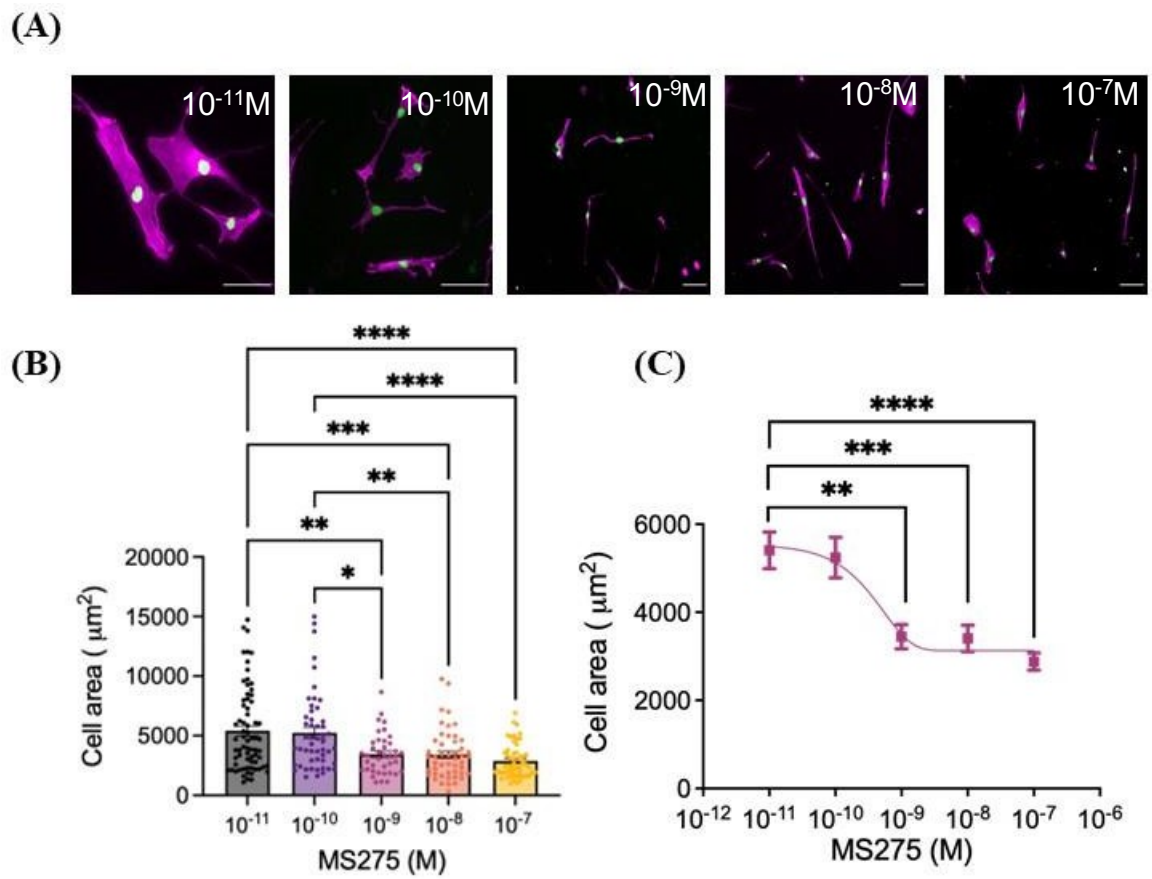

Figure 3.2 HDAC1 inhibitor (MS275) concentration response assay 72 kPa (A) *Representative immunofluorescence images showing isolated VSMC cultured on 72 kPa PAHs actin cytoskeleton stained using rhodamine phalloidin (magenta) and corresponding nuclei stained with lamin A/C (green) when treated with MS275 of increasing concentration for 1 hour. Scale bar represents 100µm. VSMCs were treated with increasing concentrations of MS275 (0.01 -100nM) for 1 hour.* ***(B)*** *Graph shows individual cell values (coloured dots) as well as the mean of 3 independent experiments with approximately ≥40 cells analysed. Significance was determined using one-way ANOVA followed by Tukey's multiple comparison test.* ***(C)*** *Corresponding line graph representing mean of 3 independent experiments with ≥40 cells. Statistical significance was determined with a one-way ANOVA (significant; ** p≤0.01,*** p≤0.001, **** p≤0.0001)*

3.4.2 HDAC2 inhibitor (Santacruzamate A) concentration response assay

Following this, I investigated the class I HDAC2 inhibitor Santacruzamate A. Santa Cruzamate A is involved in cell proliferation, inflammation and angiogenesis and has been shown to block cardiac hypertrophy (133). A concentration range between 0.001nm-100nm was tested.

Upon analysis, on the 12 kPa PAH, VSMC area increased with concentration increases of Santacruzamate A **Figure 3.3(A-C)**. Non-linear regression analysis calculated the IC50 to be 1 nM. No significant differences in VSMC area were observed on the 72 kPa PAHs Figure **3.4(A-C)**.

We saw no changes in nuclear area in VSMCs on either 12 or 72kPa PAHs when treated with HDAC2 inhibitor Santacruzamate A, this can be seen in **(Appendix-Figure A2.2)**.

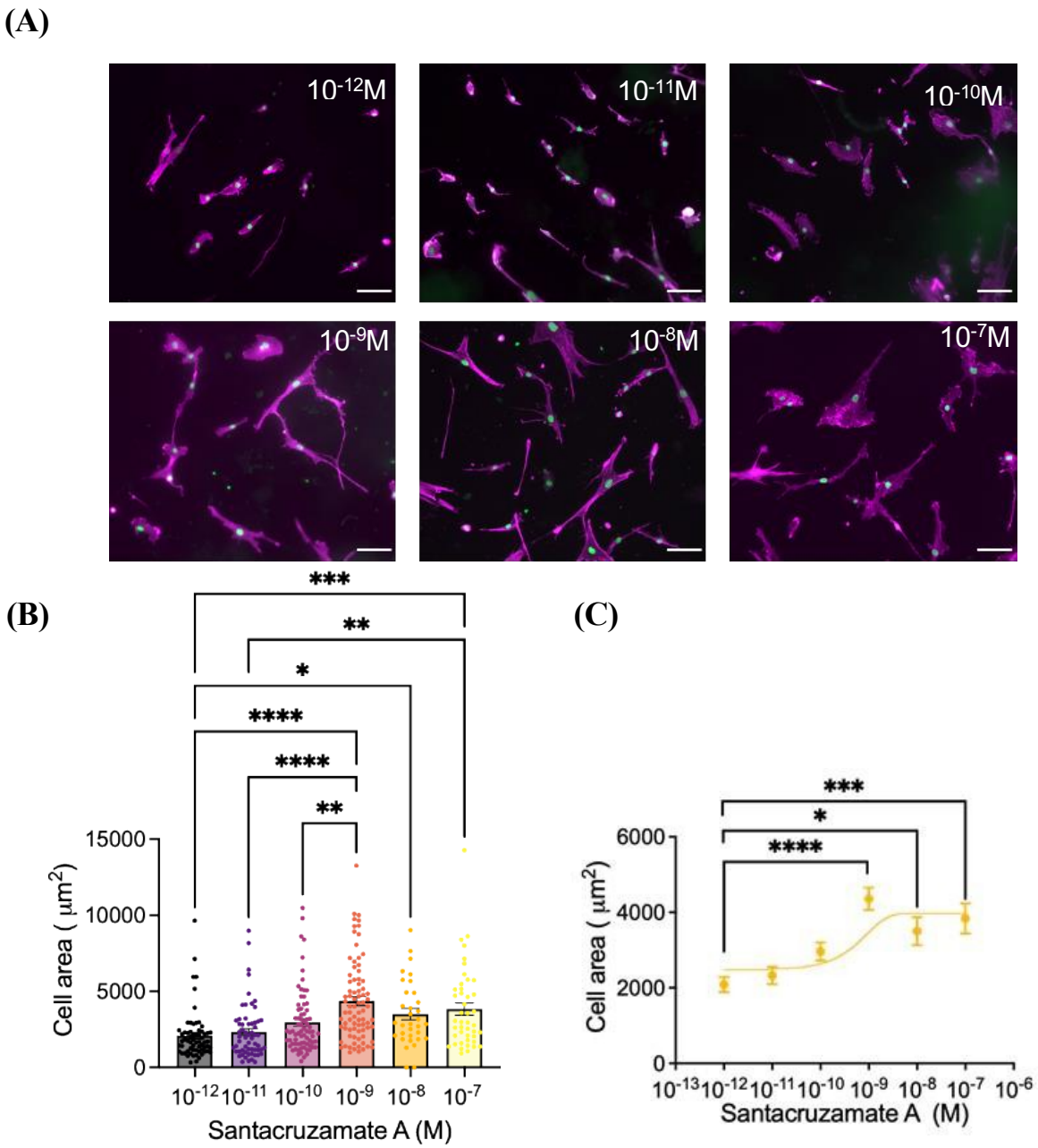

Figure 3.3 HDAC2 inhibitor (Santacruzamate A) concentration response assay 12 kPa (A) *Representative immunofluorescence images showing isolated VSMC cultured on 12 kPa PAHs actin cytoskeleton stained using rhodamine phalloidin (magenta) and corresponding nuclei stained with lamin A/C (green) when treated with Santacruzamate A of increasing concentration for 1 hour. Scale bar represents 100µm. VSMCs were treated with increasing concentrations of Santacruzamate A (0.001nM-100nM) for 1 hour.* ***(B)*** *Graph shows individual cell values (coloured dots) as well as the mean of 3 independent experiments with approximately ≥70 cells analysed. Significance was determined using one-way ANOVA followed by Tukey's multiple comparison test.* ***(C)*** *Corresponding line graph representing mean of 3 independent experiments with ≥40 cells. Statistical significance was determined with a one-way ANOVA (significant;* $p \leq 0.05$, ** $p \leq 0.01$, *** $p \leq 0.001$, **** $p \leq 0.0001$)*

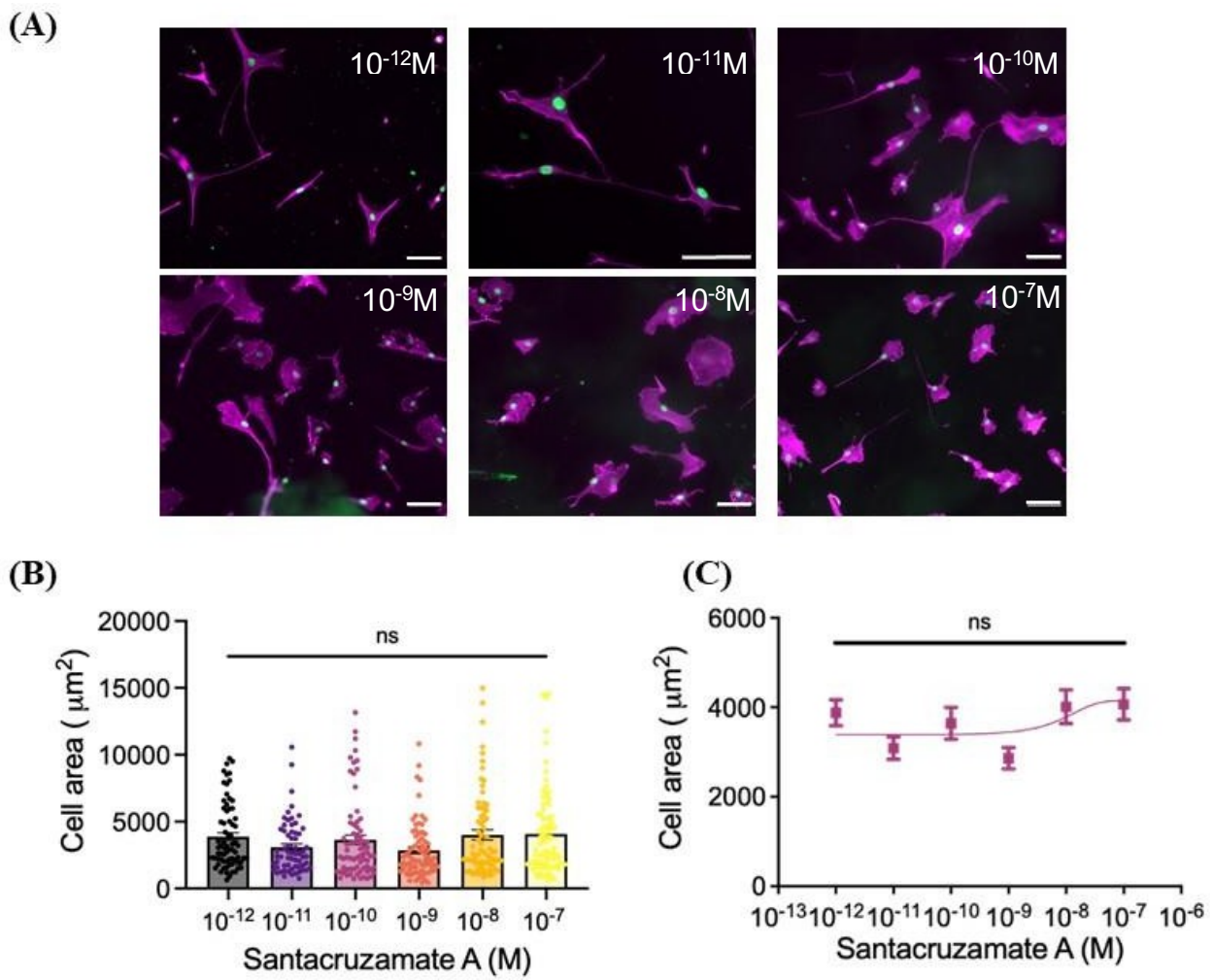

Figure 3.4 HDAC2 inhibitor (Santacruzamate A) concentration response assay 72 kPa (A) *Representative immunofluorescence images showing isolated VSMC cultured on 72 kPa PAHs actin cytoskeleton stained using rhodamine phalloidin (magenta) and corresponding nuclei stained with lamin A/C (green) when treated with Santacruzamate A of increasing concentration for 1 hour. Scale bar represents 100µm. VSMCs were treated with increasing concentrations of Santacruzamate A (0.001nM-100nM) for 1 hour.* ***(B)*** *Graph shows individual cell values (coloured dots) as well as the mean of 3 independent experiments with approximately ≥70 cells analysed. Significance was determined using one-way ANOVA followed by Tukey's multiple comparison test.* ***(C)*** *Corresponding line graph representing mean of 3 independent experiments with ≥40 cells. Statistical significance was determined with a one-way ANOVA (non-significant; p = >0.05).*

3.4.3 HDAC3 inhibitor (RGFP966) concentration response assay

Next, I tested another class I HDAC inhibitor, RGFP966 which has a selectivity for inhibiting HDAC3. HDAC3 has been identified as a target to treat atherosclerosis (135). Although it has been linked in many diseases, the specific role of HDAC3 in cardiovascular diseases remains elusive. It has been shown to regulate gene transcription in cell proliferation, cell cycle and cell survival (135). A concentration range of 0.01-100 μM was selected. Cells were also stimulated with 10 μM of angiotensin II for 30 minutes.

Image analysis of VSMCs seeded on 12 kPa PAH only showed a significant difference in cell area between those treated with 1 μM RGFP966 and 100 μM. Other cell areas showed no significant difference with one way ANOVA analysis **Figure 3.5(A-C)**.

VSMCs cultured on 72 kPa PAHs displayed a decrease in cell area with a concentration dependent increase **Figure 3.6(A-C)**.

We saw no changes in nuclear area in VSMCs on either 12 or 72kPa PAHs when treated with HDAC3 inhibitor RGFP966, this can be seen in **(Appendix-Figure A2.3)**.

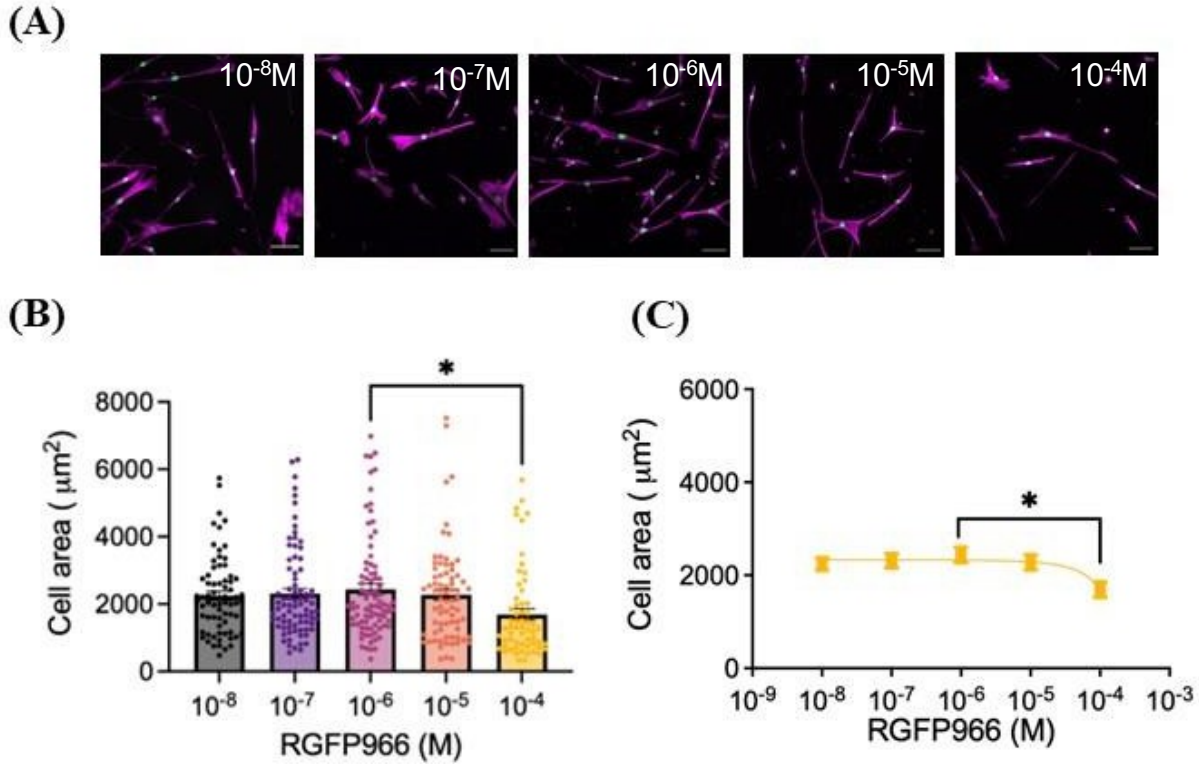

Figure 3.5 HDAC3 inhibitor (RGFP966) concentration response assay 12kPa ***(A)*** *Representative immunofluorescence images showing isolated VSMC cultured on 12 kPa PAHs actin cytoskeleton stained using rhodamine phalloidin (magenta) and corresponding nuclei stained with lamin A/C (green) when treated with RGFP966 of increasing concentration for 1 hour. Scale bar represents 100µm. VSMCs were treated with increasing concentrations of RGFP966 (0.01µM-100µM) for 1 hour.* ***(B)*** *Graph shows individual cell values (coloured dots) as well as the mean of 3 independent experiments with approximately ≥60 cells analysed. Significance was determined using one-way ANOVA followed by Tukey's multiple comparison test.* ***(C)*** *Corresponding line graph representing mean of 3 independent experiments with ≥60 cells. Statistical significance was determined with a one-way ANOVA (significant;* $p \leq 0.05$*).*

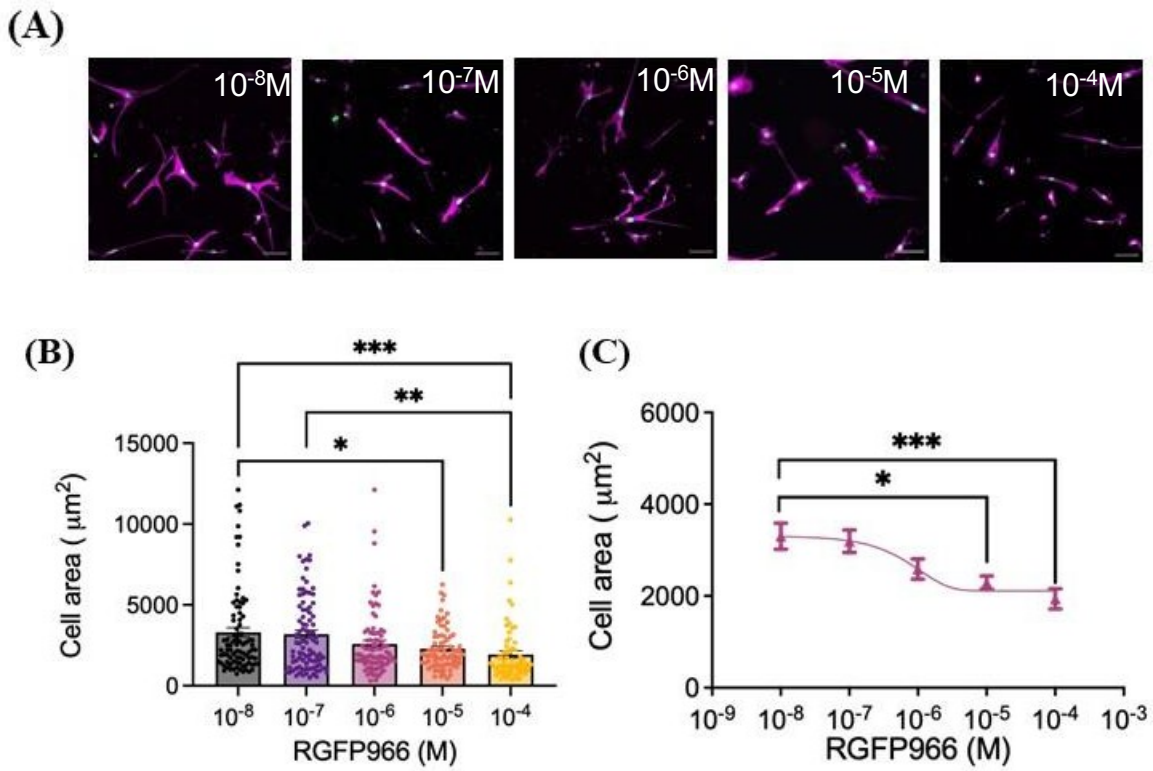

Figure 3.6 HDAC3 inhibitor (RGFP966) concentration response assay 72 kPa (A) *Representative immunofluorescence images showing isolated VSMC cultured on 72 kPa PAHs actin cytoskeleton stained using rhodamine phalloidin (magenta) and corresponding nuclei stained with lamin A/C (green) when treated with RGFP966 of increasing concentration for 1 hour. Scale bar represents 100µm. VSMCs were treated with increasing concentrations of RGFP966 (0.01µM-100µM) for 1 hour.* ***(B)*** *Graph shows individual cell values (coloured dots) as well as the mean of 3 independent experiments with approximately ≥66 cells analysed. Significance was determined using one-way ANOVA followed by Tukey's multiple comparison test.* ***(C)*** *Corresponding line graph representing mean of 3 independent experiments with ≥66 cells. Statistical significance was determined with a one-way ANOVA (significant;* * p≤0.05, ** p≤0.01, *** p≤0.001).*

3.4.4 HDAC8 inhibitor (PCI34051) concentration response assay

I tested another class I HDAC inhibitor specific for HDAC8 which has been implicated in many diseases such as cancer and parasitic infections (136). It has been seen that HDAC8 has been able to reduce vascular hypertrophy in angiotensin II hypertensive mice (137). Due to its success in other preliminary studies, we decided to utilise it with our PAH system to see if it was able to attenuate VSMC area. We tested PCI34051 at a concentration range of 0.01-10 μM was selected. Cells were also stimulated with 10 μM of angiotensin II for 30 minutes.

Upon analysis, we observed that there were no significant differences in VSMC area on either a pliable or rigid matrix with an increase in concentration of the HDAC8 inhibitor **Figure 3.7/3.8(A-C)**.

We saw no apparent changes in nuclear area in VSMCs on either 12 or 72kPa PAHs when treated with HDAC8 inhibitor PCI 34051, however, significance could not be determined as it was an N=2. This can be seen in **(Appendix-Figure A2.4)**.

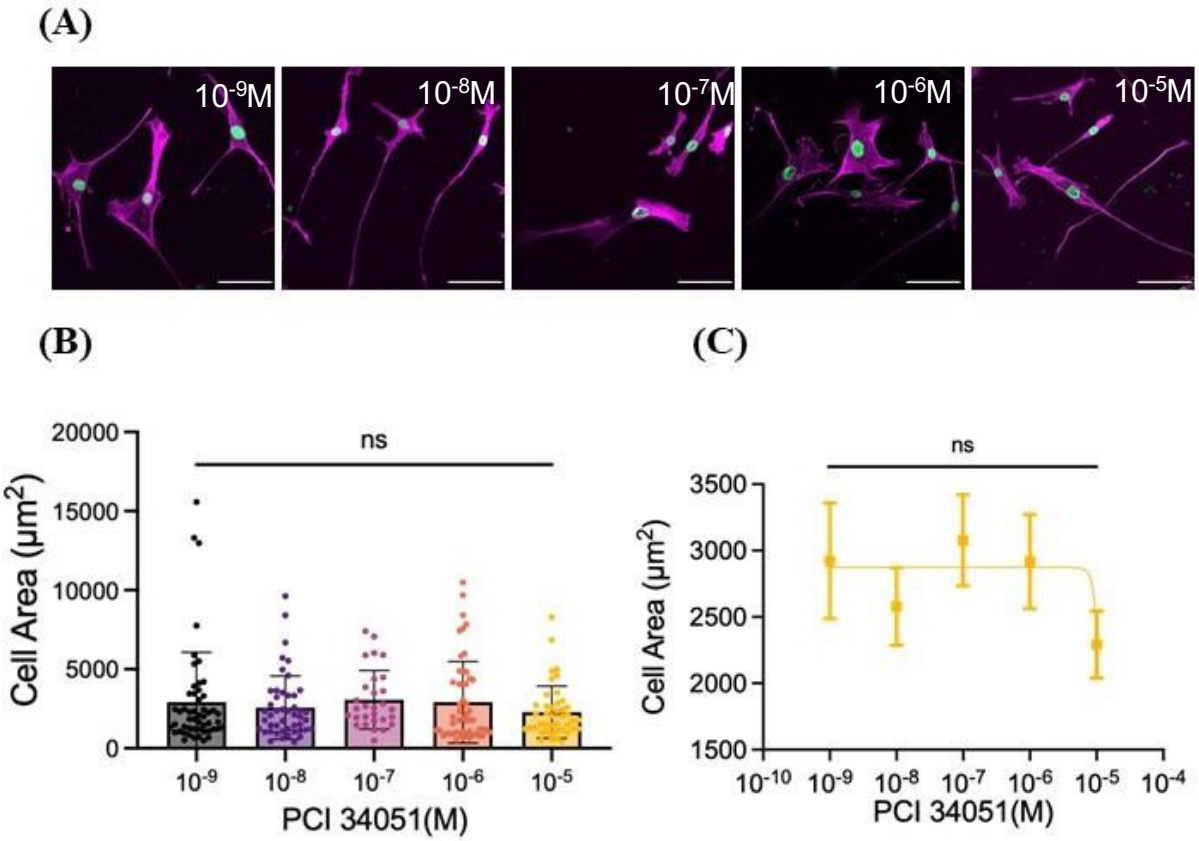

Figure 3.7 HDAC8 inhibitor (PCI34051) concentration response assay 12 kPa *(A)* *Representative immunofluorescence images showing isolated VSMC cultured on 12 kPa PAHs actin cytoskeleton stained using rhodamine phalloidin (magenta) and corresponding nuclei stained with lamin A/C (green) VSMCs were treated with increasing concentrations of PCI34051 (0.001µM-10µM) for 1 hour. Scale bar represents 100µm.* ***(B)*** *Graph shows individual cell values (coloured dots) ≥29 cells analysed.* ***(C)*** *Graph shows individual nuclei values (coloured dots) approximately ≥29 nuclei analysed. Statistical significance was determined with a one-way ANOVA (significant;* $p \leq 0.05$, ** $p \leq 0.01$, *** $p \leq 0.001$***).***

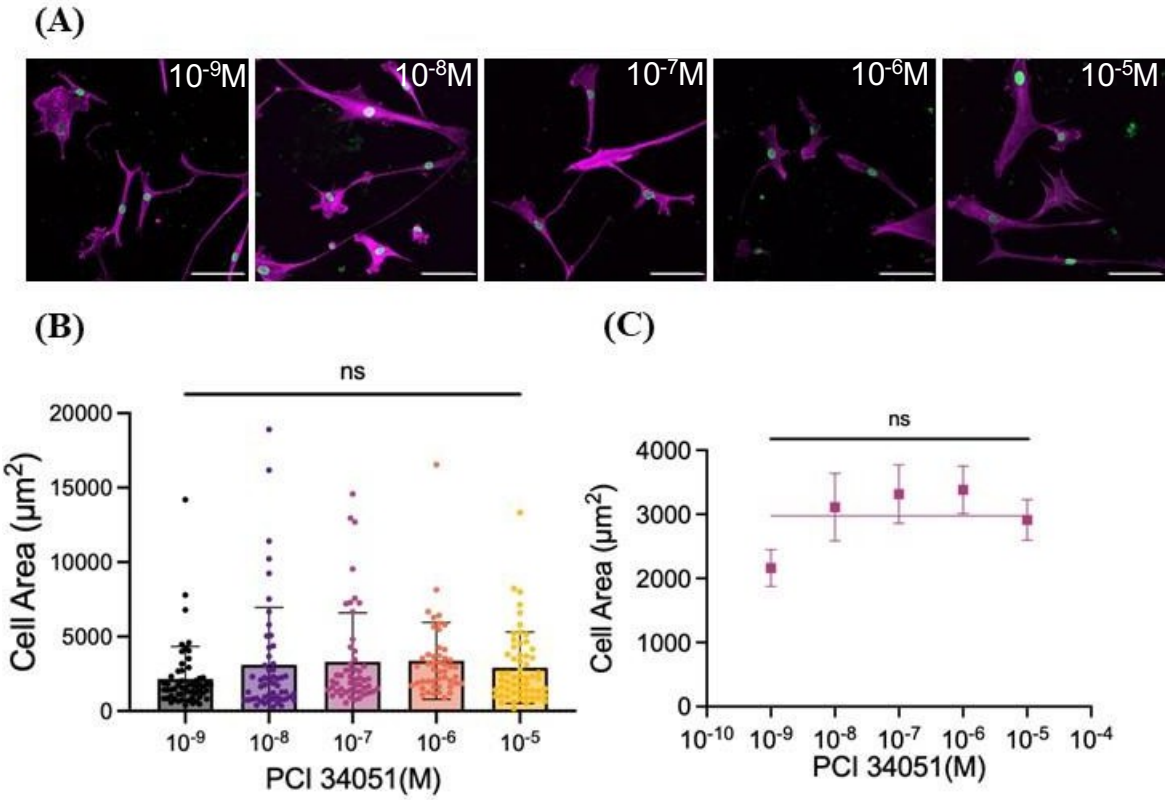

Figure 3.8 HDAC8 inhibitor (PCI34051) concentration response assay 72 kPa ***(A)*** *Representative immunofluorescence images showing isolated VSMC cultured on 72 kPa PAHs actin cytoskeleton stained using rhodamine phalloidin (magenta) and corresponding nuclei stained with lamin A/C (green) VSMCs were treated with increasing concentrations of PCI34051 (0.001µM-10µM) for 1 hour. Scale bar represents 100µm.* ***(B)*** *Graph shows individual cell values (coloured dots) ≥48 cells analysed.* ***(C)*** *Graph shows individual nuclei values (coloured dots) approximately ≥48 nuclei analysed. No statistical difference was determined, ns.*

3.4.5 HDAC6 inhibitor (Tubastatin A) concentration response assay

To further understand the roles of HDACs on VSMCs, I moved on to testing a class II inhibitor of HDAC6, Tubastatin A. Tubastatin A is involved in inducing VSMC proliferation and migration as well as inflammation and differentiation (134,138). As HDAC6 is microtubule specific, we hypothesised it may have a role in regulating microtubule stability and therefore VSMC contractility. Tubastatin A can acetylate the lysine 40 (K40) of α-tubulin. Specifically, the acetylation of K40 has caused cytoskeletal stiffness in striated muscle yet its role in the VSMC response to matrix rigidity in left unknown. The concentration range originally selected was between 0.0001-100 μM. This was later expanded to a lower concentration of 10^{-13} M as it seemed that the full response was not being seen. This was deducted with a western blot to show acetylated α-tubulin levels which can be seen in the following chapter.

Cell area of VSMC grown on 12 kPa PAH can be seen to reduce with increasing concentrations of Tubastatin A **Figure 3.9(A-C)**. Non-linear regression analysis shows the IC50 was around 10^{-9}M (1nM) **Figure 3.9(B-C)**. A significant difference was calculated with one-way ANOVA analysis. Treatment at 10^{-6} M ensured a significant effect without the observation of any cytotoxic effects. We observed that with an increase in Tubastatin A concentration it also reduced nuclear swelling on pliable PAHs **Figure 3.9(D-E)**.

VSMCs cultured on 72 kPa PAH showed a similar trend in cell area decrease with increasing concentration **Figure 3.10(A-C)**. One-way ANOVA statistical analysis showed a significant difference between these two concentrations **Figure 3.10(B-C)**. Non-linear regression analysis also calculated the IC50 as 1 nM (10^{-9}M) comparable to that on 12 kPa **Figure 3.10(C)**.

Similarly, VSMC nuclear area on 72 kpa PAHs followed the same pattern **Figure 3.10(D-E)**. With statistical analysis, one-way ANOVA showed that there was a significant difference between the lowest concentration (10^{-11}M) and 10^{-6}M (1μM).

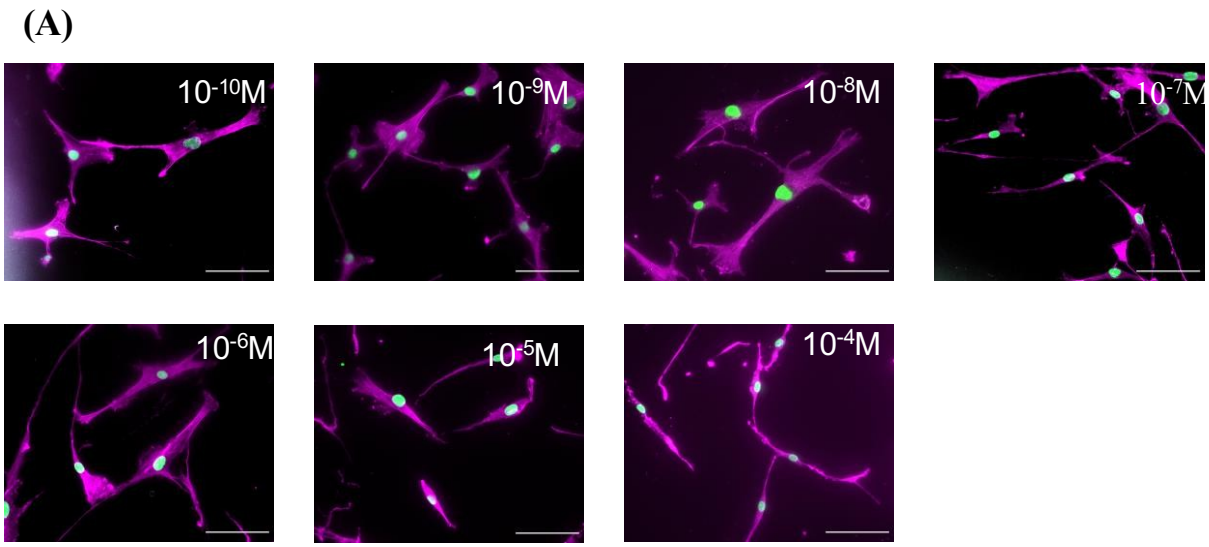
(A)
10-10M
10-9M
10-8M
10-7M
10-6M
10-5M
10-4M

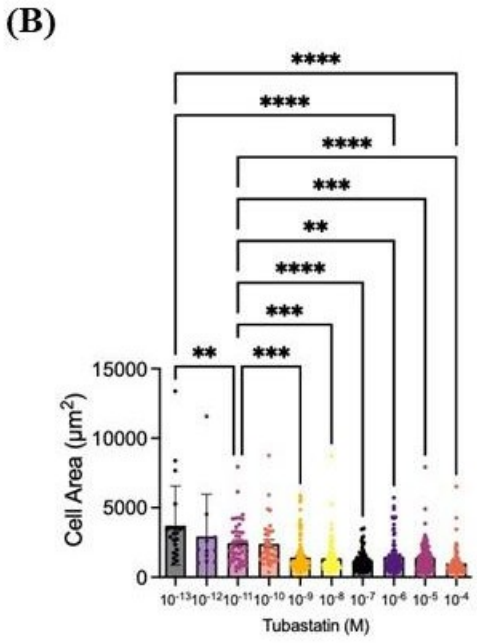
(B)
Cell Area (µm2)
Tubastatin (M)

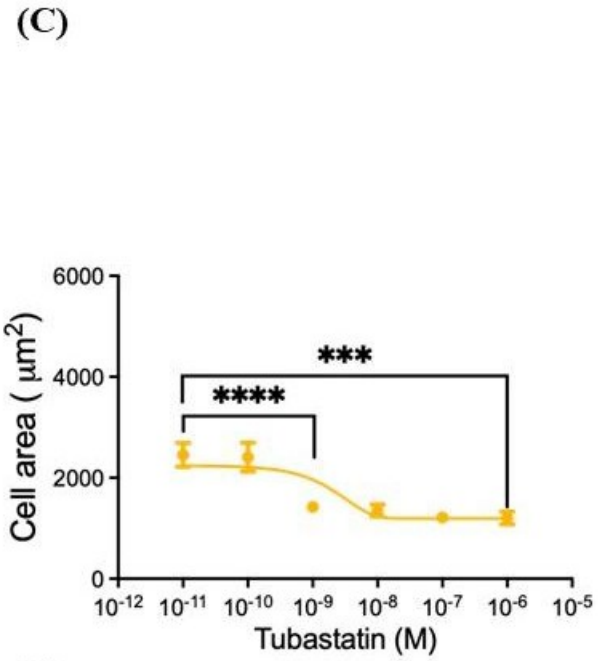
(C)
Cell area (µm2)
Tubastatin (M)

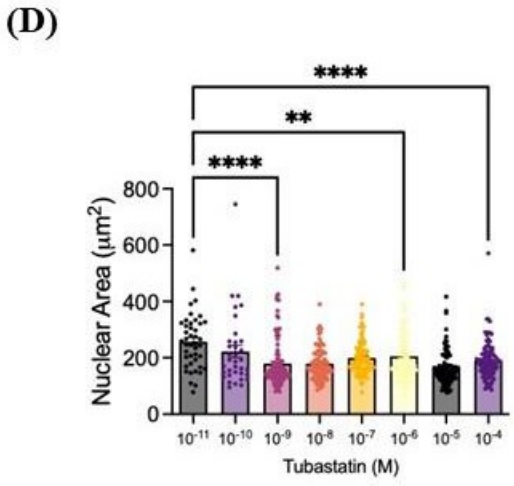
(D)
Nuclear Area (µm2)
Tubastatin (M)

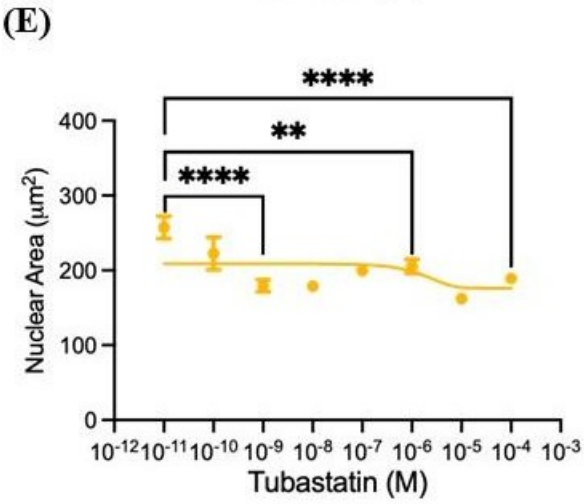
(E)
Nuclear Area (µm2)
Tubastatin (M)

Figure 3.9 HDAC6 inhibitor (Tubastatin A) concentration response assay 12 kPa (A) *Representative immunofluorescence images showing isolated VSMC cultured on 12 kPa PAHs actin cytoskeleton stained using rhodamine phalloidin (magenta) and corresponding nuclei stained with lamin A/C (green) when treated with increasing concentrations of Tubastatin (0.00001μM-100μM) for 1 hour Scale bar represents 100μm.* ***(B)*** *Graph shows individual cell values (coloured dots) as well as the mean of 3 independent experiments with approximately ≥35 cells analysed. Significance was determined using one-way ANOVA followed by Tukey's multiple comparison test.* ***(C)*** *Corresponding cell area line graph representing mean of 3 independent experiments with ≥35 cells. Statistical significance was determined with a one-way ANOVA (significant;* p≤0.05, ** p≤0.01, *** p≤0.001)* ***(D)*** *Graph shows individual nuclei values (coloured dots) as well as the mean of 3 independent experiments with approximately ≥70 nuclei analysed. Significance was determined using one- way ANOVA followed by Tukey's multiple comparison test.* ***(E)*** *Corresponding nuclear area line graph representing mean of 3 independent experiments with ≥35 cells. Statistical significance was determined with a one-way ANOVA (significant;* p≤0.05, ** p≤0.01,***p≤0.001).*

(A)

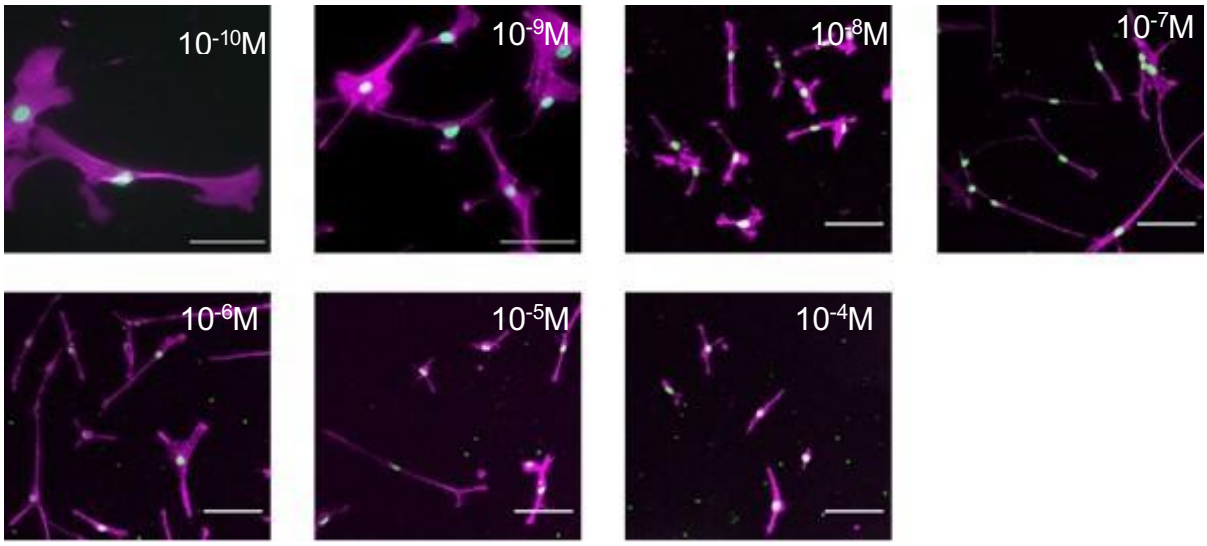
10-10M
10-9M
10-8M
10-7M
10-6M
10-5M
10-4M

(B)

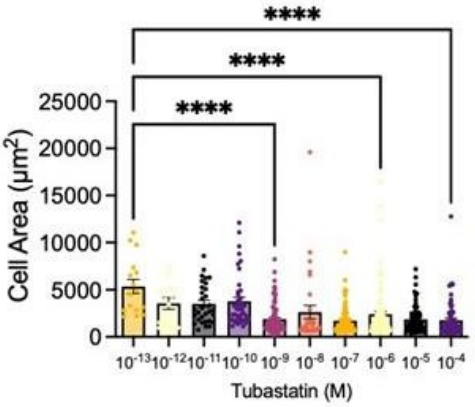
****
****
****
Cell Area (µm2)
25000
20000
15000
10000
5000
0
10-13 10-12 10-11 10-10 10-9 10-8 10-7 10-6 10-5 10-4
Tubastatin (M)

(C)

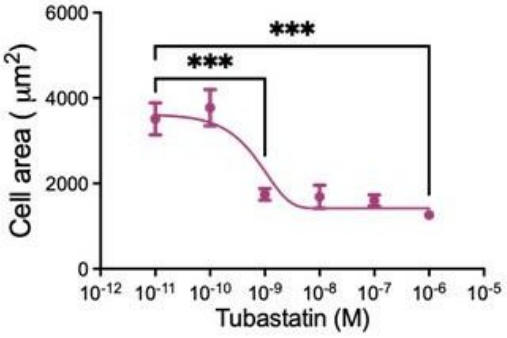
***
***
Cell area (µm2)
6000
4000
2000
0
10-12 10-11 10-10 10-9 10-8 10-7 10-6 10-5
Tubastatin (M)

(D)

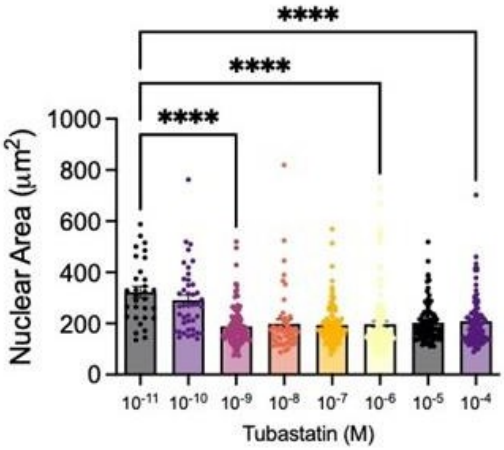
****
****
****
Nuclear Area (µm2)
1000
800
600
400
200
0
10-11 10-10 10-9 10-8 10-7 10-6 10-5 10-4
Tubastatin (M)

(E)

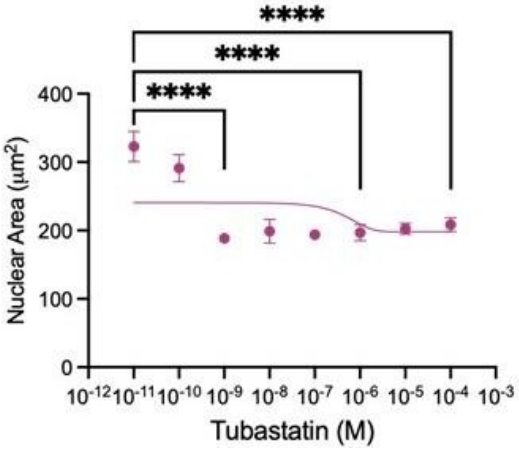
****
****
****
Nuclear Area (µm2)
400
300
200
100
0
10-12 10-11 10-10 10-9 10-8 10-7 10-6 10-5 10-4 10-3
Tubastatin (M)

Figure 3.10 HDAC6 inhibitor (Tubastatin A) concentration response assay 72 kPa (A) *Representative immunofluorescence images showing isolated VSMC cultured on 72 kPa PAHs actin cytoskeleton stained using rhodamine phalloidin (magenta) and corresponding nuclei stained with lamin A/C (green) when treated with increasing concentrations of Tubastatin (0.00001μM-100μM) for 1 hour Scale bar represents 100μm.* ***(B)*** *Graph shows individual cell values (coloured dots) as well as the mean of 3 independent experiments with approximately ≥35 cells analysed. Significance was determined using one-way ANOVA followed by Tukey's multiple comparison test.* ***(C)*** *Corresponding cell area line graph representing mean of 3 independent experiments with ≥35 cells. Statistical significance was determined with a one-way ANOVA (significant;* $p \leq 0.05$, ** $p \leq 0.01$, *** $p \leq 0.001$) ***(D)*** *Graph shows individual nuclei values (coloured dots) as well as the mean of 3 independent experiments with approximately ≥70 nuclei analysed. Significance was determined using one- way ANOVA followed by Tukey's multiple comparison test.* ***(E)*** *Corresponding nuclear area line graph representing mean of 3 independent experiments with ≥35 cells. Statistical significance was determined with a one-way ANOVA (significant;* $p \leq 0.05$, ** $p \leq 0.01$, *** $p \leq 0.001$).

3.4.6 HDAC6 inhibitor (BRD9757) concentration response assay

Another HDAC6 inhibitor was tested, BRD9757 which displays some selectivity over other class I and II HDACs. A concentration range between 0.1 -1000 nM was tested. Three repeats were conducted, however, one did not work and was excluded from the experiment. The graphs below are *N=2*, therefore no statistical analysis was conducted.

Both cell and nuclear area appear unchanged of VSMCs seeded on 12 kPa PAHs, however, this is not conclusive as a third repeat needs to be conducted **Figure 3.11(A- C)**.

On the other hand, cell area of VSMCs cultured on 72 kPa PAHs. The nuclear area of VSMCs on 72 kPa PAH were larger than their 12 kPa counterparts, as expected but remain unchanged to BRD9757 treatment **Figure 3.12(A-C)**. No further conclusions can be drawn from this experiment before an *N=3* can be completed.

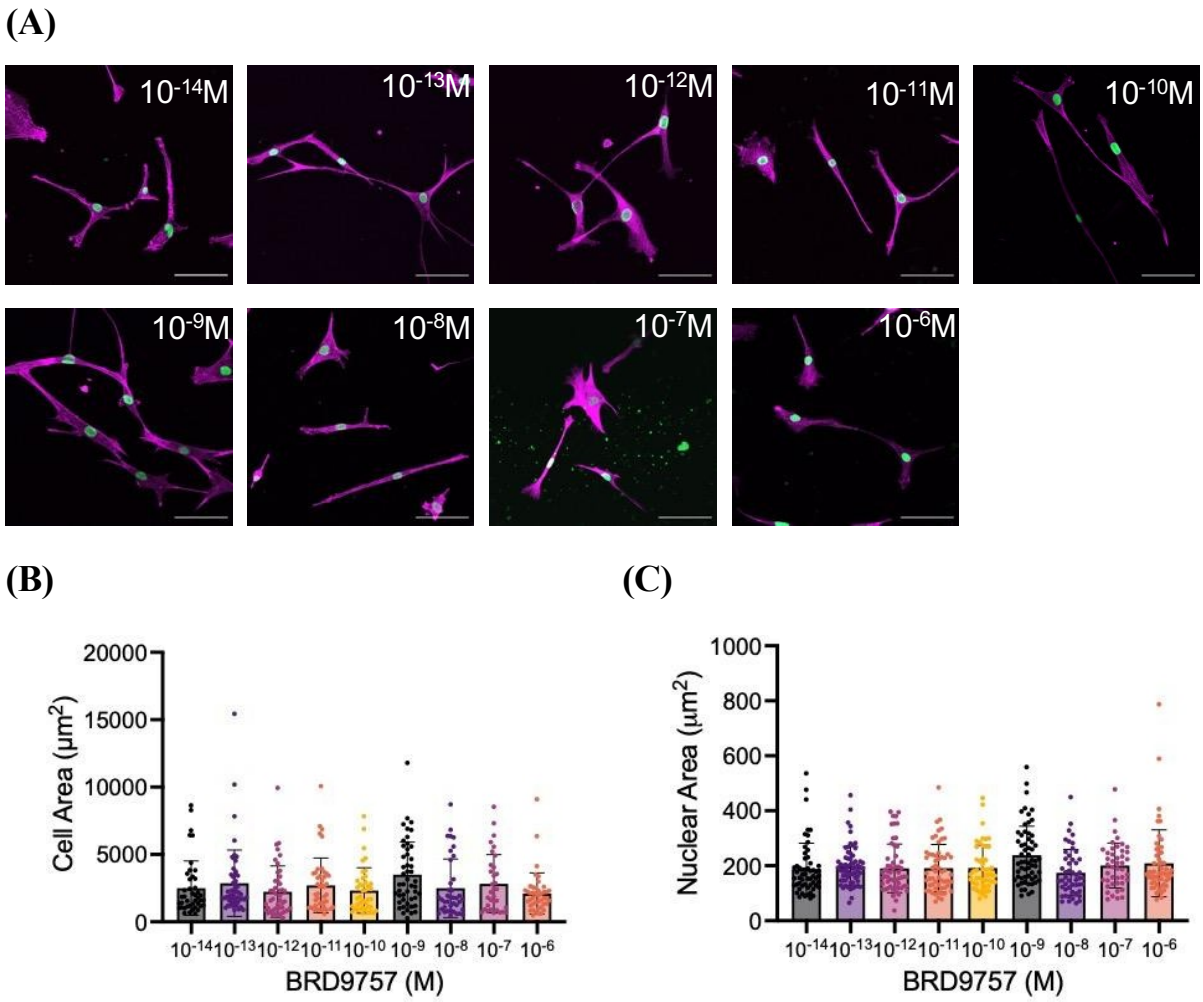

Figure 3.11 HDAC6 inhibitor (BRD9757) concentration response assay 12 kPa (A) *Representative immunofluorescence images showing isolated VSMC cultured on 12 kPa PAHs actin cytoskeleton stained using rhodamine phalloidin (magenta) and corresponding nuclei stained with lamin A/C (green) VSMCs were treated with increasing concentrations of BRD9757 (10^{-8} -1µM) for 1 hour. Scale bar represents 100µm.* ***(B)*** *Graph shows individual cell values (coloured dots) ≥33 cells analysed.* ***(C)*** *Graph shows individual nuclei values (coloured dots) approximately ≥33 nuclei analysed. Significance was not determined due to this being N=2.*

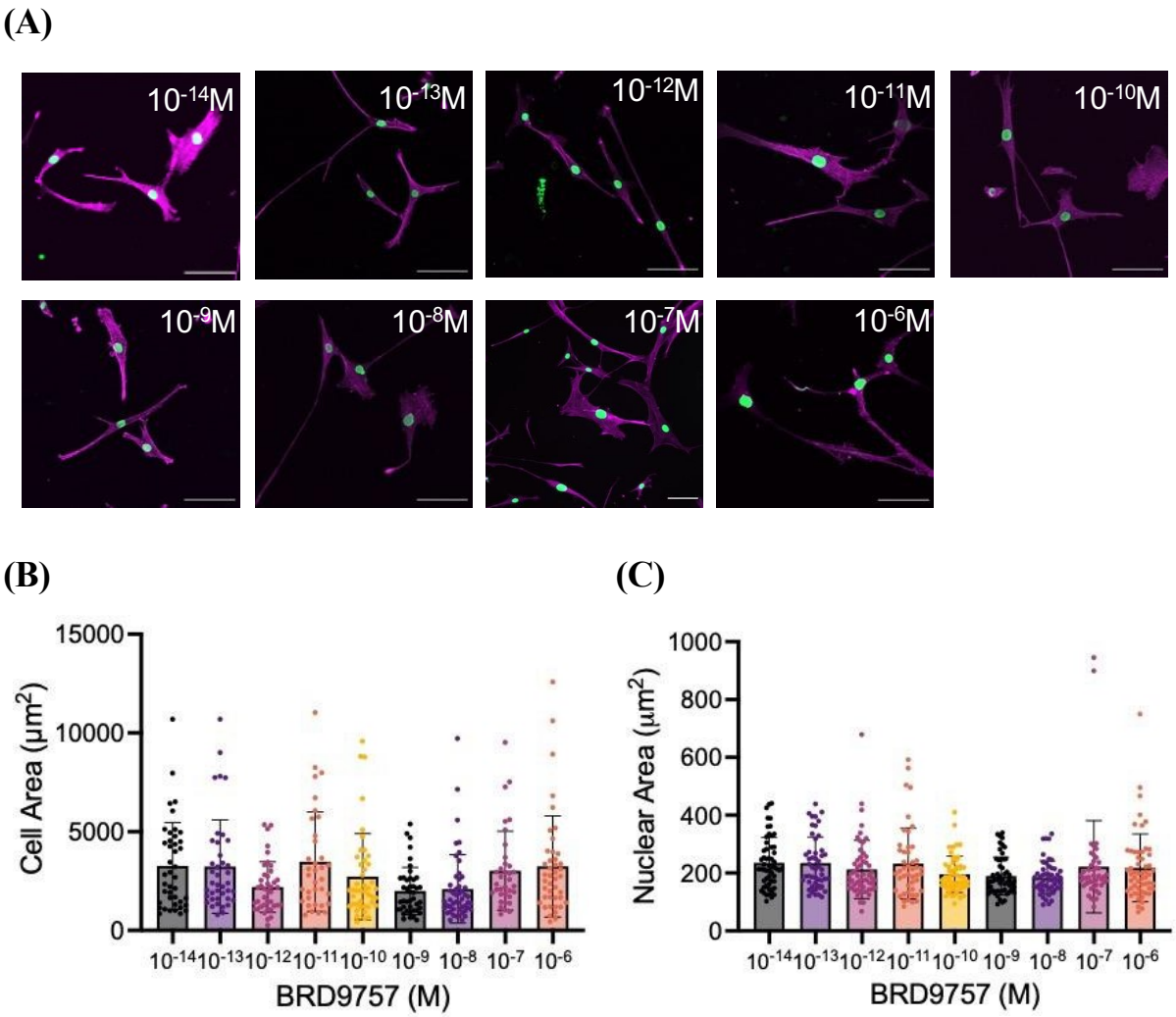

Figure 3.12 HDAC6 inhibitor (BRD9757) concentration response assay 72 kPa (A) *Representative immunofluorescence images showing isolated VSMC cultured on 72 kPa PAHs actin cytoskeleton stained using rhodamine phalloidin (magenta) and corresponding nuclei stained with lamin A/C (green) VSMCs were treated with increasing concentrations of BRD9757 (1e-8µM-1µM) for 1 hour. Scale bar represents 100µm.* ***(B)*** *Graph shows individual cell values (coloured dots) ≥35 cells analysed.* ***(C)*** *Graph shows individual nuclei values (coloured dots) approximately ≥35 nuclei analysed. Significance was not determined due to this being N=2.*

3.4.7 SIRT1 inhibitor (EX527) concentration response assay

Class III HDACs are known as sirtuins, SIRTs in short. SIRT 1 and 2 are both found in the cytoplasm, however, SIRT 1 can pass into the nucleus. SIRT 1 has been linked to endothelial cell apoptosis and senescence. Its role in VSMCs remains elusive. SIRT 1 has also been observed to have a role in migration and proliferation (134). The role of SIRT in VSMCs has not yet been fully investigated maintaining the importance of this research project. A concentration range between 0.001 nM-100 nM was selected for EX527, SIRT1 inhibitor.

VSMCs grown on 12 kPa PAHs exhibited no changes with increasing concentrations of EX527 **Figure 3.13(A-C)**. As expected, those cultured on 72 kPa PAHs are larger than their 12 kPa counterparts but also see no change with drug treatment **Figure 3.14(A-C)**. One-way ANOVA proved that there was no significant difference between the cell area on both PAHs.

We saw no changes in nuclear area in VSMCs on either 12 or 72kPa PAHs when treated with SIRT1 inhibitor EX527, this can be seen in **(Appendix-Figure A2.5)**.

(A)

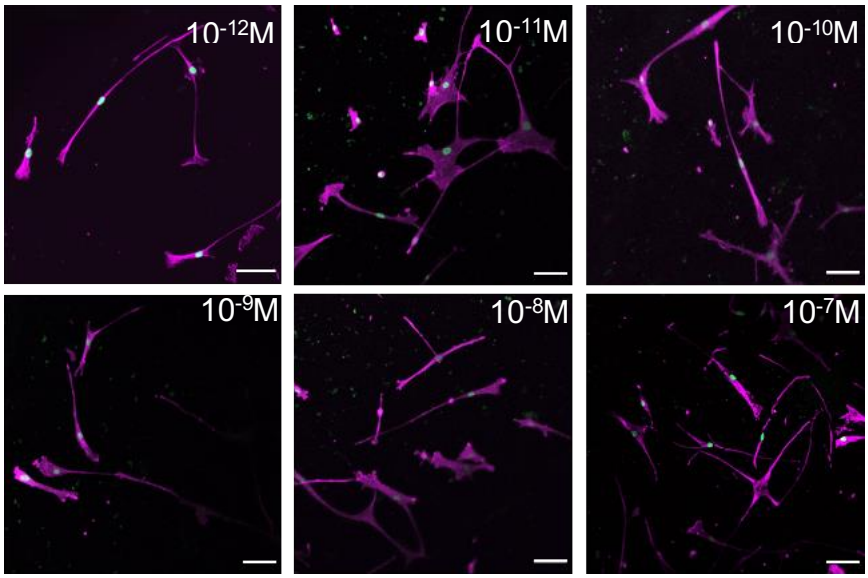

(B) **(C)**

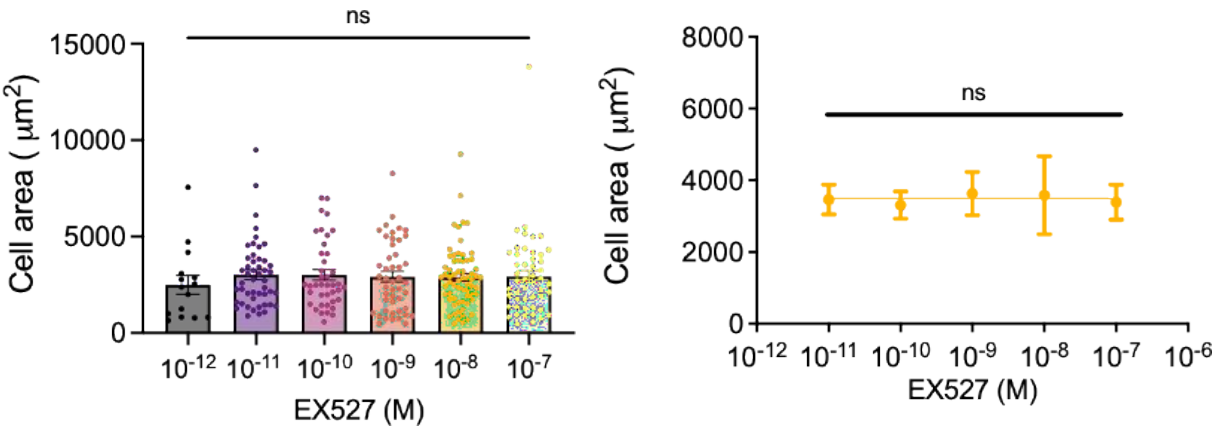

Figure 3.13 SIRT1 inhibitor (EX527) concentration assay 12 kPa (A) *Representative immunofluorescence images showing isolated VSMC cultured on 12 kPa PAHs actin cytoskeleton stained using rhodamine phalloidin (magenta) and corresponding nuclei stained with lamin A/C (green) when treated with increasing concentration of EX527 (0.001nM-10nM) for 1 hour. Scale bar represents 100µm. Significance was determined using one-way ANOVA followed by Tukey's multiple comparison test.* ***(B)*** *Graph shows the cell area of VSMC treated with increasing concentrations of EX527 (0.001nM-10nM) for 1 hour on 12 kPa PAHs, represented is individual cell values (coloured dots) as well as the mean of 3 independent experiments with approximately ≥30 cells analysed.* ***(C)*** *Corresponding cell area line graph representing mean of 3 independent experiments. Significance was determined using one- way ANOVA followed by Tukey's multiple comparison test. ANOVA (non-significant, ns. Significant;* p≤0.05, ** p≤0.01, *** p≤0.001).*

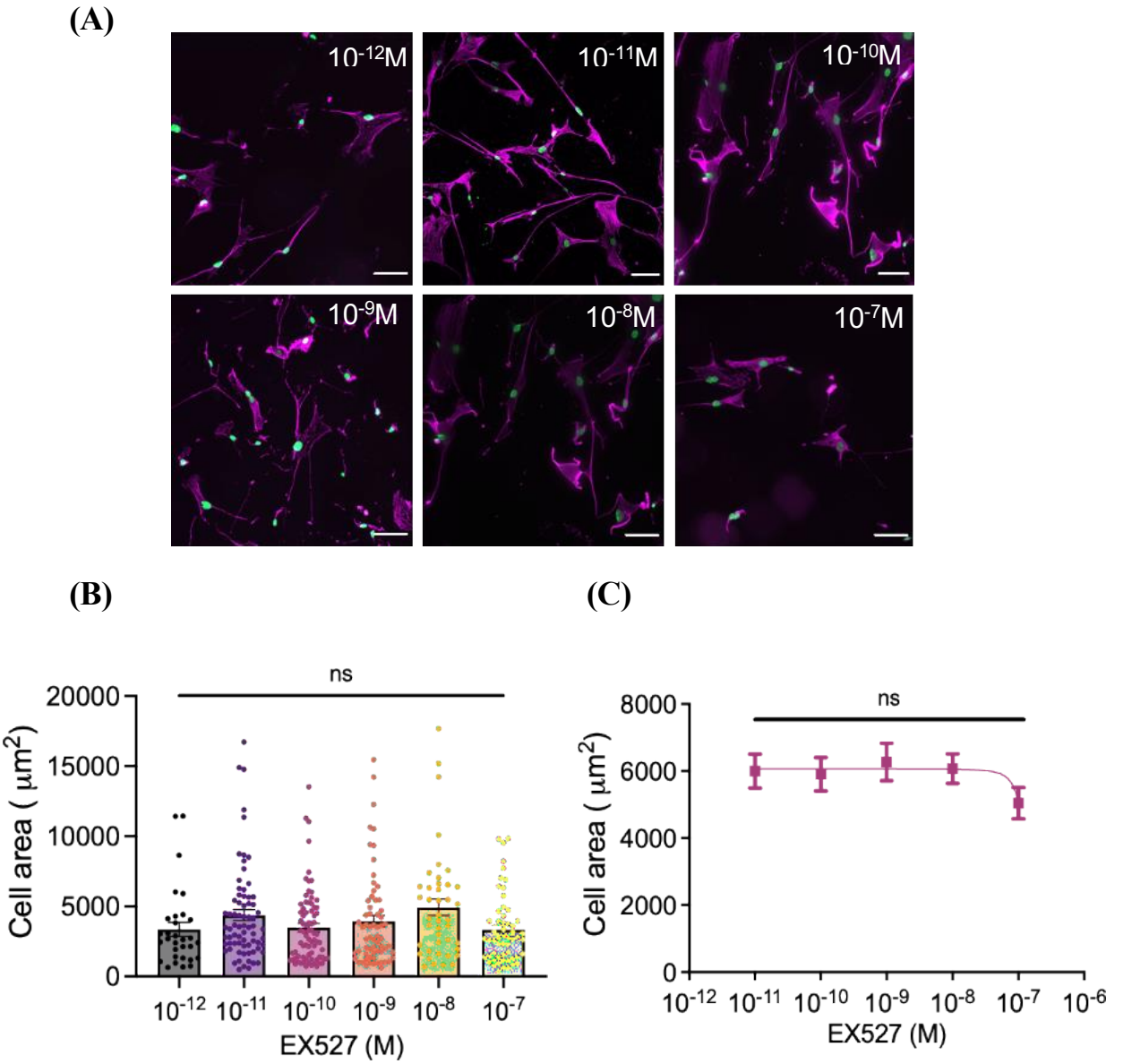

Figure 3.14 SIRT1 inhibitor (EX527) concentration response assay 72 kPa (A) *Representative immunofluorescence images showing isolated VSMC cultured on 72 kPa PAHs actin cytoskeleton stained using rhodamine phalloidin (magenta) and corresponding nuclei stained with lamin A/C (green) when treated with increasing concentration of EX527 (0.001nM-10nM) for 1 hour. Scale bar represents 100µm. Significance was determined using one-way ANOVA followed by Tukey's multiple comparison test.* ***(B)*** *Graph shows the cell area of VSMC treated with increasing concentrations of EX527 (0.001nM-10nM) for 1 hour on 72 kPa PAHs, represented is individual cell values (coloured dots) as well as the mean of 3 independent experiments with approximately ≥31 cells analysed.* ***(C)*** *Corresponding cell area line graph representing mean of 3 independent experiments. Significance was determined using one-way ANOVA followed by Tukey's multiple comparison test. ANOVA (non-significant, ns. Significant;* $p \leq 0.05$, ** $p \leq 0.01$, *** $p \leq 0.001$).*

3.4.8 SIRT2 inhibitor (AK-7) concentration response assay

A SIRT2 inhibitor, AK-7, was next to be tested. Like SIRT1 there has been some implications of SIRT 2 in cardiovascular disease. Overexpression of SIRT2 has been seen to cause cardiomyocyte hypertrophy as well as cell apoptosis in renal ischemia
(134). A concentration range of 0.01µM-100µM.

The SIRT 2 inhibitor, AK-7 also did not appear to influence cell area of VSMCs cultured on 12 kPa PAH **Figure 3.15(A-C)**. No change when treated with increasing concentrations of AK-7 on a rigid PAH **Figure 3.16(A-C)**. At least two further repeats will need to be completed to affirm any changes observed.

Unfortunately, nuclear area data was not conducted for this assay as the DAPI staining was insufficient for analysis.

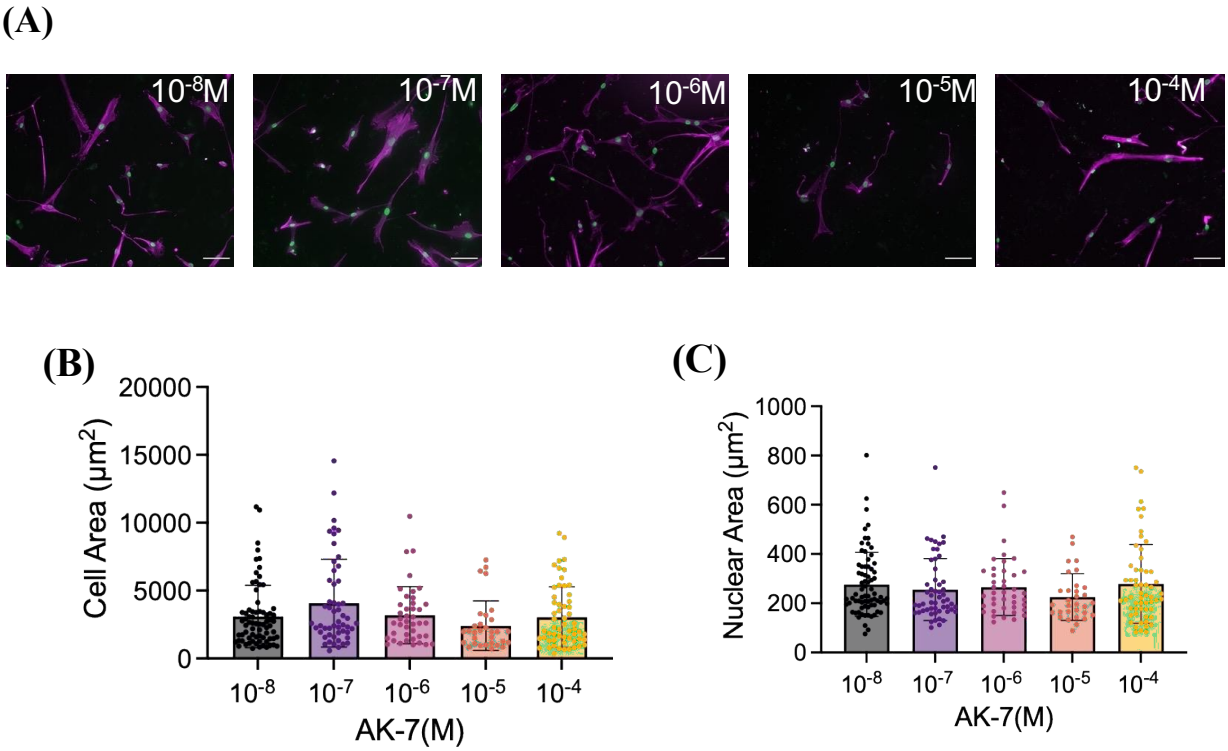

Figure 3.15 SIRT2 inhibitor (AK-7) concentration response assay 12 kPa (A) *Representative immunofluorescence images showing isolated VSMC cultured on 12 kPa PAHs actin cytoskeleton stained using rhodamine phalloidin (magenta) and corresponding nuclei stained with lamin A/C (green) VSMCs were treated with increasing concentrations of AK-7 (0.01µM-100M) for 1 hour. Scale bar represents 100µm.* ***(B)*** *Graph shows individual cell values (coloured dots) ≥31 cells analysed.* ***(C)*** *Graph shows individual nuclei values (coloured dots) approximately ≥31 nuclei analysed. Significance was not determined due to this being N=1.*

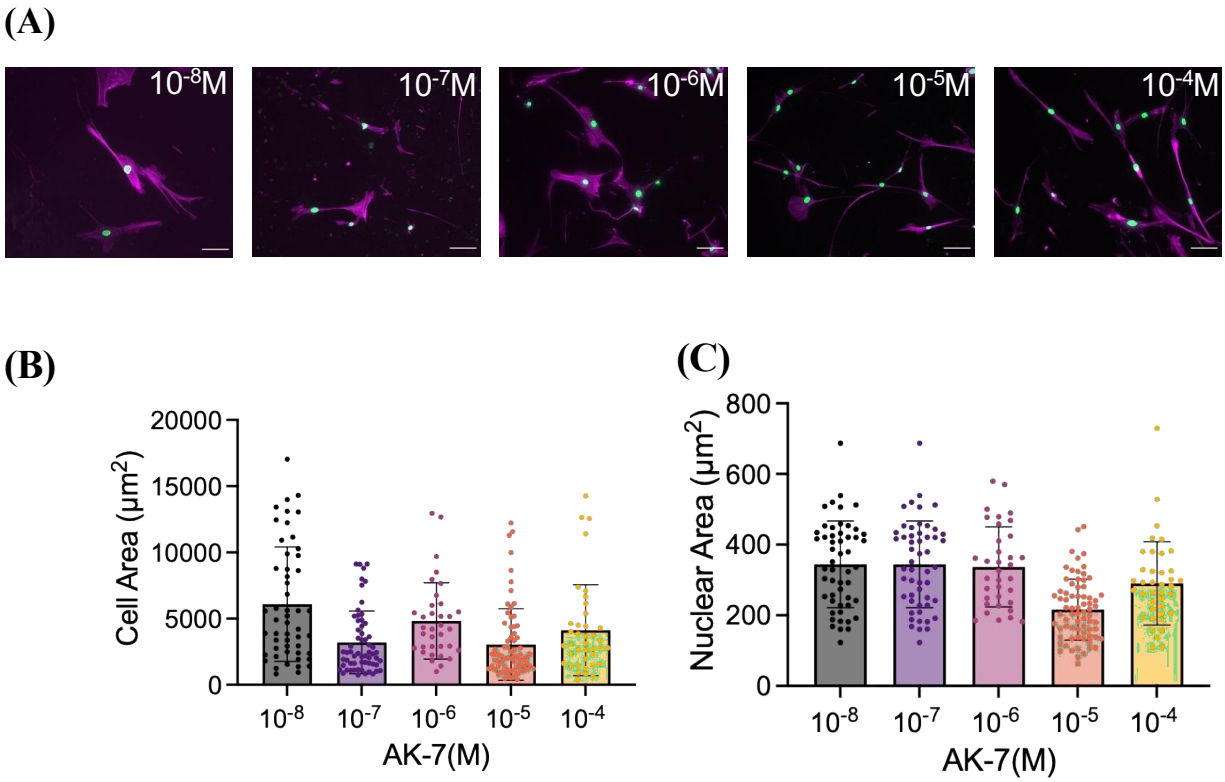

Figure 3.16 SIRT2 inhibitor (AK-7) concentration response assay 72 kPa (A) *Representative immunofluorescence images showing isolated VSMC cultured on 72 kPa PAHs actin cytoskeleton stained using rhodamine phalloidin (magenta) and corresponding nuclei stained with lamin A/C (green) VSMCs were treated with increasing concentrations of AK-7 (0.01µM-100M) for 1 hour. Scale bar represents 100µm.* ***(B)*** *Graph shows individual cell values (coloured dots) ≥35 cells analysed.* ***(C)*** *Graph shows individual nuclei values (coloured dots) approximately ≥35 nuclei analysed. Significance was not determined due to this being N=1.*

3.5 Discussion

The therapeutic effects of HDAC inhibitors have been unveiled in cancer with their potential efficacy in CVDs now garnering attention. Epigenetic regulation is essential in maintaining vascular function. HDACs are thought to be involved in causing the dysfunction of multiple vascular processes which eventually lead to CVD such as atherosclerosis (139). HDAC inhibitors are now being further investigated for this reason, however, there is still no clinical use of them for CVD. Some HDACs have beneficial roles compared to others that negatively affect the vasculature, therefore it is essential that the specific roles of each HDAC is clarified.

HDAC inhibitor	12 kPa	72 kPa
1	No effect	**Decrease in cell area**
2	**Increase in cell area**	No effect
3	**Decrease in cell area at high concentrations**	**Decrease in cell area**
8	No effect	No effect
6 (Tubastatin A)	**Decrease in cell area**	**Decrease in cell area**
6 (BRD9757)	No effect	No effect
SIRT1	No effect	No effect
SIRT2	No effect	No effect

Figure 3.17 *The table above shows the effects on cell size with increasing concentration of the corresponding HDAC inhibitors listed in the first column on either the 12 kPa or 72 kPa PAH. Red indicates a pathophysiological response, green indicates a healthy response to HDAC inhibition on the given substrate.*

Previous work in the Warren Lab showed that cells cultured on 72 kPa PAH exhibited an increase in cell spread compared to those on 12 kPa PAH when treated with a contractile agonist. This proved that VSMCs grown on a stiffer environment were unable to contract compared to those on a healthy tensile strength equivalent. The mechanism behind this was thought to be that angII stimulation on rigid PAHs induced an increase in actomyosin force generation, however, they fail to contract the surrounding ECM. It is known that the actomyosin is essential to VSMC stiffness leading to a decrease in vessel compliance. This has been observed in hypertension,

and ageing. The mechanisms of regulating VSMC stiffness is limited which leads us to investigate the roles of known epigenetic regulators such as HDACs. We have identified that microtubule stability is a key regulator of VSMC contractile response. HDAC6 is known to regulate microtubule stability and flexibility via the deacetylation of α-tubulin. It was of primary interest to us to follow the hypothesis that inhibiting the deacetylation of α-tubulin will lead to the maintenance in microtubule stability therefore reinstating VSMC contractility. With other HDACs also having various roles in cellular function, we wanted to specify which HDACs could have a beneficial effect on VSMC contractile response on rigid PAH. The unique use of PAH will also allow us to better understand the response of VSMCs in a healthy and diseased phenotype. Nuclear area was also analysed for all experiments in this chapter, this can be found in the appendix. The nucleus is also thought to function as a mechanosensor within the cell. In a contractile shape, the nucleus is elongated compared to a much rounder shape when in the synthetic state. (96) Alterations in its shape can lead to changes in chromatin structure and organisation, which, in turn, influence transcriptional regulation directly. Notably, nuclear morphology was found to be correlated with both cell shape and contractile function (224). The LINC complex connects the cytoskeleton to the nuclear envelope, this is essential in maintaining nuclear integrity, mechanotransduction and migration as external stresses can deform the nucleus (224, 225, 227, 228). Internally generated contractile stress also impacts nuclear shape in cardiac myocytes (229). This then raises the question as to whether these biophysical forces cause DNA damage over time. Collectively, these observations imply that nuclear mechanics are important regulators of cell contractility and phenotype which can then contribute to cardiovascular diseases such as hypertension and atherosclerosis. It is to be noted that we only saw nuclear changes when VSMCs were treated with Tubastatin A.

Before conducting these concentration response assay screenings, we conducted a vehicle control to ensure that DMSO had no effect on VSMCs. This is confirmed DMSO had no effect on VSMCs seeded on both 12 and 72kPa PAHs **(Appendix- Figure A1)**.

The table above (Figure 3.17) displays a general analysis of the effects of multiple HDAC inhibitors on VSMCs seeded on pliable and rigid PAH. HDAC 1,3 and 6 (Tubastatin A) inhibitors had the desired effect in reducing cell area on 72 kPa PAH.

Whilst there have been no studies on VSMC cell shape with HDAC inhibitors outside of the

Warren Lab, many have conducted research into the effects into proliferation and differentiation. Other HDAC inhibitors such as trichostatin A and Valproic acid have been seen to increase vimentin levels in endothelial cells which causes the development of the spindle shape associated with the mesenchymal cell phenotype (221).

The HDAC1 inhibitor shows great potential as a therapeutic drug for CVDs as it was able to reduce the cell area in VSMCs grown on rigid PAH (72 kPa) without affecting those on the pliable PAH. *Sun et al.* found that the downregulation of HDAC1 promoted contractile markers such as smooth muscle 22α and α-smooth muscle actin whilst simultaneously reducing VSMC migration (usually observed in the synthetic phenotype) (140). Our findings corroborate and develop on the previous work of *Sun et al.* especially regarding VSMC morphology in health and disease. These results support the targeted inhibition of HDAC1 as a viable therapeutic research avenue (141).

It is to be noted that we could further reduce the lowest concentration of HDAC3 inhibitor, RGFP966, as we are seeing a smaller cell area on 72kPa compared to other HDAC inhibitor concentration responses at the lowest concentration e.g compared to Santacruzamate A (72kPa). This suggests that we could be observing an effect as low as 0.01 μM. HDAC3 inhibitor showed a decrease in cell area of VSMCs on 12 kPa PAH at the highest concentration (100 μM). The effect of reducing cell area of VSMCs on the pliable PAH is undesirable as it would be perturbing the regular functions of a healthy VSMC. If such a drug was used within the body, one could expect the drug to affect both healthy and diseased VSMCs potentially creating adverse reactions and contributing to the diseased mechanism. In previous studies it has been suggested that the downregulation of HDAC3 reduces cell migration and proliferation, however, knowledge on the exact mechanism remains limited. Research has been conducted on the potential of HDAC3 having a major role in atherosclerosis such as promoting the inflammatory response and atherosclerotic plaque stability. Other studies have concluded that HDAC3 is essential in SMC differentiation as it regulates the SMC regulatory gene, Jagged1 (220) could push the SMC into the synthetic phenotype. In our research, we find that the inhibition of HDAC3 maintains the contractile phenotype on pliable PAHs and reverts the VSMCs to the contractile phenotype on the rigid PAHs. Nevertheless, studies of the effects on VSMCs themselves remain undocumented (135).

HDAC6 is unique amongst HDAC enzymes as it primarily resides in the cytosol and can deacetylate non-histone proteins. Unlike other HDACs, it features two catalytic domains and a

zinc-finger ubiquitin-binding domain (Zf-UBD) (218) .Tubastatin A is a hydroxamic acid based HDAC6 inhibitor that targets and binds to the zinc ion in the active site of HDAC6. BRD9757 is a concise hydroxamic acid with no surface binding group like Tubastatin A. This means that BRD9757 does not interact with the surface rim of the active site, reducing histone H3 acetylation which increases HDAC6 specific selectivity (219). Interestingly both HDAC6 inhibitors did not have the same effect on VSMCs. HDAC6 inhibitor, BRD9757 had no effect on either PAH stiffness whereas Tubastatin A influenced both cell areas. This could be explained by differences in molecular design and its promotion of different binding sites. BRD9757 has not been extensively researched thus far, due to is novel design so we are not yet able to compare to other studies. HDAC6 is microtubule specific, therefore we hypothesised it would influence VSMC contractility therefore area (142). Other studies suggest that the contractile protein α-smooth muscle actin is maintained when HDAC6 is inhibited by Tubastatin A. This same study suggested that HDAC3 reduced contractile marker proteins, which opposed our results previously discussed (143). Zhang et al. found that HDAC6 inhibitor, Tubastatin A was able to maintain α-SMC actin in VSMCs even when stimulated with platelet-derived growth factor-BB (223). The reduction in hypertrophic-like response in our study when treated with Tubastatin A on VSMCs seeded on rigid PAHs correlates with this study.

HDAC6 inhibition has previously exhibited a beneficial effect in alleviating hypertension whilst providing a cardioprotective effect (144–146). This result suggests that HDAC6 regulation of microtubule dynamics plays a role on disease mechanisms in VSMCs. The role of HDAC6 in cardiovascular diseases specifically hypertrophy remains a controversy as other work did not detect expressed levels in hypertrophic hearts of exercised adult mice. Additionally, some work found that the inhibition or knockdown of HDAC6 did not alleviate angiotensin II induced hypertension, however, did prevent kidney fibrosis *in vitro* and *in vivo* (147).

In contrast, SIRT2 demonstrated a further cell area increase on 72 kPa PAH, however these are preliminary results subject to change upon repeats. Research shows that SIRT2 activity is beneficial to vascular health. *Zhang et al* found that SIRT2 is depleted in ageing resulting in increased vessel stiffness due to ECM remodeling. With the use of old wild-type (WT) and *SIRT2-KO* mice, they found that this reduction in SIRT2 levels enhanced vascular ageing. In fact, SIRT2 has been linked by a few research groups for suppressing age-related functional decline in multiple organs (148–150).

Further research is needed to understand the role of SIRT2 in CVD to be able to certify its role in repressing age-induced vascular stiffness.

Another notable effect was the decrease in cell area when treated with a HDAC2 inhibitor. This only affected the VSMCs seeded on the pliable PAH (12 kPa) (132). This result reveals that it may not have potential as a therapeutic agent against CVD as VSMCs on rigid ECM were left unaffected. The use of HDAC2 inhibition has been explored in neurodegenerative diseases, however, its use in CVD remains elusive. A a reduction in synapse number and learning impairment was observed in HDAC2- overexpressing mice. HDAC2 has also be reported as being upregulated in various cancers (151).

HDAC8, 6 (BRD9757) and SIRT1 seemingly had no effect on either PAH stiffness. HDAC8 tends to inhibit differentiation, so it was expected that it would have a beneficial effect in VSMCs on both PAHs (132). If the ability to inhibit differentiation was repressed, a HDAC8 inhibitor this would lead to the prevention of the synthetic (de- differentiated) phenotype. SIRT1 has been seen to repress VSMC proliferation by inducing cell cycle arrest in the G1/S phase (222). The effect of BRD9757 did not support the hypothesis that inhibiting HDAC6 would decrease cell area of VSMCs on 72 kPa PAHs. It was expected that the data would at least match the effect of Tubastatin A. To further draw a conclusion, we would have to perform siRNA mediated HDAC6 knockout to further understand its role in VSMC response to matrix rigidity (152). Studies have shown that sirtuins 1 has a role in inhibiting atherosclerosis. The presence of SIRT1 induces DNA repair and promotes DNA damage markers. Some studies suggest that SIRT1 represses VSMC apoptosis. It has been suggested that SIRT1 displays a protective effect in the vasculature. Similarly to SIRT2 it is associated with inhibiting cell ageing
(153). With this knowledge, it was expected that SIRT1 would have therapeutic effect in decreasing cell area in VSMCs cultured on 72 kPa PAHs.

3.5.1 Conclusion

This chapter demonstrates that HDACs play a role in manipulating VSMC contractility and morphology with some displaying more beneficial effects than others in disease. Some HDAC inhibitors presented expected effects in VSMCs deduced from previous literature. Although there have been major developments in the use of HDACs in diseases such as cancer and Alzheimer's, our knowledge in CVD remains extremely limited.

The data in this chapter provides a promising outlook to the use of HDAC inhibitors in CVD

specifically age-related hypertension and vascular stiffness. We hypothesise that VSMC contractility and therefore morphology is microtubule (MT)-related with

Tubastatin A having an impact on MT stability. As Tubastatin A induces MT hyperacetylation, we hypothesise that this will create an increase in MT stability allowing for effective actomyosin force generation on rigid ECM. The volume of VSMCs may impact stiffness and thereby compliance, the use of HDAC inhibitors will allow us to understand if volume is also impacted with area changes. As another age- related contribution to CVD is cell senescence it would be important to look at DNA damage levels. This can be done by measuring γH2AX and 53BP1 levels in treated VSMCs. In addition to this we know some HDACs are involved in cell cycle, apoptosis and the DNA damage response. This would allow us to categorise the explicit roles of HDAC in VSMC response to a rigid matrix. Further work with siRNA-mediated knockdowns will be able to provide us with a greater insight into the effective concentrations of HDAC inhibitors.

3.5.2 Limitations

Currently, our work is conducted on 2D PAHs. Although this model has benefits over seeding cells on rigid glass substrates, the cells will never mimic native vessel structures. As previously mentioned, vessels such as the aorta are made up of multiple layers with a complex ECM as well as the existence of cell-cell interactions with endothelial cells. To improve on our current model, we would have to produce at least a co-cultured system to mitigate the lack of crosstalk between cells that would exist *in vivo*. In addition to this VSMCs exist in layers *in vivo* so we can expect to miss key morphological and mechanical changes. Another important point to consider would be cell density as it plays a crucial role in cell behaviour especially in mechanosensitive cells like VSMCs. In our studies, we have simplified for single cell study to better understand the individual VSMC processes (128). Variations in cell density such as a high cell density, could lead to an increase in cell-cell interactions leading to increase in contractile responses (230). It is also possible that higher densities could have greater coordinated contractile patterns compared to more independent contraction with lower cell densities. Cell density can be controlled to an extent with seeding at certain confluency, however, cannot be exactly the same each time. Tubastatin (HDAC6) concentration response assay was imaged with an older microscope Zeiss LSM510-META which was later found to have incorrect pixel distance data which had to be manually scaled up to be in line with new confocal microscope Zeiss LSM908-airyscan. This could imply less accurate results although

the scaling should have mitigated any discrepancies.

Chapter 4: The role of HDAC3 and HDAC6 on smooth muscle cell response to matrix stiffness

4.1 Introduction

Quiescent VSMCs cultured on rigid polyacrylamide surfaces have smaller cell areas than to those on pliable PAHs. Upon treatment with a contractile agonist, such as angiotensin II, we see that cells on the rigid PAHs have a greater cell area. These findings show that actomyosin force generation induces morphological changes on rigid PAHs. In the previous chapter we can see that HDACs play a role in VSMC matrix rigidity response. We can deduce that some HDACs have a greater beneficial role than others in restoring VSMC morphology. The mechanisms and further implications of HDACs remain unknown in VSMCs. The screening data presented in *chapter 3* indicated that HDAC3 and HDAC6 exhibited potential in altering VSMC matrix rigidity response. This chapter focuses on these two different HDACs and their effect on VSMC responses to matrix rigidity.

Actomyosin force generation may cause further impacts on other functions of the VSMC, such as microtubule stability or inducing DNA damage. In this chapter we will delve into the discovery of the role of HDAC3 and HDAC6 on these cellular functions. Microtubules compose a part of VSMCs cytoskeleton and are essential in providing structural support as well as aiding in cell division, transport, and cell signalling (94,154–156). Arguably, microtubules are a key determinant of VSMC contraction as they provide a pivotal role in impacting distribution and activity of ion channels and pumps that allow for the intracellular flux of calcium ions (157,158). They are crucial for the dynamic control of vascular tone as depolymerisation can increase VSMC contractility and force production (159). The unique characteristic that allows for the above functions of a microtubule is known as dynamic instability enabling rapid polymerisation and depolymerisation (94,127). A study has found that the overexpression of HDAC6 induced the depolymerisation of MTs which suggests it plays a key role in MTS (160).

In diseases like cancer, lung disorders, and neurological conditions, inhibiting HDAC6 has demonstrated therapeutic potential by inducing the acetylation of tubulin, leading to the stabilisation of microtubules (66,161). The reduction or inhibition of HDAC6 through siRNA-mediated knockdown resulted in enhanced tubulin acetylation in

transgenic mice expressing mutated αB-crystallin. This expression is only seen in cardiomyocytes during desmin-related cardiomyopathy. Tubulin acetylation was associated with a mitigation of the formation of detrimental protein aggregates that occurs in this disease. It remains a possibility that a beneficial effect of HDAC6 inhibition will be seen in vascular diseases and it is of paramount importance to research the roles of HDAC6 in VSMCs (65). In another study the inhibition of HDAC6 through Tubastatin A resulted in a significant increase of tubulin acetylation in C2C12 myotubes, it also showed an increase in MT acetylation confirming it is specific enough to target MTs in muscle cells (162). Tubastatin A is HDAC6 specific and has not shown any significant toxicity which highlights its potential in being a therapeutic drug if successful (163,164). P53 is a known transcription factor which when activated induces cell cycle arrest, apoptosis, and DNA repair. P53 can inhibit cell proliferation in VSMC which is beneficial in diseases such as atherosclerosis or in other types of vascular injury. The activation of P53 can also lead to an increase in senescent VSMCs. P53 activation has been seen to promote mitochondrial dysfunction which is normally seen as a result of ageing (165). It has been found that HDAC6 is a specific deacetylase of P53 suggesting it may play a role in DNA damage repair (DDR). It was found that through genetic ablation of HDAC6 there was an increase in K120 acetylation of P53 which resulted the dysfunction of mitochondria and apoptosis in mouse mesenchymal stem cells. It has also been seen that the inhibition of HDAC6 caused the acetylation of P53 which had an anticancer effect (166,167). These effects highlight the use of specific HDAC inhibition as a therapeutic effect in cancer, but it remains elusive in VSMC and CVD.

As seen in the previous chapter we can identify HDAC3 inhibition as a potential target to restore the healthy phenotype in VSMCs. However, to determine that HDAC3 has a completely beneficial role we would have to investigate further into its role in various VSMC functions. Other research groups have found that the lack of HDAC3 led to increases in DNA double-chain rupture which affected cell proliferation (135). It has been found that the deletion of HDAC3 in macrophages enables them to increase collagen by a change of phenotype. A similar role in VSMCs may contribute to ECM remodelling in the vasculature. In fact, the lack of HDAC3 in endothelial cells has been seen to accelerate the development of atherosclerosis and a reduction in cell survival.

This clearly suggests a detrimental effect, but other studies have found the opposite of increased HDAC3 expression in atherosclerotic lesions (135).

While the understanding of HDAC3/6 role in cells is still evolving, these emerging connections highlight their potential in VSMC and thereby vascular diseases. Further research is needed to fully elucidate the molecular mechanisms and specific pathways through which HDACs contribute to CVDs.

4.2 Hypothesis

We hypothesise that HDAC3 and HDAC6 inhibition will alter VSMC response to matrix rigidity. We expect that he inhibition of both HDACs will result in the decrease of cell area as well as volume. The decrease in cell/nuclear area and volume may reduce the stress placed on the nucleus and result in the reduction of DNA damage. We predict that HDAC6i via Tubastatin A will enhance tubulin acetylation and thereby microtubule stabilisation. It is expected that this alteration in response to matrix rigidity will reduce cell area and volume of VSMCs seeded on a rigid matrix.

4.3 Aims

The objective of the experiments in this chapter are:

1. To determine the impact of HDAC3 and HDAC6 inhibition on VSMC morphology on both pliable and rigid matrices.

2. To further understand the impact of HDAC3 inhibition on microtubule stability and early/ late DNA damage markers in VSMCs on pliable and rigid matrices.

3. To effectively knockdown HDAC6 levels in VSMCs and understand their impact on VSMC morphology.

4. To validate the effects of HDAC6 knockdown on DNA damage markers in VSMC seeded on a rigid PAHs.

4.4 Results

4.4.1 VSMC cell and nuclear area with RGFP966 treatment

Previous data included in Chapter 3 demonstrated that increasing concentrations of RGFP966 created morphological changes in VSMCs seeded on both pliable and rigid matrices. We saw that at high concentrations there were decreases in cell area of VSMCs seeded on 12 kPa PAHs. On 72 kPa PAHs this cell area decrease was achieved at lower concentrations. Our graphs showed an IC50 of approximately 1 μM on both PAHs therefore a working concentration of 10 μM was chosen as this was where a significant difference in cell area was observed. It was expected that no change in cell area would occur on a 12 kPa PAH, a cell area decrease was seen in VSMCs seeded on a 72 kPa PAH when treated with this HDAC3 inhibitor.

VSMCs seeded onto 12 kPa PAHs have no change in cell area when treated with RGFP966 compared to angiotensin II-only treatment **Figure 4.1(A&B)**. This is confirmed by an unpaired student's t-test. However, on 72 kPa PAHs, VSMCs possessed a smaller cell area when treated with RGFP966 **Figure 4.1(A &B)**. Furthermore, no significant changes can be seen in nuclear area **Figure 4.1(D &E)** between angiotensin II stimulated VSMCs treated with RGFP966 on both 12 kPa and 72 kPa PAHs.

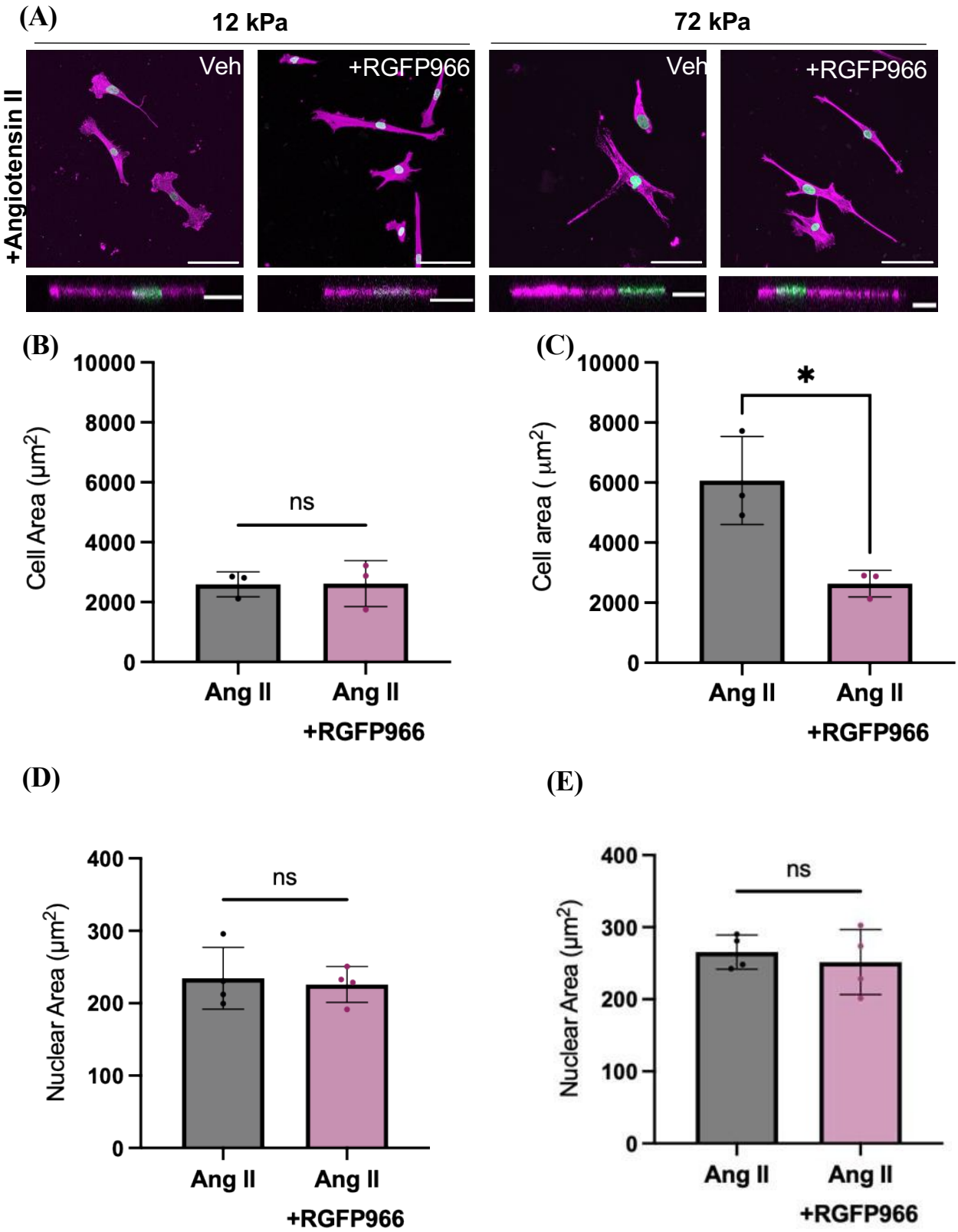
(A)
12 kPa
72 kPa
Veh
+RGFP966
Veh
+RGFP966
+Angiotensin II
(B)
Cell Area (µm²)
10000
8000
6000
4000
2000
0
ns
Ang II
Ang II
+RGFP966
(C)
Cell area (µm²)
10000
8000
6000
4000
2000
0
*
Ang II
Ang II
+RGFP966
(D)
Nuclear Area (µm²)
400
300
200
100
0
ns
Ang II
Ang II
+RGFP966
(E)
Nuclear Area (µm²)
400
300
200
100
0
ns
Ang II
Ang II
+RGFP966

Figure 4.1 VSMC cell and nuclear area with RGFP966 treatment (A) *Representative immunofluorescence images showing isolated VSMC cultured on 12 kPa and 72 kPa polyacrylamide PAHs actin cytoskeleton stained using rhodamine phalloidin (magenta) and corresponding nuclei stained with lamin A/C (green) when treated with 10μM of angiotensin II± 10μM RGFP966 for 1 hour. Scale bar represents 100μm. Orthogonal view of cell represents VSMC volume, scale bar of 20μM.* ***(B)*** *A graph to show mean cell area of VSMCs seeded on 12 kPa PAHs when treated with 10μM Angiotensin II ± 10μM RGFP966.* ***(C)*** *A graph to show mean cell area of VSMCs seeded on 72 kPa PAHs when treated with 10μM Angiotensin II ± 10μM RGFP966.* ***(D)*** *A graph to show mean nuclear area of VSMCs seeded on 12 kPa PAHs when treated with 10μM Angiotensin II ± 1μM Tubastatin A.* ***(E)*** *A graph to show mean nuclear area of VSMCs seeded on 72 kPa PAHs when treated with 10μM Angiotensin II ± 10μM RGFP966. Graphs show mean of independent experiments (coloured dots) as well as the mean of 3 independent experiments with approximately ≥70 cells analysed. Statistical significance was determined with an unpaired t-test (significant; ** $p \leq 0.01$, *** $p \leq 0.001$, **** $p \leq 0.0001$).*

4.4.2 VSMC cell and nuclear volume with RGFP966 treatment

Expanding on this, volume analysis was conducted on the same VSMCs **Figure 4.2(A- B)**. There was no difference in volume in VSMCs seeded on 12 kPa PAHs **Figure 4.2(A)**. Angiotensin II stimulated VSMCs on 72 kPa PAHs treated with RGFP966 displayed a significant decrease in volume **Figure 4.2(B)**. These results suggest that HDAC3 inhibition may have a positive role in reducing rigid matrix induced VSMC swelling. There was no significant difference in VSMC cell height on either PAH **Figure 4.2(E &F)**.

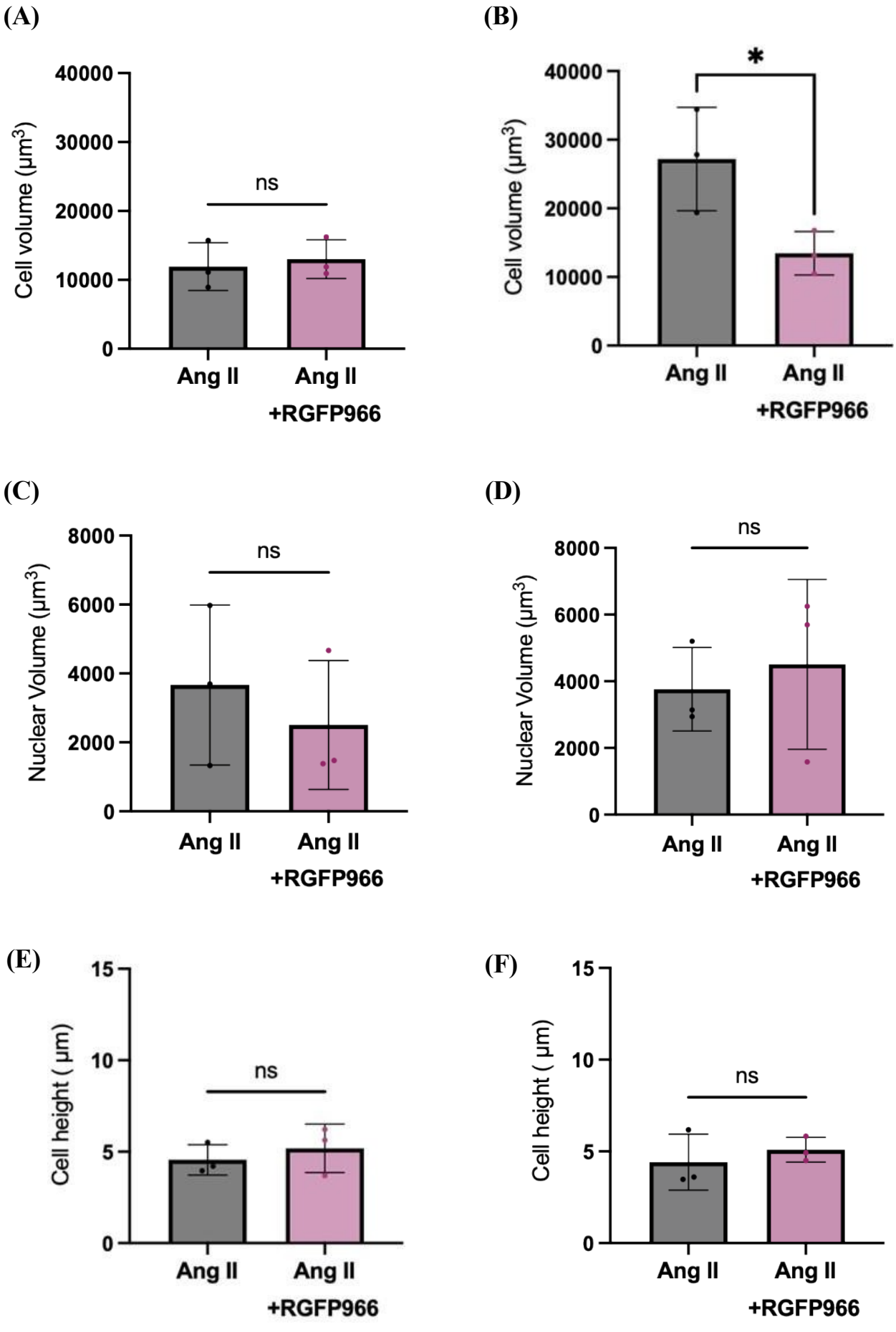
(A)
Cell volume (µm3)
40000
30000
20000
10000
0
ns
Ang II
Ang II +RGFP966
(B)
Cell volume (µm3)
40000
30000
20000
10000
0
*
Ang II
Ang II +RGFP966
(C)
Nuclear Volume (µm3)
8000
6000
4000
2000
0
ns
Ang II
Ang II +RGFP966
(D)
Nuclear Volume (µm3)
8000
6000
4000
2000
0
ns
Ang II
Ang II +RGFP966
(E)
Cell height (µm)
15
10
5
0
ns
Ang II
Ang II +RGFP966
(F)
Cell height (µm)
15
10
5
0
ns
Ang II
Ang II +RGFP966

Figure 4.2 VSMC cell and nuclear volume with RGFP966 treatment (A) *A graph to show mean cell volume of VSMCs seeded on 12 kPa PAHs when treated with 10μM Angiotensin II ± 10μM RGFP966.* ***(B)*** *A graph to show mean cell volume of VSMCs seeded on 72 kPa PAHs when treated with 10μM Angiotensin II ± 10μM RGFP966.* ***(C)*** *A graph to show mean nuclear volume of VSMCs seeded on 12 kPa PAHs when treated with 10μM Angiotensin II ± 10μM RGFP966.* ***(D)*** *A graph to show mean nuclear volume of VSMCs seeded on 72 kPa PAHs when treated with 10μM Angiotensin II ± 10μM RGFP966. Graphs show mean of each experiment (coloured dots) as well as the total mean of 3 independent experiments with approximately ≥70 cells analysed. Statistical significance was determined with an unpaired t- test (significant; ** p≤0.01, *** p≤0.001, **** p≤0.0001).*

4.4.3 Microtubule stability of VSMC with RGFP966 treatment

To determine if HDAC3 inhibition had any impact on microtubule stability in VSMCs, we performed a cold-stable microtubule assay. This experiment has only been conducted with this treatment once due to time constraints rather than the preferred standard of three repeats. I acknowledge the need for replication for these results to be validated to eliminate any uncertainty. Despite the lack of repetition, these findings suggested that there could be an increase in microtubule stability in angiotensin II stimulated VSMCs treated with RGFP966 treatment **(Figure4.3A-C)**.

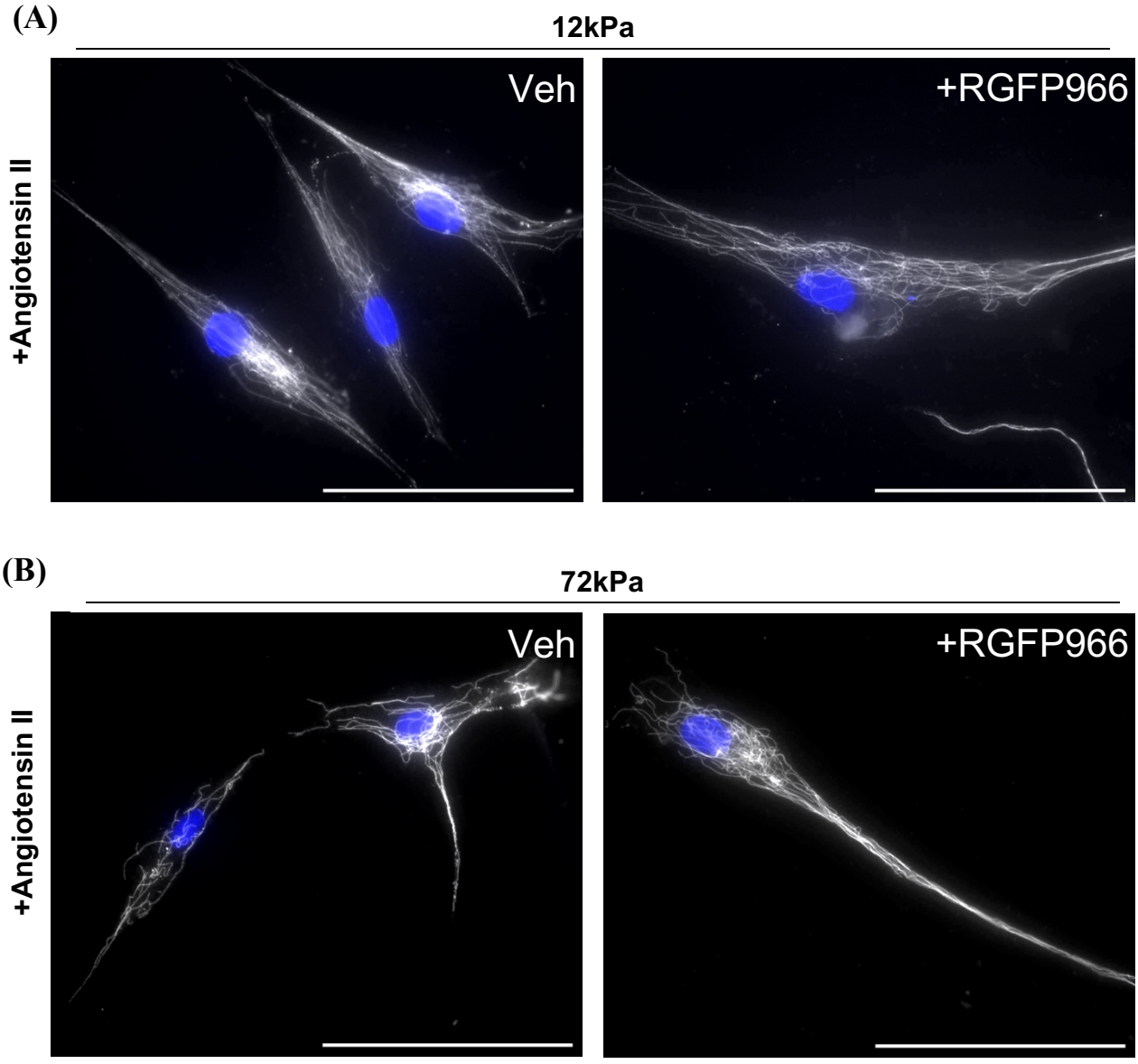

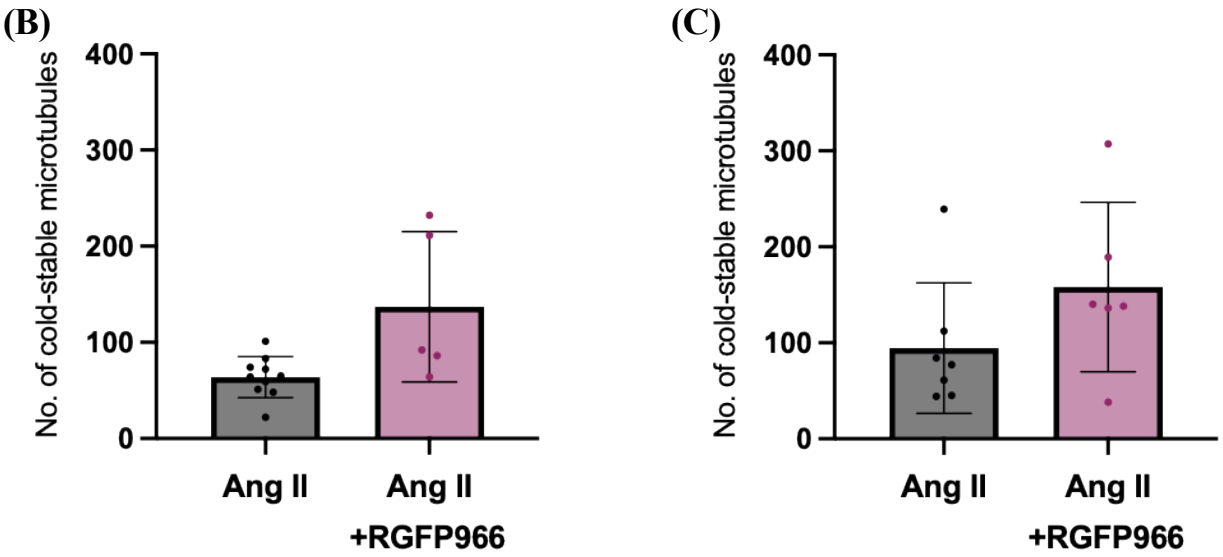

Figure 4.3 Microtubule stability of VSMC with RGFP966 treatment (A) *Representative images of cold-stable VSMC microtubules 10μM Angiotensin II ± 10μM RGFP966 treatment, actin cytoskeleton stained using rhodamine phalloidin (magenta) and corresponding nuclei stained with lamin A/C (green)* ***(B)*** *Bar graph representing number of cold-stable VSMC microtubules seeded on 12 kPa PAHs when treated with 10μM Angiotensin II ± 10μM RGFP966.* ***(C)*** *Bar graph representing number of cold-stable VSMC microtubules seeded on72 kPa PAHs when treated with 10μM Angiotensin II ± 10μM RGFP966. Graphs show individual cell values (coloured dots). 1 independent experiment with approximately ≥5 cells analysed.*

4.4.4 γH2AX levels detecting early DNA damage response in VSMCs with RGFP966 treatment

It is expected that VSMCs seeded on 12 kPa PAHs when stimulated with a contractile agonist, such as angiotensin II, will have low levels of DNA damage as they most represent VSMCs found in a healthy aorta. Furthermore, VSMCs seeded on 72 kPa represent a diseased phenotype and treatment of angiotensin II it is expected there will be DNA damage detected. This was confirmed by analysing levels of γH2AX levels. γH2AX signals DNA damage events that have occurred within cells as it is present at damaged sites, it is responsible for recruiting other repair proteins to the area.

Upon analysis there was no significant difference between γH2AX foci present in angiotensin II treated VSMCs seeded on 12 kPa PAHs ± RGFP966 treatment **Figure4.4(A&B)**. On 72 kPa PAHs, VSMCs possessed a greater number of γH2AX foci when treated with angiotensin II only to those on the pliable PAH **Figure4.4(A-C)**. Additionally, with RGFP966 treatment the number of γH2AX foci decreased significantly **(Figure4.4(A&C)**. This data suggests that a more rigid matrices not only introduces a difference in cell shape or size but also DNA damage, potentially impacting processes within the cell. RGFP966 may have beneficial effects in the early stages of DNA damage reducing the need to recruit repair proteins to the nucleus via γH2AX.

(A)

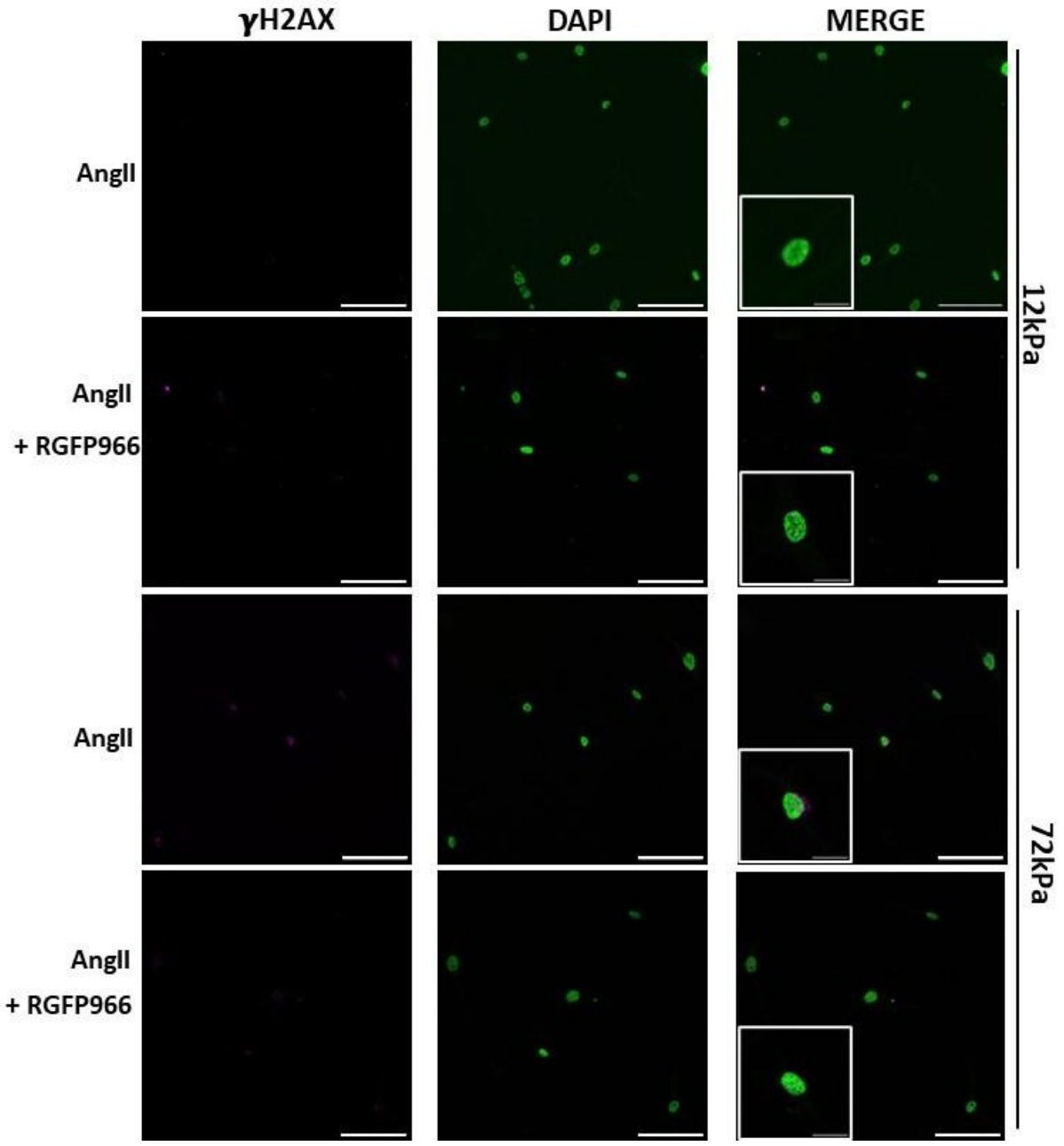
γH2AX
DAPI
MERGE
AngII
AngII
+ RGFP966
AngII
AngII
+ RGFP966
12kPa
72kPa

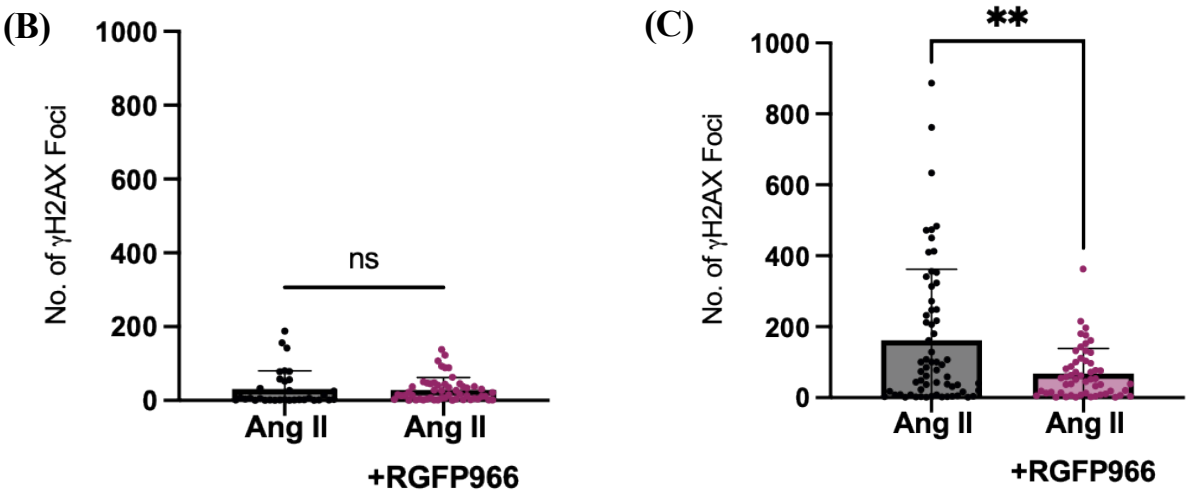

Figure 4.4 γH2AX levels in detecting early DNA damage response in VSMCs treated with RGFP966 (A) *Representative images of VSMC nuclei stained with γH2AX antibody (magenta), DAPI (blue) levels with merged column. Insets show zoomed VSMC nuclei.* ***(B)*** *Bar graph representing number of γH2AX foci on VSMC nuclei from VSMC seeded on 12 kPa PAHs when treated with 10μM Angiotensin II ± 10μM RGFP966.* ***(C)*** *Bar graph representing number of γH2AX foci on VSMC nuclei from VSMC seeded on 72 kPa PAHs when treated with 10μM Angiotensin II ± 10μM RGFP966. Graphs show individual cell values (coloured dots) as well as the mean of 3 independent experiments with approximately ≥52 nuclei analysed. Statistical significance was determined with an unpaired t-test (significant; ** p≤0.01, *** p≤0.001, **** p≤0.0001).*

4.4.5 53BP1 levels detecting DNA damage response in VSMCs with RGFP966 treatment

53BP1 is recruited after □H2AX, however, is still considered as an early-stage response to DNA damage in the nucleus. Compared to the □H2AX results, we expected that VSMCs seeded on 12 kPa PAHs will have a lower proportion of 53BP1 positive cells on 72 kPa. We also expected a similar response when co-treating with RGFP966 on both PAHs. Upon observation, we saw that there was a significant decrease in proportion of 53BP1+ cells when co-treated with HDAC3 inhibitor on the 12 kPa PAH **Figure4.5(A&B)**.

We saw a higher proportion of 53BP1+ nuclei in VSMCs seeded on 72 kPa. Statistical analysis via two-way ANOVA determined the increase to be significant between VSMCs seeded on 12 kPa and 72 kPa when treated with Angiotensin II only **Figure4.5(B&C)**. When VSMCs were co-treated with RGFP966 at working concentration there was no significant decrease (unpaired t-test) compared to Angiotensin II only treatment **Figure4.5(C)**. From this, it becomes apparent that the tensile strength of matrices that VSMCs are seeded on have an impact on the DNA damage response pathway. Rigidity of the 72 kPa PAH not only creates a hypertrophic- like response but this stretch also creates damage within the nucleus.

(A)

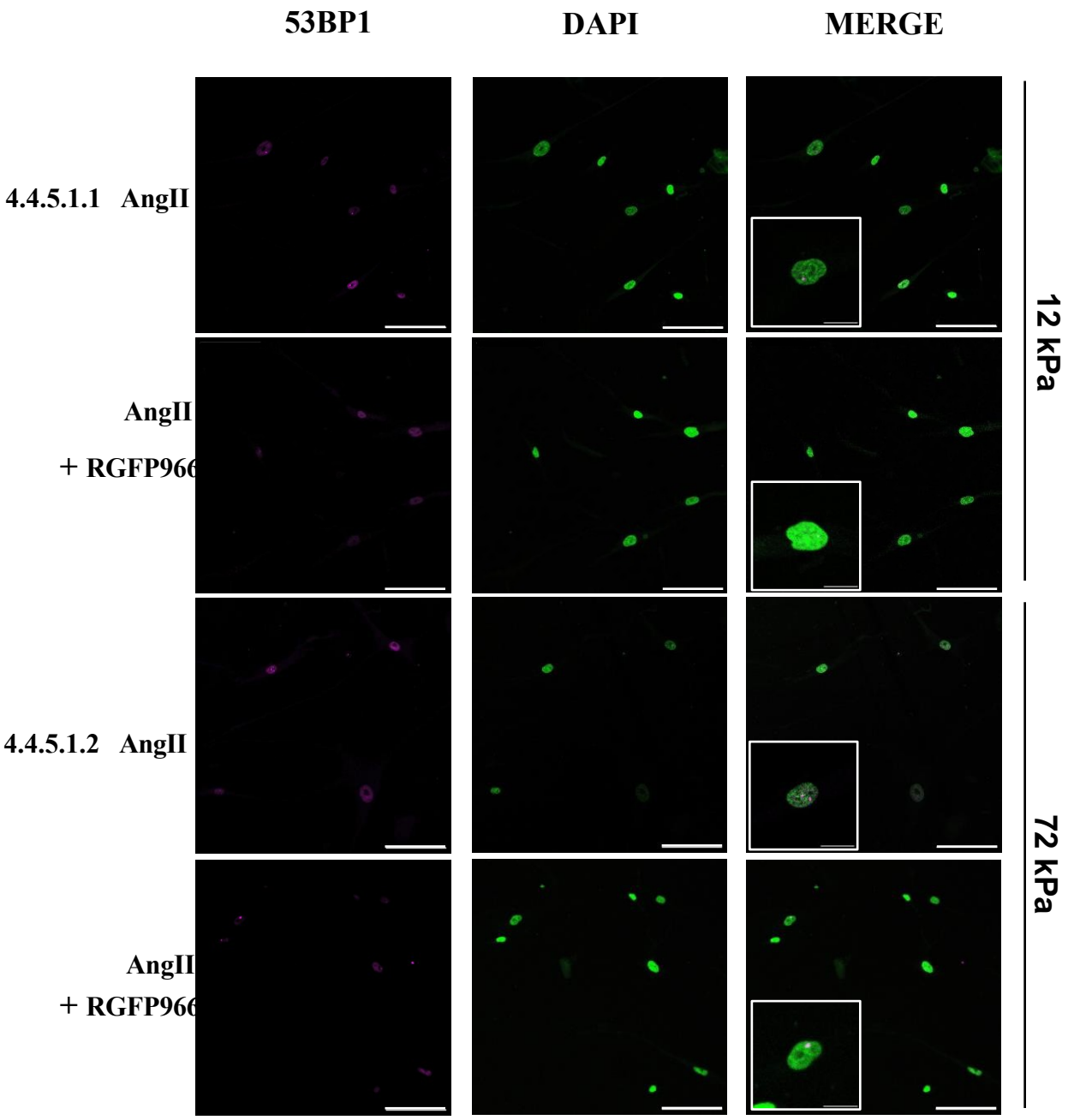
53BP1
DAPI
MERGE
4.4.5.1.1 AngII
AngII
+ RGFP966
4.4.5.1.2 AngII
AngII
+ RGFP966
12 kPa
72 kPa

(B)

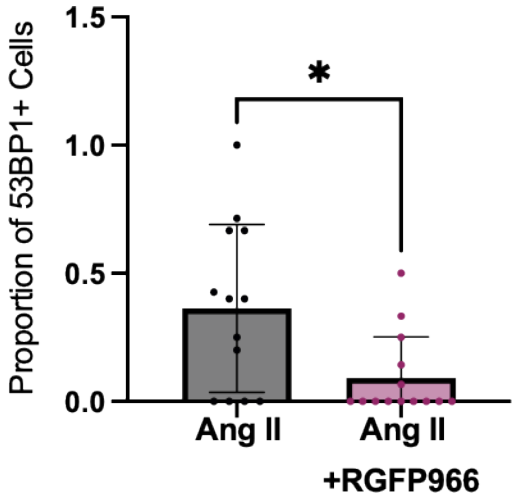

(C)

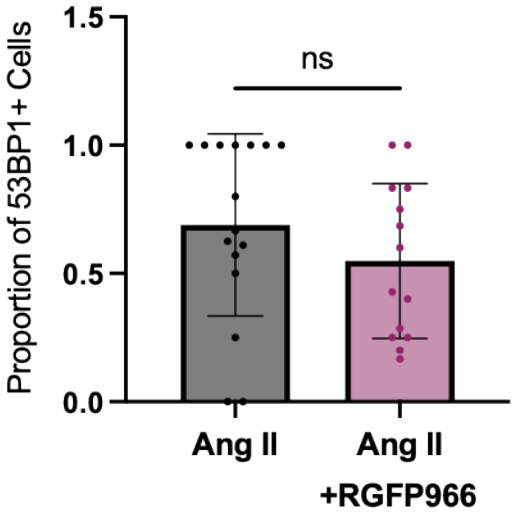

Figure 4.5 53BP1 levels detecting DNA damage in VSMC treated with RGFP966 (A) *Representative images of VSMC nuclei stained with 53BP1 antibody (magenta), DAPI (blue) levels with merged column. Insets show zoomed VSMC nuclei.* ***(B)*** *Bar graph representing proportion of 53BP1+ VSMC nuclei from VSMC seeded on 12 kPa PAHs when treated with 10μM Angiotensin II ± 10μM RGFP966.* ***(C)*** *Bar graph representing proportion of 53BP1+ VSMC nuclei from VSMC seeded on 72 kPa PAHs when treated with 10μM Angiotensin II ± 10μM RGFP966. Graphs show individual cell values (coloured dots) as well as the mean of 3 independent experiments with approximately ≥13 nuclei analysed. Statistical significance was determined with a unpaired t-test (significant; p≤ 0.05,** p≤0.01, *** p≤0.001, **** p≤0.0001).*

4.4.6 HDAC6 inhibition

To further investigate the role of HDAC inhibitors on aberrant VSMC spreading, we tested HDAC6 inhibitor, Tubastatin A. In the earlier chapter, we saw that Tubastatin inhibited the abnormal cell spreading of VSMCs seeded on 72 kPa PAH. We found that Tubastatin had an IC50 of 1 μM on VSMCs seeded on both tensile strength hydrogel. We decided of a working concentration of Tubastatin to be 1 □M to ensure reliable and effective inhibition of HDAC6 within the cells. We found that at this concentration we observed a cell response (in our concentration dose response assay) without any cytotoxic effects indicating it was too high. This is verified by a live/dead assay in the appendix. Hyperacetylation of α-tubulin occurs at 2.5 μM with hyperacetylation of the histone occurring with a 10 μM treatment.

4.4.7 Acetylated alpha tubulin levels via HDAC6 inhibition with Tubastatin A

To ascertain the efficacy of Tubastatin A on VSMCs we measure the acetylated α- tubulin levels relative to GAPDH and α-tubulin. As the major substrate of HDAC6 is α-tubulin, it is expected that upon inhibition the acetylation of this substrate would occur. A representative western blot can be seen in **Figure 4.6(A)** which shows the bands produced upon treatment with various concentrations of Tubastatin A. It is apparent that Tubastatin A increase acetylated α-tubulin in a dose dependent manner, there is especially increased acetylation of α-tubulin especially at levels of 10^{-6}M-10^{-4}M.

(A)

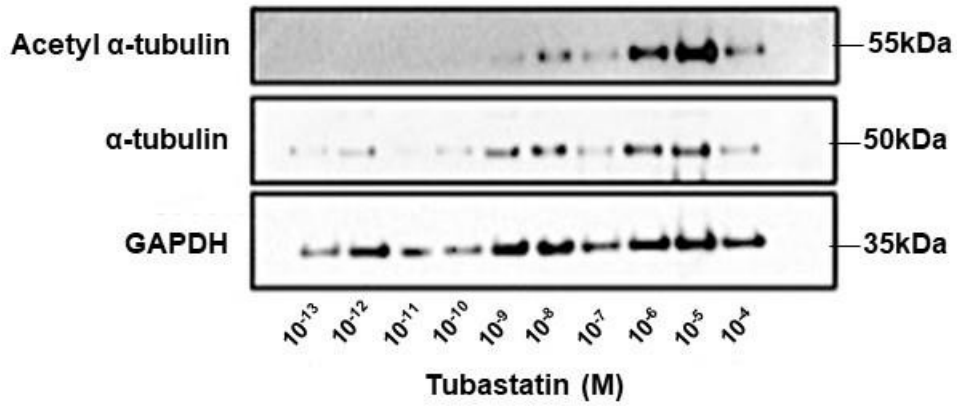

Figure 4.6 Acetylated alpha tubulin levels via HDAC6 inhibition with Tubastatin A (A) *Representative western blot image to show acetyl α-tubulin, α-tubulin and GAPDH levels with increasing levels of Tubastatin.*

4.4.8 VSMC cell and nuclear area with Tubastatin A treatment

Moving on from HDAC3 inhibition, we wanted to further comprehend the role of HDAC6 in VSMCs as it displayed a role in decreasing cell area in a dose dependent manner in the previous chapter. We treated VSMCs with Angiotensin II 10 μM, Tubastatin 1 μM seeded on both 12 kPa and 72 kPa PAHs. Upon observation, we saw a different effect to that in Chapter 3, specifically in **Figures 3.9-3.10**. This could be attributed to the concentration dose response assays were imaged using an older microscope (Zeiss LSM510-META) which did not have the correct pixel distance configuration resulting in having to manually scale up some data to match that imaged on the confocal microscope (Zeiss LSM908-Airyscan) which replaced it. This could have contributed to having different results between the concentration dose response assay and that at working concentration of Tubastin A. **Figure 4.7(A-B)** there was a decrease in cell area when VSMCs seeded on 12 kPa PAHs were co-treated with Tubastatin. In **Figure 4.7(D)** although there was a small decrease to nuclear area when treated with Tubastatin there was no significant difference when a t-test was performed. **Figure 4.7(C)**, cell area was also reduced on VSMCs on 72 kPa. There was no change in nuclear area of VSMCs seeded on 72 kPa PAHs, confirmed with no significant difference detected. It is also important to point out that we are continually seeing the trend of VSMCs on rigid PAHs being much more hypertrophic-like in nature when treated with angiotensin II only.

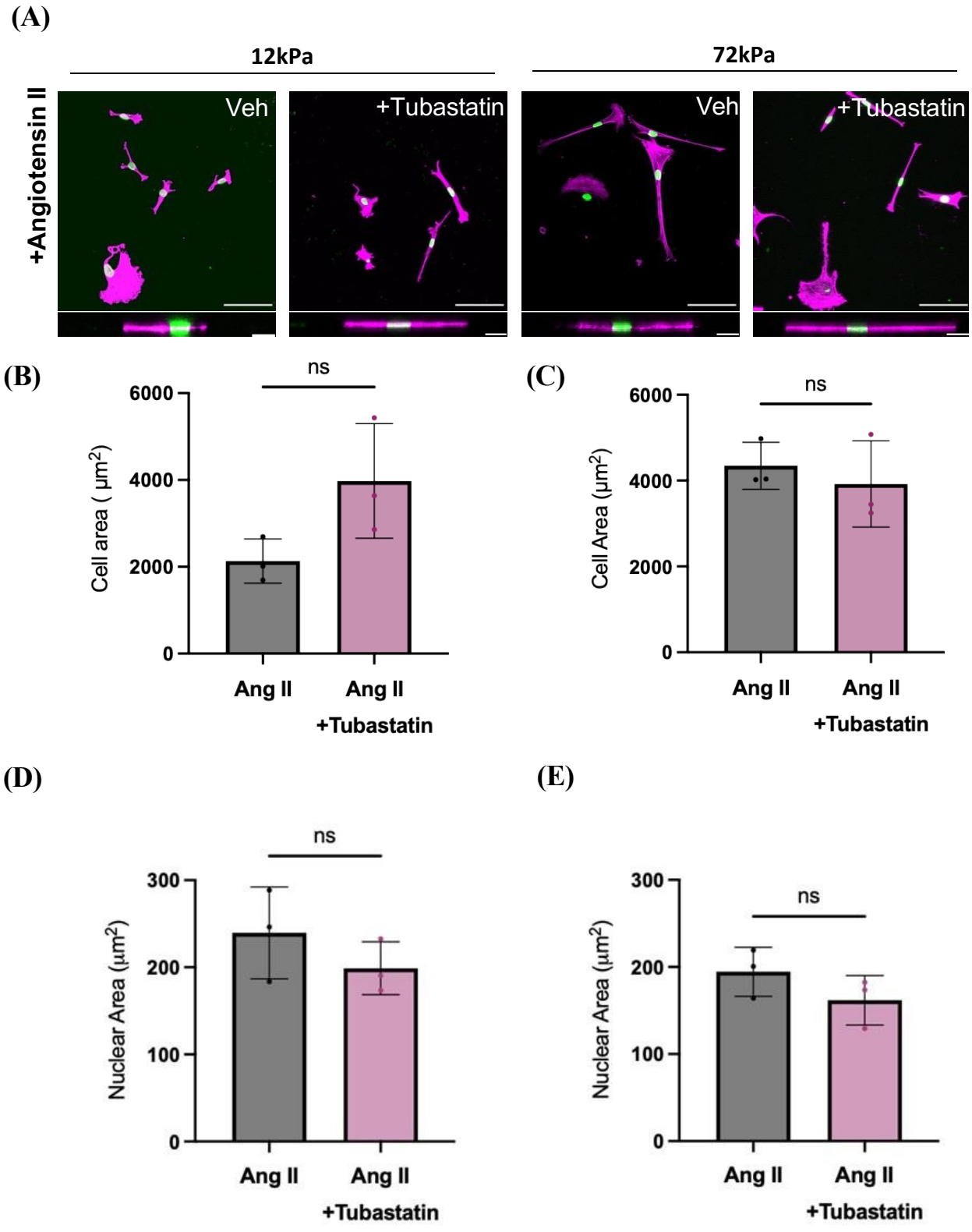
(A)
12kPa
72kPa
+Angiotensin II
Veh
+Tubastatin
Veh
+Tubastatin
(B)
ns
Cell area (µm2)
6000
4000
2000
0
Ang II
Ang II
+Tubastatin
(C)
ns
Cell Area (µm2)
6000
4000
2000
0
Ang II
Ang II
+Tubastatin
(D)
ns
Nuclear Area (µm2)
300
200
100
0
Ang II
Ang II
+Tubastatin
(E)
ns
Nuclear Area (µm2)
300
200
100
0
Ang II
Ang II
+Tubastatin

Figure 4.7 VSMC cell and nuclear area with Tubastatin A treatment (A) *Representative immunofluorescence images showing isolated VSMC cultured on 12 kPa and 72 kPa polyacrylamide PAHs actin cytoskeleton stained using rhodamine phalloidin (magenta) and corresponding nuclei stained with lamin A/C (green) when treated with 10μM of angiotensin II ± 1μM Tubastatin A for 1 hour. Scale bar represents 100μm.* ***(B)*** *A graph to show mean cell area of VSMCs seeded on 12 kPa PAHs when treated with 10μM Angiotensin II ± 1μM Tubastatin A.* ***(C)*** *A graph to show mean cell area of VSMCs seeded on 72 kPa PAHs when treated with 10μM Angiotensin II ± 1μM Tubastatin A.* ***(D)*** *A graph to show mean nuclear area of VSMCs seeded on 12 kPa PAHs when treated with 10μM Angiotensin II ± 1μM Tubastatin A.* ***(E)*** *A graph to show mean nuclear area of VSMCs seeded on 72 kPa PAHs when treated with 10μM Angiotensin II ± 1μM Tubastatin A. Graphs show individual cell values (coloured dots) as well as the mean of 3 independent experiments with approximately ≥70 cells analysed. Statistical significance was determined with an unpaired t-test (significant; ** p≤0.01, *** p≤0.001, **** p≤0.0001).*

4.4.9 VSMC cell and nuclear volume with Tubastatin A treatment

To investigate this further, we measured VSMC and nuclear volume of the same cells analysed in Figure 4.7. In **Figure 4.8(A)** we observed that treatment with Tubastatin A on VSMCs seeded on 12 kPa PAHs experienced a significant increase in cell volume in comparison to angiotensin II only treatment. VSMCs on the rigid PAHs **Figure 4.8(B)** had a slightly larger cell volume when treated with Tubastatin A but there was no significant difference. There was no significant difference in nuclear volume on either PAH when treated with Tubastatin A **Figure 4.8(C&D)**. There was also no significant difference in cell height **Figure 4.8(E&F)**. When comparing 12 kPa and 72 kPa angiotensin II only treatment, there is an increase on the rigid matrix.

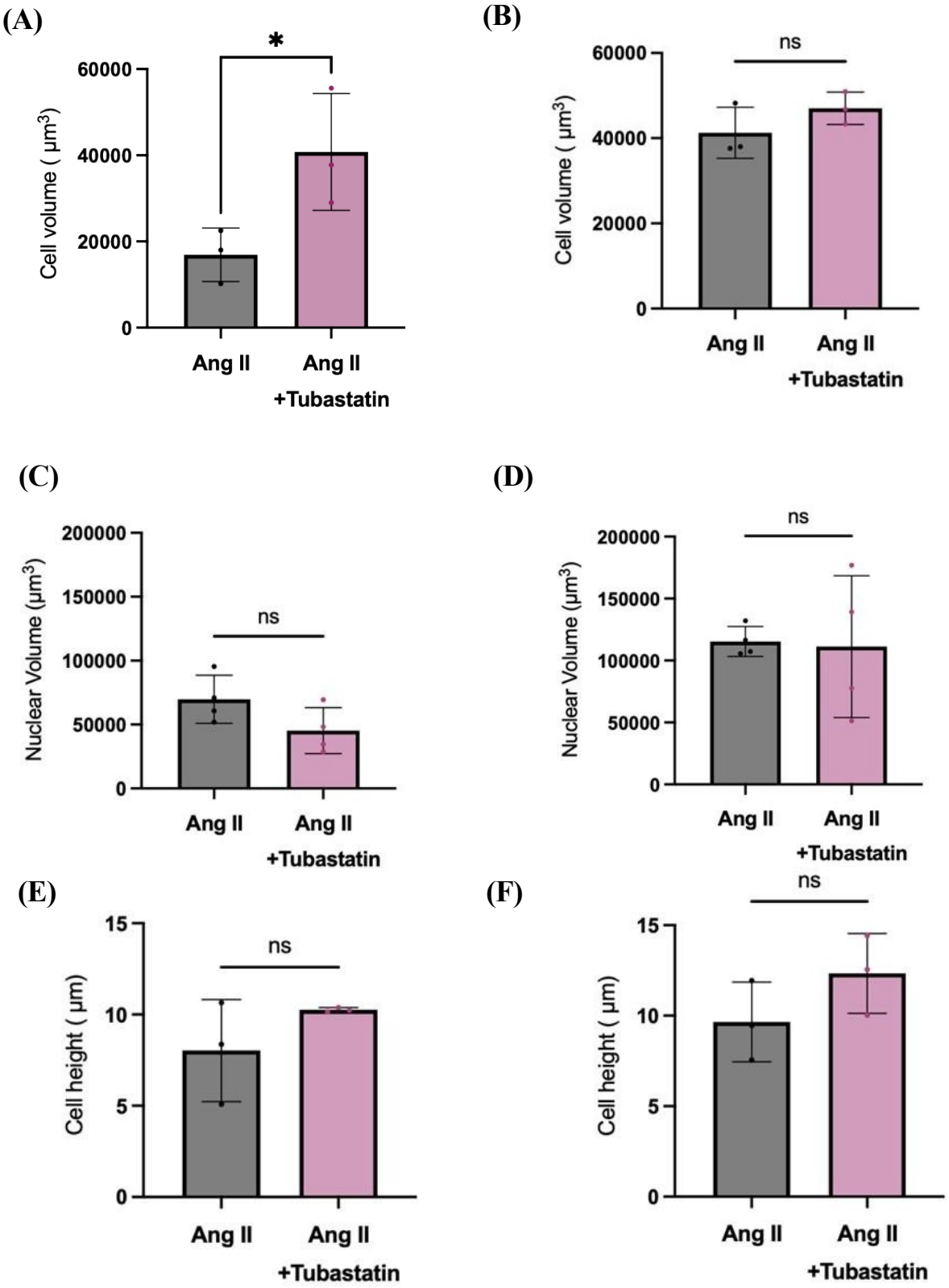
(A)
*
Cell volume (µm3)
60000
40000
20000
0
Ang II
Ang II
+Tubastatin
(B)
ns
Cell volume (µm3)
60000
40000
20000
0
Ang II
Ang II
+Tubastatin
(C)
Nuclear Volume (µm3)
200000
150000
100000
50000
0
ns
Ang II
Ang II
+Tubastatin
(D)
ns
Nuclear Volume (µm3)
200000
150000
100000
50000
0
Ang II
Ang II
+Tubastatin
(E)
ns
Cell height (µm)
15
10
5
0
Ang II
Ang II
+Tubastatin
(F)
ns
Cell height (µm)
15
10
5
0
Ang II
Ang II
+Tubastatin

Figure 4.8 VSMC cell and nuclear volume with Tubastatin A treatment (A) *A graph to show mean cell volume of VSMCs seeded on 12 kPa PAHs when treated with 10μM Angiotensin II ± 1μM Tubastatin A.* ***(B)*** *A graph to show mean cell volume of VSMCs seeded on 72 kPa PAHs when treated with 10μM Angiotensin II ± 1μM Tubastatin A.* ***(C)*** *A graph to show mean nuclear volume of VSMCs seeded on 12 kPa PAHs when treated with 10μM Angiotensin II ± 1μM Tubastatin A.* ***(D)*** *A graph to show mean nuclear volume of VSMCs seeded on 72 kPa PAHs when treated with 10μM Angiotensin II ± 1μM Tubastatin A.* ***(E)*** *A graph to show mean cell height on 12 kPa PAHs when treated with 10μM Angiotensin II ± 1μM Tubastatin A.* ***(F)*** *A graph to show mean cell height on 72 kPa PAHs when treated with 10μM Angiotensin II ± 1μM Tubastatin A. Graphs show individual cell values (coloured dots) as well as the mean of 3 independent experiments with approximately ≥70 cells analysed. Statistical significance was determined with an unpaired t-test (significant; ** p≤0.01, *** p≤0.001, **** p≤0.0001).*

4.4.10 Microtubule stability of VSMCs with Tubastatin A treatment

To further understand the changed in cell shape and size we wanted to take a closer look at the microtubules within VSMCs. Analysing the number of cold-stable microtubules (CSMs) would allow us to understand if the cell increases or decreases with HDAC inhibition were driven by microtubules or another mechanism. It was observed that there was a significant decrease in CSMs when treated with Tubastatin A compared to Angiotensin II only in VSMCs seeded on 12 kPa PAHs **Figure 4.9(A&B)**. There was minimal change seen in VSMCs on 72 kPa PAHs with no significant difference between the two treatments **Figure 4.9(A&C)**. In general, there was a decrease in the total number of CSMs. There may be involvement of microtubules in the changes of cell area and volume in VSMCs treated with HDAC6 inhibitor, Tubastatin A.

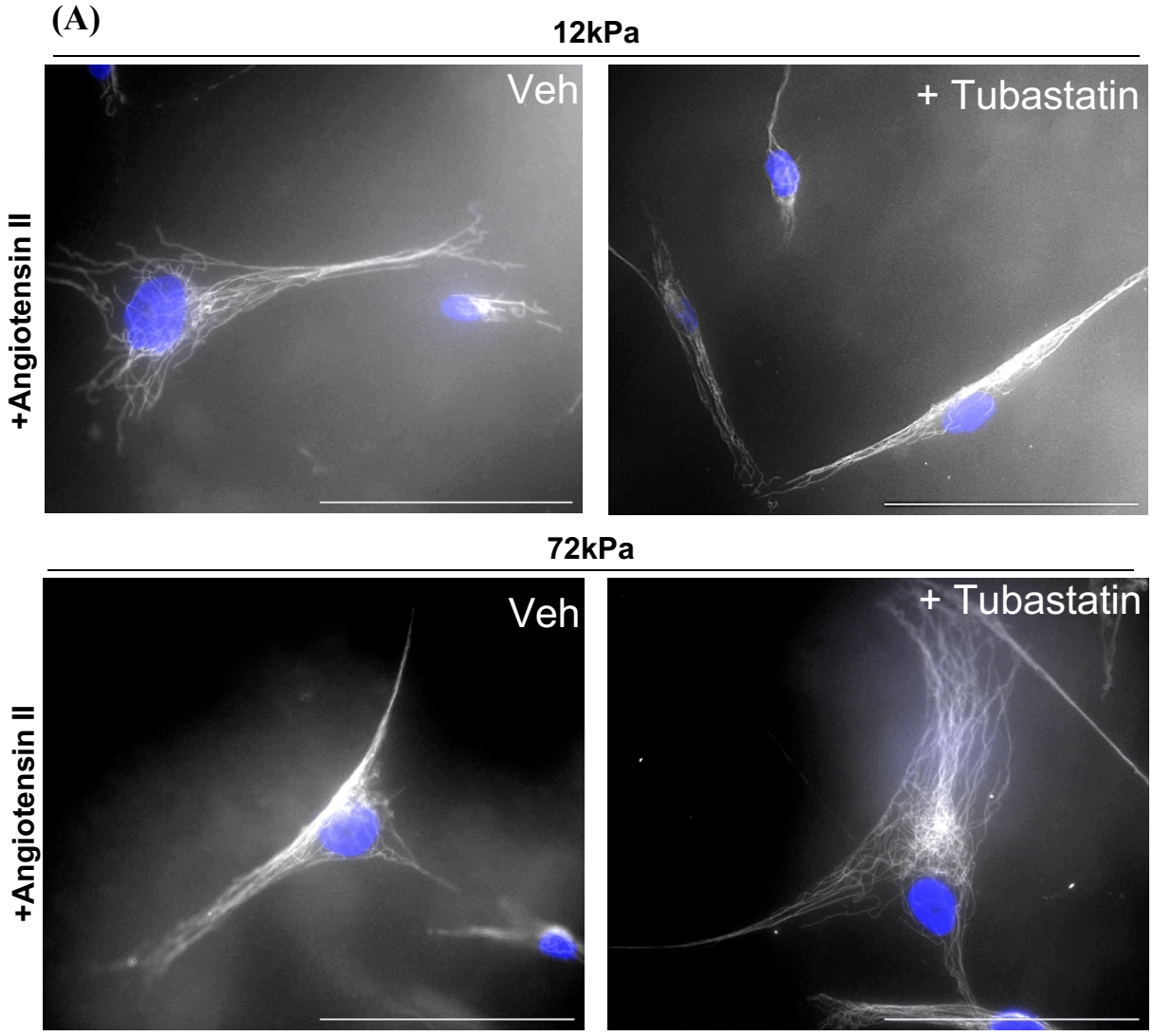

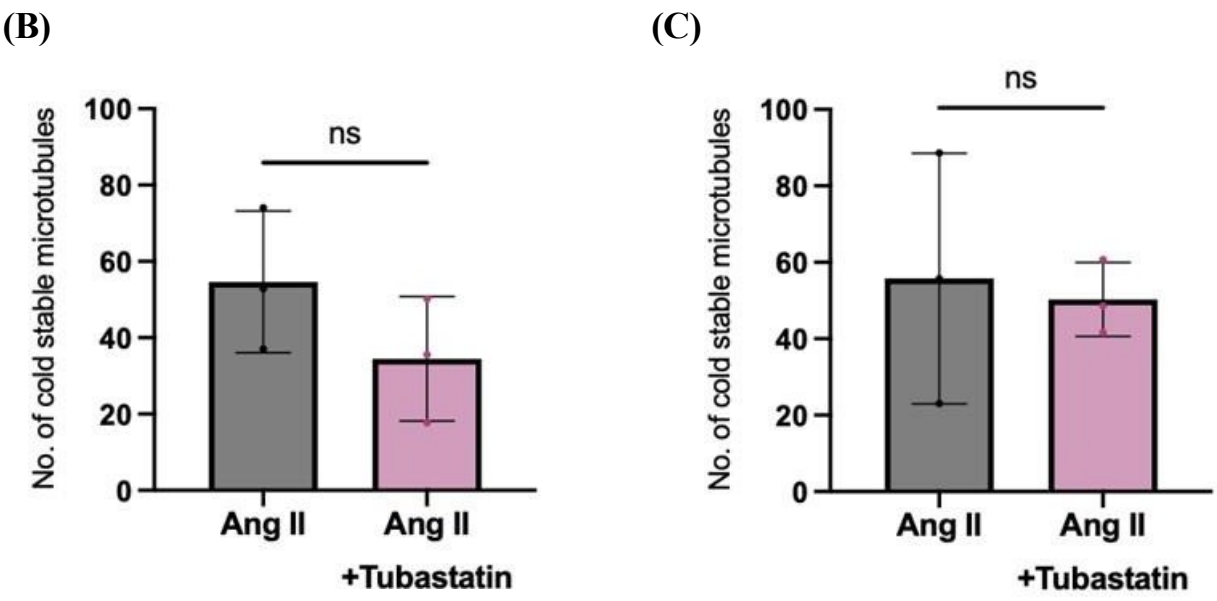

Figure 4.9 Microtubule stability of VSMC with Tubastatin A treatment ***(A)*** *Representative images of cold-stable VSMC microtubules 10μM Angiotensin II ± 1μM Tubastatin A treatment, actin cytoskeleton stained using rhodamine phalloidin (magenta) and corresponding nuclei stained with lamin A/C (green).* ***(B)*** *Bar graph representing number of cold-stable VSMC microtubules seeded on 12 kPa PAHs when treated with 10μM Angiotensin II ± 1μM Tubastatin A.* ***(C)*** *Bar graph representing number of cold-stable VSMC microtubules seeded on 72 kPa PAHs when treated with 10μM Angiotensin II ± 1μM Tubastatin A. Graphs show the mean of each independent experiment (coloured dots) as well as the mean of 3 independent experiments with approximately ≥61 cells analysed. Statistical significance was determined with an unpaired t-test (significant; ** p≤0.01, *** p≤0.001, **** p≤0.0001).*

4.4.11 H2AX levels detecting early DNA damage response in VSMCs with Tubastatin A treatment

We wanted to ascertain the levels of γH2AX within the VSMC nuclei to understand if any DNA damage was present or reduced with treatment of Tubastatin. We knew from a previous DNA damage assay with HDAC3i that VSMCs on 72 kPa exhibited more γH2AX foci. In this assay we saw a slight increase in DNA damage between angiotensin II only treatment on 12 and 72 kPa, however there was no significant difference between the two. On the 12 kPa PAH we saw that co-treatment of Tubastatin had a significant increase in the number of γH2AX foci indicating that there were greater levels of DNA damage **Figure 4.10(A-B)**. There were no significant changes on the number of γH2AX foci in VSMCs on 72 kPa PAH **Figure 4.10(A&C)** confirmed by an unpaired student's t-test. Tubacin, another HDAC6 inhibitor has been found to induce DNA damage which was verified by an increase in γH2AX foci (168).

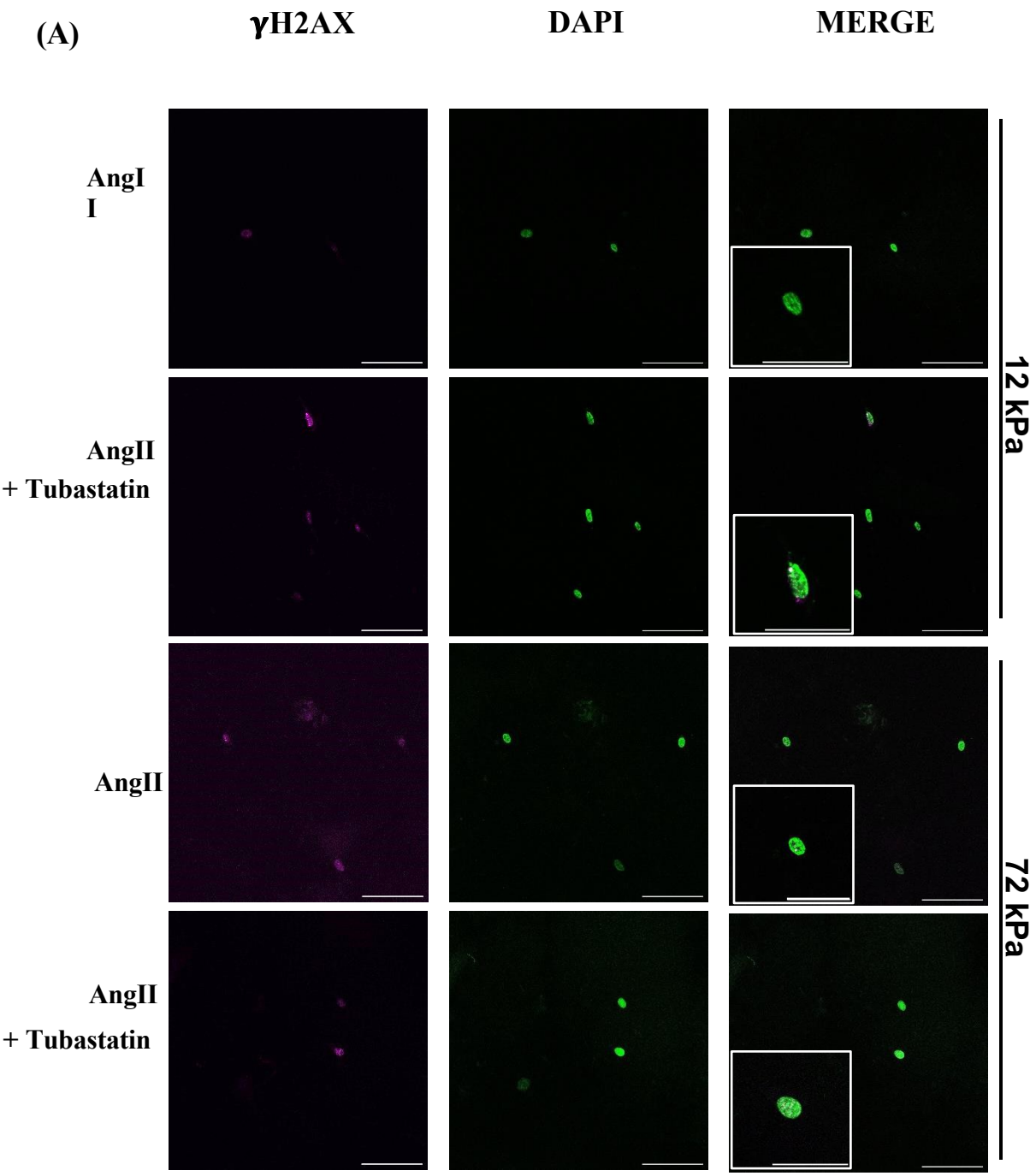
(A)
γH2AX
DAPI
MERGE
AngI
I
AngII
+ Tubastatin
AngII
AngII
+ Tubastatin
12 kPa
72 kPa

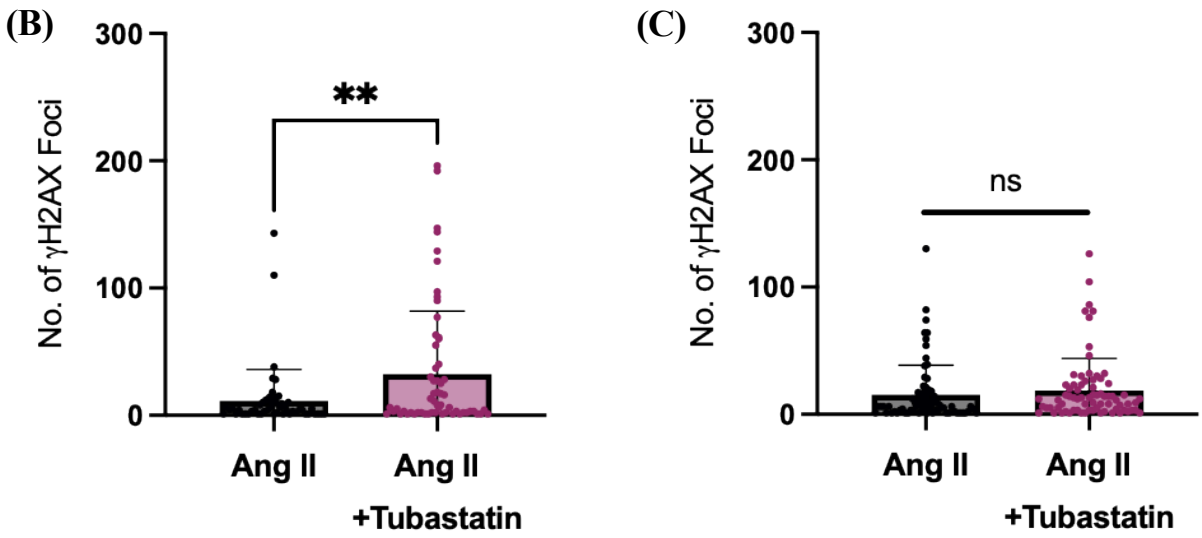

Figure 4.10 γH2AX levels detecting early DNA damage response in VSMCs with Tubastatin A treatment *(A) Representative images of VSMC nuclei stained with γH2AX antibody (magenta), DAPI (blue) levels with merged column. Insets show zoomed VSMC nuclei.* ***(B)*** *Bar graph representing number of γH2AX foci on VSMC nuclei from VSMC seeded on 12 kPa PAHs when treated with 10μM Angiotensin II ± 1μM Tubastatin A.* ***(C)*** *Bar graph representing number of γH2AX foci on VSMC nuclei from VSMC seeded on 72 kPa PAHs when treated with 10μM Angiotensin II ± 1μM Tubastatin A. Graphs show individual cell values (coloured dots) as well as the mean of 3 independent experiments with approximately ≥52 nuclei analysed. Statistical significance was determined with an unpaired t-test (significant; ** p≤0.01, *** p≤0.001, **** p≤0.0001).*

4.4.12 53BP1 levels detecting DNA damage response in VSMCs with Tubastatin A treatment

As previously performed with HDAC3i RGFP966, a 53BP1 assay was carried out with Tubastatin A treatment at working concentration of 1 μM. We can see a similar trend of increase in DNA damage presence in VSMCs seeded on 12 kPa PAHs **Figure 4.11(A&B)** when treated with Tubastatin A compared to Angiotensin II only. On 72 kPa PAHs **Figure 4.11(A&C)** we see a small decrease in DNA damage presence compared to Angiotensin II only treated VSMCs, however, this is statistically insignificant. These results confirm the trend seen number of □H2AX foci in VSMCs on 12 and 72 kPa PAHs.

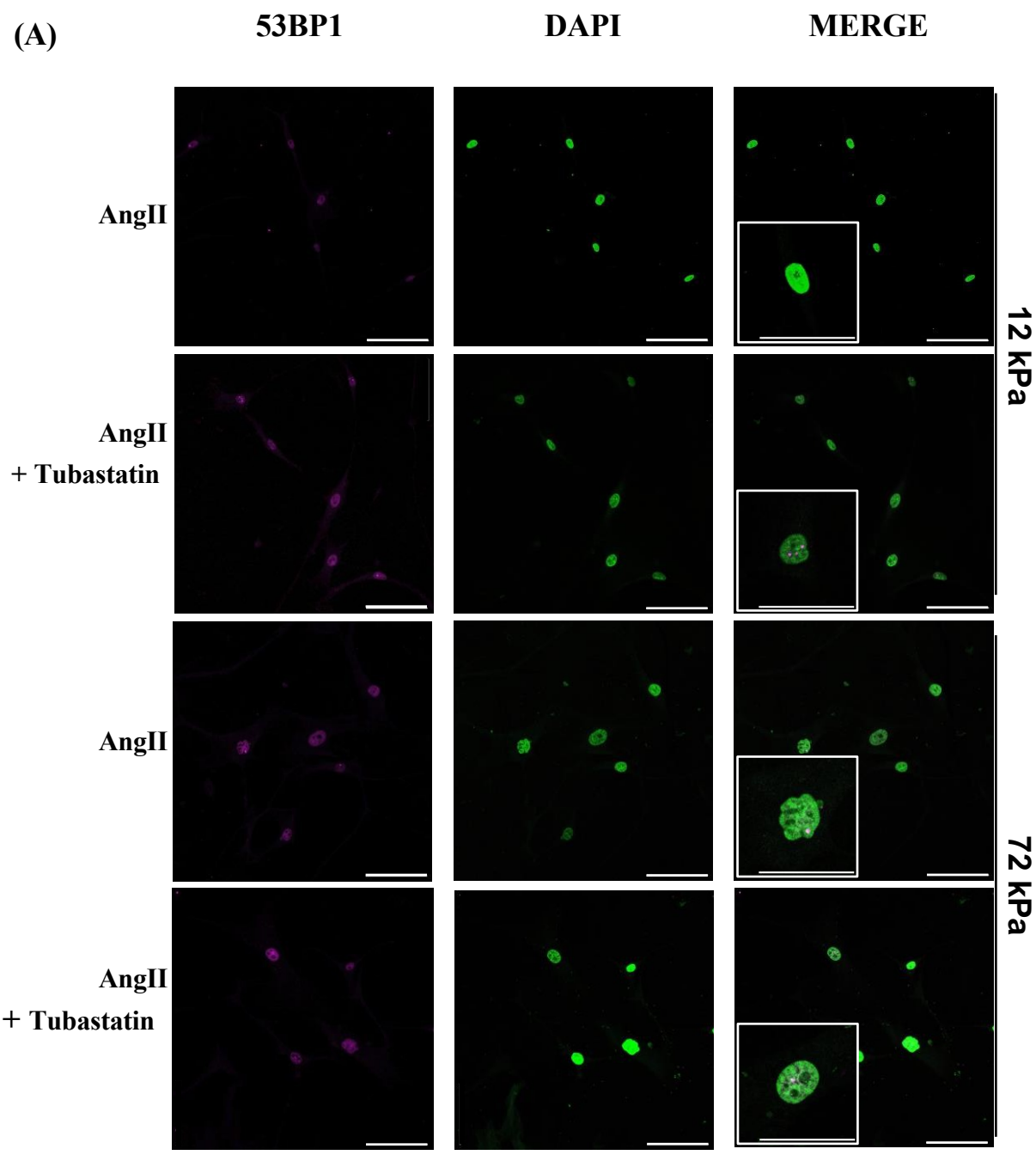
(A)
53BP1
DAPI
MERGE
AngII
AngII
+ Tubastatin
AngII
AngII
+ Tubastatin
12 kPa
72 kPa

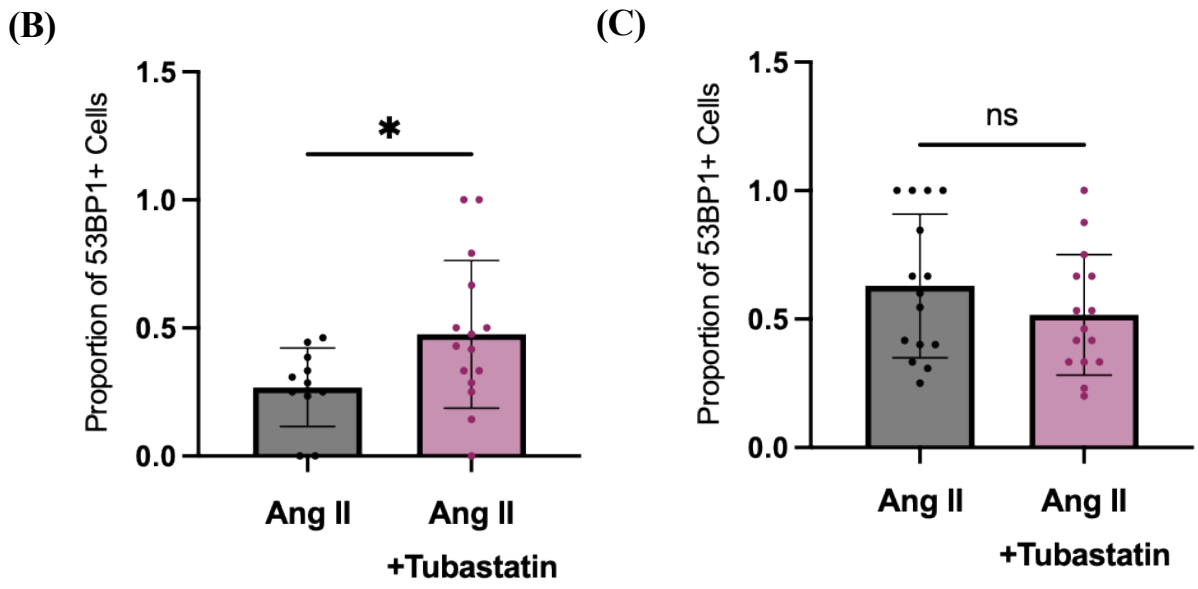

Figure 4.11 53BP1 levels detecting DNA damage response in VSMCs with Tubastatin A treatment ***(A)*** *Representative images of VSMC nuclei stained with 53BP1 antibody (magenta), DAPI (blue) levels with merged column. Insets show zoomed VSMC nuclei.* ***(B)*** *Bar graph representing number of 53BP1+ cells on VSMC nuclei from VSMC seeded on 12 kPa PAHs when treated with 10μM Angiotensin II ± 1μM Tubastatin A.* ***(C)*** *Bar graph representing number of 53BP1+ cells on VSMC nuclei from VSMC seeded on 72 kPa PAHs when treated with 10μM Angiotensin II ± 1μM Tubastatin A. Graphs show individual cell values (coloured dots) as well as the mean of 1 independent experiment with approximately ≥12 nuclei analysed. Statistical significance was determined with a t-test (significant; ** p≤0.01, *** p≤0.001, **** p≤0.0001).*

4.4.13 The SiRNA-mediated knockdown of HDAC6

To further investigate the effects of HDAC6 on VSMC morphology and mechanism, we sought to knockdown HDAC6 with siRNA. To determine whether the siRNA mediated knockdown was successful we performed a western blot testing VSMCs seeded on plastic treated with scrambled siRNA or targeted HDAC6 siRNA oligos 5 and 10. In **Figure 4.12(A-B)** HDAC6 siRNA oligos were successful in knocking down HDAC6 levels within VSMCs compared to the non-targeting treatment, however this effect was limited. Oligo 5 reduced levels to near 70%, oligo 10 reduced to approximately 53% meaning we may have an incomplete phenotypic effect.

Next, to determine whether this knockdown of HDAC6 had any effect on VSMC morphology we studied the effects on VSMC and corresponding volume. We conducted a viability assay, to ensure treatment with control or targeting siRNA had no cytotoxic effects on the VSMCs, this can be seen in **(Appendix-Figure A3.1)**. The results can be seen in **Figure 4.12(C-G)**. Overall, we see an increase in cell area **Figure 4.12(D)** when treated with oligo #5 than #10 when compared to the non-targeting siRNA (NT) on 12 kPa PAHs. On 72 kPa PAHs **Figure 4.12(E)** we do not see a change in VSMC area between the treatments. A similar trend is seen in cell volume, where on 12 kPa PAHs **Figure 4.12(F)** you see an increase in cell area with oligo #5 than #10 when compared to NT treatment. It can also be seen in **Figure 4.12(G)** that there is no change in cell volume between all three treatments in VSMC seeded on a rigid hydrogel. A minimal change can be observed in **Figured 4.12(C)** where cells are of similar size and shape across all treatments and hydrogel rigidity.

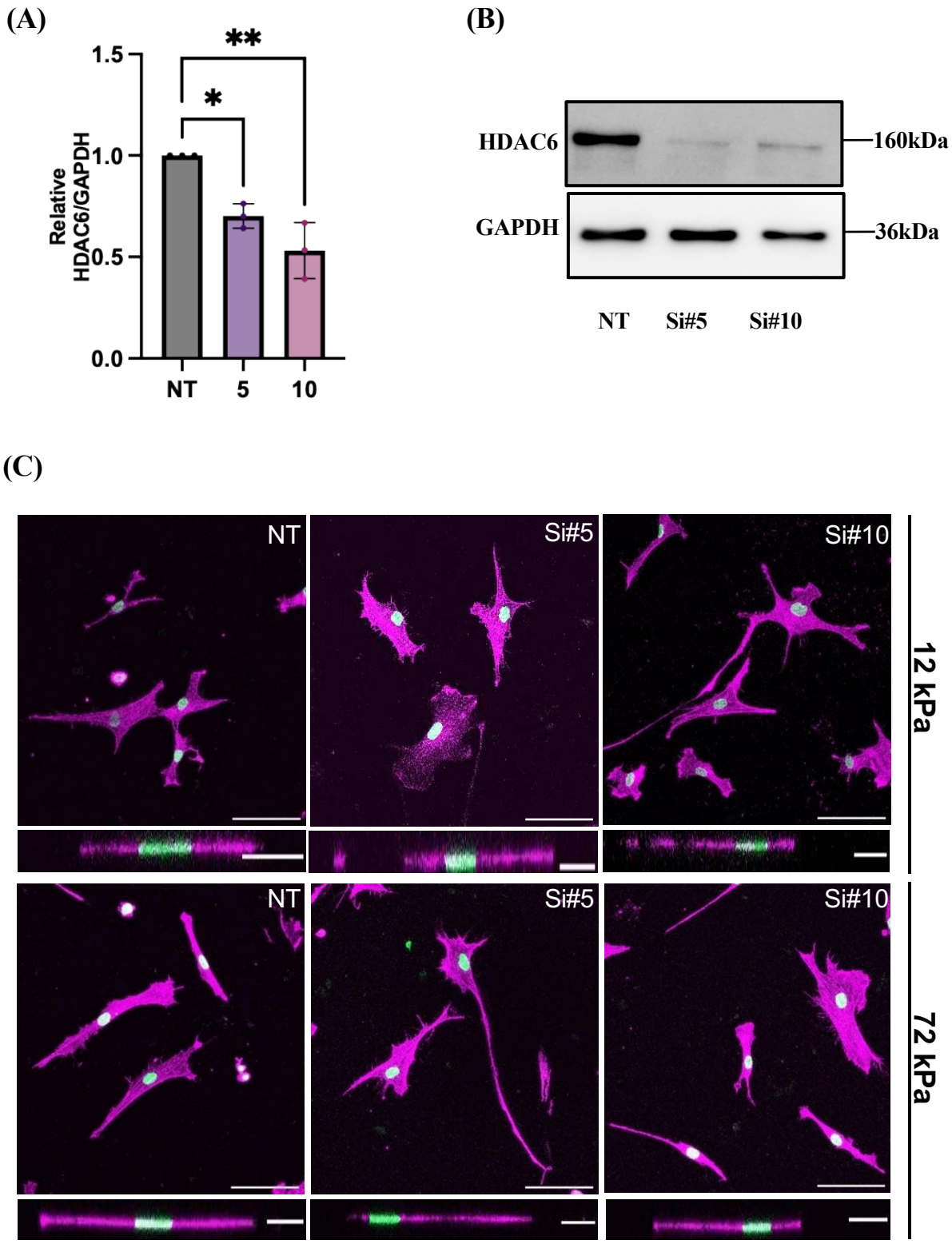
(A)
**
*
1.5
1.0
0.5
0.0
Relative HDAC6/GAPDH
NT
5
10
(B)
HDAC6
160kDa
GAPDH
36kDa
NT
Si#5
Si#10
(C)
NT
Si#5
Si#10
12 kPa
NT
Si#5
Si#10
72 kPa

(D)

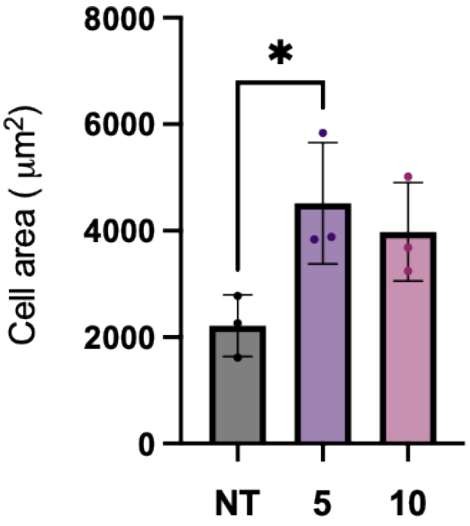
Cell area (µm²)
8000
6000
4000
2000
0
*
NT
5
10

(E)

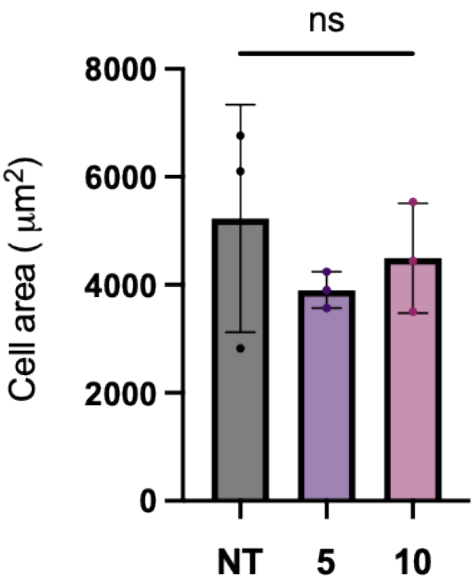
ns
Cell area (µm²)
8000
6000
4000
2000
0
NT
5
10

(F)

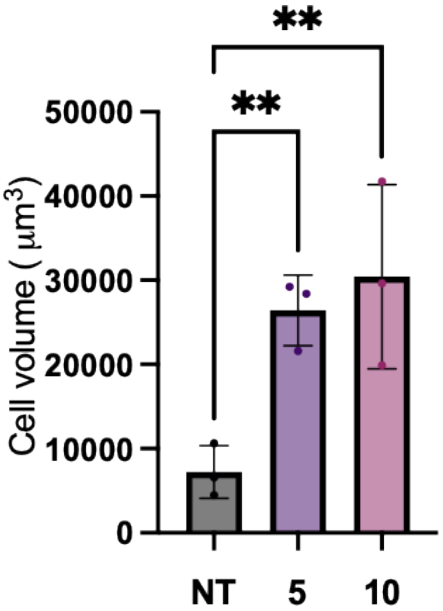
**
**
Cell volume (µm³)
50000
40000
30000
20000
10000
0
NT
5
10

(G)

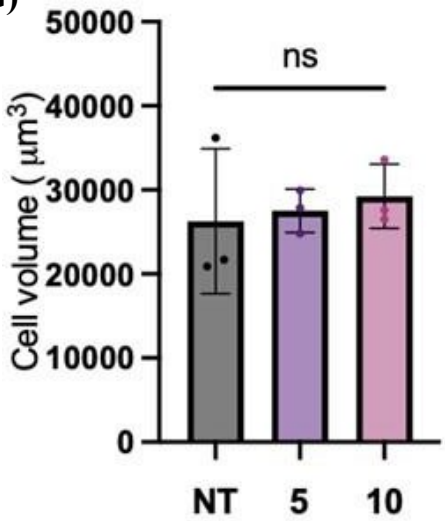
ns
Cell volume (µm³)
50000
40000
30000
20000
10000
0
NT
5
10

Figure 4.12 The siRNA mediated knockdown of HDAC6 (A) *Relative HDAC6 expression compared to GAPDH levels in VSMCs when treated with non- targeting siRNA, siRNA #5, siRNA #10 determined by western blot.* ***(B)*** *Respresentative western blot image to show levels of HDAC6 expression and GAPDH uopn treatment of non-targetting siRNA, siRNA #5 and siRNA #10. Total of 3 independent experiments represented by mean (coloured dots). Statistical significance was determined with an unpaired t-test (non-significant; p=>0.05).* ***(C)*** *Representative images of VSMCs seeded on 12 or 72 kPa PAHs treated with non-targeting siRNA, siRNA #5 and siRNA #10 as well as orthogonal view of cell to represent cell volume. Actin cytoskeleton stained using rhodamine phalloidin (magenta) and corresponding nucleistained with lamin A/C (green) Scale bars represent 100µm on VSMC area images, 20µm on VSMC volumes images.* ***(D)*** *Cell area of VSMCs seeded on 12 kPa PAHs VSMCs when treated with non-targetting siRNA, siRNA #5, siRNA #10.* ***(E)*** *Cell area of VSMCs seeded on 72 kPa PAHs when treated with non-targetting siRNA, siRNA #5, siRNA #10.* ***(F)*** *Cell volume of VSMCs seeded on 12 kPa PAHs VSMCs when treated with non-targetting siRNA, siRNA #5, siRNA #10.* ***(G)*** *Cell volume of VSMCs seeded on 72 kPa PAHs when treated with non- targetting siRNA, siRNA #5, siRNA #10. The graphs above are a mean of 3 independent experiments. Statistical significance was was determined with a one-way ANOVA. (significant;** p≤0.01, *** p≤0.001, **** p≤0.0001).*

4.4.14 Microtubule stability of VSMCs with HDAC6 siRNA treatment

Similarly to assays performed with Tubastatin A treatment, we conducted an MTS assay to understand more fine-tuned morphological changes in VSMCs when HDAC6 is knocked-down. From **(Figure 4.13A-B)** we can deduct that there was no significant change in the number of cold-stable microtubules (CSMs) in VSMCs seeded on 12 kPa PAH between all treatments. This is further confirmed by a t-test. On 72 kPa PAHs **(Figure 4.13A/C)** we also see no significant change in the number of CSMs, however, we do see a small decrease comparing the non-targeting scrambled siRNA to oligos #5 and #10. These results may indicate that there is no specific role for HDAC6 knockdown on VSMC MTS on either stiffness, suggesting this is not a mechanism driving variations in VSMC morphology. The impact of not being able to completely knockdown HDAC6 levels may have had an impact on why this result would not be similar to what has been seen in Tubastatin treated MTS assays.

(A)

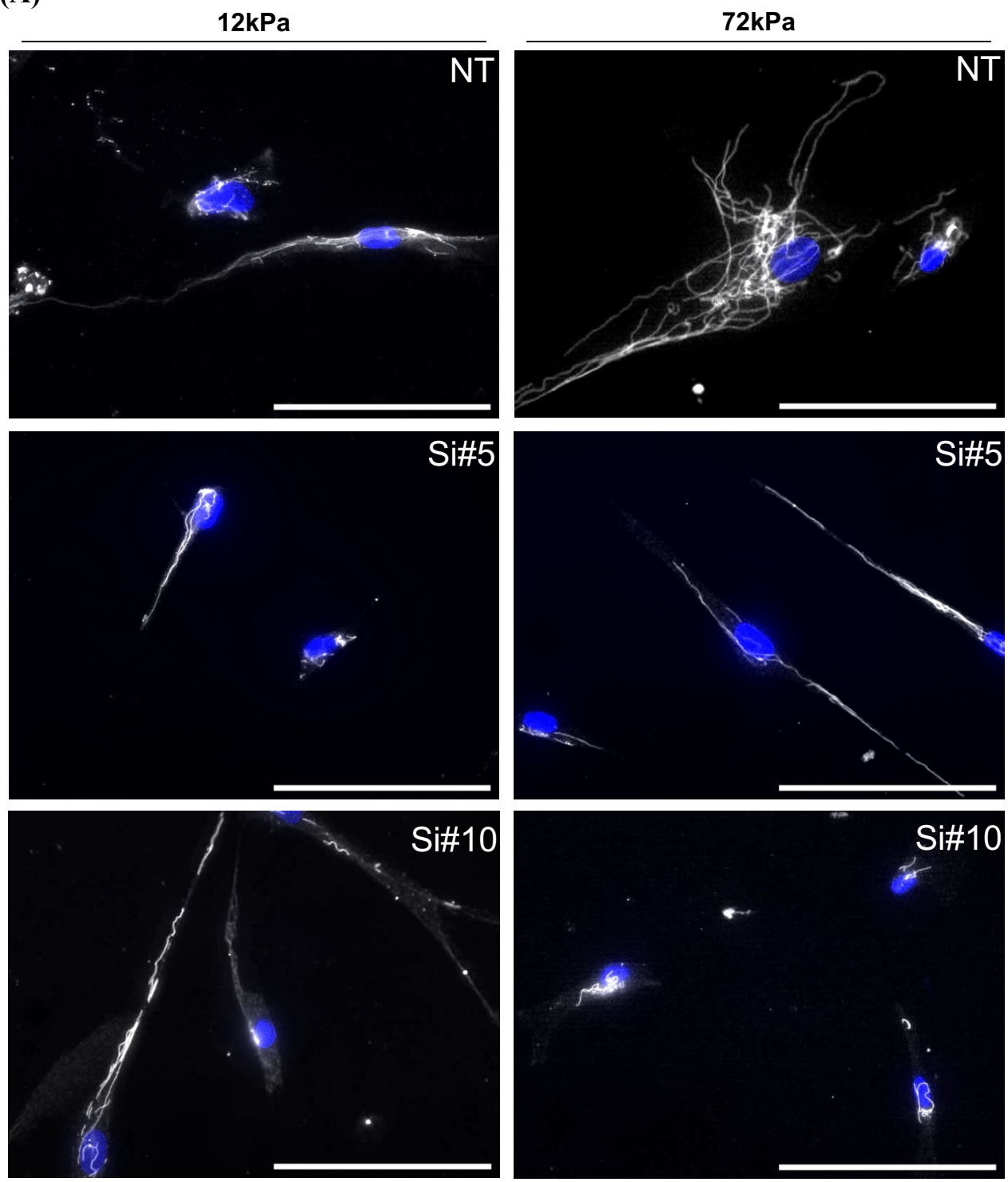

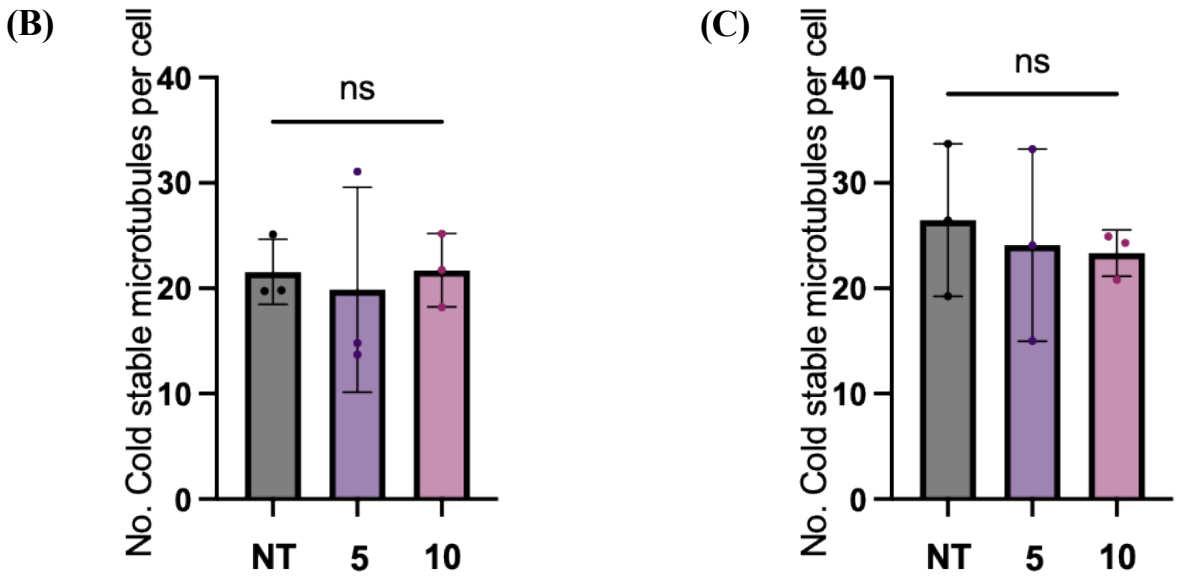

Figure 4.13 Microtubule stability of VSMCs with HDAC6 siRNA treatment ***(A)*** *Representative images of cold-stable VSMC microtubules treated with non-targeting siRNA, siRNA #5, siRNA #10 on 12 kPa and 72 kPa PAHs. Actin cytoskeleton stained using rhodamine phalloidin (magenta) and corresponding nuclei stained with lamin A/C (green)* ***(B)*** *Bar graph representing number of cold-stable VSMC microtubules seeded on 12 kPa PAHs when treated with non-targeting siRNA, siRNA #5, siRNA #10.* ***(C)*** *Bar graph representing number of cold-stable VSMC microtubules seeded on 72 kPa PAHs when treated with non- targeting siRNA, siRNA #5, siRNA #10. Graphs show mean of three individual experiments. Statistical significance was determined with a one-way ANOVA as non-significant.*

4.4.15 γH2AX levels detecting DNA damage response in siRNA mediated HDAC6 knockdown VSMCs

Next, we looked at the number of γH2AX foci in VSMC with HDAC6 siRNA knockdown. We saw in **Figure 4.14(B)** that with treatment with oligo #5 and #10 the number of γH2AX foci displays no significant difference to VSMCs treated with scrambled siRNA. There was also no significant difference observed between treatments on **Figure 4.14(C)** 72 kPa PAH. Although we seem to see a decrease in γH2AX foci on the 72 kPa PAHs, we can see that there is a lot of variation between each experiment. Compared to VSMCs treated with Tubastatin, in **Figure 4.14(A-C)** where Tubastatin (HDAC6 inhibitor) caused an increase in γH2AX foci on 12 kPa with no change on 72 kPa PAHs. This suggests that there is still speculation as to whether HDAC6 knockdown plays a stiffness-based role in DNA damage detected by γH2AX.

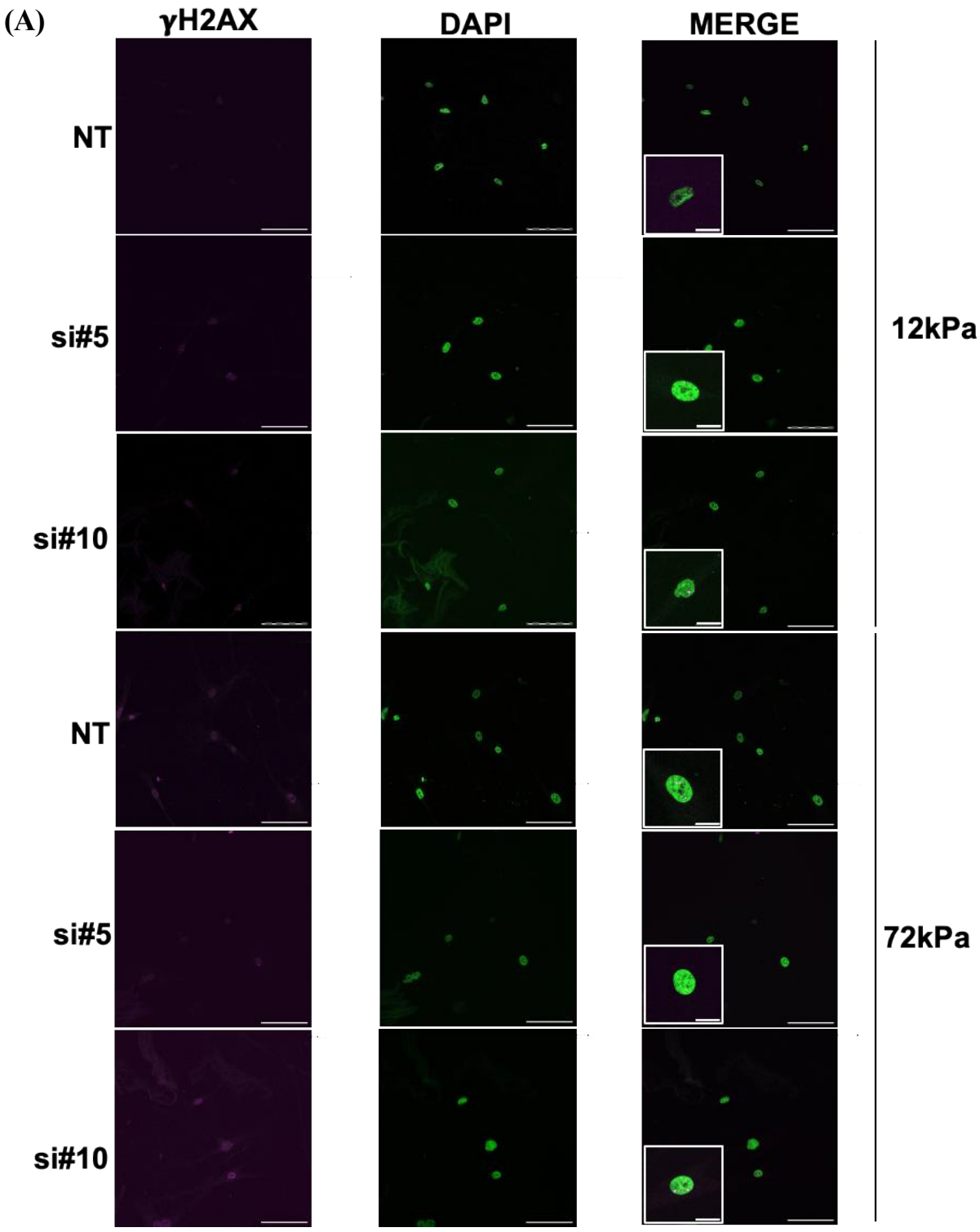
(A)
γH2AX
DAPI
MERGE
NT
si#5
si#10
NT
si#5
si#10
12kPa
72kPa

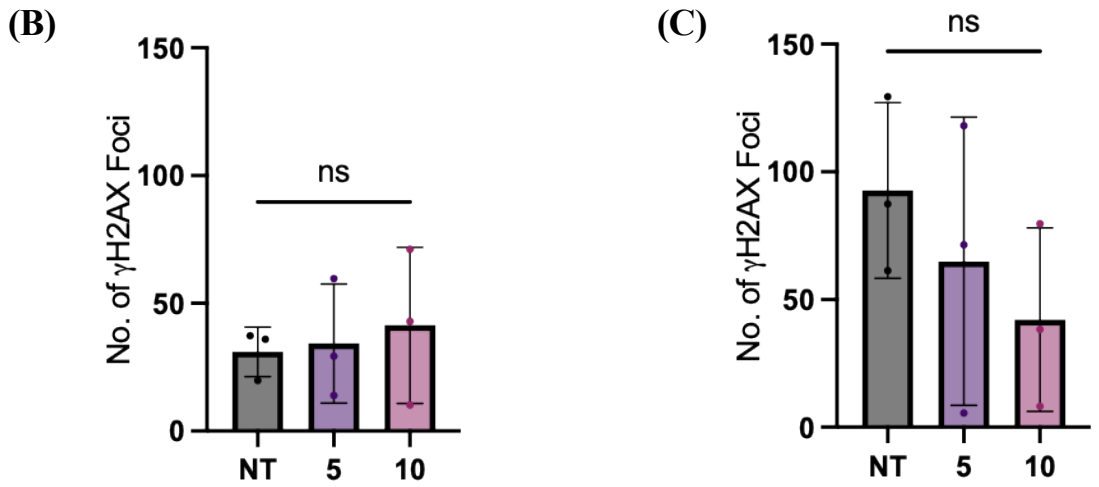

Figure 4.14 γH2AX levels detecting early DNA damage response in siRNA mediated knockdown of HDAC6 VSMCs ***(A)*** *Representative images of VSMC nuclei stained with 53BP1 antibody (magenta), DAPI (blue) levels with merged column. Insets show zoomed VSMC nuclei.* ***(B)*** *Bar graph representing number of 53BP1+ cells on VSMC nuclei from VSMC seeded on 12 kPa PAHs when treated with non-targeting siRNA, siRNA #5, siRNA #10.* ***(C)*** *Bar graph representing number of 53BP1+ cells on VSMC nuclei from VSMC seeded on 72 kPa PAHs when treated with non-targeting siRNA, siRNA #5, siRNA #10. Graphs show individual cell values (coloured dots) as well as the mean of 1 independent experiment with approximately ≥5 nuclei analysed. Statistical significance was determined with a one-way ANOVA (significant; ** p≤0.01, *** p≤0.001, **** p≤0.0001).*

4.4.16 53BP1 levels detecting DNA damage response in siRNA mediated HDAC6 knockdown VSMCs

We progressed to determine the proportion of 53BP1+ VSMCs when treated to a HDAC6 siRNA knockdown. This is the results from one independent experiment therefore statistical analysis is not available and can only be used as an indicator until atleast two further experiments are completed. We can see in **(Figure 4.15A-B)** that 53BP1+ cells increase when treated to oligo #5 compared to NT control and decrease with oligo #10 treatment. The increase when treated with oligo #5 may be due to an outlier, however, this can only be deduced with further experiments. In **(Figure 4.15A/C)**, we can see a decrease in the proportion of 53BP1+ cells with those treated to oligos #5 and #10 compared to non-targeting treatment on those seeded on 72 kPa. We can see that there was a similar trend with Tubastatin A treatment that 53BP1+cells were increased to that on control on 12 kPa and had a small decrease on 72 kPa **Figure 4.11(A/C)**. This may indicate that the inhibition or knockdown of HDAC6 may play a role in DNA damage levels on a stiffness-basis in VSMCs.

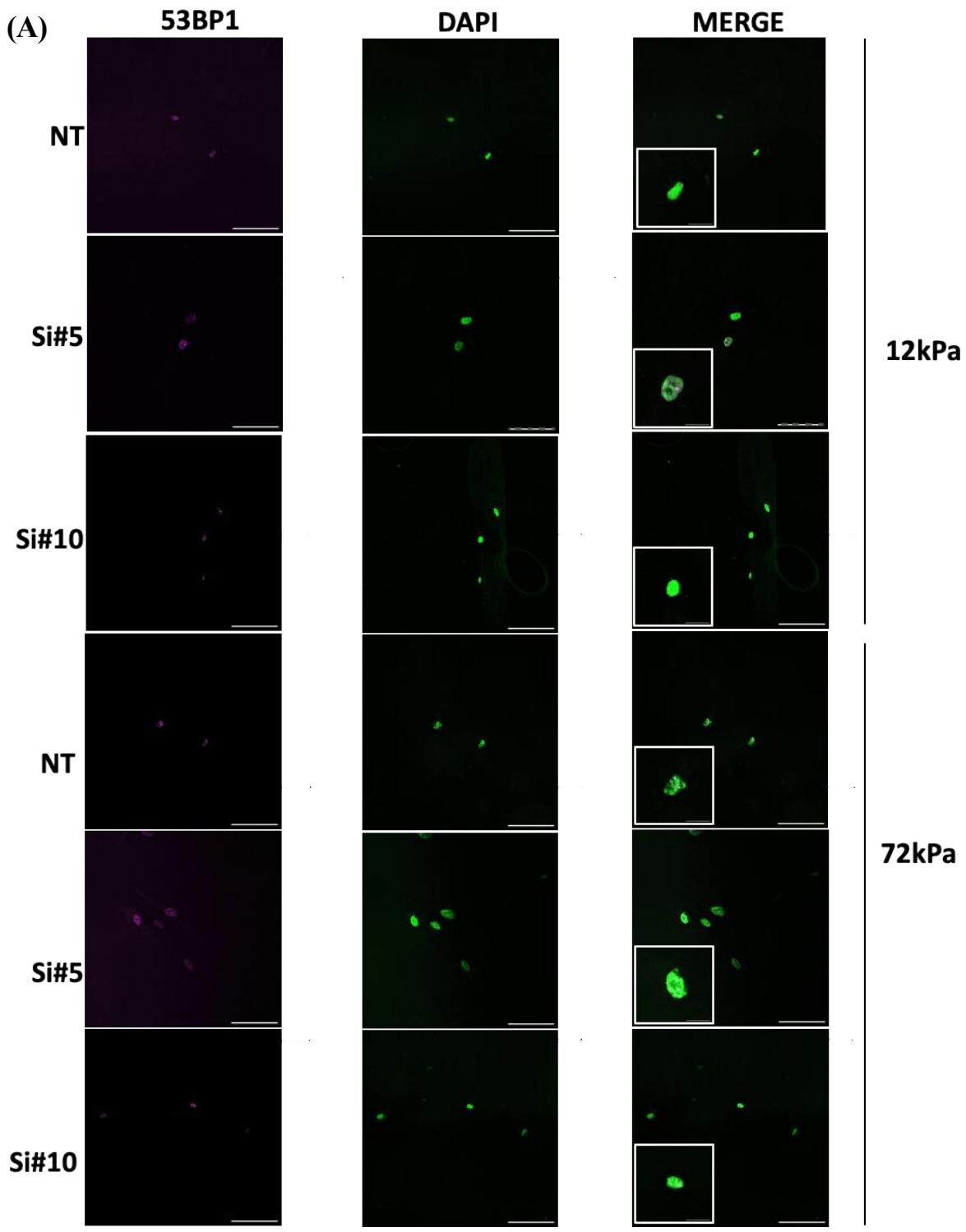
(A)
53BP1
DAPI
MERGE
NT
Si#5
Si#10
NT
Si#5
Si#10
12kPa
72kPa

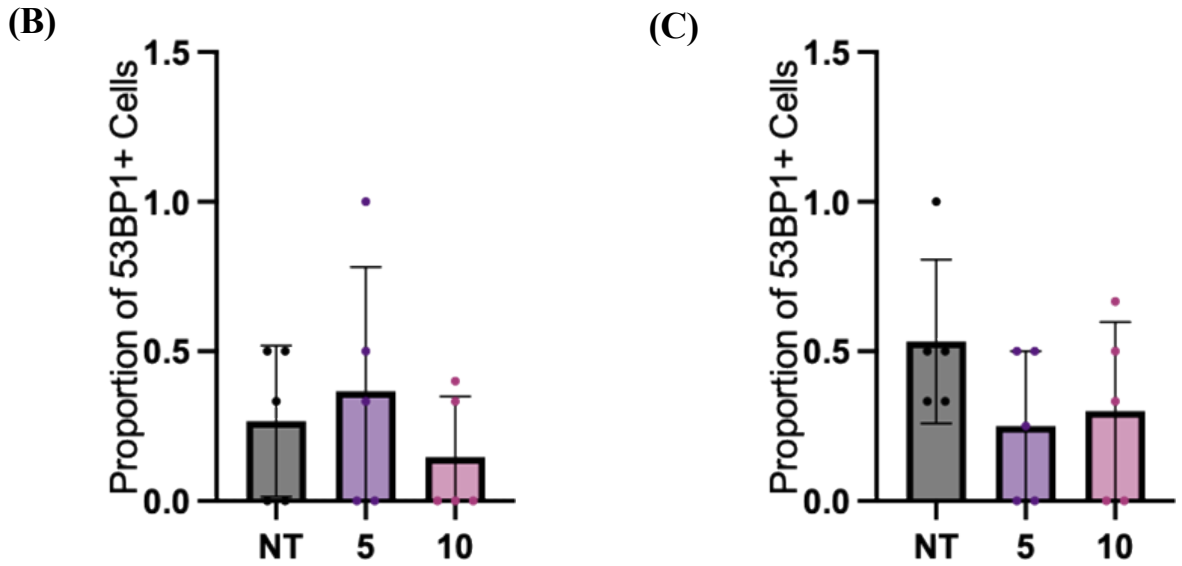

Figure 4.15 53BP1 levels detecting DNA damage response in siRNA mediated knockdown of HDAC6 *(A) Representative images of VSMC nuclei stained with 53BP1 antibody (magenta), DAPI (blue) levels with merged column. Insets show zoomed VSMC nuclei.* ***(B)*** *Bar graph representing number of 53BP1+ cells on VSMC nuclei from VSMC seeded on 12 kPa PAHs when treated with non-targeting siRNA, siRNA #5, siRNA #10.* ***(C)*** *Bar graph representing number of 53BP1+ cells on VSMC nuclei from VSMC seeded on 72 kPa PAHs when treated with non-targeting siRNA, siRNA #5, siRNA #10. Graphs show individual cell values (coloured dots) as well as the mean of 1 independent experiment with approximately ≥5 nuclei analysed. Statistical significance was determined with a one-way ANOVA (significant; ** p≤0.01, *** p≤0.001, **** p≤0.0001).*

4.5 Discussion

This chapter investigated the effects of HDAC3 and HDAC6 on VSMCs morphology and DNA damage. These effects were explored via the use of specific HDAC inhibitors and siRNA knockdowns allowing for a better understanding of their roles in VSMCs. We observed how drug treatments such as Tubastatin A which has shown promise in cancer management, may regulate multiple processes within VSMCs. Furthermore, we have also explored the impact on the nucleus in terms of morphology and DNA damage indicators with their relationship to matrix-stiffness. We are now able to provide a better mechanistic insight to the efficacy/toxicity of specific HDAC inhibitors and their role within the cardiovascular system.

4.5.1 The Role of HDAC3 inhibitor (RGFP966) on VSMC morphology

As we age our aortic wall and VSMCs stiffen resulting in a decreased aortic compliance, a major risk factor of various cardiovascular diseases. The current gold- standard to measure aortic compliance is pulse wave velocity (PWV) (169–171). This rigidity is often paired with age-dependent extracellular matrix stiffening further reducing compliance. As mechanosensitive cells, it has been observed that VSMCs increase actomyosin force generation in response to the increased rigidity of their surrounding environment (172–174). It has been observed in some CVDs such as hypertension that VSMCs display a hypertrophic-like response which in turn feeds in the cyclical nature of aortic rigidity (175–179)

Previous studies have shown that Angiotensin II induces VSMC hypertrophy creating an augmentation in cell size and protein synthesis. Prior work in the Warren Lab have shown that ECM rigidity causes an increase in cell area and volume when stimulated with contractile agonist Angiotensin II (180,181).

In the previous chapter we saw that some histone deacetylase inhibitors (HDACi) had an impact on VSMC area on both healthy aorta bio-mimic hydrogel (12 kPa) and the diseased aorta bio-mimic hydrogel (72 kPa). Some HDACi were able to selectively inhibit the hypertrophic effects observes in VSMCs seeded on 72 kPa PAHs. These

HDACi were chosen for further testing to provide a better mechanistic insight and their regulation in cell area. As mentioned earlier, we know that typically VSMCs on rigid substrates present a greater cell volume when stimulated with angiotensin II. We wanted to further understand if HDACi have a role in augmenting VSMC volume as well as area. This increased volume response feeds into aortic wall rigidity, therefore, some HDACi that can impede this response may be beneficial in treating various cardiovascular diseases.

HDAC3i, RGFP966 was successful in reducing cell area in a dose-dependent manner in our previous assays of VSMCs seeded on rigid 72 kPa PAHs. At higher doses we saw that this reduction in cell area also occurred in VSMCs on 12 kPa PAHs. Our concentration response assays in the previous chapter allowed us to choose a working concentration of 10 μM. At working concentration, HDAC3 inhibition expectedly recapitulated the changes seen in the previous dose response assay. We saw a decrease in VSMC area and volume when treated with the HDAC3 inhibitor. We did not observe any changes with nuclear cell area of volume. This was unexpected as HDAC3 has been observed as present within the nucleus as well as the cytoplasm suggesting its potential to manipulate nuclear volume (139).

The lack of changes could be due to an ineffective working concentration, with a stronger concentration needed to have a significant response in a smaller population of cells. We observed that there were no changes in cell area on VSMCs seeded on 12 kPa PAHs at 100 μM of RGFP966 in the previous chapter, suggesting that we may be able to increase our working concentration to yield the desired effect of area reduction in VSMCs on 72 kPa PAHs without affecting those on 12 kPa PAHs. An issue we may face with a concentration increase is off-target effects with inhibition for other HDACs. RGFP966 can inhibit HDAC8 at concentrations above 100 μM. At concentrations of 9.7 μM we may see inhibition of HDAC2 which may be responsible for off-target effects resulting in undesired results.

To further understand why we didn't obtain the results expected, we would want to question the stability of the inhibitor. It could be possible that it expired and therefore had no effect compared to control in further experiments after the concentration response assays. With this knowledge it warrants further investigation, however due

to time limitations this was not possible. We were following up on more successful Tubastatin A assays to understand the mechanism of HDAC6 inhibition in VSMCs.

Other studies have shown that HDAC3i decreases migration and proliferation which is usually seen in VSMCs displaying the proliferative phenotype (diseased) suggesting HDAC3 plays a critical role in VSMC. At this point further investigation is needed to determine its role in VSMC volume regulation (133). To follow up on the location of HDAC3 within the VSMCs, we could quantify HDAC3 expression. This would allow us to further understand where HDAC3 inhibition would have a major role (135).

4.5.2 Characterising VSMC morphological changes associated with HDAC6 with HDAC6 inhibitor Tubastatin A

Some research has indicated a therapeutic role for HDAC6 inhibition in cardiovascular diseases as it has been seen to prevent atherosclerosis and endothelial injury (182). HDAC6 is thought to induce vasoconstriction and thereby increase blood pressure as well as increase vascular hyperplasia, which is the accumulation of cells in the tunica intima resulting in a thickened intima. Vascular hyperplasia is often seen as a response to vessel injury which can lead to VSMC dedifferentiation to the proliferative phenotype (183). Other studies have shown that Tubastatin A has a role in reducing Ang-II mediated vasoconstriction which is often seen in atherosclerosis. Additionally, Tubastatin A has been shown to decrease VSMC proliferation in the tunica intima (133,139).

In the previous chapter, we saw that HDAC6 inhibitor, Tubastatin A had the ability to influence the VSMC matrix rigidity response as it decreased cell area on both VSMCs seeded on pliable and rigid PAHs. We wanted to further assess its role in other morphological changes within VSMCs. Western blot analysis, although not significantly different allowed us to confirm the increase in acetylated α-tubulin levels with an increase in Tubastatin A concentration. A working concentration of 1 μM was found to be the most appropriate. VSMC had an increase in cell area when treated with Tubastatin at working concentration on VSMCs on pliable PAHs although not significant. This increase was to a similar cell area seen in VSMCs seeded on rigid PAHs. Tubastatin treatment of those on rigid PAHs showed minimal changes. Upon

analysing cell volume, there was a similar trend in VSMCs seeded on pliable and rigid PAHs.

We tested to confirm if these changes in VSMC area and volume were microtubule driven as Tubastatin is tubulin-specific. Adaptations to the stability of the microtubules would have impact on the VSMCs ability to contract. This data showed minimal changes of no significance in stability on both the pliable and rigid PAHs.
We also analysed the effects of Tubastatin on VSMC DNA as we hypothesised that the hypertrophic effect seen on 12 kPa PAHs may cause stress within the nucleus. Both γH2AX and 53BP1 levels increased in VSMCs on pliable PAHs when treated with Tubastatin compared to its vehicle counterpart. This suggested that there were defections in the DNA-repair pathway as well as double-strand breaks. On the rigid PAHs, we saw that Tubastatin had no significant changes on DNA damage as both γH2AX and 53BP1 levels remained undeterred.

We performed a siRNA mediated HDAC6 depletion experiment to confirm that these morphological changes were driven by the inhibition of HDAC6. We were able to confirm the efficient depletion of HDAC6 via two different oligomers compared to the non-targeted control via western blot. The decrease in cell area and volume of VSMCs on pliable PAHs with the depletion of HDAC6 suggests that HDAC6 may play a specific role in healthy cells compared to those that bio-mimic diseased VSMCs (those on 72 kPa). Other suggestions for why VSMCs on rigid PAHs could be because other pathways have already been altered and the depletion of HDAC6 may not have enough of an impact. Although oligomers 5 and 10 can decrease HDAC6 levels within VSMCs, its effect is limited to a maximum 50% knockdown. The siRNA mediated knockdown of HDAC6 also had no effect on microtubule stability compared to the non- targeting control. The siRNA-mediated knockdown of HDAC6 creates an increase in γH2AX detected DNA damage in VSMCs seeded on 12 kPa PAHs with no detected changes on 72 kPa PAHs and none on either rigidities with 53BP1 levels. These results suggest that the depletion of HDAC6 have potential effects on the nucleus. The impact of cell area and volume may contribute to the DNA damage detected in VSMCs on 12 kPa PAHs as these hypertrophic changes can increase pressure within the cell and its nucleus.

This result shows us that Tubastatin and the siRNA-mediated knockdown of HDAC6 is specific in targeting VSMCs seeded on pliable PAHs i.e. bio-mimic of healthy VSMCs. A comparison of baseline siRNA mediated knockdown levels on both 12 and 72 kPa may help us understand the differential effect between the two rigidities. There has been further investigation into compensatory mechanisms such as calcium ion homeostasis, which has been performed by another member of the lab. The results of this investigation so far, has determined an increase in calcium ion influx which may be activating downstream targets influencing VSMC volume. Recently, the Warren Lab also investigated the effect of Tubastatin on cell height to determine if this hypertrophic effect on the pliable PAH also affects the cell vertically. It is known the mechanotransduction can be affected by cell shape and height, therefore changes to both could cause further issues in the many processes involved in the VSMC response to matrix rigidity. The results also show that the depletion or inhibition of HDAC6 is causing maladaptive changes in these VSMCs potentially leading to detrimental effects on the cardiovascular system if followed through as treatment in cancers. The mechanism causing an increase in cell area and volume in VSMCs when Tubastatin treatment remains elusive.

4.5.3 Limitations

These specific HDAC inhibitors were chosen for further investigation as were part of the first drugs I screened that had interesting results in cell and nuclear area. Due to time constraints, I was not able to further investigate HDAC1 which showed a positive result in decreasing VSMC area on rigid matrices. This would be an area to be investigated in future work.

Chapter 5: Piezo1 regulates VSMC volume response to ECM stiffness

5.1 Introduction

VSMC contraction is essential in maintaining vascular tone in healthy aortae, this contraction becomes disrupted when changes in ECM such as an increase in rigidity occur. A rigid ECM reduces aortic compliance and results in increased blood pressure which overtime can contribute to vascular damage and atherosclerosis. As the rigidity of the ECM increases, VSMCs also become stiffer attempting to adapt to their surroundings, this is due to their ability to be mechanosensitive. This further feeds into a stiffer environment. Our knowledge on the mechanisms driving this remain limited.

Intracellular Ca^{2+} levels play a central role in regulating VSMC contraction. Calcium stores are tightly regulated as they need to respond fast to constant blood flow within the vessel. This is done via the extracellular intake of Ca^{2+} via membrane channels or intracellular stores such as the sarcoplasmic reticulum. These processes are accelerated into a state of dysfunction as we age, with VSMC stiffness leading to hypertension. Overtime VSMC become hypertrophic which is the increase in cell mass without the increase in number of cells (128,178,184). Hypertrophy is a combination of an increase in cell volume and protein synthesis. This results in an increase in aortic wall thickness contributing to arterial rigidity further decreasing vessel compliance
(128). Previous work in the Warren Lab has proven that angiotensin II stimulated VSMCs possess an increase cell volume when seeded on a rigid PAH, however, the exact mechanisms of this are yet to be determined. It is known that in cardiac fibroblasts, ECM rigidity promotes the activation of stretch activated channels as they enable the influx of extracellular Ca^{2+} (185). This is thought to occur as an increase in intraluminal pressure triggers stretch activation in VSMCs causing the aorta to expand (185,186). Furthermore, this stretch activation stimulates downstream signalling pathways initiating VSMC contraction via Ca^{2+} influx. Stretch activated ion channels (SACs) are essential for mechanosensitivity in VSMCs, examples including Piezo1, TRPV1 and others in the TRP (transient receptor potential) (187–189). Piezo1 has been implicated in causing VSMC dysfunction leading to atherosclerosis and abdominal aortic aneurysm induced vascular remodelling (190,191).SAC blockers have been used in attenuating cell volume in rabbit ventricular myocytes under

hypoosmotic stress. Certain SAC blockers such as Gadolinium (Gd3+) and Streptomycin have proven to reduce the influx of Ca^{2+} ions (192,193).
The D-enantiomer of another SAC blocker, GSMTx4 has been proven to be a potent cardioprotectant and has been the target of new research for ischemic reperfusion injury (194). Further research is necessary to clarify whether VSMC volume impacts VSMC stiffness in response to ECM rigidity.

Other cell types have been known to regulate the cell volume response by utilising ion transporters. Volume decreases promote potassium chloride influx which can be combatted using K+/Cl- or individual transporters whereas volume increases utilise the Na+/K+/2Cl- cotransporter to encourage chloride ions back into the cell (195). Additionally, cell swelling is also due to water transport into the cell suggesting the involvement of aquaporins. Due to osmosis, increases in chloride ions into the cell are followed by an influx of water resulting in cell swelling. On the contrary, the efflux of chloride ions out of the cell and water would cause cell shrinking (128). In healthy cells, any perturbations in cell volume will result in a quick response via ion or water transport to adjust back to homeostasis (196). Other members of the lab conducted concentration response assays of different types of aquaporins, with aquaporin-1 having a greater effect on VSMCs. Protein kinase C is a known regulator of aquaporin- 1, with its activation triggering the membrane translocation of aquaporin-1 in HEK293 cells. This translocation resulted in greater water influx into the cell thereby causing an increase in cell volume (197). This was yet to be proven true in VSMCs, the Warren Lab also conducted pilot studies on the concentration-dependent responses of VSMCs with PKC inhibitor, Go 6983 and aquaporin-1 inhibitor, TCAQP1. This data uncovered novel pathways to explore and expand upon. More specifically, we wanted to further confirm our results and understand the longer-term response of VSMCs to these inhibitors in supplemented growth media (154).

5.2 Hypothesis

The activation of SACs on VSMC membrane facilitate the intracellular accumulation of Ca^{2+}.The increase in Ca^{2+} will trigger aquaporin-1 driving water into the cell causing VSMC swelling. Using a SAC blocker, GsMTx-4 will reduce cell volume in VSMCs seeded on a rigid PAH. The effective knockdown or inhibition of Piezo1 and aquaporin- 1 will prohibit/reduce VSMC volume increase. The allosteric activator Yoda-1 would be able to increase VSMC volume on pliable hydrogels as it is activating the SAC, Piezo1. The inhibition

of PKC, an aquaporin-1 regulator will also reduce VSMC volume as well as being able to regulate aquaporin-1 in VSMCs.

5.3 Aims

1. To be able to confirm that VSMC volume increase on a rigid PAH is sustained in the longer term by seeding in growth or basal media on both PAHs stiffnesses for a period of 24 hours.

2. To determine if SACs are involved in causing a cell volume increase on rigid PAHs by using a SAC blocker, GsMTx4 in long term assay with growth media. Further confirming this via the use of allosteric activator of Piezo1 (Yoda1) with co-treatment of Angiotensin II.

3. To understand the effects of siRNA-mediated knockdown of Piezo1 in VSMCs seeded on both pliable and rigid PAHs over a long term with growth media.

4. To understand the role of aquaporin-1 in the VSMC response to rigid matrices by inhibiting its function with TCAQP1 on both 12 and 72 kPa PAHs in growth media in the long term.

5. To determine if PKC plays a role in the VSMC response to a rigid matrix with use of PKC inhibitor Go6983 in the longer term incubated in growth media.

6. To investigate if PKC plays a role in regulating aquaporin-1 in VSMCs by conducting localisation assays with pre-treatment with PKC inhibitor. This will be compared to aquaporin-1 localisation without pre-treatment in both 12 and 72 kPa PAHs.

5.4 Results

5.4.1 VSMCs possess increased cell volume on rigid PAHs

To investigate the long-term effects of matrix rigidity on vascular smooth muscle cells (VSMCs), we analysed cell volume using confocal microscopy. VSMCs were incubated in either growth or basal media on both types of PAHs. No significant differences were found in area or volume of VSMCs incubated for 24 hours in growth or basal media on 12 kPa PAHs **Figure 5.1(A,B,D)**. However, on 72 kPa PAHs, VSMCs incubated in growth media had an increase in area and volume compared to their basal media incubated counterparts **Figure 5.1(A,C,E)**. Additionally, there was also an increase in cell area and volume of VSMCs seeded on rigid PAHs compared to pliable PAHs when incubated with growth media **Figure 5.1(A-E)**. There were no significant differences in cell height between the conditions **Figure 5.1(F-G)**.

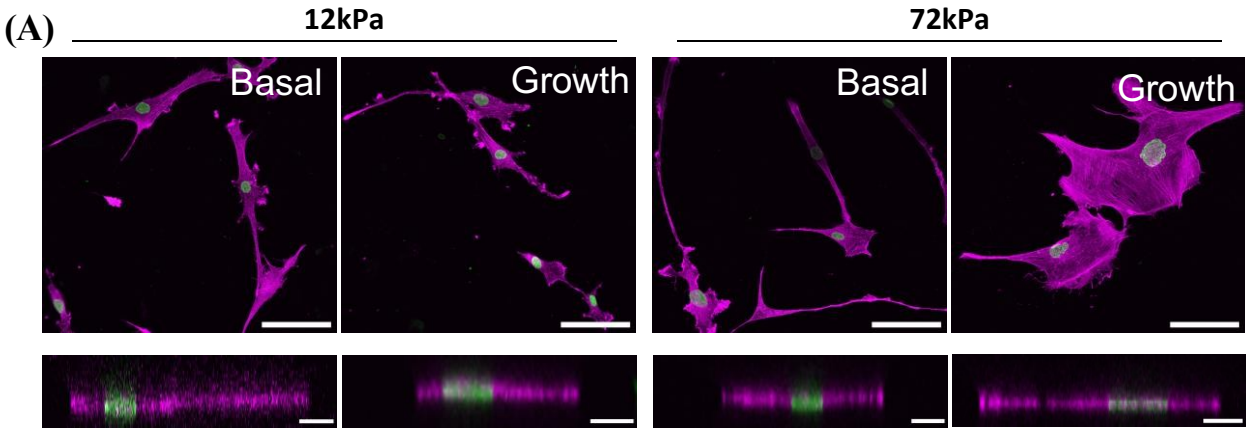
(A)
12kPa
72kPa
Basal
Growth
Basal
Growth

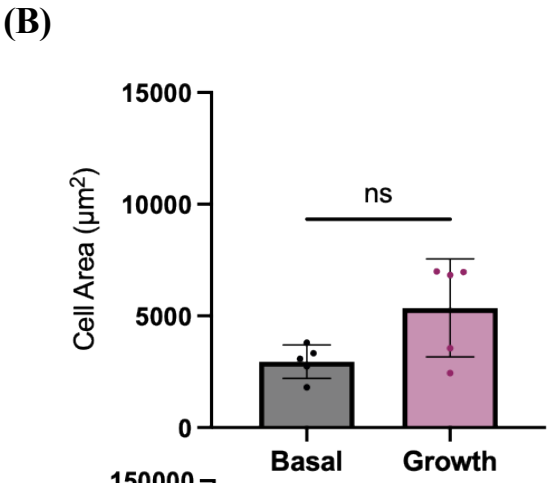
(B)
Cell Area (µm²)
15000
10000
5000
0
ns
Basal
Growth

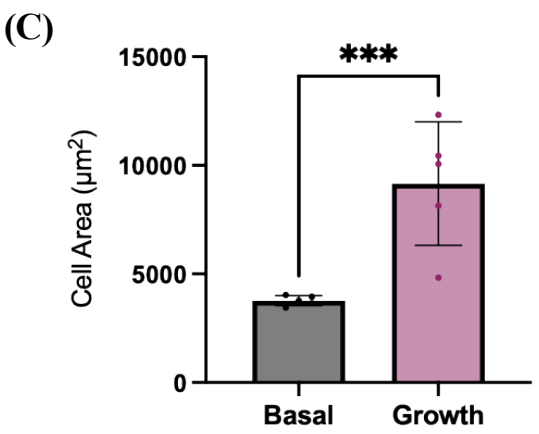
(C)
Cell Area (µm²)
15000
10000
5000
0
***
Basal
Growth

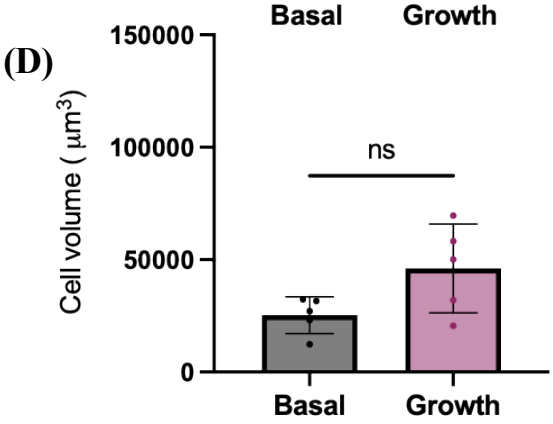
(D)
Cell volume (µm³)
150000
100000
50000
0
ns
Basal
Growth

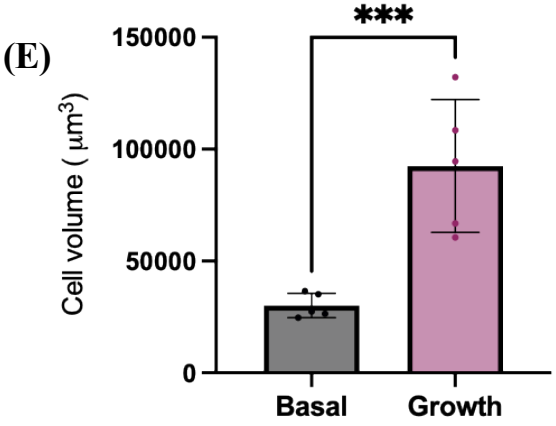
(E)
Cell volume (µm³)
150000
100000
50000
0
***
Basal
Growth

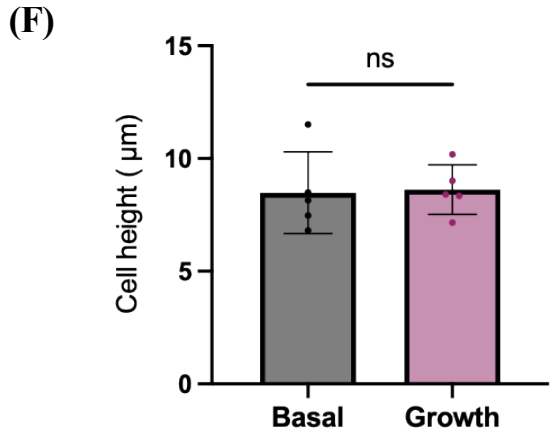
(F)
Cell height (µm)
15
10
5
0
ns
Basal
Growth

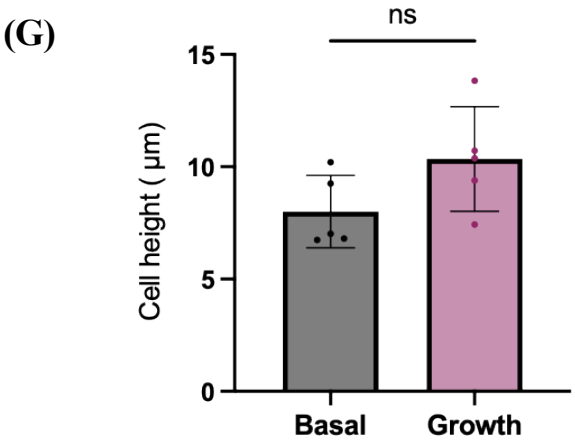
(G)
Cell height (µm)
15
10
5
0
ns
Basal
Growth

Figure 5.1 *VSMCs possess increased cell volume on rigid PAHs (A) Representative images of VSMCs seeded on 12- or 72 kPa PAHs incubated in growth or basal media for 24 h. Actin cytoskeleton (magenta) and DAPI labelled nuclei (green). Top panel shows representative XY images of VSMC area, scale bar = 100μm. Bottom panel shows representative XZ images of VSMC height, scale bar = 20μm. Graphs show VSMC (B) VSMC area on 12 kPa PAHs, (C) VSMC area on 72 kPa PAHs, (D) VSMC volume on 12 kPa PAHs, (E) VSMC volume on 72 kPa PAHs and (f) VSMC height on 12 kPa PAHs, (G) VSMC height on 72 kPa PAHs. Graphs represent combined data from five independent experiments with ≥50 cells analysed per condition. Mean data from each individual repeat of the five independent experiments are shown by a colour dot. Significance was determined using an unparalleled t-test (significant; * $p<0.05$ ** $p\leq0.01$, *** $p\leq0.001$, **** $p\leq0.0001$).*

5.4.2 Inhibiting VSMC hypertrophy through SAC blockade, GsMTx-4

It is known that in other cell types such as, human atrial fibroblast cells, that ECM rigidity promotes the activation of SACs which thereby causes the influx of extracellular Ca^{2+} (198–201). We tested if this remained true in VSMCs by utilising a SAC blocker, GsMTx-4. This was tested for a longer term of an 18-hour incubation in growth media compared to our standard short assay with quiescent VSMC. GsMTx-4 had no significant effect on VSMCs seeded on 12 kPa PAHs compared to vehicle only treatment **Figure 5.2(A&B)**. Conversely, GsMTx-4 reduced cell area in VSMCs on 72 kPa PAHs compared to control treatment **Figure 5.2(A&C)**. A similar analysis to VSMC area can be made for VSMC volume when pre-treated with GsMTx-4 **Figure 5.2(A,D&E)**. Cell height remained unaffected, **Figure 5.2(G)**.

The GSMTx-4 data proved that stretch activated channels were involved in the regulation of VSMC hypertrophy on rigid matrices. This led to us exploring Piezo1 a SAC, known to be involved in atherosclerosis and abdominal aortic aneurysm- mediated VSMC dysfunction (190).

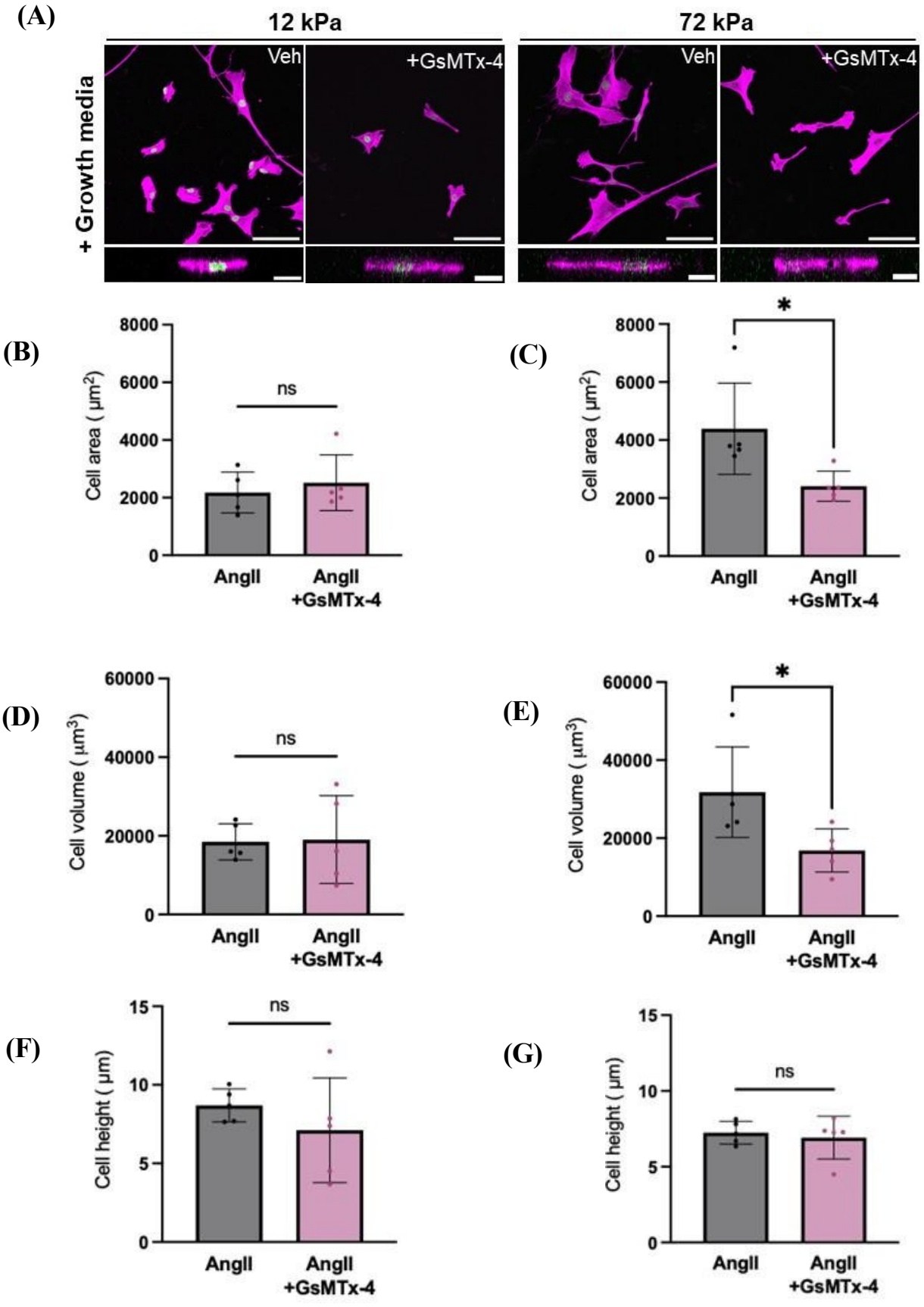
(A)
12 kPa
72 kPa
Veh
+GsMTx-4
Veh
+GsMTx-4
+ Growth media
(B)
Cell area (μm²)
8000
6000
4000
2000
0
ns
AngII
AngII +GsMTx-4
(C)
Cell area (μm²)
8000
6000
4000
2000
0
*
AngII
AngII +GsMTx-4
(D)
Cell volume (μm³)
60000
40000
20000
0
ns
AngII
AngII +GsMTx-4
(E)
Cell volume (μm³)
60000
40000
20000
0
*
AngII
AngII +GsMTx-4
(F)
Cell height (μm)
15
10
5
0
ns
AngII
AngII +GsMTx-4
(G)
Cell height (μm)
15
10
5
0
ns
AngII
AngII +GsMTx-4

Figure 5.2 Inhibiting hypertrophy through SAC blockade via GsMTx-4 (A) *Representative images of isolated VSMCs seeded on 12 or 72 kPa PAHs incubated in growth media for 18 h ± GsMTx-4. Actin cytoskeleton (magenta) and DAPI labelled nuclei (green). Top panel shows representative XY images of VSMC area, scale bar = 100μm. Bottom panel shows representative XZ images of VSMC height, scale bar = 20μm. Graphs show* ***(B)*** *VSMC area on 12 kPa PAHs,* ***(C)*** *VSMC area on 72 kPa PAHs,* ***(D)*** *VSMC volume on 12 kPa PAHs,* ***(E)*** *VSMC volume on 72 kPa PAHs and* ***(F)*** *VSMC height on 12 kPa PAHs,* ***(G)*** *VSMC height on 72 kPa PAHs. Graphs represent combined data from five independent experiments with ≥50 cells analysed per condition. Mean data from each individual repeat of the five independent experiments are shown by a black dot. Significance was determined using an unparalleled t- test (significant; * $p<0.05$, ** $p\leq0.01$, *** $p\leq0.001$, **** $p\leq0.0001$).*

5.4.3 The siRNA-mediated knockdown of Piezo1 in VSMCs

We used SiRNA-mediated knockdown of Piezo-1 to investigate its involvement in VSMC volume regulation. Initial western blot of the siRNA knockdown were conducted by Rob Johnson. We conducted longer term assay in growth media to study the effect of piezo depletion in VSMCs over a period of 24 hours on both 12 and 72 kPa PAHs. Upon analysis, we concluded that there was no change in cell area or volume in VSMCs on pliable hydrogels compared to the vehicle control **Figure 5.3(A,B&D)**. In contrast, VSMCs on rigid hydrogels displayed a reduction in cell area and volume when treated with siRNA compared to the si-control(NT) **Figure 5.3(A,C&E)**. There were no significant differences in cell height of VSMCs on either PAH **Figure 5.3(F&G)**.

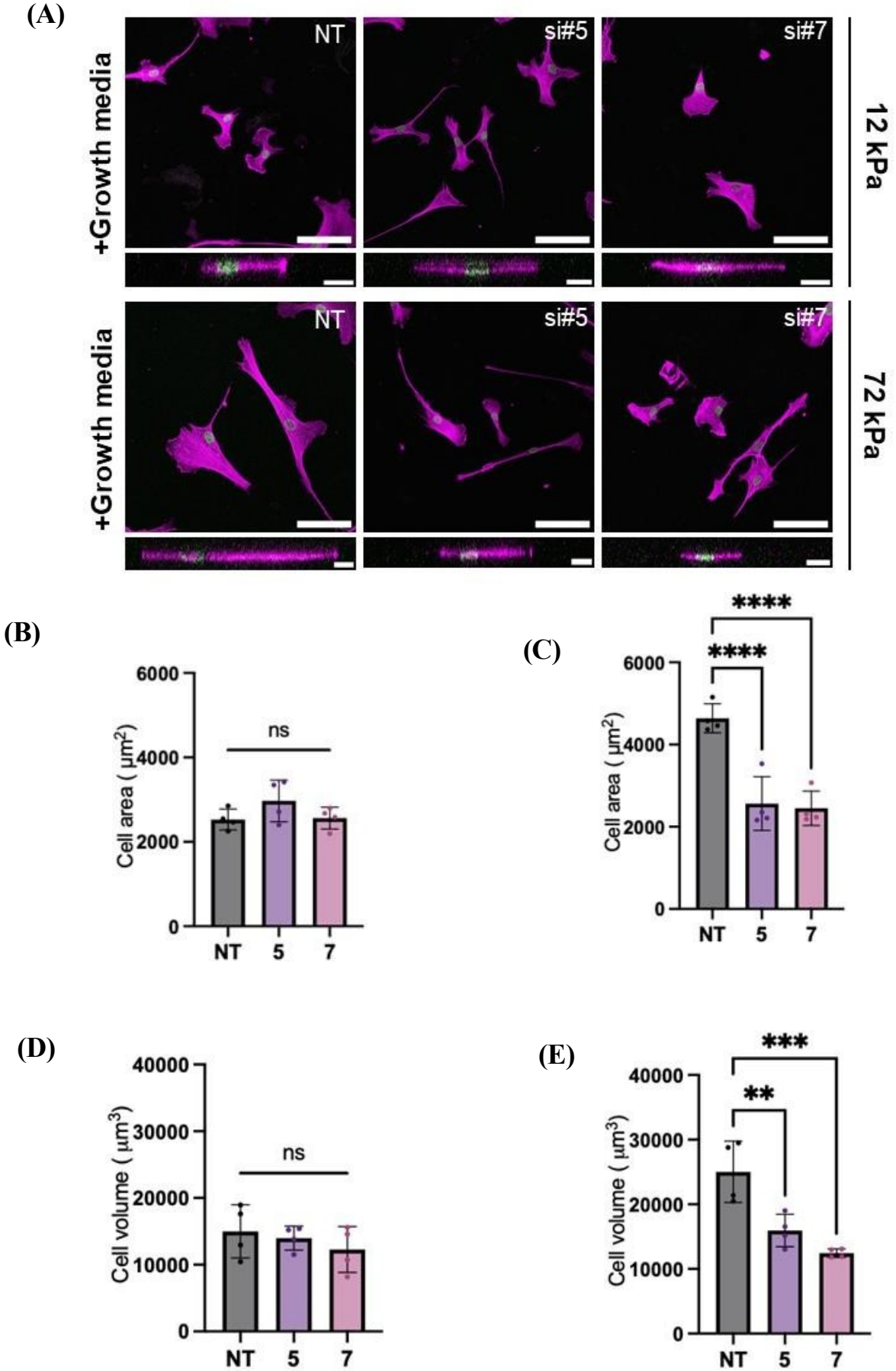
(A)
NT
si#5
si#7
+Growth media
12 kPa
72 kPa
(B)
Cell area (µm²)
ns
NT
5
7
(C)
****
****
Cell area (µm²)
(D)
Cell volume (µm³)
ns
(E)
***
**
Cell volume (µm³)

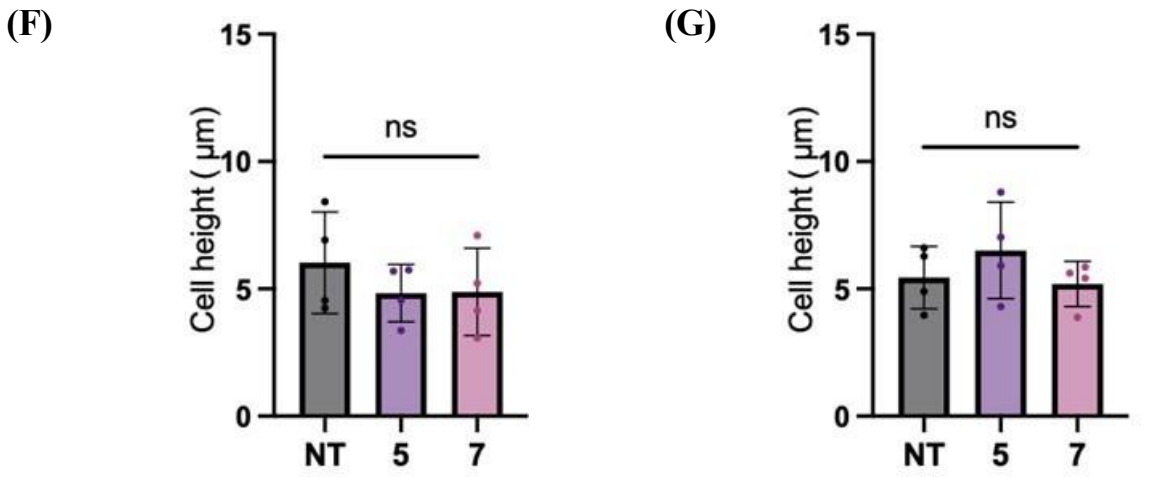

Figure 5.3 SiRNA-mediated knockdown of Piezo1 in VSMCs (A) *Representative images of piezo1-depleted VSMCs incubated in growth media on 12 or 72 kPa PAHs for 24 hours. NT = non-targeting siRNA. Actin cytoskeleton (magenta) and DAPI labelled nuclei (green). Top panel shows representative XY images of VSMC area, scale bar = 10 µm. Bottom panel shows representative XZ images of VSMC height, scale bar = 20µm. Graphs show* ***(B)*** *VSMC area on 12 kPa PAH,* ***(C)*** *VSMC area on 72 kPa PAH,* ***(D)*** *VSMC volume on 12 kPa PAH,* ***(E)*** *VSMC volume on 72 kPa PAH* ***(F)*** *VSMC height on 12 kPa PAH* ***(G)*** *VSMC height on 72 kPa PAH and represent the combined data of 4 independent experiments with ≥50 cells analysed per condition. Mean data of individual repeats of the 4 independent experiments are shown as dots. Significance was determined using a one-way ANOVA followed by Tukey's test (significant; * $p<0.05$ ** $p\leq0.01$, *** $p\leq0.001$, **** $p\leq0.0001$).*

5.4.4 Yoda1 treatment does not alter the volume of angiotensin II treated VSMCs on rigid PAHs

Yoda1 was used at a working concentration of 1 μM. It was expected that Yoda1 would increase the volume of angiotensin II stimulated VSMCs seeded on 12 kPa PAHs. This hypothesis was constructed due to previous research in the lab concluded that Yoda1 caused a sustained increase of Ca^{2+} influx in VSMCs seeded on both pliable and rigid PAHs. There were no significant differences in cell area of either VSMCs on 12 or 72 kPa PAHs **Figure 5.4(A-C)**. We were able to confirm our hypothesis as VSMC volume increased on 12 kPa PAHs, **Figure 5.4(A&D)**, when cotreated with angiotensin II and Yoda1 compared to angiotensin II only treatment. There were no changes in volume on the rigid PAHs **Figure 5.4(A&E)**. Additionally, there was no changes in cell height on either PAH as seen in **Figure 5.4(F-G)**.

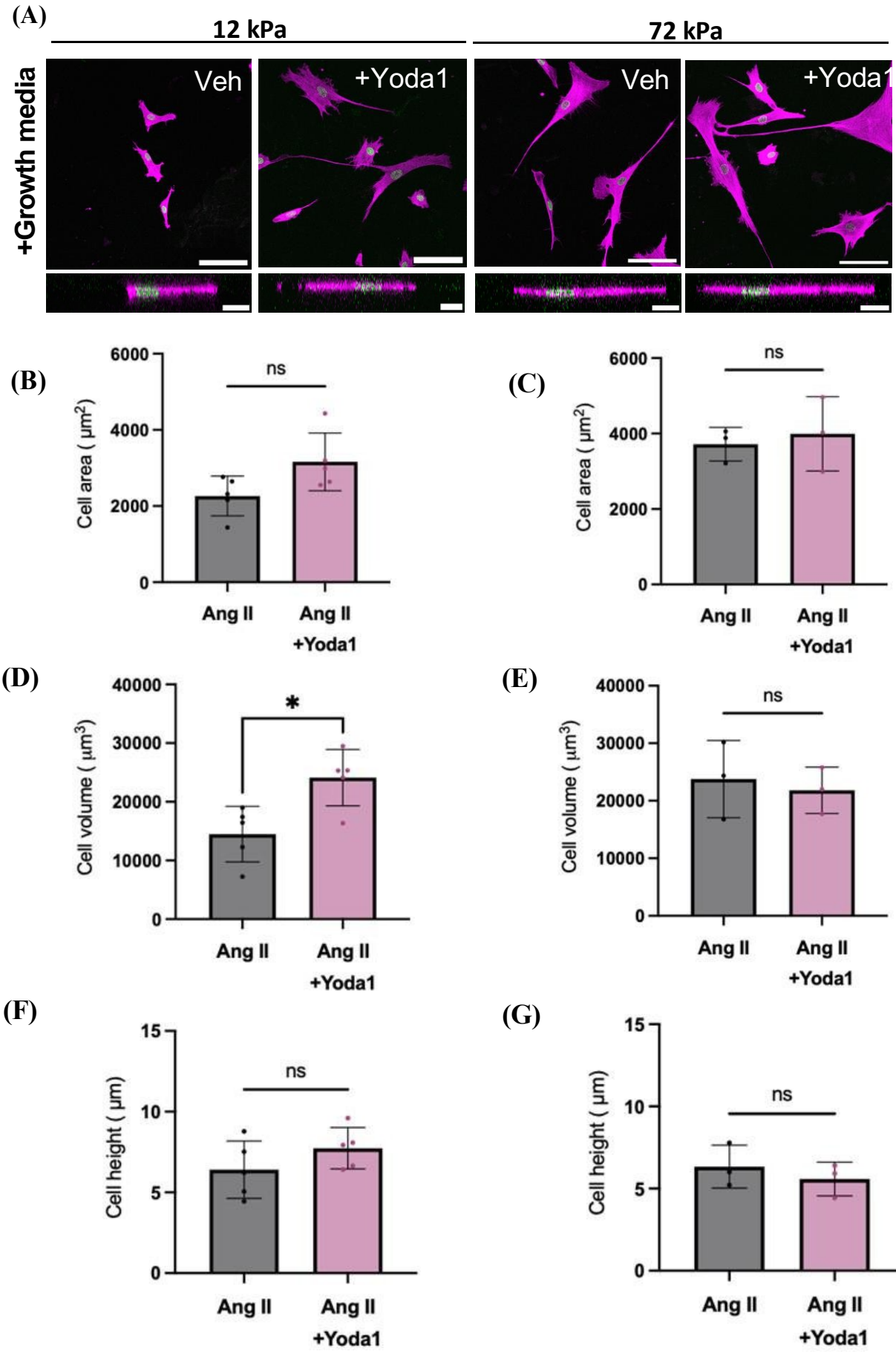
(A)
12 kPa
72 kPa
+Growth media
Veh
+Yoda1
Veh
+Yoda1
(B)
Cell area (µm2)
6000
4000
2000
0
ns
Ang II
Ang II +Yoda1
(C)
Cell area (µm2)
6000
4000
2000
0
ns
Ang II
Ang II +Yoda1
(D)
Cell volume (µm3)
40000
30000
20000
10000
0
*
Ang II
Ang II +Yoda1
(E)
Cell volume (µm3)
40000
30000
20000
10000
0
ns
Ang II
Ang II +Yoda1
(F)
Cell height (µm)
15
10
5
0
ns
Ang II
Ang II +Yoda1
(G)
Cell height (µm)
15
10
5
0
ns
Ang II
Ang II +Yoda1

Figure 5.4 Yoda1 treatment does not alter the volume on rigid PAHs (A) *Representative images of DMSO Vehicle control and Yoda1 pretreated Quiescent VSMCs prior to angiotensin II stimulation on 12 or 72 kPa PAHs. Actin cytoskeleton (magenta) and DAPI labelled nuclei (green). Top panel shows representative XY images of VSMC area, scale bar = 100 μm. Bottom panel shows representative XZ images of VSMC height, scale bar = 20 μm.* ***(B)*** *VSMC area on 12 kPa PAH,* ***(C)*** *VSMC area on 72 kPa PAH,* ***(D)*** *VSMC volume on 12 kPa PAH,* ***(E)*** *VSMC volume on 72 kPa PAH* ***(F)*** *VSMC height on 12 kPa PAH* ***(G)*** *VSMC height on 72 kPa PAH and represent 3 independent experiments with ≥42 cells analysed per condition. Mean data of individual repeats of the 3 independent experiments are shown as dots. Significance was determined using a one-way ANOVA followed by Tukey's test (significant; * $p < 0.05$, ** $p \leq 0.01$, *** $p \leq 0.001$, **** $p \leq 0.0001$).*

5.4.5 The inhibition of aquaporin-1 reduces VSMC volume on rigid PAHs

Other research in our lab confirmed that piezo-1 drove extracellular Ca^{2+} into the VSMCs leading to increases in cell volume on rigid PAHs. We investigated aquaporin 1, predicting its involvement in the downstream processes that drive VSMC volume increase. VSMCs were incubated in TCAQP1, (aquaporin-1 blocker) for a period of 18 hours in growth media on pliable and rigid PAHs. The results confirm a matrix rigidity induced response as there was no significant difference between control and TCAQP1 treated area and volume of VSMCs seeded on 12 kPa PAHs **Figure 5.5(A,B&D)**. Additionally, there was a reduction in both cell area and volume in TCAQP1 treated VSMCs on rigid PAHs **Figure 5.5(A,C&E)**. There was no change in cell height on either PAH **Figure 5.5(F&G)**. These results suggest that VSMCs that are on rigid matrices have an increase in AQP1 levels resulting in the influx of water into the cell causing the increase in cell volume.

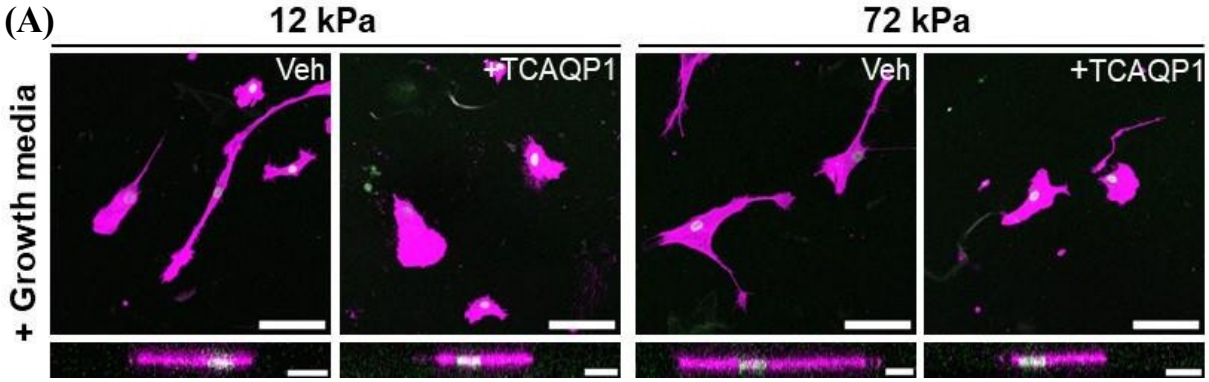
(A)
12 kPa
72 kPa
+ Growth media
Veh
+TCAQP1
Veh
+TCAQP1

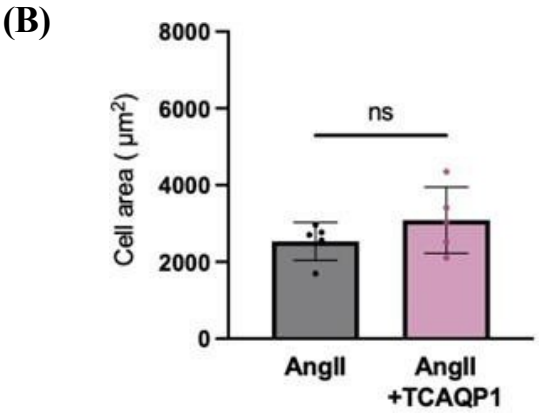
(B)
Cell area (µm2)
8000
6000
4000
2000
0
ns
AngII
AngII +TCAQP1

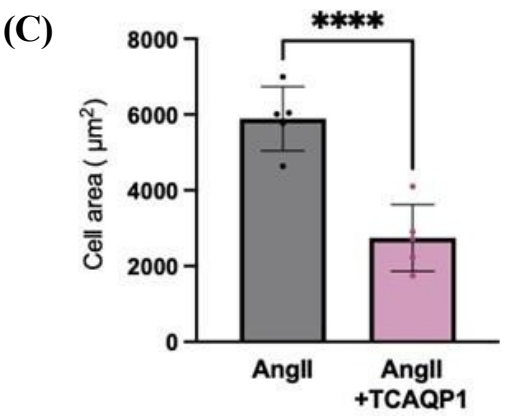
(C)
****
Cell area (µm2)
8000
6000
4000
2000
0
AngII
AngII +TCAQP1

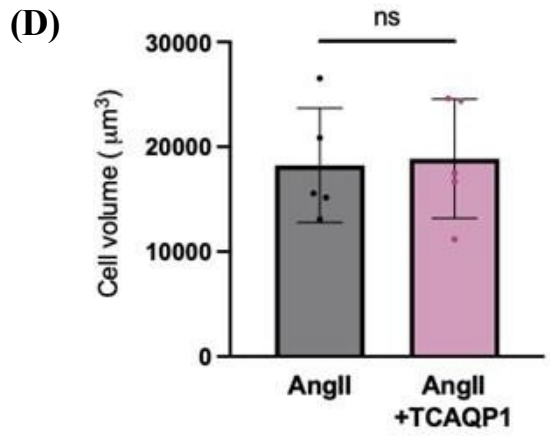
(D)
ns
Cell volume (µm3)
30000
20000
10000
0
AngII
AngII +TCAQP1

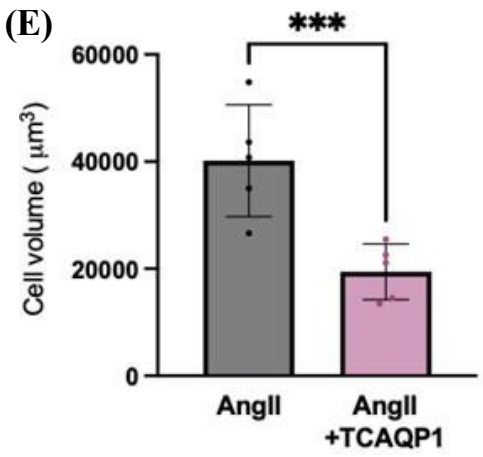
(E)
***
Cell volume (µm3)
60000
40000
20000
0
AngII
AngII +TCAQP1

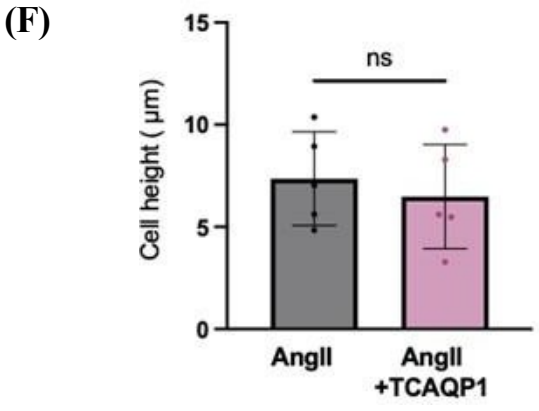
(F)
Cell height (µm)
15
10
5
0
ns
AngII
AngII +TCAQP1

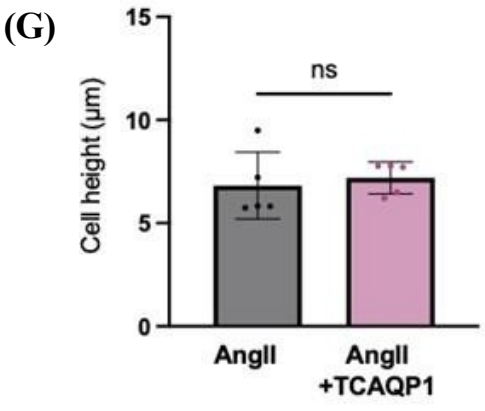
(G)
Cell height (µm)
15
10
5
0
ns
AngII
AngII +TCAQP1

Figure 5.5 The inhibition of aquaporin-1 reduces VSMC volume on rigid PAHs (A) *Representative images of isolated VSMCs seeded on 12 or 72 kPa polyacrylamide hydrogels incubated in growth media for 18 h ± TCAQP1. Actin cytoskeleton (magenta) and DAPI labelled nuclei (green). Top panel shows representative XY images of VSMC area, scale bar = 100μm. Bottom panel shows representative XZ images of VSMC height, scale bar = 20μm. Graphs show* ***(B)*** *VSMC area on 12 kPa PAHs,* ***(C)*** *VSMC area on 72 kPa PAHs,* ***(D)*** *VSMC volume on 12 kPa PAHs,* ***(E)*** *VSMC volume on 72 kPa PAHs and* ***(F)*** *VSMC height on 12 kPa PAHs,* ***(G)*** *VSMC height on 72 kPa PAHs. Graphs represent combined data from five independent experiments with ≥50 cells analysed per condition. Mean data from each individual repeat of the five independent experiments are shown by a dot. Significance was determined using an unparalleled t-test (significant; * p< 0.05, ** p≤0.01, *** p≤0.001, **** p≤0.0001).*

5.4.6 PKC inhibition reduces VSMC volume on rigid PAHs

We screened for ion transport channels that are known to play a role in regulatory volume increase in other cell types such as NKCC and WNK (202). This was done by other members of the lab in angiotensin II treated VSMCs. This was done to elucidate if they impacted or regulated aquaporin-1 expression in VSMCs. Furthermore, I screened PKC which is a known regulator for aquaporin-1 in other cell types such as Xenopus oocytes (203). I utilised PKC inhibitor Go6983 in growth media for a period of 18 hours to study if there were long term effects on VSMC area and volume. Analysis via confocal microscopy showed that treatment with Go6983 had no effect on VSMC area or volume on 12 kPa PAHs **Figure 5.6(A,B&D)**. On 72 kPa PAHs, we saw a reduced VSMC area and volume when treated with Go6983 compared to the control **Figure 5.6(A,C&E)**. There were no significant differences in cell height on either PAH **Figure 5.6(F&G)**.

Following on from this, we wanted to know if PKC was able to cause the cellular trafficking of AQP1 in VSMCs similarly to what had been studied in HEK293 cells (203,204).

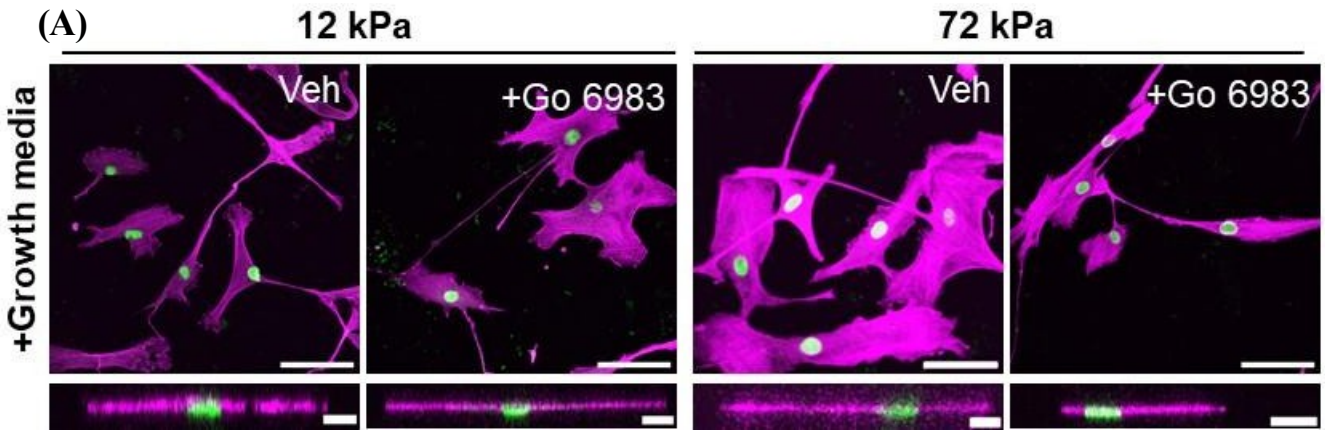
(A)
12 kPa
72 kPa
+Growth media
Veh
+Go 6983
Veh
+Go 6983

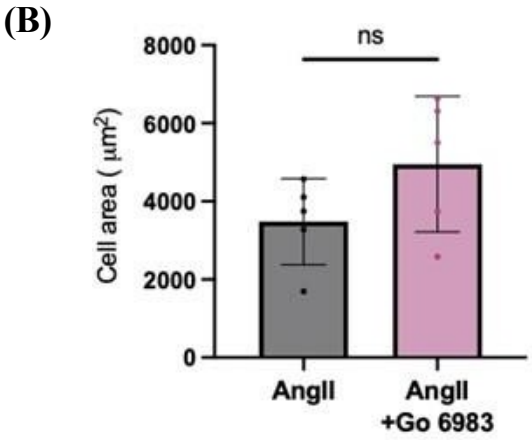
(B)
Cell area (µm²)
8000
6000
4000
2000
0
ns
AngII
AngII
+Go 6983

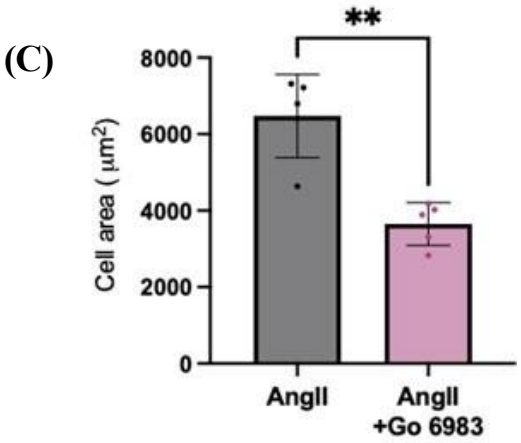
(C)
Cell area (µm²)
8000
6000
4000
2000
0
**
AngII
AngII
+Go 6983

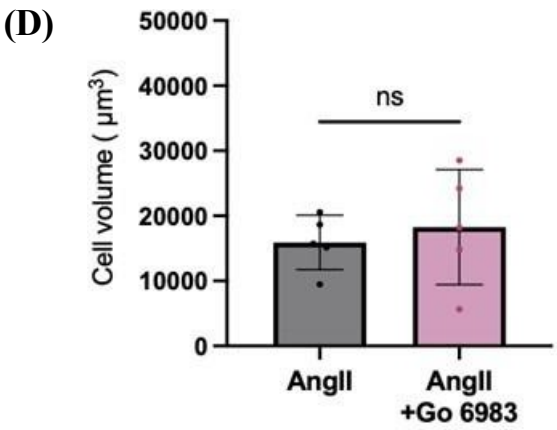
(D)
Cell volume (µm³)
50000
40000
30000
20000
10000
0
ns
AngII
AngII
+Go 6983

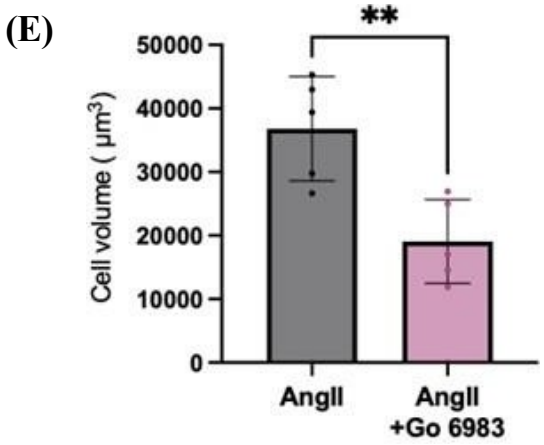
(E)
Cell volume (µm³)
50000
40000
30000
20000
10000
0
**
AngII
AngII
+Go 6983

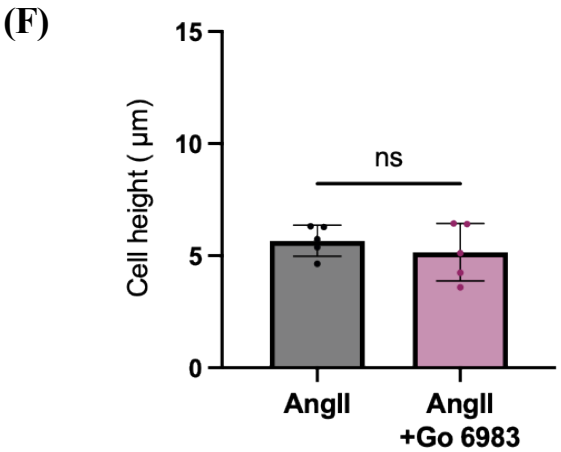
(F)
Cell height (µm)
15
10
5
0
ns
AngII
AngII
+Go 6983

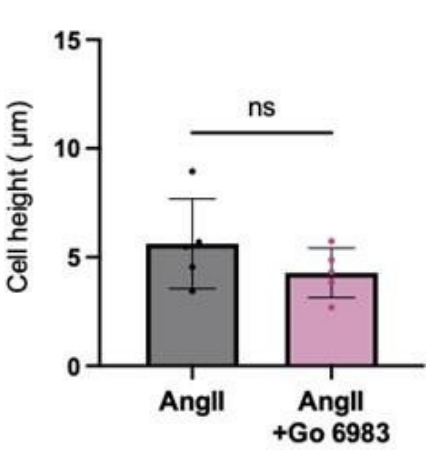
(G)
Cell height (µm)
15
10
5
0
ns
AngII
AngII
+Go 6983

Figure 5.6 PKC inhibition reduces VSMC volume on rigid PAHs (A) *Representative images of isolated VSMCs seeded on 12 or 72 kPa PAHs incubated in growth media for 18 h ± Go 6983. Actin cytoskeleton (magenta) and DAPI labelled nuclei (green). Top panel shows representative XY images of VSMC area, scale bar = 100μm. Bottom panel shows representative XZ images of VSMC height, scale bar = 20μm. Graphs show* ***(B)*** *VSMC area on 12 kPa PAHs,* ***(C)*** *VSMC area on 72 kPa PAHs,* ***(D)*** *VSMC volume on 12 kPa PAHs,* ***(E)*** *VSMC volume on 72 kPa PAHs and* ***(F)*** *VSMC height on 12 kPa PAHs,* ***(G)*** *VSMC height on 72 kPa PAHs. Graphs represent combined data from five independent experiments with ≥50 cells analysed per condition. Mean data from each individual repeat of the five independent experiments are shown by a black dot. Significance was determined using an unparalleled t- test (significant; * $p < 0.05$, ** $p \leq 0.01$, *** $p \leq 0.001$, **** $p \leq 0.0001$).*

5.4.7 Protein Kinase C regulates aquaporin-1 localisation in VSMCs

It has been seen in *Xenopus* oocytes that PKC regulates aquaporin-1 activity and promotes aquaporin-1 membrane translocation in HEK cells (197,203). We conducted a localisation assay to determine the localisation of aquaporin-1 in VSMCs both on a pliable and rigid PAH. It can be seen in **Figure 5.7(A)** that aquaporin-1 is distributed in both the nucleus and cytoplasm when stimulated by angiotensin II for the quiescent phenotype on both PAHs. Aquaporin-1 was localised towards the basal membrane in VSMCs on 12 kPa PAHs, compared to an apical localisation on the 72 kPa PAH **Figure 5.7(B)**. It was observed that aquaporin-1 was redistributed into the nucleus from cytoplasmic regions on both pliable **Figure 5.8(A&B)** and rigid PAHs **Figure 5.8(C&D)**.

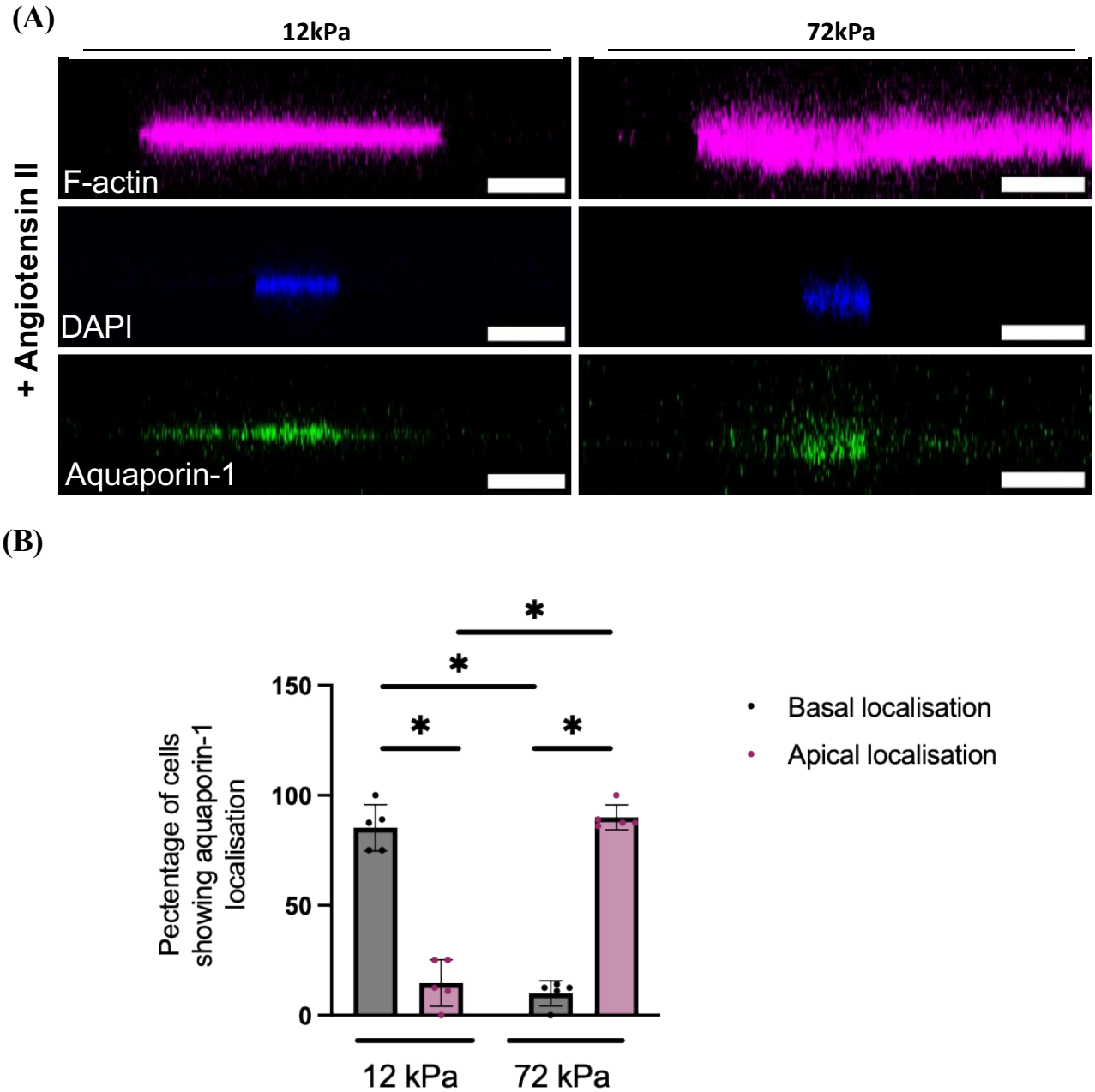

Figure 5.7 Protein Kinase C regulates aquaporin-1 localisation*in VSMCs seeded on 12 or 72 kPa PAHs.* ***(A)*** *Representative XZ images of aquaporin-1 (green), DAPI (blue) and F- actin (magenta) organisation in angiotensin II stimulated VSMCs on 12 and 72 kPa hydrogels. Scale bar = 20µm.* ***(B)*** *Graph shows percentage of VSMCs displaying basal and apical localisation of aquaporin-1 and represents the combined data of 5 independent experiments with ≥40 cells analysed per condition. Mean data of individual repeats of the 5 independent experiments are shown as black dots (basal) or purple dots (apical). Significance determined using a one-way ANOVA followed by Tukey's multiple comparison test. (* = $p < 0.05$, error bars represent ± SEM).*

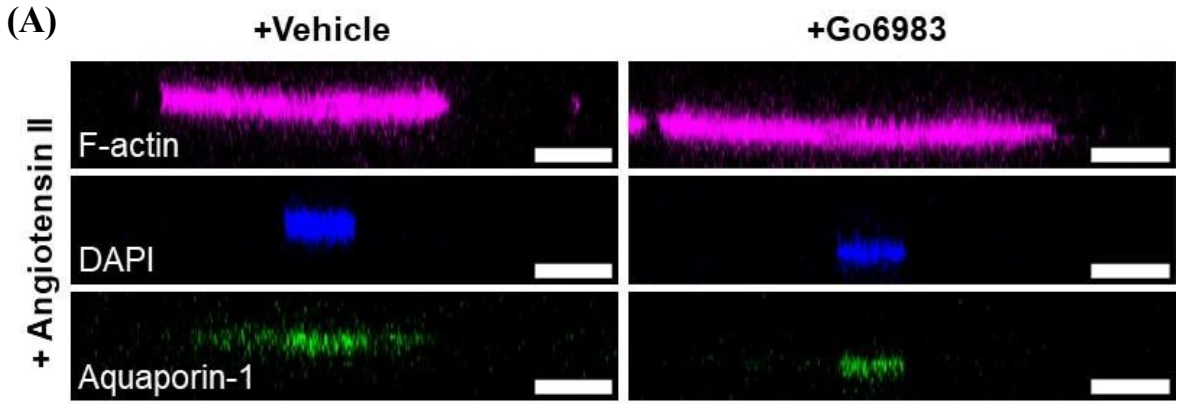
(A)
+Vehicle
+Go6983
+ Angiotensin II
F-actin
DAPI
Aquaporin-1

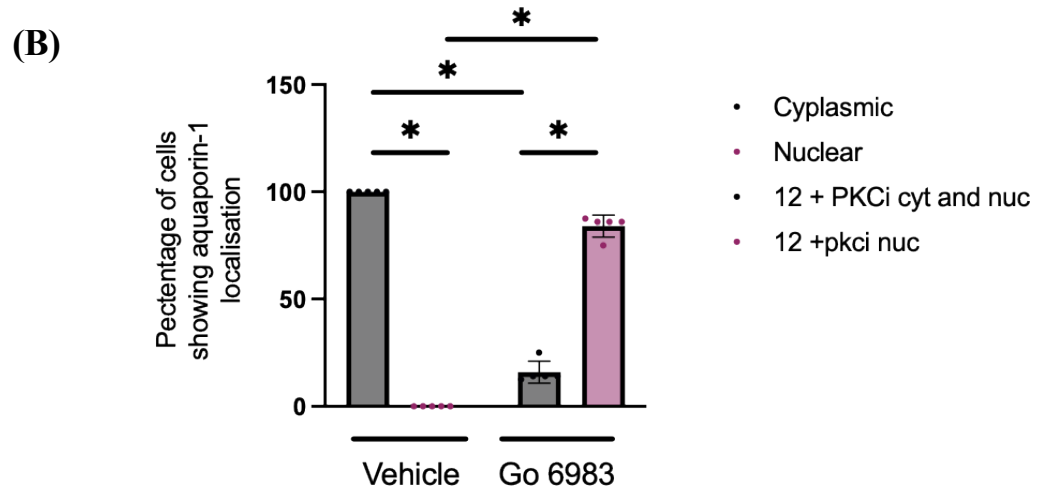
(B)
Pectentage of cells showing aquaporin-1 localisation
150
100
50
0
Vehicle
Go 6983
Cyplasmic
Nuclear
12 + PKCi cyt and nuc
12 +pkci nuc

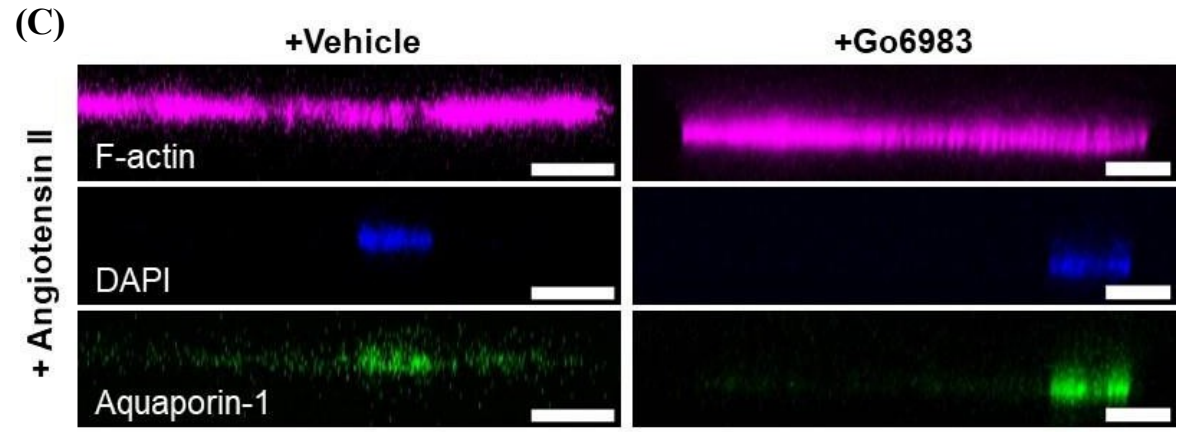
(C)
+Vehicle
+Go6983
+ Angiotensin II
F-actin
DAPI
Aquaporin-1

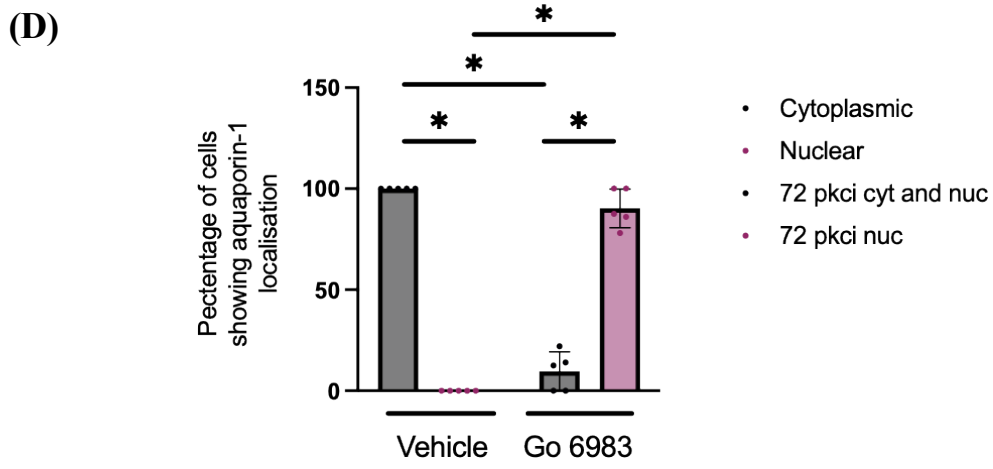
(D)
Pectentage of cells showing aquaporin-1 localisation
150
100
50
0
Vehicle
Go 6983
Cytoplasmic
Nuclear
72 pkci cyt and nuc
72 pkci nuc

Figure 5.8 (A) Protein Kinase C regulates aquaporin-1 localisation *Representative XZ images of aquaporin-1 (green), DAPI (blue) and F-actin (magenta) organisation in angiotensin II stimulated VSMCs on 12 kPa hydrogels treated with either vehicle control (DMSO) or Go 6983 prior to angiotensin II stimulation. Scale bar = 20 µm.* ***(B)*** *Graph shows percentage of VSMCs seeded on 12 kPa PAHs showing cytoplasmic and nuclear localisation of aquaporin-1. Combined data of 5 independent experiments with ≥37 cells analysed per condition.* ***(C)*** *Representative XZ images of aquaporin-1 (green), DAPI (blue) and F-actin (magenta) organisation in angiotensin II stimulated VSMCs on 72 kPa hydrogels treated with either vehicle control (DMSO) or Go 6983 prior to angiotensin II stimulation. Scale bar = 20µm.* ***(D)*** *Graph shows percentage of VSMCs seeded on 12 kPa PAHs showing cytoplasmic and nuclear localisation of aquaporin-1. Combined data of 5 independent experiments with ≥37 cells analysed per condition. Mean data of individual repeats of the 5 independent experiments are shown as black dots (cytoplasmic) or purple dots (nuclear). Significance determined using a one-way ANOVA followed by Tukey's multiple comparison test. (* = $p < 0.05$, error bars represent ± SEM).*

5.5 Discussion

VSMC hypertrophy has been linked to hypertension due to its contribution to aortic wall thickening, increasing aortic stiffness thereby reducing aortic compliance (93). This relationship between hypertrophy and hypertension is cyclic in nature but the mechanisms causing this are poorly understood.

In this chapter we investigated and identified the pathways that led to the increase of VSMC volume on rigid matrices. Other studies from our lab have shown that the increase of Ca^{2+} from internal stores in VSMC are not only key drivers to contraction but cause an increased volume response to Angiotensin II stimulation on rigid matrices (128). Through the assays conducted in this chapter we have also uncovered the greater influx of extracellular Ca^{2+} through mechanosensitive SACs. Through the inhibition and knockdown of Piezo1 we have been able to identify it as an important regulator of VSMC swelling when VSMCs are exposed to rigid matrices. The data yielded in this chapter provides strong evidence that Piezo1 is upregulated in VSMCs that are on a rigid matrix. We observed that VSMCs seeded on 72 kPa PAHs when treated with non-targeting siRNA Piezo1 an increase compared to that on 12 kPa PAHs. This was especially true in our growth media assay in the longer period of 24 hours. This hypothesis was further confirmed when Piezo1 depleted VSMCs possessed a decrease in cell volume. The inhibition of Piezo1 has been confirmed to prevent mice from developing abdominal aortic aneurysms. (190)Additionally, Piezo1 agonist Yoda1 induced apoptosis in VSMCs via Ca^{2+} overload, the generation of ROS and mitochondrial dysfunction (191). Yoda1 treatment on Angiotensin II stimulated VSMCs resulted in increased volume on 12 kPa PAHs. We did not see this similar increase in volume in VSMCs seeded on 72 kPa PAHs, suggesting that the VSMCs are at their maximum size and cannot further respond to their rigid environment. GSMTx-4 another inhibitor of mechanosensitive ion channels such as Piezo1 caused a reduction in VSMC area and volume in VSMCs on 72 kPa PAHs. This data further confirms that Piezo1 Ca^{2+} influx drives the increase of VSMC volume.

Additional data performed by other lab members that compliments that in this chapter includes the shorter angiotensin II treatment assays which represent the effect of a drug on quiescent VSMCs. Other complimentary data was fluo-4 calcium imaging where we were able to capture the levels of Ca^{2+} within the VSMCs on either PAH with or without drug treatment. By measuring fluo-4 fluorescence we could see that Ca^{2+} was tightly regulated in VSMCs on pliable hydrogels when treated with angiotensin II compared to those on a rigid PAH. VSMCs

on 72 kPa PAHs, had a broader, multiple, and sustained peaks of Ca^{2+} influx. Increased piezo1 activity in VSMCs resulted in a sustained increase in intracellular Ca^{2+}.This suggests a mechanism that results in VSMC swelling.

We hypothesised the involvement of aquaporins in matrix-induced VSMC swelling in addition to the Piezo1 driven Ca^{2+} influx. Aquaporin-1 is expressed within VSMCs, but there is limited knowledge on its function. Our data shows it is involved in VSMC swelling as its inhibition results in a decrease of cell area and volume. Furthermore, we investigated PKC as it is a known membrane trafficker of aquaporin-1, its inhibition also led to the reduction in VSMC area and volume (197,205). ***Figure 5.9*** represents our hypothesis of a novel pathway that drives VSMC swelling in rigid environments. The increase of intracellular Ca^{2+} via the activation of piezo1 channels activates PKC. The aquaporin-1 localisation assay allowed us to confirm that PKC caused aquaporin- 1 channels to move to the plasma membrane increasing water transport into the VSMC. Moreover, single cell RNA-sequencing (scRNA-seq) performed by a collaborator emphasised our findings as piezo1 and aquaporin-1 gene expression was increased in disease relevant VSMC phenotypes (128). This also affirms our hypothesis that the components of this pathway are up-regulated in aortic disease.

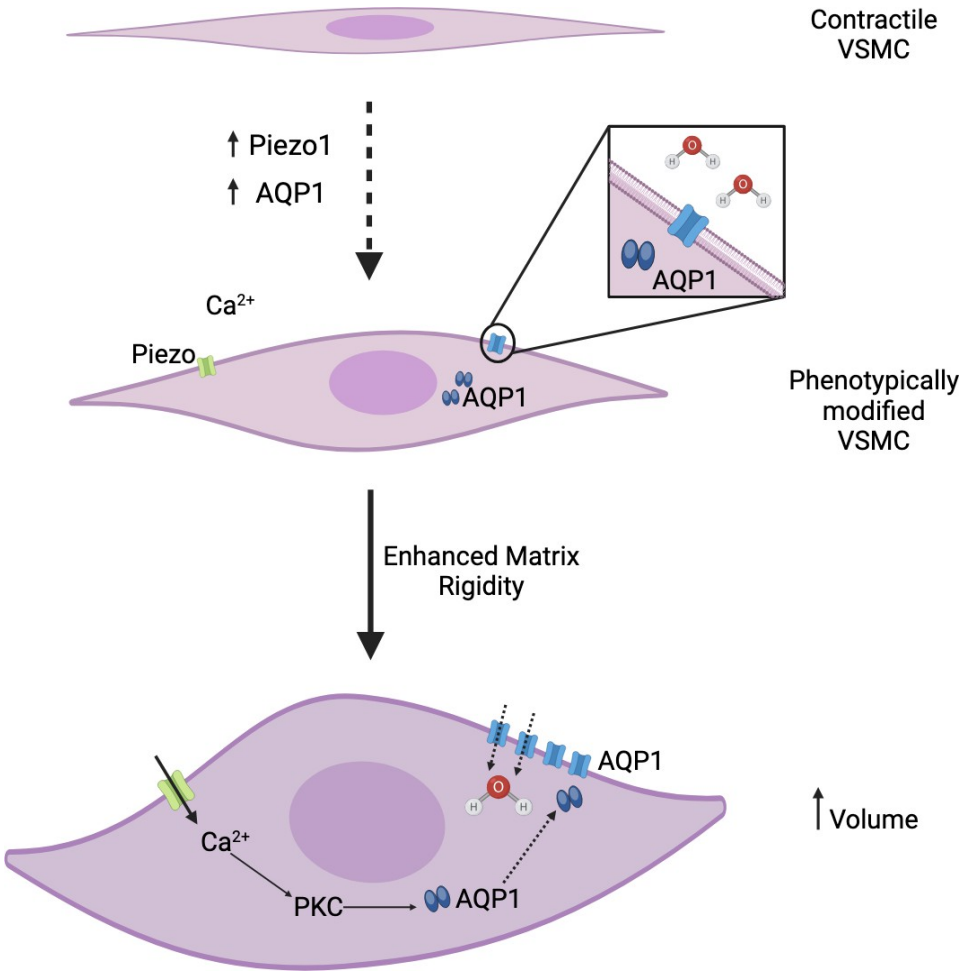

Figure 5.9 *A figure to represent the novel mechanical pathway that induces vascular smooth muscle cell swelling when exposed to enhanced matrix rigidity.*

Chapter 6: Final discussion and conclusion

6.1 Final discussion

Overall this thesis has shown the mechanisms driving VSMC dysfunction in response to matrix rigidity, a key factor in diseases like atherosclerosis and hypertension. VSMCs, typically quiescent in healthy vessels, can become proliferative and contribute to vascular stiffening in ageing or diseased arteries, where the extracellular matrix (ECM) is stiffer. Using PAHs to manipulate matrix stiffness, we investigated how VSMCs react to both physiological and pathological conditions. We identified key players in this process, such as HDACs, particularly HDAC3 and HDAC6, which regulate VSMC volume and DNA damage. Inhibition of HDAC3 was shown to reduce VSMC hypertrophy on rigid matrices, while HDAC6 played a role in tubulin acetylation, influencing VSMC hypertrophy through microtubule dynamics. Further work in HDACs was halted due to my contributions towards a paper in the British Journal of Pharmacology where I helped to identify a Piezo1/PKC/Aquaporin-1 pathway driving VSMC dysfunction in cardiovascular diseases. This significant shift in focus toward Piezo1 revealed its role in promoting VSMC hypertrophy in response to rigid matrices, with calcium influx being critical for this process. Additionally, we linked aquaporin-1 to VSMC hypertrophy, showing its potential as a therapeutic target. Through these findings, this thesis presents novel insights into how matrix rigidity contributes to VSMC dysfunction and suggests potential therapeutic pathways for improving aortic compliance and alleviating vascular stiffness in diseases.

VSMCs are the majority cell type in the middle layer of the arterial wall, the tunica media (206). VSMCs typically exist in a quiescent state and express proteins consistent with the contractile phenotype. This allows them to maintain vascular tone. Vessel tone and compliance is essential for regulation of blood pressure within the arterial network. In aged or damaged vessels, VSMCs can dedifferentiate into a proliferative state. The disease phenotype is also associated with an ECM of a greater elastic modulus, 60-250 kPa, compared to a healthy modulus of 10 - 20 kPa. Pathological remodelling of the aorta from CVDs such as atherosclerosis, results in stiffened arteries further contributing to the disease cycle (49,175,207).

Increased vascular stiffness is also accompanied by increases in VSMC stiffness as well as increased cell-matrix adhesion. This contributes to the decline of vascular function and vascular stiffening. This concept is known as smooth muscle cell stiffness syndrome (SMCSS)(208).

Our work utilises polyacrylamide hydrogels with a defined elastic modulus allowing us to control the stiffness that VSMCs are cultured on. This work was performed on a 2D system that allowed us to isolate the contractile pathway of the VSMCs. This is critical to understanding the mechanisms that drive VSMC dysfunction in response to rigid matrices. The VSMC response to pliable and rigid PAHs highlights the importance of matrix stiffness in VSMC studies compared to those on plastic/glass. This response via loss of contractility on stiffer matrices would have been overlooked in other studies using standard cell culture methods. VSMCs treated with angiotensin II on a 72 kPa PAHs are unable to contract as much as those on 12 kPa PAHs. We have also linked increased matrix stiffness to increased actomyosin force generation in VSMCs (209,210). Elucidating the mechanism of this VSMC response to rigid matrices is essential in identifying novel therapeutic targets to relieve vascular and VSMC stiffening in both ageing and disease. Previous work has shown that using 2D substrates could differ from accurate *in vivo* responses as there are cell-cell interactions that could effect VSMC behaviour. An example of this can be vasodilation of the vessel caused by nitric oxide-mediated relaxation of the VSMCs by the intimal layer of endothelial cells. Therefore, we need to take into account external cues beyond our system to gain a clearer understanding of the relationship between aortic compliance, VSMC function and vessel tone regulation.

HDACs play a pivotal role in regulating gene expression and cellular behaviour. They are therefore targets of interest in CVD research. Examples of processes regulated by these post-translational modifications include cell proliferation, inflammation, differentiation and migration (132). Understanding how HDACs control these processes is vital, as they directly contribute to pathological changes in blood vessels, such as atherosclerosis, hypertension, and vascular calcification. The role of HDACs in VSMCs is not extensively understood and our work is essential in unveiling mechanisms for future therapeutic strategies.

In Chapter 3, we were able to show which HDACs affected VSMC area through the screening of multiple inhibitors. More importantly, our use of PAHs allows us to understand the effect of these inhibitors in both physiological and pathological conditions. This allows us to find targets that only implicate diseased or aged VSMCs. We found that not all HDACs have beneficial effects in VSMCs or no effect in attenuating the increase in cell area of those seeded on 72 kPa PAHs. We discovered that HDAC1, 3 and 6 had potential in decreasing cell area of VSMCs seeded on 72 kPa PAHs. Due to time constraints, we were only able to perform follow-up studies

on HDAC 3 and 6. Interestingly, only one of the two HDAC 6 inhibitors we tested influenced VSMCs on either pliable or stiff PAHs. To further determine whether these specific HDACs played any role in attenuating VSMC hypertrophy we examined their impact on VSMC volume. HDAC3 was able to decrease VSMC volume at working concentration which validates the previous HDAC3 screening work. The initial working model from our work in Chapter 3 is highlighted in **Figure 6.1**, we have only included the effects of HDAC3 and HDAC6 inhibitors as we further investigated them in Chapter 4. HDAC3 is thought to be a predominantly nuclear HDAC, despite this there was an absence of nuclear area or volume changes on either PAH. This may be explained by some earlier studies that suggest that HDAC3 is able to move out of the nucleus into the cytoplasm (135). More specifically, other studies confirm that HDAC3 possesses a unique ability to localise to both the nucleus and cytoplasm compared to other class I HDACs (211– 213).

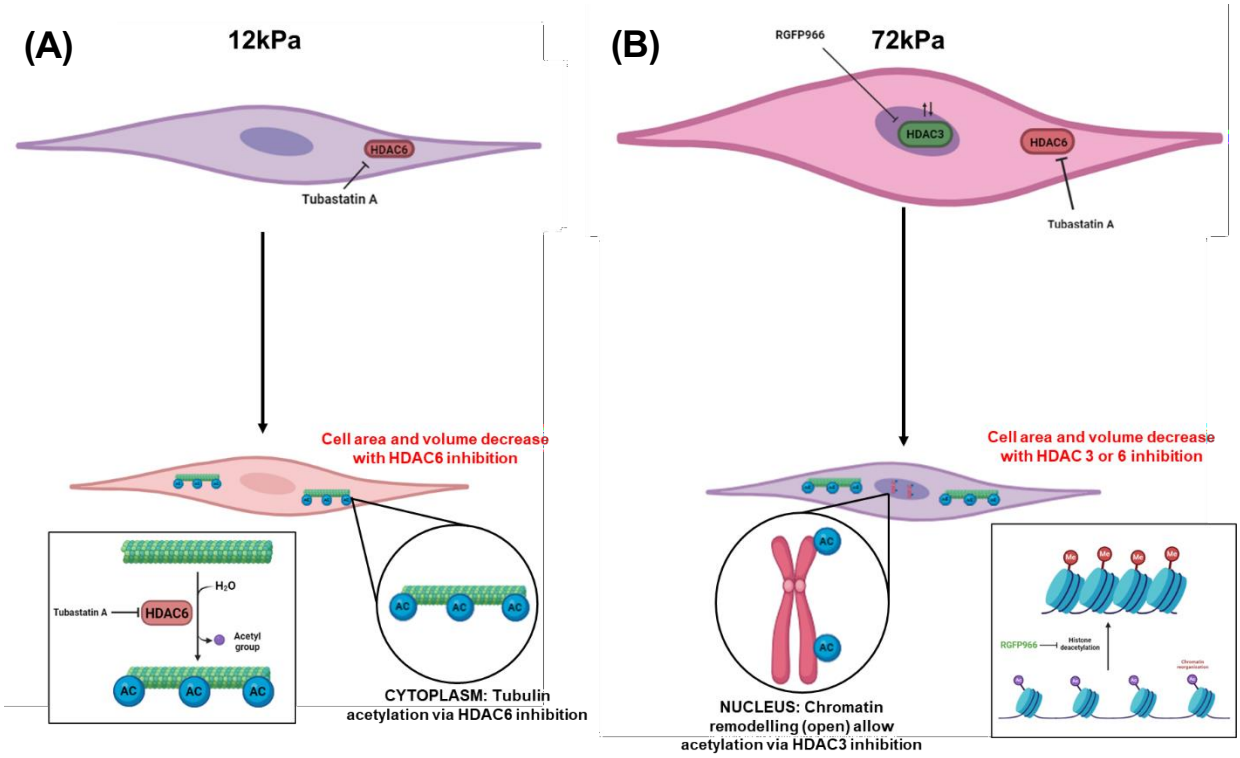

Figure 6.1 *The initial working model revealing the effects of HDAC3 and -6 in VSMCs on* ***(A)*** *12 kPa PAHs* ***(B)*** *72 kPa PAHs. HDAC3 inhibition acetylates the histone moving it into the open position allowing key gene activation and changes to cell function. HDAC3 more commonly localised in nucleus and is inhibited by RGFP966. HDAC6 localised in cytoplasm, inhibited by Tubastatin A. Tubastatin A acetylates α-tubulin and causes cell volume increase on pliable and rigid PAHs.*

We additionally explored the role of microtubules to determine the mechanism causing these changes in cell area and volume. Due to time constraints, we were only able to perform one repeat of our cold-stable microtubule (CSM) assay with RGFP966 treatment in VSMCs on 12

and 72 kPa PAHs. Although we were not able to perform statistical analysis, it seems that the number of CSMs increases on both PAHs. Additionally, we found that the number of γH2AX foci increased in VSMCs seeded on 72 kPa with angiotensin II stimulation. This suggests that the hypertrophy experienced by VSMCs on rigid matrices put pressure on the nucleus increasing levels of DNA damage. Furthermore, we observed that there was no significant change in 53BP1 presence with RGFP966 treatment on 72 kPa PAHs, suggesting that it may not have a role in rectifying DNA damage at a later stage than γH2AX. We found that with RGFP966 treatment, we were able to reduce the levels of DNA damage in VSMCs seeded on a rigid matrix. We show that HDAC3 may have a beneficial role in attenuating DNA damage in aged and diseased VSMCs. This shows potential to inhibit the effects of cell senescence observed in CVD (214).

Although a lot is known of the role of HDAC in cancer therapies with some de novo inhibitors entering clinical trials the role of HDAC6 in VSMCs is currently unknown. HDAC6 is another unique HDAC as it can act on non-histone substrates such as □- tubulin and tau protein. Earlier studies note that HDAC6 contributes to maladaptive remodelling in heart and skeletal muscle (145). Other studies link HDAC6 activity to cardiac hypertrophy, pulmonary hypertension and atherosclerosis (215). HDAC6 is a member of Class-IIb HDACs, which are able to alter microtubule dynamics via tubulin acetylation (216). Our initial screenings showed that the HDAC6 inhibitor, Tubastatin A, was able to decrease VSMC area on both 12 and 72 kPa PAHs. As HDAC6 inhibition has been characterised as beneficial in different CVDs, we expected to see a reduction in cell area and volume in VSMCs seeded on rigid PAHs. Interestingly, Tubastatin A treated VSMCs were of greater volume than angiotensin II only treated cells on pliable PAHs. Tubastatin had no effect in quiescent VSMCs on rigid PAHs. These results of HDAC3 and HDAC6 inhibition at working concentrations on VSMC cell area and volume can be summarised in **Figure 6.2** below. To ensure that this effect was driven by HDAC6 disruption, we performed an siRNA-mediated knockdown. It was confirmed that HDAC6 depleted VSMCs possessed an increased volume compared to VSMCs treated with a scrambled control. The knockdown of HDAC6 had no effect on VSMCs seeded on rigid PAHs. We hypothesised that the change in volume in VSMCs on pliable PAHs may be due to tubulin acetylation altering microtubule stability. However, the number of cold stable microtubules remained unaltered with Tubastatin treatment. Other concurrent studies from the Warren Lab performed by Finn Wostear found that Ca^{2+} influx was prolonged in Tubastatin treated VSMCs on pliable PAHs, with no change on rigid PAHs (129). These findings imply that tubulin acetylation may be involved in triggering stretch activated channels allowing the influx of Ca^{2+}. We also tested the effects of

HDAC6 inhibition on DNA damage. We observed that there was an increase in both γH2AX and 53BP1+ foci in VSMCs treated with Tubastatin A on pliable PAHs. Similar effects were seen in siRNA-mediated HDAC6 knockdowns. This result correlates an increase of area and volume with increased levels of DNA damage. With this data we have been able to confirm that epigenetic modifications such as acetylation play a role in VSMC response to matrix rigidity via chromatin reorganisation.

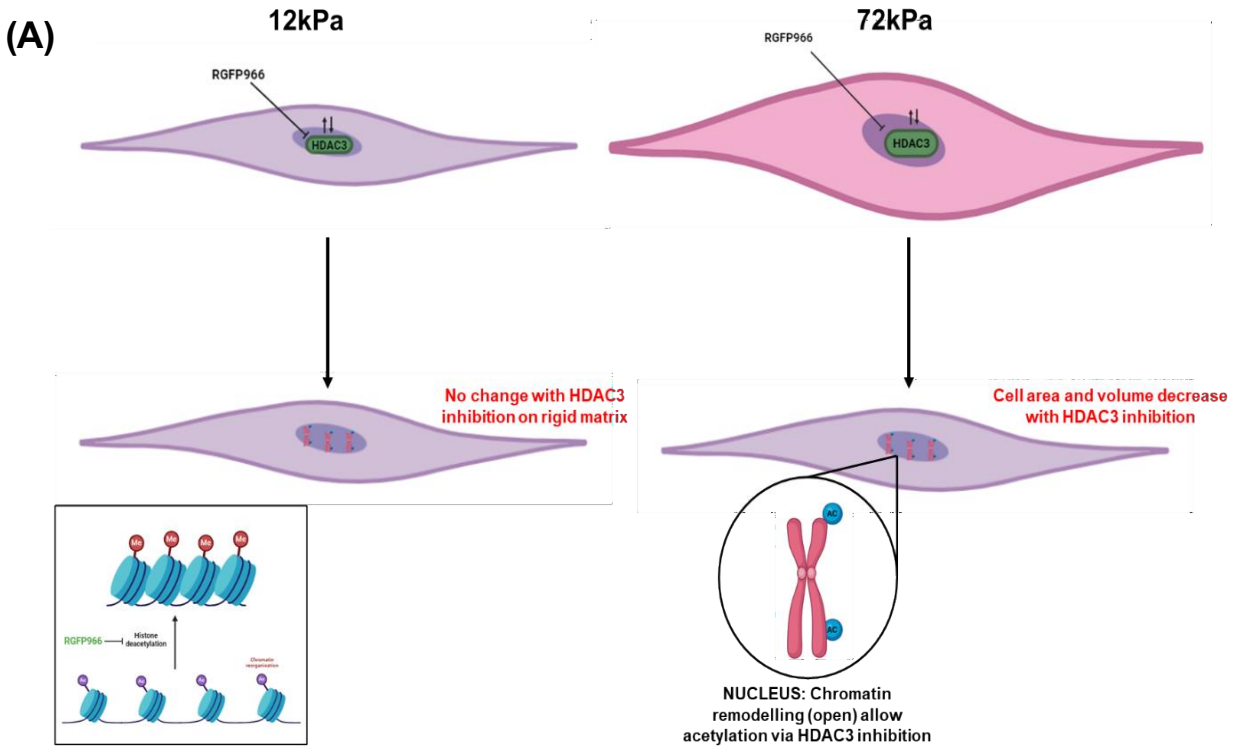
(A)
12kPa
72kPa
RGFP966
HDAC3
RGFP966
HDAC3
No change with HDAC3 inhibition on rigid matrix
Cell area and volume decrease with HDAC3 inhibition
Me
RGFP966
Histone deacetylation
AC
NUCLEUS: Chromatin remodelling (open) allow acetylation via HDAC3 inhibition

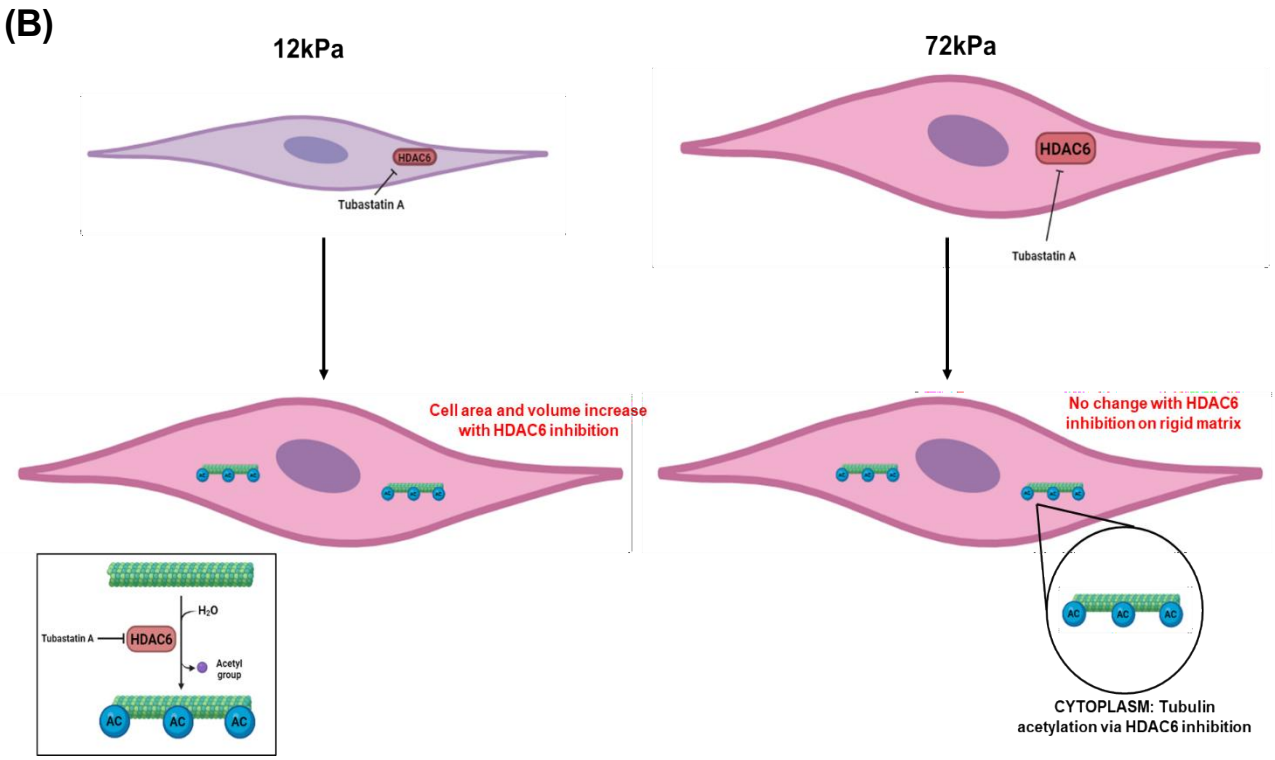
(B)
12kPa
72kPa
HDAC6
Tubastatin A
HDAC6
Tubastatin A
Cell area and volume increase with HDAC6 inhibition
No change with HDAC6 inhibition on rigid matrix
Tubastatin A
HDAC6
H2O
Acetyl group
AC
AC
AC
AC
AC
AC
CYTOPLASM: Tubulin acetylation via HDAC6 inhibition

Figure 6.2 *An update working hypothesis to represent HDAC inhibitor roles in VSMCs* ***(A)*** *An updated working model to represent the effect of HDAC3 inhibitor, RGFP966 on VSMCs on either a 12- or 72 kPa PAH.RGFP966 acetylated the histone leading to an "open" conformation. This chromatin remodelling allows for gene activation, inhibiting hypertrophy of VSMCs on rigid matrices.* ***(B)*** *A working model to show the effects of Tubastatin A at working concentration, 1μM, on VSMCs on either 12- or 72 kPa. Tubastatin A acetylates α-tubulin which causes VSMC hypertrophy on pliable matrices, no change on rigid matrices. Tubulin acetylation may be triggering SACs causing influx of* Ca^{2+} *leading to hypertrophy.*

Future work on HDAC roles in VSMC response to matrix rigidity could include the siRNA-mediated knockdown of HDAC3, similar to our HDAC6 studies. We would like to further explore the effects of HDAC1 inhibition on VSMC hypertrophy as our initial screening demonstrated a decrease in cell area on rigid matrices. The class I HDACs are pro-hypertrophic (217). The role of HDAC1 in VSMC stiffness and hypertrophy is less well defined but due to its suspected involvement in cardiac hypertrophy, it warrants further investigation.

In chapter 5, I changed the course of my investigation. However, the overall aim of this thesis remained the same, to investigate the mechanisms contributing to VSMC response to rigid matrices. I decided to refocus my efforts towards investigating the role of piezo1 on promoting VSMC hypertrophy on rigid matrices. The reason for this was that we were submitting a paper to the British Journal of Pharmacology, of which I was a co-first author. Piezo1 has been implicated in the VSMC response to matrix rigidity in earlier studies from the Warren Lab. We previously found that Piezo1 expression was upregulated in VSMCs in rigid environments, however, its role in hypertrophy and mechanisms driving VSMC dysfunction remain unknown. Our findings in this paper highlighted that calcium influx is essential for contraction and volume regulation. In addition to release of Ca^{2+} from internal stores the increased volume response is also driven by influx of extracellular Ca^{2+} through SACs. Specifically piezo-1 promoted VSMC hypertrophy as a response to increased matrix rigidity. Additionally, our study suggests that VSMC hypertrophy may contribute to vessel stiffness seen in disease and ageing.

I conducted long-term assays in growth media in this study as well as some short-term angiotensin II assays. We wanted to ensure that the effects we were seeing in our short-term assays were sustained over a longer period. We found that the inhibition of SACs with GsMTx-4 reduced VSMC hypertrophy on rigid matrices. The siRNA- mediated knockdown of piezo1

conducted in growth media also inhibited VSMC hypertrophy on rigid matrices. These studies confirmed SAC involvement in ECM rigidity mediated VSMC hypertrophy. The allosteric activator of piezo1, Yoda 1, did not increase VSMC area or volume on the rigid hydrogels. This result suggests that VSMCs are at their maximum capacity on the 72 kPa PAH and are unable to expand any further.

Downstream to piezo1, we implicated aquaporin-1 in the VSMC hypertrophic response. Until now, the functional significance of aquaporin-1 in VSMCs had yet to be confirmed. Our findings show that inhibition of aquaporin-1 reduces VSMC hypertrophy. This was further validated by single cell sequencing datasets that revealed the upregulation of aquaporin-1 in pathological VSMC populations. Single cell sequencing also demonstrated the upregulation of piezo1. This suggests that piezo1 and aquaporin-1 are involved in the pathophysiology of diseases such as atherosclerosis. This data was collected by collaborators at the University of Cambridge. Our study also found that PKC, a known regulator of aquaporin-1, was able to reduce VSMC hypertrophy on rigid matrices even over a longer time period. In this study, we have been able to prove that PKC can regulate aquaporin-1 in VSMCs. Our studies show that PKC activity contributes to aquaporin-1 relocation from the nucleus to the cell membrane.

We have been able to provide novel mechanistic insights into VSMC response to matrix rigidity that have not been previously demonstrated. We have presented potential therapeutic pathways for the reduction of VSMC hypertrophy and aortic rigidity allowing for the reinstatement of efficient aortic compliance.

6.2 Strengths, Limitations and Future Directions

Whilst we have been able to provide new mechanistic insights into the VSMC response to matrix rigidity, we have a number of limitations to our study. Our use of primary human aortic VSMCs, this contributes to the variation we see in the data. This is a 2D and single cell approach, which reduces the effects of cell-cell interactions that we would see *in vivo* or future 3D systems. We are able to effectively interrogate the signalling pathways in our system however this differs from an organized 3D co-culture environment. Future work will include validating these findings in both *ex vivo* and *in vivo* systems to confirm the robustness of our approach. However, the significance of our results is underscored by gene expression data from single-cell sequencing, which show increased expression of Piezo1 and Aquaporin-1 in disease-relevant VSMC phenotypes.

To further understand the role of HDACs in VSMC dysfunction, further work with HDAC3 such as siRNA knockdown and HDAC1 should be investigated.

6.3 Conclusion

VSMCs play an essential role in the normal functioning of the aorta, with any aberrant changes leading to cell senescence and disease progression. Aortic rigidity and VSMC stiffness have emerged as important biomarkers in multiple CVDs. However, the mechanisms driving this loss of compliance have remained elusive. In this thesis we have be able to identify several pathways with therapeutic potential to inhibit VSMC hypertrophy and thereby rigidity, with the potential to remediate declining aortic compliance often seen in disease. We have also found that DNA damage and microtubule stability are affected by matrix and VSMC stiffness. Although some pan-HDAC inhibitor drugs have reached clinical trials, we observe that some have a greater beneficial effect than others. Further investigation is necessary to unveil their mechanisms of action within VSMCs. We have been able to build on and publish our knowledge of SAC involvement in CVD. Following on from this, we will have to address the limitations of our study. Our 2D-assay does not fully capitulate the natural environment of VSMCs in the aortic wall. Although our PAH approach provides essential insight into cell-matrix interactions, VSMCs also experience cell-cell adhesions which can contribute to the VSMC matrix rigidity response. Further research via *ex vivo* and *in vivo* settings will allow us to validate our findings. Examples of this would be co-culture models on our PAHs or biophysical stimulation via 4Dcell static cell confiner.

References

1. Coll PP, editor. Healthy Aging: A Complete Guide to Clinical Management [Internet]. Cham: Springer International Publishing; 2019. Available from: http://link.springer.com/10.1007/978-3-030-06200-2
2. BHF. British Heart Foundation. 2023 [cited 2023 Oct 20]. 1.BHF UK CVD Factsheet 2023. Available from: https://www.bhf.org.uk/-/media/files/for-professionals/research/heart-statistics/bhf-cvd-statistics-uk-factsheet.pdf2023
3. Tedstone A, Duval D, Peacock E. Dietary health and CVD: implications for dietary policy in England. Proceedings of the Nutrition Society. 2020 Feb 30;79(1):95–102.
4. Stewart J, Manmathan G, Wilkinson P. Primary prevention of cardiovascular disease: A review of contemporary guidance and literature. JRSM Cardiovasc Dis [Internet]. 2017 Jan [cited 2023 Oct 20];6:204800401668721. Available from: /pmc/articles/PMC5331469/
5. Jani B. Ageing and vascular ageing. Postgrad Med J [Internet]. 2006 [cited 2023 Oct 20];82:357–62. Available from: https://academic.oup.com/pmj/article/82/968/357/7045254
6. Harvey A, Montezano AC, Touyz RM. Vascular biology of ageing—Implications in hypertension. J Mol Cell Cardiol [Internet]. 2015 Jun 1 [cited 2023 Dec 1];83:112. Available from: /pmc/articles/PMC4534766/
7. Lacolley P, Regnault V, Segers P, Laurent S. Vascular smooth muscle cells and arterial stiffening: Relevance in development, aging, and disease. Physiol Rev [Internet]. 2017 Oct 1 [cited 2023 Oct 20];97(4):1555–617. Available from: https://journals.physiology.org/doi/10.1152/physrev.00003.2017
8. Wang M, Deshpande DA, Pintus G, Reinhart-King CA, Kohn JC, Lampi MC. Age-related vascular stiffening: causes and consequences. 2015 [cited 2023 Oct 20]; Available from: www.frontiersin.org
9. Gasser TC, Ogden RW, Holzapfel GA. Hyperelastic modelling of arterial layers with distributed collagen fibre orientations. [cited 2023 Oct 20]; Available from: https://royalsocietypublishing.org/
10. Brown BA, Williams H, George SJ. Evidence for the Involvement of Matrix-Degrading Metalloproteinases (MMPs) in Atherosclerosis. [cited 2023 Dec 1]; Available from: http://dx.doi.org/10.1016/bs.pmbts.2017.01.004

11. Bacakova L, Travnickova M, Filova E, Matějka R, Stepanovska J, Musilkova J, et al. The Role of Vascular Smooth Muscle Cells in the Physiology and Pathophysiology of Blood Vessels. In: Sakuma K, editor. Muscle Cell and Tissue [Internet]. Rijeka: IntechOpen; 2018. Available from: https://doi.org/10.5772/intechopen.77115
12. Sandoo A, Veldhuijzen Van Zanten JJCS, Metsios GS, Carroll D, Kitas GD. The Endothelium and Its Role in Regulating Vascular Tone. Open Cardiovasc Med J. 2010;4:302–12.
13. Dworatzek E, Baczko I, Kararigas G. Effects of aging on cardiac extracellular matrix in men and women. Proteomics Clin Appl. 2016 Jan 25;10(1):84–91.
14. Belz GG. Elastic Properties and of the Human Aorta Windkessel Function. Cardiovasc Drugs Ther. 1995;9:73–83.
15. Qiu H, Zhu Y, Sun Z, Trzeciakowski JP, Gansner M, Depre C, et al. Short Communication Vascular Smooth Muscle Cell Stiffness As a Mechanism for Increased Aortic Stiffness With Aging. 2010 [cited 2023 Oct 23]; Available from: http://circres.ahajournals.org.
16. Glasser SP, Arnett DK, Mcveigh GE, Finkelstein SM, Bank AJ, Morgan DJ, et al. Vascular Compliance and Cardiovascular Disease A Risk Factor or a Marker? 1997 [cited 2023 Oct 23]; Available from: https://academic.oup.com/ajh/article/10/10/1175/156506
17. Lemarié CA, Tharaux PL, Lehoux S. Extracellular matrix alterations in hypertensive vascular remodeling. J Mol Cell Cardiol. 2009;48:433–9.
18. Sazonova O V, Isenberg BC, Herrmann J, Lee KL, Purwada A, Valentine AD, et al. Extracellular matrix presentation modulates vascular smooth muscle cell mechanotransduction. 2014 [cited 2023 Oct 23]; Available from: http://dx.doi.org/10.1016/j.matbio.2014.11.001
19. Ahmed S, Warren DT, Warren D. A model for estimating traction force magnitude reveals differential regulation of actomyosin activity and matrix adhesion number in response to smooth 2 muscle cell spreading. [cited 2023 Oct 23]; Available from: https://doi.org/10.1101/612267
20. Webb RC. Smooth muscle contraction and relaxation. American Journal of Physiology - Advances in Physiology Education [Internet]. 2003 [cited 2023 Oct 23];27(1–4):201–6. Available from: https://journals.physiology.org/doi/10.1152/advan.00025.2003

21. Ghosh D, Syed AU, Prada MP, Nystoriak MA, Santana LF, Nieves-Cintrón M, et al. Calcium Channels in Vascular Smooth Muscle. Adv Pharmacol [Internet]. 2017 [cited 2023 Oct 23];78:49–87. Available from: https://pubmed.ncbi.nlm.nih.gov/28212803/
22. Kuo IY, Ehrlich BE. Signaling in Muscle Contraction. Cold Spring Harb Perspect Biol [Internet]. 2015 [cited 2023 Oct 23];7(2). Available from: /pmc/articles/PMC4315934/
23. He WQ, Peng YJ, Zhang WC, Lv N, Tang J, Chen C, et al. Myosin light chain kinase is central to smooth muscle contraction and required for gastrointestinal motility in mice. Gastroenterology [Internet]. 2008 [cited 2023 Oct 23];135(2). Available from: https://pubmed.ncbi.nlm.nih.gov/18586037/
24. Ahmed S, Warren DT. Vascular smooth muscle cell contractile function and mechanotransduction. Vessel Plus [Internet]. 2018 Nov 5 [cited 2023 Oct 23];2(0):null-null. Available from: https://www.oaepublish.com/articles/vp.2883.YXJ0aWNsZWlk
25. Zhang WC, Peng YJ, Zhang GS, He WQ, Qiao YN, Dong YY, et al. Myosin light chain kinase is necessary for tonic airway smooth muscle contraction. J Biol Chem [Internet]. 2010 Feb 19 [cited 2023 Oct 23];285(8):5522–31. Available from: https://pubmed.ncbi.nlm.nih.gov/20018858/
26. Amano M, Nakayama M, Kaibuchi K. Rho-kinase/ROCK: A key regulator of the cytoskeleton and cell polarity. Cytoskeleton. 2010 Sep;67(9):545–54.
27. Lipskaia L, Limon I, Bobe R, Hajjar R, Lipskaia L, Limon I, et al. Calcium Cycling in Synthetic and Contractile Phasic or Tonic Vascular Smooth Muscle Cells. Current Basic and Pathological Approaches to the Function of Muscle Cells and Tissues - From Molecules to Humans [Internet]. 2012 Jul 18 [cited 2023 Oct 23]; Available from: https://www.intechopen.com/chapters/37876
28. Ribeiro-Silva JC, Miyakawa AA, Krieger JE. Focal adhesion signaling: vascular smooth muscle cell contractility beyond calcium mechanisms. Clin Sci [Internet]. 2021 [cited 2023 Dec 1];135:1189–207. Available from: https://doi.org/10.1042/CS20201528
29. Zhang MJ, Zhou Y, Chen · Lei, Wang YQ, Wang · Xu, Pi Y, et al. An overview of potential molecular mechanisms involved in VSMC phenotypic modulation. Histochem Cell Biol. 2016;145:119–30.

30. Cao G, Xuan X, Hu J, Zhang R, Jin H, Dong H. How vascular smooth muscle cell phenotype switching contributes to vascular disease. Cell Commun Signal [Internet]. 2022 Dec 1 [cited 2024 Sep 13];20(1). Available from: /pmc/articles/PMC9677683/
31. Chen R, McVey DG, Shen D, Huang X, Ye S. Phenotypic Switching of Vascular Smooth Muscle Cells in Atherosclerosis. J Am Heart Assoc [Internet]. 2023 Oct 17 [cited 2024 Sep 13];12(20):31121. Available from: https://www.ahajournals.org/doi/10.1161/JAHA.123.031121
32. Raines EW. The extracellular matrix can regulate vascular cell migration, proliferation, and survival: relationships to vascular disease. Int J Exp Pathol [Internet]. 2000 [cited 2024 Sep 13];81(3):173. Available from: /pmc/articles/PMC2517724/
33. Regulation and characteristics of vascular smooth muscle cell phenotypic diversity.
34. Lacolley P, Ronique Regnault V, Nicoletti A, Li Z, Michel JB. The vascular smooth muscle cell in arterial pathology: a cell that can take on multiple roles. [cited 2023 Oct 23]; Available from: https://academic.oup.com/cardiovascres/article/95/2/194/293314
35. Chen Y, Su X, Qin Q, Yu Y, Jia M, Zhang H, et al. New insights into phenotypic switching of VSMCs induced by hyperhomocysteinemia: Role of endothelin-1 signaling. 2019 [cited 2023 Oct 23]; Available from: https://doi.org/10.1016/j.biopha.2019.109758
36. Sorokin V, Vickneson K, Kofidis T, Woo CC, Lin XY, Foo R, et al. Role of Vascular Smooth Muscle Cell Plasticity and Interactions in Vessel Wall Inflammation. Front Immunol [Internet]. 2020 Nov 26 [cited 2023 Oct 23];11:1. Available from: /pmc/articles/PMC7726011/
37. Carraher CL, Schwarzbauer JE. Regulation of Matrix Assembly through Rigidity-dependent Fibronectin Conformational Changes *. 2013;
38. Saleh Al-Shehabi T, Iratni R, Eid AH. Anti-atherosclerotic plants which modulate the phenotype of vascular smooth muscle cells. Phytomedicine. 2016 Oct 15;23(11):1068–81.
39. Sazonova O V., Isenberg BC, Herrmann J, Lee KL, Purwada A, Valentine AD, et al. Extracellular matrix presentation modulates vascular smooth muscle cell mechanotransduction. Matrix Biology. 2015 Jan 1;41:36–43.

40. Zhang L, Xu Z, Wu Y, Liao J, Zeng F, Shi L, et al. Akt/eNOS and MAPK Signaling Pathways Mediated the Phenotypic Switching of Thoracic Aorta Vascular Smooth Muscle Cells in Aging/Hypertensive Rats. Physiol Res [Internet]. 2018 [cited 2024 Sep 13];67:543–53. Available from: www.biomed.cas.cz/physiolres
41. Gardner SE, Humphry M, Bennett MR, Clarke MCH. Senescent vascular smooth muscle cells drive inflammation through an interleukin-1α-dependent senescence-associated secretory phenotype. Arterioscler Thromb Vasc Biol [Internet]. 2015 Sep 28 [cited 2024 Sep 13];35(9):1963–74. Available from: https://www.ahajournals.org/doi/10.1161/ATVBAHA.115.305896
42. Tsai MC, Chen L, Zhou J, Tang Z, Hsu TF, Wang Y, et al. Shear stress induces synthetic-to-contractile phenotypic modulation in smooth muscle cells via peroxisome proliferator-activated receptor α/δ activations by prostacyclin released by sheared endothelial cells. Circ Res [Internet]. 2009 Aug 28 [cited 2023 Oct 23];105(5):471–80. Available from: http://circres.ahajournals.org
43. Hsu S, Chu JS, Chen FF, Wang A, Li S. Effects of Fluid Shear Stress on a Distinct Population of Vascular Smooth Muscle Cells. Cell Mol Bioeng [Internet]. 2011 Dec [cited 2024 Sep 13];4(4):627. Available from: /pmc/articles/PMC3425612/
44. Wang G, Qiu J, Zheng Y, Hu J, Liao D, Gregersen H, et al. Biomechanical regulation of vascular smooth muscle cell functions: from in vitro to in vivo understanding.
45. Jaminon A, Reesink K, Kroon A, Schurgers L. Molecular Sciences The Role of Vascular Smooth Muscle Cells in Arterial Remodeling: Focus on Calcification-Related Processes. [cited 2023 Oct 23]; Available from: www.mdpi.com/journal/ijms
46. Zhu Y, Qu J, He L, Zhang F, Zhou Z, Yang S, et al. Calcium in Vascular Smooth Muscle Cell Elasticity and Adhesion: Novel Insights Into the Mechanism of Action. Front Physiol. 2019 Aug 7;10.
47. Millard M, Odde S, Neamati N. Integrin Targeted Therapeutics. Theranostics. 2011 Feb 17;1:154–88.
48. Sun Z, Martinez-Lemus LA, Hill MA, Meininger GA. Extracellular matrix-specific focal adhesions in vascular smooth muscle produce mechanically

active adhesion sites. Am J Physiol Cell Physiol [Internet]. 2008 [cited 2023 Oct 23];295:268–78. Available from: www.ajpcell.org

49. Sehgel NL, Sun Z, Hong Z, Hunter WC, Hill MA, Vatner DE, et al. Augmented Vascular Smooth Muscle Cell Stiffness and Adhesion When Hypertension Is Superimposed on Aging. Hypertension. 2015 Feb;65(2):370–7.
50. Cunningham KS, Gotlieb AI. The role of shear stress in the pathogenesis of atherosclerosis. Laboratory Investigation [Internet]. 2005 [cited 2023 Oct 23];85:9–23. Available from: www.laboratoryinvestigation.org
51. Ye GJC, Nesmith AP, Parker KK. The role of mechanotransduction on vascular smooth muscle myocytes cytoskeleton and contractile function. Anatomical Record. 2014;297(9):1758–69.
52. Matis M. The Mechanical Role of Microtubules in Tissue Remodeling. BioEssays. 2020 May 1;42(5).
53. Stamenović D. Microtubules may harden or soften cells, depending of the extent of cell distension. J Biomech. 2005 Aug 1;38(8):1728–32.
54. Nishida K, Matsumura K, Tamura M, Nakamichi T, Shimamori K, Kuragano M, et al. Effects of three microtubule-associated proteins (MAP2, MAP4, and Tau) on microtubules' physical properties and neurite morphology. Scientific Reports 2023 13:1 [Internet]. 2023 May 31 [cited 2024 Sep 13];13(1):1–12. Available from: https://www.nature.com/articles/s41598-023-36073-9
55. Li L, Zhang Q, Zhang X, Zhang J, Wang X, Ren J, et al. Microtubule associated protein 4 phosphorylation leads to pathological cardiac remodeling in mice. EBioMedicine. 2018 Nov 1;37:221–35.
56. Qin YS, Li H, Wang SZ, Wang ZB, Tang CK. Microtubule affinity regulating kinase 4: A promising target in the pathogenesis of atherosclerosis. J Cell Physiol. 2022 Jan 1;237(1):86–97.
57. Warner EF, Li Y, Li X. Targeting Microtubules for the Treatment of Heart Disease. Circ Res [Internet]. 2022 May 27 [cited 2024 Sep 13];130(11):1723–41. Available from: https://www.ahajournals.org/doi/10.1161/CIRCRESAHA.122.319808
58. Kadavath H, Hofele R V., Biernat J, Kumar S, Tepper K, Urlaub H, et al. Tau stabilizes microtubules by binding at the interface between tubulin heterodimers. Proc Natl Acad Sci U S A [Internet]. 2015 Jun 16 [cited 2024

Sep 13];112(24):7501–6. Available from: https://www.pnas.org/doi/abs/10.1073/pnas.1504081112

59. Khwaja S, Kumar K, Das R, Negi AS. Microtubule associated proteins as targets for anticancer drug development. Bioorg Chem. 2021 Nov 1;116:105320.

60. Luciani M, Montalbano M, Troncone L, Bacchin C, Uchida K, Daniele G, et al. TRANSLATIONAL RESEARCH Heart failure and cardiomyopathies Big tau aggregation disrupts microtubule tyrosination and causes myocardial diastolic dysfunction: from discovery to therapy. Eur Heart J [Internet]. 2023 [cited 2024 Sep 13];44:1560–70. Available from: https://doi.org/10.1093/eurheartj/ehad205

61. Portran D, Schaedel L, Xu Z, Théry M, Nachury M V. Tubulin acetylation protects long-lived microtubules against mechanical ageing. Nature Cell Biology 2017 19:4 [Internet]. 2017 Feb 27 [cited 2024 Sep 13];19(4):391–8. Available from: https://www.nature.com/articles/ncb3481

62. Loscalzo J, Handy DE. Epigenetic modifications: Basic mechanisms and role in cardiovascular disease (2013 Grover Conference series). Pulm Circ. 2014 Jun 1;4(2):169–74.

63. Ferreira JP, Pitt B, Zannad F. Histone deacetylase inhibitors for cardiovascular conditions and healthy longevity. 2021 [cited 2023 Dec 1];2. Available from: www.thelancet.com/healthy-longevity

64. Li G, Tian Y, Zhu WG. The Roles of Histone Deacetylases and Their Inhibitors in Cancer Therapy. Front Cell Dev Biol. 2020 Sep 29;8:576946.

65. McLendon PM, Ferguson BS, Osinska H, Shenuarin Bhuiyan M, James J, McKinsey TA, et al. Tubulin hyperacetylation is adaptive in cardiac proteotoxicity by promoting autophagy. Proc Natl Acad Sci U S A [Internet]. 2014 Nov 17 [cited 2023 Oct 25];111(48):E5178–86. Available from: https://www.pnas.org/doi/abs/10.1073/pnas.1415589111

66. Asthana J, Kapoor S, Mohan R, Panda D. Inhibition of HDAC6 Deacetylase Activity Increases Its Binding with Microtubules and Suppresses Microtubule Dynamic Instability in MCF-7 Cells. J Biol Chem [Internet]. 2013 Aug 8 [cited 2023 Oct 25];288(31):22516. Available from: /pmc/articles/PMC3829339/

67. Kee HJ, Bae EH, Park S, Lee KE, Suh SH, Kim SW, et al. HDAC inhibition suppresses cardiac hypertrophy and fibrosis in DOCA-salt hypertensive rats via regulation of HDAC6/HDAC8 enzyme activity. Kidney Blood Press Res

[Internet]. 2013 Nov [cited 2023 Oct 25];37(4–5):229–39. Available from: https://pubmed.ncbi.nlm.nih.gov/23868068/

68. Demos-Davies KM, Ferguson BS, Cavasin MA, Mahaffey JH, Williams SM, Spiltoir JI, et al. HDAC6 contributes to pathological responses of heart and skeletal muscle to chronic angiotensin-II signaling. Am J Physiol Heart Circ Physiol [Internet]. 2014 [cited 2023 Oct 25];307:252–8. Available from: www.ajpheart.org
69. Choi J, Park S, Kwon TK, Sohn SI, Park KM, Kim JI. Role of the histone deacetylase inhibitor valproic acid in high-fat diet-induced hypertension via inhibition of HDAC1/angiotensin II axis. Int J Obes [Internet]. 2017 [cited 2023 Dec 1];41:1702–9. Available from: www.nature.com/ijo
70. Bondarev AD, Attwood MM, Jonsson J, Chubarev VN, Tarasov V V., Schiöth HB. Recent developments of HDAC inhibitors: Emerging indications and novel molecules. Br J Clin Pharmacol. 2021 Dec 1;87(12):4577–97.
71. Bhaskara S, Knutson SK, Jiang G, Chandrasekharan MB, Wilson AJ, Zheng S, et al. Article Hdac3 Is Essential for the Maintenance of Chromatin Structure and Genome Stability.
72. Bhaskara S, Chyla BJ, Amann JM, Knutson SK, Cortez D, Sun ZW, et al. Article Deletion of Histone Deacetylase 3 Reveals Critical Roles in S Phase Progression and DNA Damage Control.
73. Xin-Ping Ouyang and, Jiang LP, Yu XH, Chen JZ, Hu M, Zhang YK, et al. Histone Deacetylase 3: A Potential Therapeutic Target for Atherosclerosis. 2021 [cited 2023 Dec 1]; Available from: http://dx.doi.org/10.14336/AD.2021.1116
74. Chen X, Barozzi I, Termanini A, Prosperini E, Recchiuti A, Dalli J, et al. Requirement for the histone deacetylase Hdac3 for the inflammatory gene expression program in macrophages. Proc Natl Acad Sci U S A [Internet]. 2012 Oct 16 [cited 2023 Dec 1];109(42):E2865–74. Available from: https://www.pnas.org/doi/abs/10.1073/pnas.1121131109
75. Mullican SE, Gaddis CA, Alenghat T, Nair MG, Giacomin PR, Everett LJ, et al. Histone deacetylase 3 is an epigenomic brake in macrophage alternative activation. Genes Dev [Internet]. 2011 Dec 1 [cited 2023 Dec 1];25(23):2480–8. Available from: http://genesdev.cshlp.org/content/25/23/2480.full

76. Kim JY, Cho H, Yoo J, Kim GW, Jeon YH, Lee SW, et al. Pathological Role of HDAC8: Cancer and Beyond. Cells [Internet]. 2022 Oct 1 [cited 2023 Dec 1];11(19). Available from: /pmc/articles/PMC9563588/
77. Yan M, Chen C, Gong W, Yin Z, Zhou L, Chaugai S, et al. miR-21-3p regulates cardiac hypertrophic response by targeting histone deacetylase-8. [cited 2023 Dec 1]; Available from: https://academic.oup.com/cardiovascres/article/105/3/340/455502
78. Chelladurai P, Dabral S, Basineni SR, Chen CN, Schmoranzer M, Bender N, et al. Isoform-specific characterization of class I histone deacetylases and their therapeutic modulation in pulmonary hypertension. 2020 [cited 2023 Dec 1];10:12864. Available from: https://doi.org/10.1038/s41598-020-69737-x
79. Li L, Zhang HN, Chen HZ, Gao P, Zhu LH, Li HL, et al. SIRT1 Acts as a Modulator of Neointima Formation Following Vascular Injury in Mice. 2011 [cited 2023 Dec 1]; Available from: http://circres.ahajournals.org
80. Epstein FH, Guarente L. franklin h. epstein lecture Sirtuins, Aging, and Medicine. N Engl J Med. 2011;364:2235–79.
81. Melnick A, Licht JD. Histone deacetylases as therapeutic targets in hematologic malignancies. Curr Opin Hematol [Internet]. 2002;9(4). Available from: https://journals.lww.com/co-hematology/fulltext/2002/07000/histone_deacetylases_as_therapeutic_targets_in.10.aspx
82. Diamond JR, Pitts TM, Ungermannova D, Nasveschuk CG, Zhang G, Phillips AJ, et al. Preclinical Development of the Class-I-Selective Histone Deacetylase Inhibitor OKI-179 for the Treatment of Solid Tumors. [cited 2023 Dec 1]; Available from: http://aacrjournals.org/mct/article- pdf/21/3/397/3052588/397.pdf
83. Kong Y, Tannous P, Lu G, Berenji K, Rothermel BA, Olson EN, et al. Suppression of Class I and II Histone Deacetylases Blunts Pressure-Overload Cardiac Hypertrophy. 2006 [cited 2023 Dec 1]; Available from: http://www.circulationaha.org
84. Kee HJ, Sohn S, Kwang ;, Nam I, Jong ;, Park E, et al. Inhibition of Histone Deacetylation Blocks Cardiac Hypertrophy Induced by Angiotensin II Infusion and Aortic Banding. 2006 [cited 2023 Dec 1]; Available from: http://circ.ahajournals.org/cgi/content/full/

85. Harman JL, Dobnikar L, Chappell J, Stokell BG, Dalby A, Foote K, et al. Epigenetic Regulation of Vascular Smooth Muscle Cells by Histone H3 Lysine 9 Dimethylation Attenuates Target Gene-Induction by Inflammatory Signaling. Arterioscler Thromb Vasc Biol [Internet]. 2019 Nov 1 [cited 2023 Oct 25];39(11):2289–302. Available from: https://pubmed.ncbi.nlm.nih.gov/31434493/
86. Jiang W, Agrawal DK, Boosani CS. Cell-specific histone modifications in atherosclerosis (Review). Vol. 18, Molecular Medicine Reports. Spandidos Publications; 2018. p. 1215–24.
87. Wei X, Yi X, Zhu XH, Jiang DS. Histone methylation and vascular biology. Clinical Epigenetics 2020 12:1 [Internet]. 2020 Feb 18 [cited 2023 Oct 25];12(1):1–17. Available from: https://clinicalepigeneticsjournal.biomedcentral.com/articles/10.1186/s13148- 020-00826-4
88. Toscano-Marquez F, Romero Y, Espina-Ordoñez M, Cisneros J. Absence of HDAC3 by Matrix Stiffness Promotes Chromatin Remodeling and Fibroblast Activation in Idiopathic Pulmonary Fibrosis. Cells [Internet]. 2023 Apr 1 [cited 2023 Dec 1];12(7):1020. Available from: https://www.mdpi.com/2073-4409/12/7/1020/htm
89. Spin JM, Maegdefessel L, Tsao PS. Vascular smooth muscle cell phenotypic plasticity: focus on chromatin remodelling. [cited 2023 Oct 25]; Available from: https://academic.oup.com/cardiovascres/article/95/2/147/291599
90. Chi C, Li DJ, Jiang YJ, Tong J, Fu H, Wu YH, et al. Vascular smooth muscle cell senescence and age-related diseases: State of the art. Biochimica et Biophysica Acta (BBA) - Molecular Basis of Disease. 2019 Jul 1;1865(7):1810– 21.
91. Ekholm M, Kahan T. The Impact of the Renin-Angiotensin-Aldosterone System on Inflammation, Coagulation, and Atherothrombotic Complications, and to Aggravated COVID-19. Vol. 12, Frontiers in Pharmacology. Frontiers Media S.A.; 2021.
92. Pfeifer CR, Alvey CM, Irianto J, Discher DE. Current Opinion in Systems Biology. 2017 [cited 2023 Oct 25];2:103–14. Available from: http://dx.doi.org/10.1016/j.coisb.2017.04.0052452-3100/

93. Brown IAM, Diederich L, Good ME, DeLalio LJ, Murphy SA, Cortese-Krott MM, et al. Vascular Smooth Muscle Remodeling in Conductive and Resistance Arteries in Hypertension: VSMC in hypertension. Arterioscler Thromb Vasc Biol [Internet]. 2018 [cited 2023 Oct 25];38(9):1969. Available from: /pmc/articles/PMC6205219/
94. Ahmed S, Johnson RT, Solanki R, Afewerki T, Wostear F, Warren DT. Using Polyacrylamide Hydrogels to Model Physiological Aortic Stiffness Reveals that Microtubules Are Critical Regulators of Isolated Smooth Muscle Cell Morphology and Contractility. Front Pharmacol [Internet]. 2022 Jan 27 [cited 2024 Sep 13];13. Available from: https://pubmed.ncbi.nlm.nih.gov/35153800/
95. Jaminon A, Reesink K, Kroon A, Schurgers L. Molecular Sciences The Role of Vascular Smooth Muscle Cells in Arterial Remodeling: Focus on Calcification-Related Processes. [cited 2023 Dec 1]; Available from: www.mdpi.com/journal/ijms
96. Johnson RT, Solanki R, Warren DT. Mechanical programming of arterial smooth muscle cells in health and ageing. [cited 2023 Dec 1]; Available from: https://doi.org/10.1007/s12551-021-00833-6
97. Owens GK, Schwartz SM. Vascular smooth muscle cell hypertrophy and hyperploidy in the Goldblatt hypertensive rat. Circ Res [Internet]. 1983 [cited 2023 Oct 25];53(4):491–501. Available from: https://www.ahajournals.org/doi/abs/10.1161/01.res.53.4.491
98. Jaminon A, Reesink K, Kroon A, Schurgers L. Molecular Sciences The Role of Vascular Smooth Muscle Cells in Arterial Remodeling: Focus on Calcification-Related Processes. [cited 2023 Dec 1]; Available from: www.mdpi.com/journal/ijms
99. Baumgarten CM. Origin of Mechanotransduction: Stretch-Activated Ion Channels [Internet]. Landes Bioscience; 2013 [cited 2023 Oct 25]. Available from: https://www.ncbi.nlm.nih.gov/books/NBK6374/
100. Haller H, Lindschau C, Quass P, Distler A, Luft FC. Differentiation of Vascular Smooth Muscle Cells and the Regulation of Protein Kinase C-α. Circ Res [Internet]. 1995 Jan 1 [cited 2023 Oct 25];76(1):21–9. Available from: https://www.ahajournals.org/doi/abs/10.1161/01.RES.76.1.21
101. Cole WC, Welsh DG. Role of myosin light chain kinase and myosin light chain phosphatase in the resistance arterial myogenic response to intravascular

pressure. Arch Biochem Biophys [Internet]. 2011 Jun 15 [cited 2023 Oct 25];510(2):160–73. Available from: https://pubmed.ncbi.nlm.nih.gov/21392499/

102. Douguet D, Patel A, Xu A, Vanhoutte PM, Honoré E. Piezo Ion Channels in Cardiovascular Mechanobiology. Trends Pharmacol Sci. 2019 Dec 1;40(12):956–70.

103. De Vecchis D, Beech DJ, Kalli AC. Molecular dynamics simulations of Piezo1 channel opening by increases in membrane tension. [cited 2023 Dec 1]; Available from: https://doi.org/10.1016/j.bpj.2021.02.006

104. Lin CY, Song X, Ke Y, Raha A, Wu Y, Wasi M, et al. Yoda1 Enhanced Low-Magnitude High-Frequency Vibration on Osteocytes in Regulation of MDA-MB- 231 Breast Cancer Cell Migration. Cancers (Basel). 2022 Jul 1;14(14).

105. Shanahan CM, Connolly DL, Tyson KL, Cary NRB, Osbourn JK, Agre P, et al. Aquaporin-1 Is Expressed by Vascular Smooth Muscle Cells and Mediates Rapid Water Transport across Vascular Cell Membranes. J Vasc Res [Internet]. 1999 Oct 1 [cited 2023 Oct 25];36(5):353–62. Available from: https://dx.doi.org/10.1159/000025674

106. Sachs F, Sivaselvan M V. Cell volume control in three dimensions: Water movement without solute movement. Journal of General Physiology. 2015 May 1;145(5):373–80.

107. King LS, Nielsen S, Agre P, Brown RH. Decreased pulmonary vascular permeability in aquaporin-1-null humans. Proc Natl Acad Sci U S A [Internet]. 2002 Jan 22 [cited 2023 Oct 25];99(2):1059–63. Available from: www.pnas.orgcgidoi10.1073pnas.022626499

108. Al-Samir S, Goossens D, Cartron JP, Nielsen S, Scherbarth F, Steinlechner S, et al. Maximal oxygen consumption is reduced in aquaporin-1 knockout mice. Front Physiol. 2016 Aug 10;7(AUG):209079.

109. Shangzu Z, Dingxiong X, Chengjun M, Yan C, Yangyang L, Zhiwei L, et al. Aquaporins: Important players in the cardiovascular pathophysiology. Pharmacol Res [Internet]. 2022 [cited 2023 Oct 25];183:1043–6618. Available from: https://doi.org/10.1016/j.phrs.2022.106363

110. Madonna R, Doria V, Görbe A, Cocco N, Ferdinandy P, Geng YJ, et al. Co-expression of glycosylated aquaporin-1 and transcription factor NFAT5 contributes to aortic stiffness in diabetic and atherosclerosis-prone mice. J Cell Mol Med. 2020 Mar 1;24(5):2857–65.

111. Fontijn RD, Volger OL, Van Der Pouw-Kraan TC, Doddaballapur A, Leyen T, Baggen JM, et al. Expression of Nitric Oxide-Transporting Aquaporin-1 Is Controlled by KLF2 and Marks Non-Activated Endothelium In Vivo. PLoS One [Internet]. 2015 Dec 1 [cited 2023 Oct 25];10(12):e0145777. Available from: https://journals.plos.org/plosone/article?id=10.1371/journal.pone.0145777
112. Wintmo P, Johansen SH, Hansen PBL, Lindholt JS, Urbonavicius S, Rasmussen LM, et al. The water channel AQP1 is expressed in human atherosclerotic vascular lesions and AQP1 deficiency augments angiotensin II- induced atherosclerosis in mice. Acta Physiologica [Internet]. 2017 Aug 1 [cited 2023 Oct 25];220(4):446–60. Available from: https://onlinelibrary.wiley.com/doi/full/10.1111/apha.12853
113. Fontijn RD, Volger OL, Van Der Pouw-Kraan TC, Doddaballapur A, Leyen T, Baggen JM, et al. Expression of Nitric Oxide-Transporting Aquaporin-1 Is Controlled by KLF2 and Marks Non-Activated Endothelium In Vivo. PLoS One [Internet]. 2015 Dec 1 [cited 2023 Oct 25];10(12):e0145777. Available from: https://journals.plos.org/plosone/article?id=10.1371/journal.pone.0145777
114. Beamish JA, He P, Kottke-Marchant K, Marchant RE. Molecular Regulation of Contractile Smooth Muscle Cell Phenotype: Implications for Vascular Tissue Engineering.
115. Hartman CD, Isenberg BC, Chua SG, Wong JY. Vascular smooth muscle cell durotaxis depends on extracellular matrix composition. Proc Natl Acad Sci U S A [Internet]. 2016 Oct 4 [cited 2023 Oct 25];113(40):11190–5. Available from: https://www.pnas.org/doi/abs/10.1073/pnas.1611324113
116. Zhu Y, Qiu H, Trzeciakowski JP, Sun Z, Li Z, Hong Z, et al. Temporal analysis of vascular smooth muscle cell elasticity and adhesion reveals oscillation waveforms that differ with aging. Aging Cell. 2012 Oct;11(5):741–50.
117. Hee Park J, Bin Jo S, Lee JH, Lee HH, Knowles JC, Kim HW. Materials and extracellular matrix rigidity highlighted in tissue damages and diseases: Implication for biomaterials design and therapeutic targets. 2022 [cited 2023 Dec 1]; Available from: http://creativecommons.org/licenses/by-nc-nd/4.0/
118. Tang HY, Chen AQ, Zhang H, Gao XF, Kong XQ, Zhang JJ. Vascular Smooth Muscle Cells Phenotypic Switching in Cardiovascular Diseases. Cells [Internet]. 2022 Dec 1 [cited 2024 Sep 13];11(24). Available from: /pmc/articles/PMC9777337/

119. Chakraborty R, Chatterjee P, Dave JM, Ostriker AC, Greif DM, Rzucidlo EM, et al. Targeting smooth muscle cell phenotypic switching in vascular disease. JVS Vasc Sci [Internet]. 2021 Jan 1 [cited 2024 Sep 13];2:79. Available from: /pmc/articles/PMC8489222/
120. Ageing causes an aortic contractile dysfunction phenotype by targeting the expression of members of the extracellular signal-regulated kinase pathway. 2022;
121. Ma Z, Mao C, Jia Y, Fu Y, Kong W. Tissue Remodeling: From Regeneration to Fibrosis: Extracellular matrix dynamics in vascular remodeling. Am J Physiol Cell Physiol [Internet]. 2020 Sep 9 [cited 2024 Sep 13];319(3):C481. Available from: /pmc/articles/PMC7509265/
122. Ye Z, Zhu S, Li G, Lu J, Huang S, Du J, et al. Early matrix softening contributes to vascular smooth muscle cell phenotype switching and aortic dissection through down-regulation of microRNA-143/145. J Mol Cell Cardiol [Internet]. 2024 Jul 1 [cited 2024 Sep 13];192:1–12. Available from: http://www.jmcc-online.com/article/S0022282824000671/fulltext
123. Talwar S, Kant A, Xu T, Shenoy VB, Assoian RK. Mechanosensitive smooth muscle cell phenotypic plasticity emerging from a null state and the balance between Rac and Rho. Cell Rep. 2021 Apr 20;35(3):109019.
124. Claudie P, Alain G, Stéphane A. Traction Force Measurements of Human Aortic Smooth Muscle Cells Reveal a Motor-Clutch Behavior. Molecular & Cellular Biomechanics [Internet]. 1970 Jan 1 [cited 2024 Sep 13];16(2):87–108. Available from: https://www.techscience.com/mcb/v16n2/28635
125. Sanyour HJ, Li N, Rickel AP, Childs JD, Kinser CN, Hong Z. Membrane cholesterol and substrate stiffness co-ordinate to induce the remodelling of the cytoskeleton and the alteration in the biomechanics of vascular smooth muscle cells. Cardiovasc Res [Internet]. 2019 Jul 1 [cited 2024 Sep 13];115(8):1369–80. Available from: https://dx.doi.org/10.1093/cvr/cvy276
126. Ye GJC, Nesmith AP, Parker KK. The role of mechanotransduction on vascular smooth muscle myocytes cytoskeleton and contractile function. Anat Rec (Hoboken) [Internet]. 2014 [cited 2024 Sep 13];297(9):1758. Available from: /pmc/articles/PMC4863956/
127. Johnson RT, Solanki R, Warren DT. Mechanical programming of arterial smooth muscle cells in health and ageing. Biophysical Reviews 2021 13:5

[Internet]. 2021 Aug 30 [cited 2024 Sep 13];13(5):757–68. Available from: https://link.springer.com/article/10.1007/s12551-021-00833-6

128. Johnson RT, Solanki R, Wostear F, Ahmed S, Taylor JCK, Rees J, et al. Piezo1-mediated regulation of smooth muscle cell volume in response to enhanced extracellular matrix rigidity. Br J Pharmacol [Internet]. 2024 Jun 1 [cited 2024 Sep 13];181(11):1576–95. Available from: https://onlinelibrary.wiley.com/doi/full/10.1111/bph.16294
129. Johnson R, Wostear F, Solanki R, Steward O, Morris C, Bidula S, et al. A microtubule stability switch alters isolated vascular smooth muscle calcium. [cited 2024 Sep 13]; Available from: https://doi.org/10.1101/2022.11.23.517637
130. Niu X, Mao CX, Wang S, Wang X, Zhang Y, Hu J, et al. α-Tubulin acetylation at lysine 40 regulates dendritic arborization and larval locomotion by promoting microtubule stability in Drosophila. PLoS One [Internet]. 2023 Feb 1 [cited 2024 Sep 13];18(2):e0280573. Available from: https://journals.plos.org/plosone/article?id=10.1371/journal.pone.0280573
131. Howes SC, Alushin GM, Shida T, Nachury M V., Nogales E. Effects of tubulin acetylation and tubulin acetyltransferase binding on microtubule structure. Mol Biol Cell [Internet]. 2014 Jan 1 [cited 2024 Sep 13];25(2):257. Available from: /pmc/articles/PMC3890346/
132. Yoon S, Eom GH. HDAC and HDAC Inhibitor: From Cancer to Cardiovascular Diseases. Chonnam Med J [Internet]. 2016 [cited 2024 Sep 12];52(1):1. Available from: /pmc/articles/PMC4742605/
133. Luan Y, Liu H, Luan Y, Yang Y, Yang J, Ren K Di. New Insight in HDACs: Potential Therapeutic Targets for the Treatment of Atherosclerosis. Front Pharmacol [Internet]. 2022 Apr 21 [cited 2024 Sep 13];13:863677. Available from: www.frontiersin.org
134. Shi Y, Zhang H, Huang S, Yin L, Wang F, Luo P, et al. Epigenetic regulation in cardiovascular disease: mechanisms and advances in clinical trials. Signal Transduction and Targeted Therapy 2022 7:1 [Internet]. 2022 Jun 25 [cited 2024 Sep 13];7(1):1–28. Available from: https://www.nature.com/articles/s41392-022-01055-2
135. Jiang LP, Yu XH, Chen JZ, Hu M, Zhang YK, Lin HL, et al. Histone Deacetylase 3: A Potential Therapeutic Target for Atherosclerosis. Aging Dis

[Internet]. 2022 May 18 [cited 2024 Sep 12];13(3):773–86. Available from: https://www.aginganddisease.org/EN/10.14336/AD.2021.1116

136. Chakrabarti A, Oehme I, Witt O, Oliveira G, Sippl W, Romier C, et al. HDAC8: a multifaceted target for therapeutic interventions. Trends Pharmacol Sci. 2015 Jul 1;36(7):481–92.

137. Kee HJ, Ryu Y, Seok YM, Choi SY, Sun S, Kim GR, et al. Selective inhibition of histone deacetylase 8 improves vascular hypertrophy, relaxation, and inflammation in angiotensin II hypertensive mice. Clin Hypertens [Internet]. 2019 Jun 15 [cited 2024 Sep 13];25(1). Available from: /pmc/articles/PMC6570901/

138. Chen TQ, Guo X, Huo B, Zhong XX, Wang QH, Chen Y, et al. BRD4770 inhibits vascular smooth muscle cell proliferation via SUV39H2, but not EHMT2 to protect against neointima formation. Hum Cell [Internet]. 2023 Sep 1 [cited 2024 Sep 13];36(5):1672–88. Available from: https://link.springer.com/article/10.1007/s13577-023-00924-4

139. Chen X, He Y, Fu W, Sahebkar A, Tan Y, Xu S, et al. Histone Deacetylases (HDACs) and Atherosclerosis: A Mechanistic and Pharmacological Review. Front Cell Dev Biol [Internet]. 2020 Nov 12 [cited 2024 Sep 13];8:581015. Available from: www.frontiersin.org

140. Sun L, Wang C, Yuan Y, Guo Z, He Y, Ma W, et al. Downregulation of HDAC1 suppresses media degeneration by inhibiting the migration and phenotypic switch of aortic vascular smooth muscle cells in aortic dissection. J Cell Physiol [Internet]. 2020 Nov 1 [cited 2024 Sep 13];235(11):8747–56. Available from: https://pubmed.ncbi.nlm.nih.gov/32324261/

141. Ryu Y, Kee HJ, Sun S, Seok YM, Choi SY, Kim GR, et al. Class I histone deacetylase inhibitor MS-275 attenuates vasoconstriction and inflammation in angiotensin II-induced hypertension. PLoS One [Internet]. 2019 Mar 1 [cited 2024 Sep 13];14(3). Available from: /pmc/articles/PMC6398866/

142. Hubbert C, Guardiola A, Shao R, Kawaguchi Y, Ito A, Nixon A, et al. HDAC6 is a microtubule-associated deacetylase. Nature 2002 417:6887 [Internet]. 2002 May 23 [cited 2024 Sep 13];417(6887):455–8. Available from: https://www.nature.com/articles/417455a

143. Zhang M, Urabe G, Little C, Wang B, Kent AM, Huang Y, et al. HDAC6 Regulates the MRTF-A/SRF Axis and Vascular Smooth Muscle Cell Plasticity. JACC Basic Transl Sci. 2018 Dec 1;3(6):782–95.
144. Boucherat O, Chabot S, Paulin R, Trinh I, Bourgeois A, Potus F, et al. HDAC6: A Novel Histone Deacetylase Implicated in Pulmonary Arterial Hypertension. Scientific Reports 2017 7:1 [Internet]. 2017 Jul 3 [cited 2024 Sep 13];7(1):1–14. Available from: https://www.nature.com/articles/s41598-017-04874-4
145. Demos-Davies KM, Ferguson BS, Cavasin MA, Mahaffey JH, Williams SM, Spiltoir JI, et al. HDAC6 contributes to pathological responses of heart and skeletal muscle to chronic angiotensin-II signaling. Am J Physiol Heart Circ Physiol [Internet]. 2014 Jul 15 [cited 2024 Sep 12];307(2). Available from: https://pubmed.ncbi.nlm.nih.gov/24858848/
146. Choi SY, Kee HJ, Sun S, Seok YM, Ryu Y, Kim GR, et al. Histone deacetylase inhibitor LMK235 attenuates vascular constriction and aortic remodelling in hypertension. J Cell Mol Med [Internet]. 2019 Apr 1 [cited 2024 Sep 13];23(4):2801–12. Available from: https://onlinelibrary.wiley.com/doi/full/10.1111/jcmm.14188
147. Lemon DD, Horn TR, Cavasin MA, Jeong MY, Haubold KW, Long CS, et al. Cardiac HDAC6 catalytic activity is induced in response to chronic hypertension. J Mol Cell Cardiol. 2011 Jul 1;51(1):41–50.
148. North BJ, Rosenberg MA, Jeganathan KB, Hafner A V, Michan S, Dai J, et al. SIRT 2 induces the checkpoint kinase BubR1 to increase lifespan . EMBO J [Internet]. 2014 Jul 13 [cited 2024 Sep 13];33(13):1438–53. Available from: https://www.embopress.org/doi/10.15252/embj.201386907
149. He M, Chiang HH, Luo H, Zheng Z, Qiao Q, Wang L, et al. An Acetylation Switch of the NLRP3 Inflammasome Regulates Aging-Associated Chronic Inflammation and Insulin Resistance. Cell Metab [Internet]. 2020 Mar 3 [cited 2024 Sep 13];31(3):580-591.e5. Available from: https://pubmed.ncbi.nlm.nih.gov/32032542/
150. Tang X, Chen XF, Wang NY, Wang XM, Liang ST, Zheng W, et al. SIRT2 acts as a cardioprotective deacetylase in pathological cardiac hypertrophy. Circulation [Internet]. 2017 Nov 1 [cited 2024 Sep 13];136(21):2051–67. Available from: https://www.ahajournals.org/doi/10.1161/CIRCULATIONAHA.117.028728

151. Guan JS, Haggarty SJ, Giacometti E, Dannenberg JH, Joseph N, Gao J, et al. HDAC2 negatively regulates memory formation and synaptic plasticity. Nature [Internet]. 2009 May 7 [cited 2024 Sep 13];459(7243):55–60. Available from: https://pubmed.ncbi.nlm.nih.gov/19424149/
152. Wu YX, Li BQ, Yu XQ, Liu YL, Chui RH, Sun K, et al. Histone deacetylase 6 as a novel promising target to treat cardiovascular disease. Cancer Innovation [Internet]. 2024 Jun 1;3(3):e114. Available from: https://doi.org/10.1002/cai2.114
153. Gorenne I, Kumar S, Gray K, Figg N, Yu H, Mercer J, et al. Vascular smooth muscle cell sirtuin 1 protects against dna damage and inhibits atherosclerosis. Circulation [Internet]. 2013 Jan 22 [cited 2024 Sep 13];127(3):386–96. Available from: https://www.ahajournals.org/doi/10.1161/CIRCULATIONAHA.112.124404
154. Touyz RM, Alves-Lopes R, Rios FJ, Camargo LL, Anagnostopoulou A, Arner A, et al. Vascular smooth muscle contraction in hypertension. Cardiovasc Res [Internet]. 2018 Mar 15 [cited 2024 Sep 15];114(4):529–39. Available from: https://dx.doi.org/10.1093/cvr/cvy023
155. Afewerki TL, Ahmed S, Warren D. Emerging regulators of vascular smooth muscle cell migration. J Muscle Res Cell Motil [Internet]. 2019 Jun 1 [cited 2024 Sep 15];40(2):185. Available from: /pmc/articles/PMC6726670/
156. Sheridan BC, McIntyre RC, Meldrum DR, Cleveland JC, Agrafojo J, Banerjee A, et al. Microtubules Regulate Pulmonary Vascular Smooth Muscle Contraction. Journal of Surgical Research. 1996 May 1;62(2):284–7.
157. Smyth JW, Shaw RM. Forward Trafficking of Ion Channels: What the Clinician Needs to Know. Heart rhythm : the official journal of the Heart Rhythm Society [Internet]. 2010 [cited 2024 Sep 15];7(8):1135. Available from: /pmc/articles/PMC2917321/
158. Steele DF, Fedida D. Cytoskeletal roles in cardiac ion channel expression. Biochimica et Biophysica Acta (BBA) - Biomembranes. 2014 Feb 1;1838(2):665–73.
159. Leite R, Webb RC. Microtubule disruption potentiates phenylephrine-induced vasoconstriction in rat mesenteric arterial bed. Eur J Pharmacol. 1998 Jun 12;351(1):R1–3.

160. Matsuyama A, Shimazu T, Sumida Y, Saito A, Yoshimatsu Y, Seigneurin-Berny D, et al. In vivo destabilization of dynamic microtubules by HDAC6-mediated deacetylation. EMBO J [Internet]. 2002 Dec 12 [cited 2024 Sep 15];21(24):6820. Available from: /pmc/articles/PMC139102/
161. D'Ydewalle C, Krishnan J, Chiheb DM, Van Damme P, Irobi J, Kozikowski AP, et al. HDAC6 inhibitors reverse axonal loss in a mouse model of mutant HSPB1–induced Charcot-Marie-Tooth disease. Nature Medicine 2011 17:8 [Internet]. 2011 Jul 24 [cited 2024 Sep 15];17(8):968–74. Available from: https://www.nature.com/articles/nm.2396
162. Osseni A, Ravel-Chapuis A, Thomas JL, Gache V, Schaeffer L, Jasmin BJ. HDAC6 regulates microtubule stability and clustering of AChRs at neuromuscular junctions. Journal of Cell Biology [Internet]. 2020 Aug 3 [cited 2024 Sep 15];219(8). Available from: https://doi.org/10.1083/jcb.201901099
163. Butler K V., Kalin J, Brochier C, Vistoli G, Langley B, Kozikowski AP. Rational Design and Simple Chemistry Yield a Superior, Neuroprotective HDAC6 Inhibitor, Tubastatin A. J Am Chem Soc [Internet]. 2010 Aug 8 [cited 2024 Sep 15];132(31):10842. Available from: /pmc/articles/PMC2916045/
164. Zhang D, Wu CT, Qi XY, Meijering RAM, Hoogstra-Berends F, Tadevosyan A, et al. Activation of histone deacetylase-6 induces contractile dysfunction through derailment of α-tubulin proteostasis in experimental and human atrial fibrillation. Circulation [Internet]. 2014 Jan 21 [cited 2024 Sep 15];129(3):346–58. Available from: https://www.ahajournals.org/doi/10.1161/CIRCULATIONAHA.113.005300
165. Phadwal K, Tang QY, Luijten I, Zhao JF, Corcoran B, Semple RK, et al. p53 Regulates Mitochondrial Dynamics in Vascular Smooth Muscle Cell Calcification. Int J Mol Sci [Internet]. 2023 Jan 1 [cited 2024 Sep 15];24(2). Available from: https://pubmed.ncbi.nlm.nih.gov/36675156/
166. Eckschlager T, Plch J, Stiborova M, Hrabeta J. Histone Deacetylase Inhibitors as Anticancer Drugs. Int J Mol Sci [Internet]. 2017 Jul 1 [cited 2024 Sep 15];18(7). Available from: /pmc/articles/PMC5535906/
167. Mrakovcic M, Kleinheinz J, Fröhlich LF. p53 at the Crossroads between Different Types of HDAC Inhibitor-Mediated Cancer Cell Death. Int J Mol Sci [Internet]. 2019 May 2 [cited 2024 Sep 15];20(10). Available from: /pmc/articles/PMC6567317/

168. Namdar M, Perez G, Ngo L, Marks PA. Selective inhibition of histone deacetylase 6 (HDAC6) induces DNA damage and sensitizes transformed cells to anticancer agents. Proc Natl Acad Sci U S A [Internet]. 2010 Nov 16 [cited 2024 Sep 15];107(46):20003–8. Available from: /pmc/articles/PMC2993347/
169. Safar ME, Henry O, Meaume S. Aortic Pulse Wave Velocity: An Independent Marker of Cardiovascular Risk. Am J Geriatr Cardiol [Internet]. 2002 Sep 1 [cited 2024 Sep 15];11(5):295–304. Available from: https://onlinelibrary.wiley.com/doi/full/10.1111/j.1076-7460.2002.00695.x
170. Sequí-Domínguez I, Cavero-Redondo I, Álvarez-Bueno C, Pozuelo- Carrascosa DP, de Arenas-Arroyo SN, Martínez-Vizcaíno V. Accuracy of Pulse Wave Velocity Predicting Cardiovascular and All-Cause Mortality. A Systematic Review and Meta-Analysis. Journal of Clinical Medicine 2020, Vol 9, Page 2080 [Internet]. 2020 Jul 2 [cited 2024 Sep 15];9(7):2080. Available from: https://www.mdpi.com/2077-0383/9/7/2080/htm
171. Zhong Q, Hu MJ, Cui YJ, Liang L, Zhou MM, Yang YW, et al. Carotid–Femoral Pulse Wave Velocity in the Prediction of Cardiovascular Events and Mortality: An Updated Systematic Review and Meta-Analysis. Angiology [Internet]. 2018 Aug 1 [cited 2024 Sep 15];69(7):617–29. Available from: https://journals.sagepub.com/doi/10.1177/0003319717742544
172. Sanyour HJ, Li N, Rickel AP, Childs JD, Kinser CN, Hong Z. Membrane cholesterol and substrate stiffness co-ordinate to induce the remodelling of the cytoskeleton and the alteration in the biomechanics of vascular smooth muscle cells. Cardiovasc Res [Internet]. 2019 Jul 1 [cited 2024 Sep 15];115(8):1369–80. Available from: https://dx.doi.org/10.1093/cvr/cvy276
173. Claudie P, Alain G, Stéphane A. Traction Force Measurements of Human Aortic Smooth Muscle Cells Reveal a Motor-Clutch Behavior. Molecular & Cellular Biomechanics [Internet]. 1970 Jan 1 [cited 2024 Sep 15];16(2):87–108. Available from: https://www.techscience.com/mcb/v16n2/28635
174. Johnson RT, Solanki R, Warren DT. Mechanical programming of arterial smooth muscle cells in health and ageing. Biophysical Reviews 2021 13:5 [Internet]. 2021 Aug 30 [cited 2024 Sep 15];13(5):757–68. Available from: https://link.springer.com/article/10.1007/s12551-021-00833-6

175. Sehgel NL, Zhu Y, Sun Z, Trzeciakowski JP, Hong Z, Hunter WC, et al. Increased vascular smooth muscle cell stiffness: A novel mechanism for aortic stiffness in hypertension. Am J Physiol Heart Circ Physiol [Internet]. 2013 Nov 1 [cited 2024 Sep 12];305(9):1281–7. Available from: https://journals.physiology.org/doi/10.1152/ajpheart.00232.2013
176. Zhang Y, Griendling KK, Dikalova A, Owens GK, Taylor WR. Vascular hypertrophy in angiotensin II-induced hypertension is mediated by vascular smooth muscle cell-derived H2O2. Hypertension [Internet]. 2005 Oct 1 [cited 2024 Sep 15];46(4):732–7. Available from: https://www.ahajournals.org/doi/10.1161/01.HYP.0000182660.74266.6d
177. Schiffrin EL. Vascular remodeling in hypertension: Mechanisms and treatment. Hypertension [Internet]. 2012 Feb [cited 2024 Sep 15];59(2 SUPPL. 1):367–74. Available from: https://www.ahajournals.org/doi/10.1161/HYPERTENSIONAHA.111.187021
178. Rizzoni D, Porteri E, Guefi D, Piccoli A, Castellano M, Pasini G, et al. Cellular hypertrophy in subcutaneous small arteries of patients with renovascular hypertension. Hypertension [Internet]. 2000 [cited 2024 Sep 15];35(4):931–5. Available from: https://www.ahajournals.org/doi/10.1161/01.HYP.35.4.931
179. Owens GK, Schwartz SM. Vascular smooth muscle cell hypertrophy and hyperploidy in the Goldblatt hypertensive rat. Circ Res [Internet]. 1983 [cited 2024 Sep 15];53(4):491–501. Available from: https://www.ahajournals.org/doi/10.1161/01.RES.53.4.491
180. Johnson RT, Solanki R, Wostear F, Ahmed S, Taylor JCK, Rees J, et al. Piezo1-mediated regulation of smooth muscle cell volume in response to enhanced extracellular matrix rigidity. Br J Pharmacol. 2024 Jun 1;181(11):1576–95.
181. Mondaca-Ruff D, Riquelme JA, Quiroga C, Norambuena-Soto I, Sanhueza-Olivares F, Villar-Fincheira P, et al. Angiotensin II-Regulated Autophagy Is Required for Vascular Smooth Muscle Cell Hypertrophy. Front Pharmacol [Internet]. 2019 [cited 2024 Sep 15];9(February). Available from: https://pubmed.ncbi.nlm.nih.gov/30804791/
182. Xu S, Chen H, Ni H, Dai Q. Targeting HDAC6 attenuates nicotine-induced macrophage pyroptosis via NF-κB/NLRP3 pathway. Atherosclerosis [Internet].

2021 Jan 1 [cited 2024 Sep 15];317:1–9. Available from: https://pubmed.ncbi.nlm.nih.gov/33321327/

183. Déglise S, Bechelli C, Allagnat F. Vascular smooth muscle cells in intimal hyperplasia, an update. Front Physiol [Internet]. 2022 Jan 4 [cited 2024 Sep 15];13. Available from: /pmc/articles/PMC9845604/

184. Owens GK, Schwartz SM. Alterations in Vascular Smooth Muscle Mass in the Spontaneously Hypertensive Rat Role of Cellular Hypertrophy, Hyperploidy, and Hyperplasia. [cited 2024 Sep 15]; Available from: http://ahajournals.org

185. Stewart L, Turner NA. Channelling the Force to Reprogram the Matrix: Mechanosensitive Ion Channels in Cardiac Fibroblasts. Cells [Internet]. 2021 May 1 [cited 2024 Sep 15];10(5). Available from: https://pubmed.ncbi.nlm.nih.gov/33922466/

186. Liu S, Lin Z. Vascular Smooth Muscle Cells Mechanosensitive Regulators and Vascular Remodeling. J Vasc Res [Internet]. 2022 Mar 22 [cited 2024 Sep 15];59(2):90–113. Available from: https://dx.doi.org/10.1159/000519845

187. Inoue R, Jian Z, Kawarabayashi Y. Mechanosensitive TRP channels in cardiovascular pathophysiology. Pharmacol Ther. 2009 Sep 1;123(3):371–85.

188. Lowis C, Ramara Winaya A, Kumari P, Rivera CF, Vlahos J, Hermantara R, et al. Mechanosignals in abdominal aortic aneurysms. Front Cardiovasc Med. 2023 Jan 9;9:1021934.

189. Davis MJ, Earley S, Li YS, Chien S. Vascular mechanotransduction. Physiol Rev [Internet]. 2023 Apr 4 [cited 2024 Sep 15];103(2):1247. Available from: /pmc/articles/PMC9942936/

190. Qian W, Hadi T, Silvestro M, Ma X, Rivera CF, Bajpai A, et al. Microskeletal stiffness promotes aortic aneurysm by sustaining pathological vascular smooth muscle cell mechanosensation via Piezo1. Nature Communications 2022 13:1 [Internet]. 2022 Jan 26 [cited 2024 Sep 15];13(1):1–19. Available from: https://www.nature.com/articles/s41467-021-27874-5

191. Yin Q, Zang G, Li N, Sun C, Du R. Agonist-induced Piezo1 activation promote mitochondrial-dependent apoptosis in vascular smooth muscle cells. BMC Cardiovasc Disord [Internet]. 2022 Dec 1 [cited 2024 Sep 15];22(1):1–12. Available from: https://link.springer.com/articles/10.1186/s12872-022-02726-2

192. Suleymanian MA, Clemo HF, Cohen NM, Baumgarten CM. Stretch-activated channel blockers modulate cell volume in cardiac ventricular myocytes. J Mol

Cell Cardiol [Internet]. 1995 [cited 2024 Sep 15];27(1):721–8. Available from: https://pubmed.ncbi.nlm.nih.gov/7539086/

193. Dobner S, Amadi OC, Lee RT. Cardiovascular Mechanotransduction. Muscle: Fundamental Biology and Mechanisms of Disease. 2012 Jan 1;1–2:173–86.
194. Wang J, Ma Y, Sachs F, Li J, Suchyna TM. GsMTx4-D is a cardioprotectant against myocardial infarction during ischemia and reperfusion. J Mol Cell Cardiol [Internet]. 2016 Sep 1 [cited 2024 Sep 15];98:83–94. Available from: https://pubmed.ncbi.nlm.nih.gov/27423272/
195. McManus ML, Churchwell KB, Strange K. Regulation of Cell Volume in Health and Disease. New England Journal of Medicine [Internet]. 1995 Nov 9 [cited 2024 Sep 15];333(19):1260–7. Available from: https://www.nejm.org/doi/full/10.1056/NEJM199511093331906
196. Delpire E, Gagnon KB. Water Homeostasis and Cell Volume Maintenance and Regulation. Curr Top Membr [Internet]. 2018 Jan 1 [cited 2024 Sep 15];81:3. Available from: /pmc/articles/PMC6457474/
197. Conner MT, Conner AC, Brown JEP, Bill RM. Membrane trafficking of aquaporin 1 is mediated by protein kinase C via microtubules and regulated by tonicity. Biochemistry [Internet]. 2010 Feb 9 [cited 2024 Sep 15];49(5):821–3. Available from: https://pubs.acs.org/doi/full/10.1021/bi902068b
198. Li X, Garcia-Elias A, Benito B, Nattel S. The effects of cardiac stretch on atrial fibroblasts: analysis of the evidence and potential role in atrial fibrillation. Cardiovasc Res [Internet]. 2022 Feb 1 [cited 2024 Sep 15];118(2):440. Available from: /pmc/articles/PMC8803074/
199. Wu Y, Xu X, Liu F, Jing Z, Shen D, He P, et al. Three-Dimensional Matrix Stiffness Activates the Piezo1-AMPK-Autophagy Axis to Regulate the Cellular Osteogenic Differentiation. ACS Biomater Sci Eng [Internet]. 2023 Aug 14 [cited 2024 Sep 15];9(8):4735–46. Available from: https://pubs.acs.org/doi/full/10.1021/acsbiomaterials.3c00419
200. Emig R, Knodt W, Krussig MJ, Zgierski-Johnston CM, Gorka O, Groß O, et al. Piezo1 Channels Contribute to the Regulation of Human Atrial Fibroblast Mechanical Properties and Matrix Stiffness Sensing. Cells 2021, Vol 10, Page 663 [Internet]. 2021 Mar 16 [cited 2024 Sep 15];10(3):663. Available from: https://www.mdpi.com/2073-4409/10/3/663/htm

201. Lopez-Cavestany M, Hahn S Bin, Hope JM, Reckhorn NT, Greenlee JD, Schwager SC, et al. Matrix stiffness induces epithelial-to-mesenchymal transition via Piezo1-regulated calcium flux in prostate cancer cells. iScience. 2023 Apr 21;26(4):106275.
202. Day RE, Kitchen P, Owen DS, Bland C, Marshall L, Conner AC, et al. Human aquaporins: Regulators of transcellular water flow. Biochimica et Biophysica Acta (BBA) - General Subjects. 2014 May 1;1840(5):1492–506.
203. Zhang W, Zitron E, Hömme M, Kihm L, Morath C, Scherer D, et al. Aquaporin- 1 channel function is positively regulated by protein kinase C. J Biol Chem [Internet]. 2007 Jul 20 [cited 2024 Sep 15];282(29):20933–40. Available from: https://pubmed.ncbi.nlm.nih.gov/17522053/
204. Markou A, Unger L, Abir-Awan M, Saadallah A, Halsey A, Baklava Z, et al. Molecular mechanisms governing aquaporin relocalisation. Biochimica et Biophysica Acta (BBA) - Biomembranes. 2022 Apr 1;1864(4):183853.
205. Shanahan CM, Connolly DL, Tyson KL, Cary NRB, Osbourn JK, Agre P, et al. Aquaporin-1 Is Expressed by Vascular Smooth Muscle Cells and Mediates Rapid Water Transport across Vascular Cell Membranes. J Vasc Res [Internet]. 1999 Oct 1 [cited 2024 Sep 15];36(5):353–62. Available from: https://dx.doi.org/10.1159/000025674
206. Ahmed S, Johnson RT, Solanki R, Afewerki T, Wostear F, Warren DT. Using Polyacrylamide Hydrogels to Model Physiological Aortic Stiffness Reveals that Microtubules Are Critical Regulators of Isolated Smooth Muscle Cell Morphology and Contractility. Front Pharmacol [Internet]. 2022 Jan 27 [cited 2023 Dec 1];13. Available from: /pmc/articles/PMC8830533/
207. Tracqui P, Broisat A, Toczek J, Mesnier N, Ohayon J, Riou L. Mapping elasticity moduli of atherosclerotic plaque in situ via atomic force microscopy. J Struct Biol [Internet]. 2011 [cited 2024 Sep 12];174(1):115–23. Available from: https://pubmed.ncbi.nlm.nih.gov/21296163/
208. Sehgel NL, Vatner SF, Meininger GA. "Smooth Muscle Cell Stiffness Syndrome"—Revisiting the Structural Basis of Arterial Stiffness. Front Physiol [Internet]. 2015 [cited 2024 Sep 12];6(NOV):335. Available from: /pmc/articles/PMC4649054/
209. Sazonova O V., Isenberg BC, Herrmann J, Lee KL, Purwada A, Valentine AD, et al. Extracellular matrix presentation modulates vascular smooth muscle cell

mechanotransduction. Matrix Biol [Internet]. 2015 Jan 1 [cited 2024 Sep 12];41:36–43. Available from: https://pubmed.ncbi.nlm.nih.gov/25448408/

210. Hytönen VP, Wehrle-Haller B. Mechanosensing in cell-matrix adhesions - Converting tension into chemical signals. Exp Cell Res [Internet]. 2016 Apr 10 [cited 2024 Sep 12];343(1):35–41. Available from: https://pubmed.ncbi.nlm.nih.gov/26518118/
211. Yang WM, Tsai SC, Wen Y Der, Fejé G, Seto E. Functional domains of histone deacetylase-3. J Biol Chem [Internet]. 2002 Mar 15 [cited 2024 Sep 12];277(11):9447–54. Available from: https://pubmed.ncbi.nlm.nih.gov/11779848/
212. Gao Z, He Q, Peng B, Chiao PJ, Ye J. REGULATION OF NUCLEAR TRANSLOCATION OF HDAC3 BY IKBα IS REQUIRED FOR TNF-INHIBITION OF PPARγ FUNCTION. J Biol Chem [Internet]. 2006 Feb 2 [cited 2024 Sep 12];281(7):4540. Available from: /pmc/articles/PMC1447600/
213. Baek SH, Ohgi KA, Rose DW, Koo EH, Glass CK, Rosenfeld MG. Exchange of N-CoR corepressor and Tip60 coactivator complexes links gene expression by NF-κB and β-amyloid precursor protein. Cell [Internet]. 2002 Jul 12 [cited 2024 Sep 12];110(1):55–67. Available from: http://www.cell.com/article/S0092867402008097/fulltext
214. Hu C, Zhang X, Teng T, Ma ZG, Tang QZ. Cellular Senescence in Cardiovascular Diseases: A Systematic Review. Aging Dis [Internet]. 2022 Feb 1 [cited 2024 Sep 12];13(1):103. Available from: /pmc/articles/PMC8782554/
215. Wu YX, Li BQ, Yu XQ, Liu YL, Chui RH, Sun K, et al. Histone deacetylase 6 as a novel promising target to treat cardiovascular disease. Cancer Innovation [Internet]. 2024 Jun 1 [cited 2024 Sep 12];3(3):e114. Available from: https://onlinelibrary.wiley.com/doi/full/10.1002/cai2.114
216. McKinsey TA. Derepression of pathological cardiac genes by members of the CaM kinase superfamily. Cardiovasc Res [Internet]. 2007 Mar 1 [cited 2024 Sep 12];73(4):667–77. Available from: https://dx.doi.org/10.1016/j.cardiores.2006.11.036
217. Bagchi RA, Weeks KL. Histone deacetylases in cardiovascular and metabolic diseases. J Mol Cell Cardiol. 2019 May 1;130:151–9.
218. Jha S, Kim JH, Kim M, Nguyen AH, Ali KH, Gupta SK, et al. Design, synthesis, and biological evaluation of HDAC6 inhibitors targeting L1 loop and serine 531 residue. Eur J Med Chem. 2024 Feb 5;265:116057.
219. Wagner FF, Olson DE, Gale JP, Kaya T, Weïwer M, Aidoud N, et al. Potent and

selective inhibition of histone deacetylase 6 (HDAC6) does not require a surface-binding motif. J Med Chem [Internet]. 2013 Feb 28 [cited 2025 Mar 26];56(4):1772–6. Available from: https://pubs.acs.org/doi/full/10.1021/jm301355j

220. Singh N, Trivedi CM, Lu M, Mullican SE, Lazar MA, Epstein JA. Histone deacetylase 3 regulates smooth muscle differentiation in neural crest cells and development of the cardiac outflow tract. Circ Res [Internet]. 2011 Nov 11 [cited 2025 Mar 26];109(11):1240–9. Available from: https://pubmed.ncbi.nlm.nih.gov/21959220/

221. HDAC inhibitors, trichostatin A and valproic acid, increase E-cadherin and vimentin expression but inhibit migration and invasion of cholangiocarcinoma cells [Internet]. [cited 2025 Mar 26]. Available from: https://www.spandidos-publications.com/10.3892/or.2018.6441#b6-or-40-01-0346

222. Yang H, Guo K, Ding P, Ning J, Zhang Y, Wang Y, et al. Histone deacetylases: Regulation of vascular homeostasis via endothelial cells and vascular smooth muscle cells and the role in vascular pathogenesis. Genes Dis. 2024 Nov 1;11(6):101216.

223. Wagner FF, Olson DE, Gale JP, Kaya T, Weïwer M, Aidoud N, et al. Potent and selective inhibition of histone deacetylase 6 (HDAC6) does not require a surface-binding motif. J Med Chem [Internet]. 2013 Feb 28 [cited 2025 Mar 26];56(4):1772–6. Available from: https://pubs.acs.org/doi/full/10.1021/jm301355j

224. Maniotis AJ, Chen CS, Ingber DE. Demonstration of mechanical connections between integrins, cytoskeletal filaments, and nucleoplasm that stabilize nuclear structure. Proc Natl Acad Sci U S A [Internet]. 1997 Feb 4 [cited 2025 Mar 26];94(3):849–54. Available from: https://www.pnas.org/doi/abs/10.1073/pnas.94.3.849

225. Dahl KN, Ribeiro AJS, Lammerding J. Nuclear shape, mechanics, and mechanotransduction. Circ Res [Internet]. 2008 Jun 6 [cited 2025 Mar 26];102(11):1307–18. Available from: https://www.ahajournals.org/doi/10.1161/CIRCRESAHA.108.173989

226. Alford PW, Nesmith AP, Seywerd JN, Grosberg A, Parker KK. Vascular Smooth Muscle Contractility Depends on Cell Shape. Integr Biol (Camb) [Internet]. 2011 Nov [cited 2025 Mar 26];3(11):1063. Available from: https://pmc.ncbi.nlm.nih.gov/articles/PMC8388149/

227. Sims JR, Karp S, Ingber DE. Altering the cellular mechanical force balance results in integrated changes in cell, cytoskeletal and nuclear shape. J Cell Sci [Internet]. 1992 Dec 1 [cited 2025 Mar 26];103(4):1215–22. Available from:

https://dx.doi.org/10.1242/jcs.103.4.1215

228. Zhou C, Li R, Warren DT, Shanahan CM, Zhang Q. Mouse models of nesprin-related diseases. Biochem Soc Trans [Internet]. 2018 Jun 19 [cited 2025 Mar 26];46(3):669–81. Available from: /biochemsoctrans/article/46/3/669/67441/Mouse-models-of-nesprin-related-diseases

229. Bray MAP, Adams WJ, Geisse NA, Feinberg AW, Sheehy SP, Parker KK. Nuclear morphology and deformation in engineered cardiac myocytes and tissues. Biomaterials. 2010 Jul 1;31(19):5143–50.

230. Mudera V, Smith AST, Brady MA, Lewis MP. The effect of cell density on the maturation and contractile ability of muscle derived cells in a 3D tissue-engineered skeletal muscle model and determination of the cellular and mechanical stimuli required for the synthesis of a postural phenotype. J Cell Physiol [Internet]. 2010 Dec 1 [cited 2025 Mar 26];225(3):646–53. Available from: https://onlinelibrary.wiley.com/doi/full/10.1002/jcp.22271

Appendix

8.1 Appendix for Chapter 3:

8.1.1 A1 DMSO dilution controls

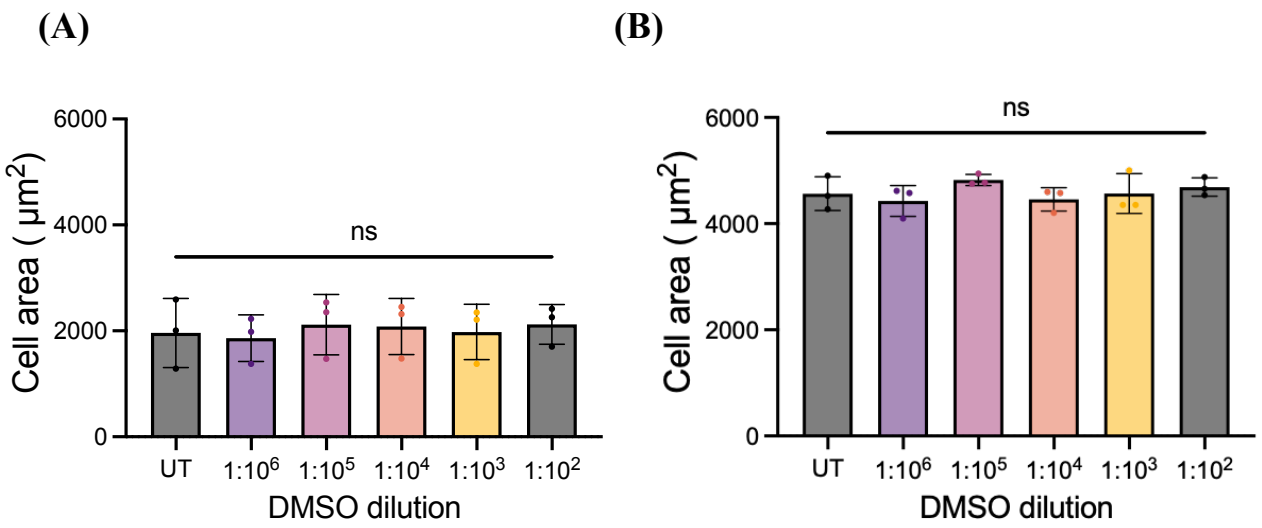

Figure A1 *DMSO vehicle control assay (A) Graph shows the cell area of VSMC treated with dilution range of DMSO vehicle control for 30 minutes prior to angiotensin II (10µM) stimulation on 12kPa PAHs. (UT = only treated with angiotensin II). (B) VSMC area on 72 kPa PAHs. Represented are individual cell values (coloured dots) as well as the mean of 3 independent experiments with approximately ≥53 cells analysed. Significance was determined using one-way ANOVA followed by Tukey's multiple comparison test (non-significant, ns. Significant; * p≤0.05, ** p≤0.01, *** p≤0.001).*

8.1.2 A2 HDAC Inhibitor nuclear data

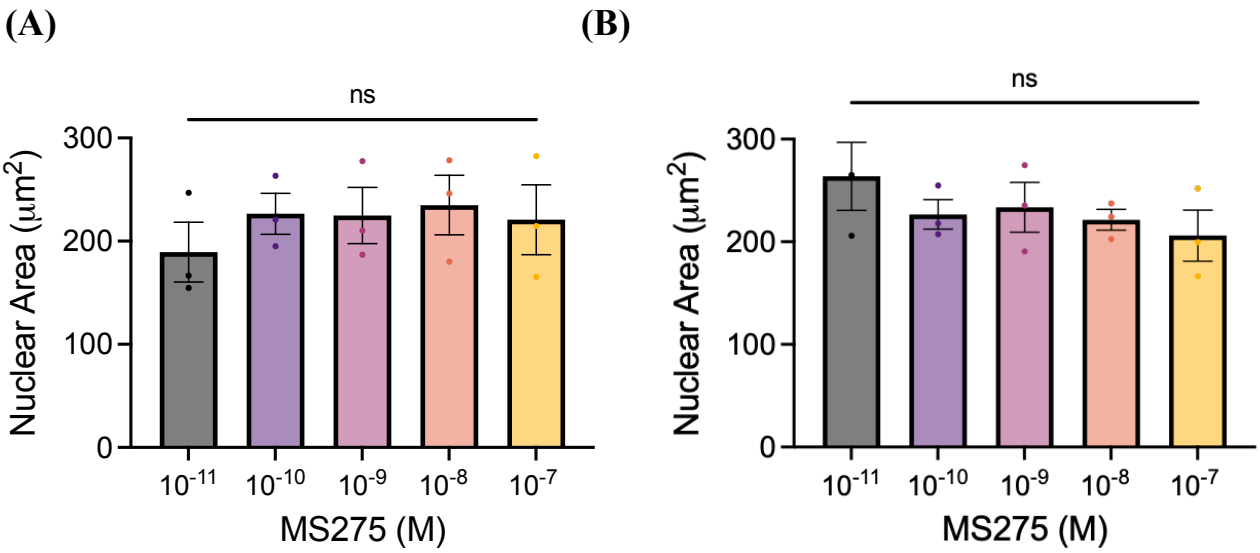

Figure A2.1 *HDAC1 inhibitor (MS275) concentration response assay VSMCs were treated with increasing concentrations of MS275 (0.01µM-100µM) for 1 hour. (A) Graph shows nuclear area data of VSMCs seeded on 12kPa PAH individual cell values (coloured dots) as well as the mean of 3 independent experiments with approximately ≥60 cells analysed. (B) Graph shows nuclear area data of VSMCs seeded on 72kPa PAH individual cell values (coloured dots) as well as the mean of 3 independent experiments with approximately ≥60 cells analysed. Significance was determined using one-way ANOVA followed by Tukey's multiple comparison test (non-significant, ns. Significant; * p≤0.05, ** p≤0.01, *** p≤0.001).*

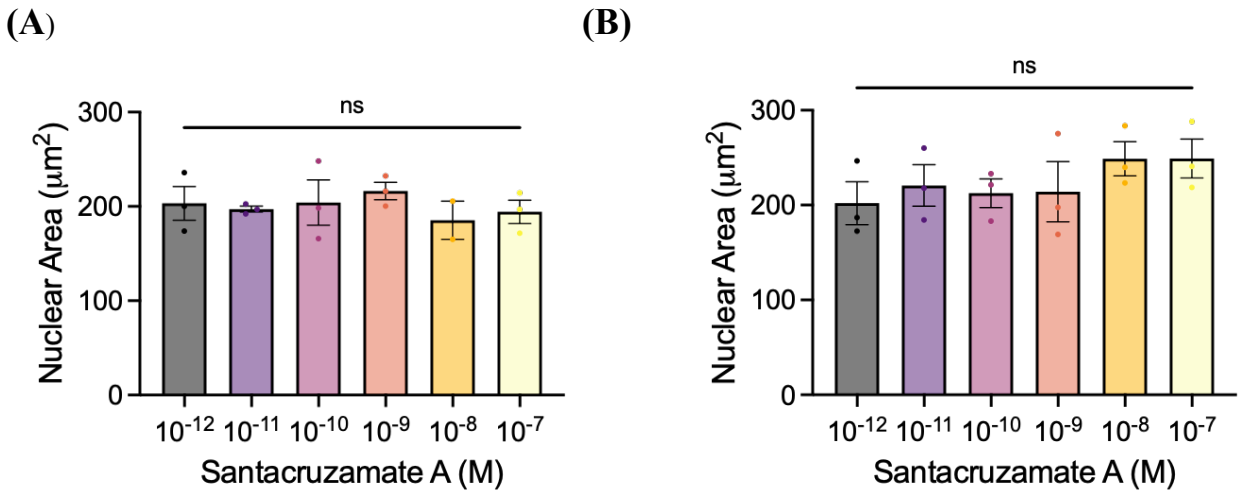

Figure A2.2 *HDAC2 inhibitor (Santacruzamate A) concentration response assay VSMCs were treated with increasing concentrations of Santacruzamate A (0.01µM-100µM) for 1 hour. (A) Graph shows nuclear area data of VSMCs seeded on 12kPa PAH individual cell values (coloured dots) as well as the mean of 3 independent experiments with approximately ≥60 cells analysed. (B) Graph shows nuclear area data of VSMCs seeded on 72kPa PAH individual cell values (coloured dots) as well as the mean of 3 independent experiments with approximately ≥60 cells analysed. Significance was determined using one-way ANOVA followed by Tukey's multiple comparison test (non-significant, ns. Significant; * p≤0.05, ** p≤0.01, *** p≤0.001).*

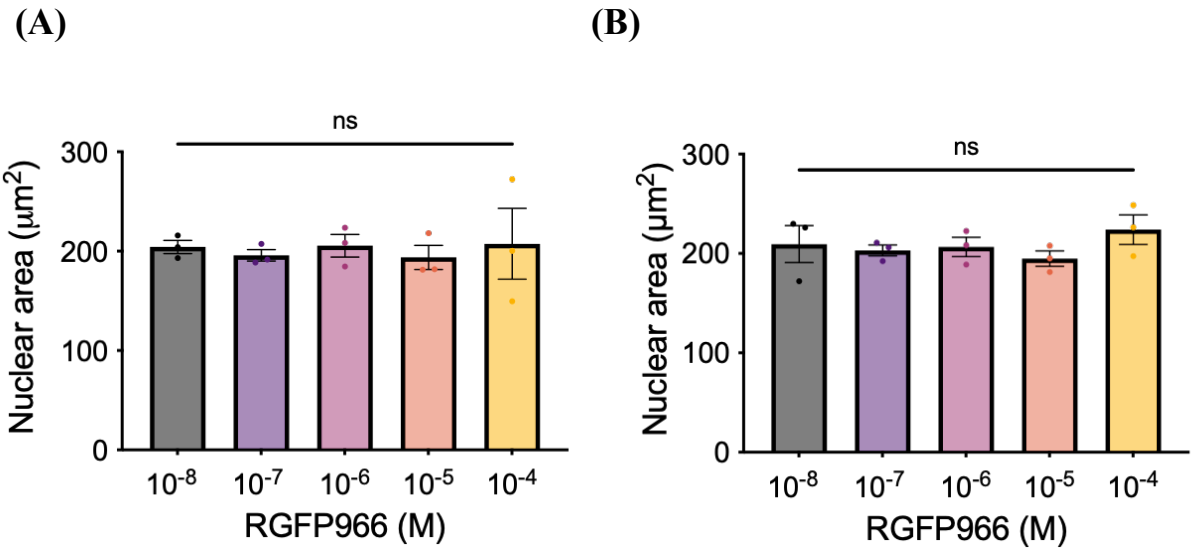

Figure A2.3 *HDAC3 inhibitor (RGFP966) concentration response assay VSMCs were treated with increasing concentrations of RGFP966 (0.01µM-100µM) for 1 hour. (A) Graph shows nuclear area data of VSMCs seeded on 12kPa PAH individual cell values (coloured dots) as well as the mean of 3 independent experiments with approximately ≥60 cells analysed. (B) Graph shows nuclear area data of VSMCs seeded on 72kPa PAH individual cell values (coloured dots) as well as the mean of 3 independent experiments with approximately ≥60 cells analysed. Significance was determined using one-way ANOVA followed by Tukey's multiple comparison test (non-significant, ns. Significant; * p≤0.05, ** p≤0.01, *** p≤0.001).*

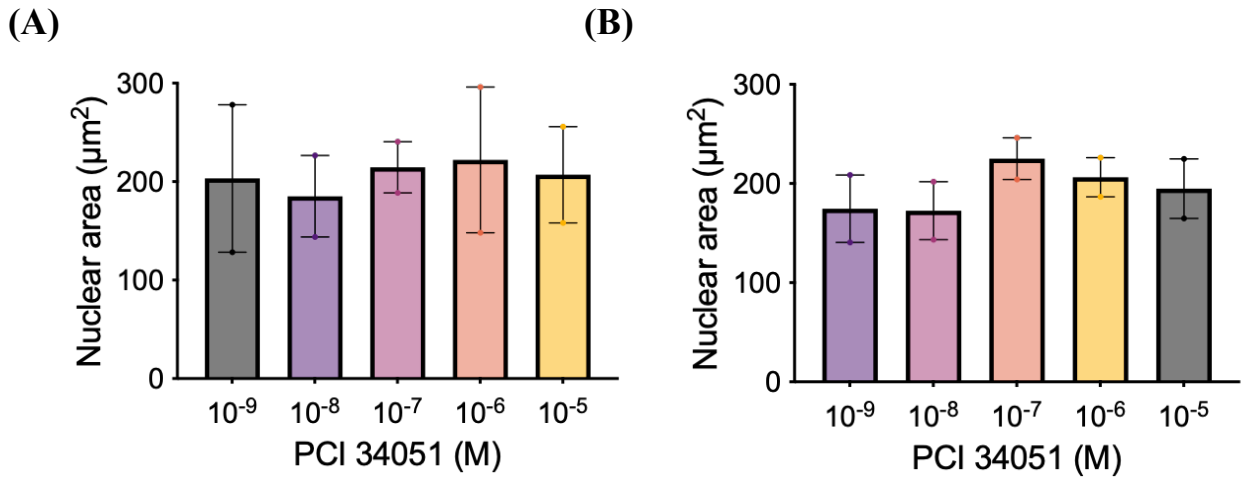

Figure A2.4 *HDAC8 inhibitor (PCI 34051) concentration response assay VSMCs were treated with increasing concentrations of PCI 34051 (0.01µM-100µM) for 1 hour. (A) Graph shows nuclear area data of VSMCs seeded on 12kPa PAH individual cell values (coloured dots) as well as the mean of 2 independent experiments with approximately ≥30 cells analysed. (B) Graph shows nuclear area data of VSMCs seeded on 72kPa PAH individual cell values (coloured dots) as well as the mean of 2 independent experiments with approximately ≥30 cells analysed. Significance was not determined as only N=2.*

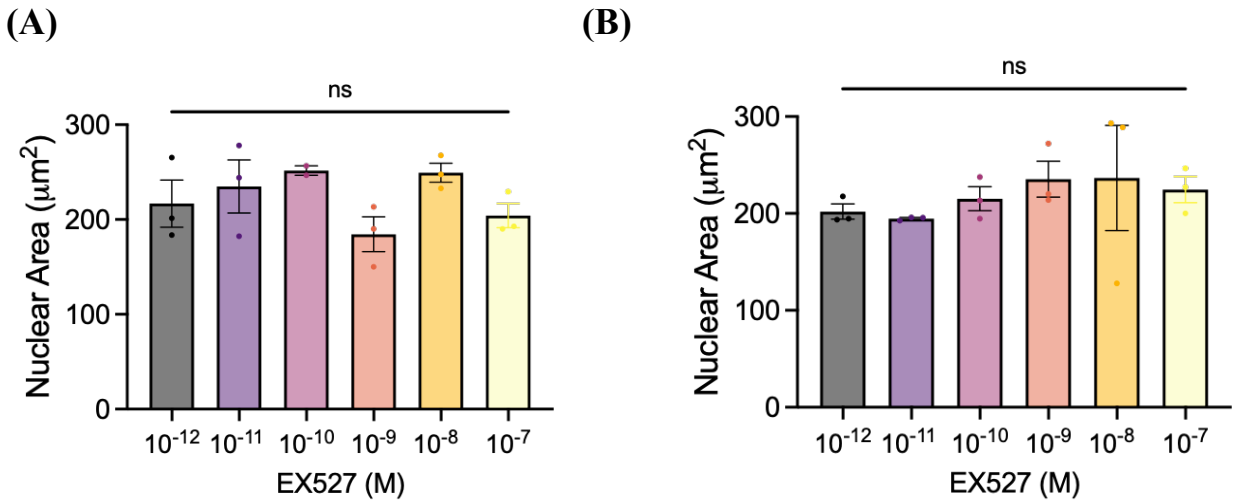

Figure A2.5 *SIRT1 inhibitor (EX527) concentration response assay VSMCs were treated with increasing concentrations of EX527 (0.01µM-100µM) for 1 hour. (A) Graph shows nuclear area data of VSMCs seeded on 12kPa PAH individual cell values (coloured dots) as well as the mean of 3 independent experiments with approximately ≥60 cells analysed. (B) Graph shows nuclear area data of VSMCs seeded on 72kPa PAH individual cell values (coloured dots) as well as the mean of 3 independent experiments with approximately ≥60 cells analysed. Significance was determined using one-way ANOVA followed by Tukey's multiple comparison test (non-significant, ns. Significant; * p≤0.05, ** p≤0.01, *** p≤0.001).*

8.2 Appendix for Chapter 4

8.2.1 HDAC6 SiRNA viability data

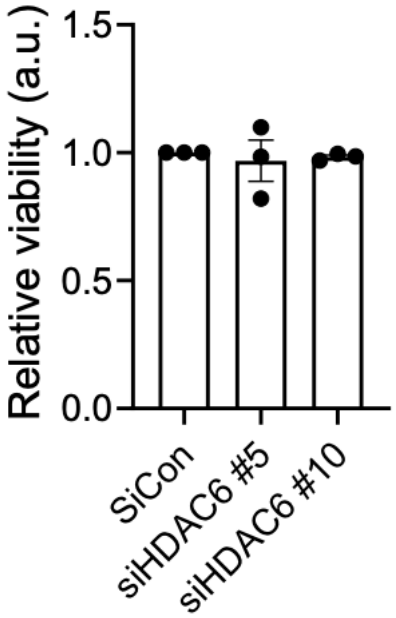

Figure A3.1 *Graph shows relative VSMC viability following a 72-hour treatment with scrambled (siCon) or HDAC6-targeting (siHDAC6 #5/#10) siRNA. Black dots represent mean values for each independent experimental repeats performed in triplicate. One-way ANOVA followed by Tukey's test determined that no significant differences existed between the experimental groups. Error bars represent ± SEM).*